論文 / 著書情報
Article / Book Information

題目(和文)	ロドプシンおよびバクテリオロドプシンにおける発色団 : タンパク質相互作用に関する量子化学的研究
Title(English)	Quantum chemical study of chromophore-protein interactions in rhodopsin and bacteriorhodopsin
著者(和文)	北條博彦
Author(English)	Hirohiko Houjou
出典(和文)	学位:博士(工学), 学位授与機関:東京工業大学, 報告番号:甲第3781号, 授与年月日:1998年3月26日, 学位の種別:課程博士, 審査員:
Citation(English)	Degree:Doctor (Engineering), Conferring organization: Tokyo Institute of Technology, Report number:甲第3781号, Conferred date:1998/3/26, Degree Type:Course doctor, Examiner:
学位種別(和文)	博士論文
Type(English)	Doctoral Thesis

Quantum Chemical Study of Chromophore-Protein Interactions in Rhodopsin and Bacteriorhodopsin

Hirohiko Houjou

A Thesis for Doctorate

at

Tokyo Institute of Technology

January, 1998

Contents

List of Abbreviations

Rh	rhodopsin
bR	bacteriorhodopsin
MO	molecular orbital
CI	configuration interaction
SCRF	self-consistent reaction field
PCM	polarizable continuum model
NMR	nuclear magnetic resonance
UV-VIS	ultraviolet-visible
RSB	retinal Schiff base
PRSB	protonated retinal Schiff base

List of Notations

σ_{iso}	isotropic shielding constant
ε	dielectric constant
n	refractive index
ε_{stat}	static dielectric constant
ε_{opt}	optical dielectric constant
λ	wavelength
ν	wavenumber
ν_{max}	absorption maximum

List of Publications

Chapter 2

(1) Houjou, H.; Sakurai, M.; Asakawa, N.; Inoue, Y.; Tamura Y.; Watanabe, Y. "*Ab Initio* Study of the C12-C13 Conformation of 11-*cis*-retinal" *Chem. Lett.* **1995**, 1039-1040.

(2) Houjou, H.; Sakurai, M.; Asakawa, N.; Inoue, Y.; Tamura, Y. "*Ab Initio* Study of ^{13}C Shieldings for Linear π-Conjugated Systems. Theoretical Determination of the C12-C13 Conformation in the Chromophore of Rhodopsin" *J. Am. Chem. Soc.* **1996**, *118*, 8904-8915.

Chapter 3

(3) Houjou, H.; Sakurai, M.; Inoue, Y. "Theoretical Evaluation of Medium Effects on Absorption Maxima of Molecular Solutes 1. Formulation of a New Method Based on the Self-Consistent Reaction Field Theory" *J. Chem. Phys.* **1997**, *107*, 5652-5660.

Chapter 4

(4) Houjou, H.; Sakurai, M.; Inoue, Y. "Medium Effects on Absorption Maxima of Protonated Retinylidene Schiff Bases as Models of Rhodopsin" *Chem. Lett.* **1996**, 1075-1076.

(5) Houjou, H.; Inoue, Y.; Sakurai, M. "Theoretical Evaluation of Medium Effects on Absorption Maxima of Molecular Solutes 2. Comprehensive Analysis of the Opsin shift of Bacteriorhodopsin" *J. Am. Chem. Soc.*, submitted.

Chapter 5

(6) Houjou, H.; Inoue, Y.; Sakurai, M. "Full-Atomic Calculation Involving Electronic Polarization Effect. A New Interpretation for the Opsin Shift of Bacteriorhodopsin" to be published.

Chapter 1. Introduction

§1.1 Retinal Proteins

"Rays are not coloured."[1] Color recognition by animals arises from a difference in response of the optic nerve to visual light with various wavelengths in quite a narrow region. Extremely fine distinguishability for color is attributed to the precise regulation of the absorption spectra of photoreceptive pigments of animals. Recent progress in spectroscopy, biochemistry and electrophysiology, combined with molecular genetics, has provided new and exciting findings, which may make us expect to understand the mechanism of vision at the molecular level. In the visual pigments studied so far, a retinal molecule functions as a receptor of a photon. Similar proteins are also found in the cytoplasmic membrane of *Halobacteria.*

1.1.1 Visual Pigments

In the retina of eyes of animals, there are a number of light sensitive cells (visual cells). There are two types of visual cells: rods and cones. Photoreceptive proteins are contained in the integral membrane of the outer segment of each cell (Figure 1.1). Those proteins in rods and cones are called rhodopsin (Rh) and cone pigments, respectively.[2] Rhodopsin shows its absorption maximum around 500 nm, and initiates the signal transduction in twilight vision with a high quantum yield. Cone pigments are further classified into several types, which show distinct absorption maxima from each other. In contrast to Rh, cone pigments initiate the signal transduction in daylight vision, and are responsible for color recognition. The dexterous action of these cells enables a human eye to have a wide dynamic range for brightness from starlight to daylight.

The number ratio of cones to rods depends on species of animals, and the

(a) The human eye

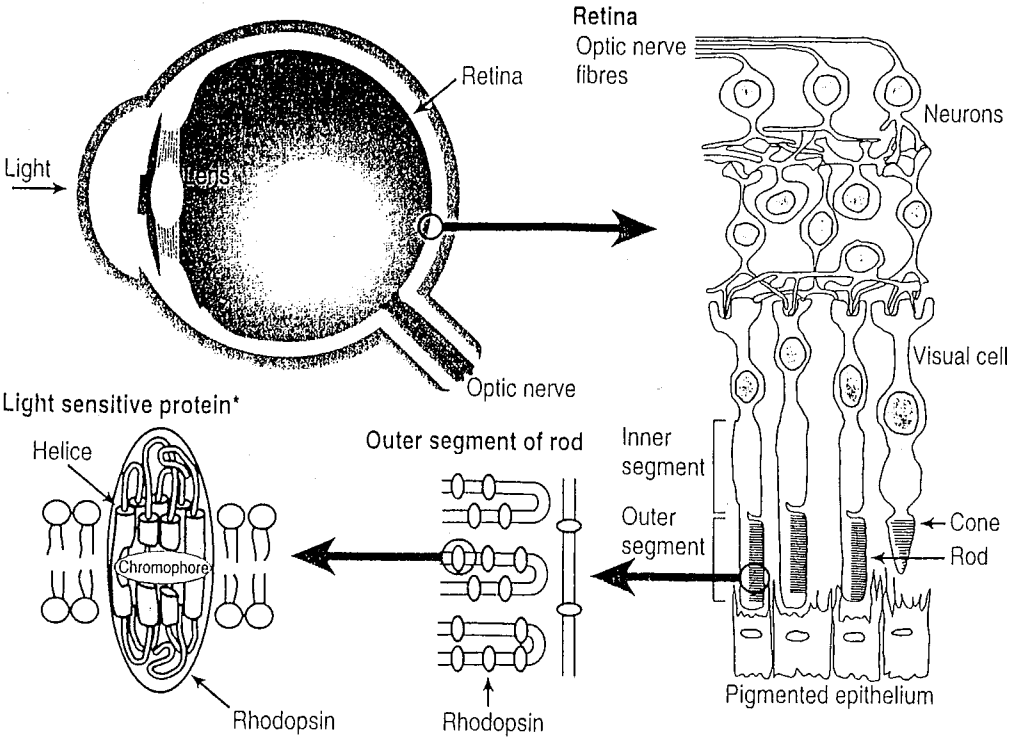

(b)

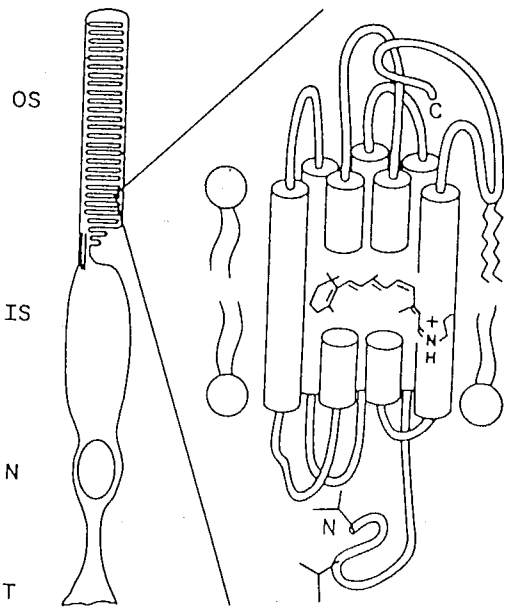

Figure 1.1 Photoreceptive pigments in human retina. (a) cited from ref. 2g, and (b) cited from ref. 3.

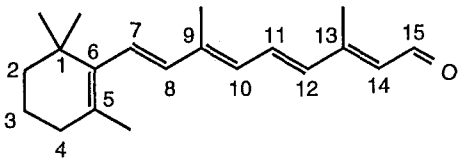

all-trans-retinal

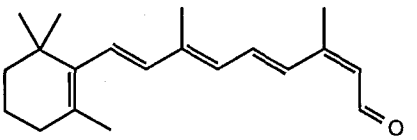

13-*cis*-retinal

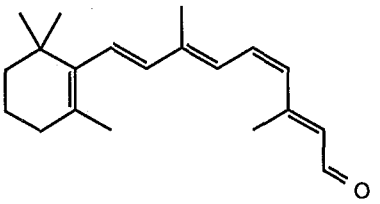

11-*cis*-retinal

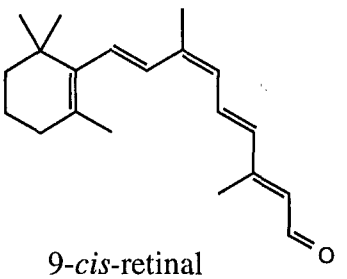

9-*cis*-retinal

Table 1.1 Absorption maxima of visual pigments in various vertebrates (given in nm)

	Rh	Red	Green	Blue	Violet
Human[a]	493	552, 557	530	426	-
Bovine[b]	500	-	-	-	-
Dog[c]	508				
Chicken[d]		571	508	455	415
Mouse[c]	498				
Gekko[c]			521	467	
Goldfish[c]	492	525	511	506	441

a) Nathans, J., *Biochemistry* **1992**, *31*, 4923.
b) Nakanishi,K. *Pure & Appl. Chem.* **1991**, *63*, 161.
c) Yokoyama, S. *Mol. Biol. Evol.* **1995**, *12*, 53.
d) Yoshizawa, T.; Kuwata, O. *Photochem. Photobiol.* **1991**, *54*, 1061.

number of the types of cones does as well. Table 1.1 summarizes the absorption maxima of visual pigments in various animals. A human eye has three kinds of cones (the receptors of red, green, and blue light, respectively) with their absorption maxima at 552 (or 557), 530, and 426 nm.[3]

Among the known visual pigments, bovine Rh has been most extensively investigated. Bovine Rh consists of an apoprotein opsin and the 11-*cis*-retinal.[2] Opsin is a protein that is composed of 348 amino acid residues (MW = 40 kD), organized into seven highly hydrophobic segments. These segments, which are arranged into the form of a helical bundle, traverse the membrane bilayer. Figure 1.2 shows the primary structure of bovine Rh. The 11-*cis*-retinal chromophore is contained inside the helical bundle, and is covalently bound to the ε-amino group of Lys296 via protonated Schiff base linkage. The counterion of the positively charged chromophore is presumed to be Glu113. Other visual pigments seem to have tertiary structures similar to that of bovine Rh. The amino acid sequences of bovine, chicken, human, mouse, and sheep rhodopsins are all greater than 87% identical.[3] The cone pigments from human, chicken, and cavefish are approximately 40% identical to the respective Rh.[3]

Visual activation of Rh starts with the absorption of a photon by the chromophore. Subsequently, Rh undergoes sequential transformation to spectroscopically distinct intermediates photo (570 nm), batho (535 nm) and lumi (497 nm), finally leading to the equilibrium of meta I (478 nm) and meta II (380 nm).[2] On the way from Rh to batho intermediates, the chromophore is isomerized from the 11-*cis* to the *all-trans* form. Dynamics in the primary process on going from Rh to photo intermediate was investigated by means of femtsecond fluorescence spectroscopy of Rh analogues having artificial chromophores.[4] The results revealed that the isomerization around the C11–C12 double bond occurs as fast as vibrational motions of the chromophore. Meta II, where the Schiff base

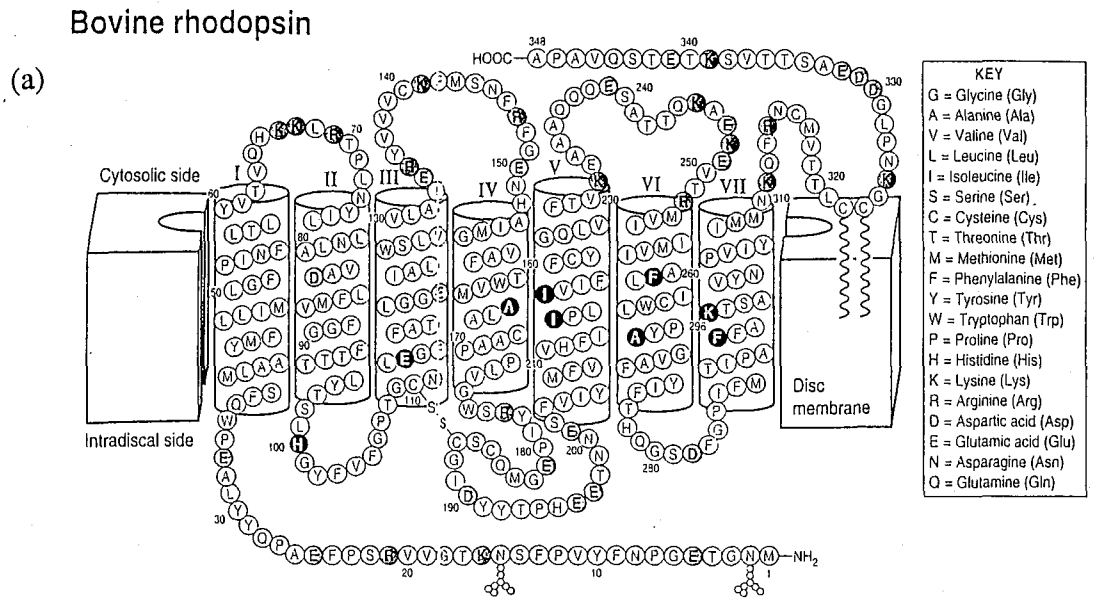

It is the lysine at 296 that forms a Schiff base with 11-*cis* retinal, while the glutamic acid at 113 becomes the protonated counter ion. At the cytosolic side, rhodopsin activates transducin through a specific protein-protein interaction.
Acidic amino acids (aspartic acid and glutamic acid) are highlighted in red; basic amino acids (arginine and lysine) are in blue.
The asparagines at 2 and 15 are sites of *N*-linked glycosylation.[51,52]
The cysteines at 110 and 187 form an essential disulphide bond,[53] and those at 322 and 323 are the sites of palmitylation.[54]
The residues highlighted in green are related to the colour determinants of human red and green

Amino acid residues for pigments

Position	*Bovine rhodopsin*	*Human green*	*Human red*
100	His	Tyr	Ser
164	Ala	Ala	Ser
214	Ile	Thr	Ile
217	Ile	Ser	Ala
261	Phe	Phe	Tyr
269	Ala	Ala	Thr
293	Phe	Phe	Tyr

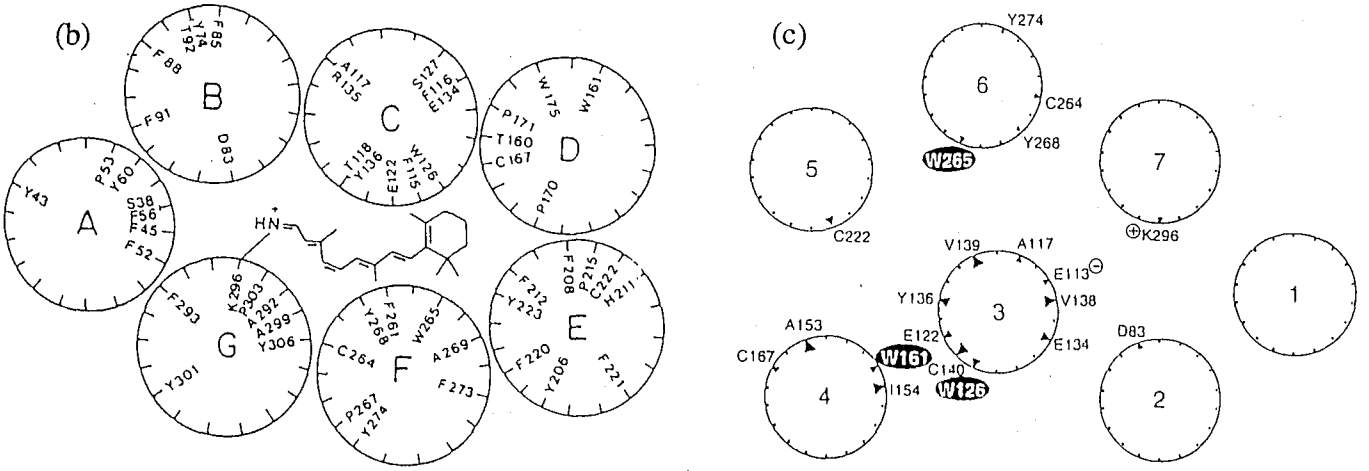

Figure 1.2 Amino acid sequence of bovine rhodopsin. A secondary structure model (a) (cited from ref. 2g), and a helical wheel projection maps (b) (cited from ref. 59b) and (c) (cited from ref. 60).

proton is lost, is the only intermediate that can activate the G protein transducin.[2] Therefore, the life time of meta II dominates the sensitivity and time-resolution of the vision: the lifetime of meta II of Rh is ten times longer than that of similar intermediates of cone pigments.[5] The activated G protein subsequently activates PDE (phosphodiesterase), which rapidly hydrolyses cGMP to produce GMP. The reduction of cGMP concentration induces the closing of cation channels in the rod cell membrane, resulting in the generation of a nerve impulse. The activity decays rapidly as a result of the actions of rhodopsin kinase and arrestin, and then meta II is dissociated to *all-trans*-retinal and the apoprotein.

1.1.2 Bacteriorhodopsin

Bacteriorhodopsin (bR) is a retinal protein that functions as a light-driven proton pump in the purple membrane of *Halobacterium halobium* (*H. salinarium*). Bacteriorhodopsin is a transmembrane protein composed of 248 amino acid residues (MW = 26 kD), and have a helical bundle structure similar to Rh (Figure 1.3). The chromophore *all-trans*-retinal is bound to the protein via protonated Schiff base linkage with Lys216. The carboxyl group of Asp85 is dissociated, and regarded as the counterion of the chromophore. In the protein interior, Asp212 and Arg82 are also presumed to be charged.[2] The protonated Schiff base would take part in a hydrogen bonding network including some charged and polar residues and some water molecules.

Under sufficient brightness, bR is present in the so-called light-adapted state (bR_{568}), where the chromophore takes *all-trans* form. The absorption maximum of bR_{568} appears at 568 nm. In the dark, bR is present in the dark-adapted state (bR_{558}), where the chromophore is in equilibrium between *all-trans* and 13-*cis* forms, and the absorption maximum appears at 555 nm. Under the condition of pH<3.5, the purple to blue transition is observed, and hence the resulting pigment is

called acidic purple membrane or blue membrane (λ_{max} = 605 nm).[6] bR_{568} is the only state that possesses the proton pump function. Upon absorption of light, bR_{568} undergoes sequential photoreaction cycle including spectroscopically distinct intermediates K(590 nm), L(550 nm), M(412 nm), N(550 nm), and O(640 nm).[7] During this cycle, bR takes in a proton from the intracellular side, and releases another proton into the extracellular side. This process is particularly active under the anaerobic conditions and in light, and provides an alternative source of metabolic energy instead of respiration. The proton gradient generated is used by the cell for the synthesis of ATP.

By means of FT-IR measurements, Maeda's group intensively investigated the pathway of the proton transfer and the hydrogen bonding network formed in each intermediate.[8] They identified Glu204 as the residue finally releasing a proton into the extracellar side.[9] According to the experimental results accumulated so far, the scheme of the proton transportation is summarized as follows: in $bR_{568} \rightarrow$K, the chromophore isomerizes from the *all-trans* to the 13-*cis* form, and then the Schiff base linkage is detached from Asp85; in K→L, the protein undergoes some structural changes, resulting in the re-approach of the Schiff base moiety toward Asp85; in L→M, the Schiff base proton is passed to Asp85, and simultaneously the proton of Glu204 is released into the extracellular side; in M→N, the proton of Asp96 is passed to the Schiff base; in N→O, retinal thermally re-isomerizes into the *all-trans* form, and Asp96 regains a proton from the intracellular side; finally in O $\rightarrow bR_{568}$, the proton of Asp85 is passed to Glu204. This scheme is illustrated in Figure 1.4.

Bacteriorhodopsin forms a two-dimensional crystal in the purple membrane, i.e., the trimer of bR is arranged into a hexagonal lattice. Recently, Henderson's group has published the results from electron diffraction analysis, where the crystal structure was obtained in a resolution of 3.5Å.[10] The electron diffraction

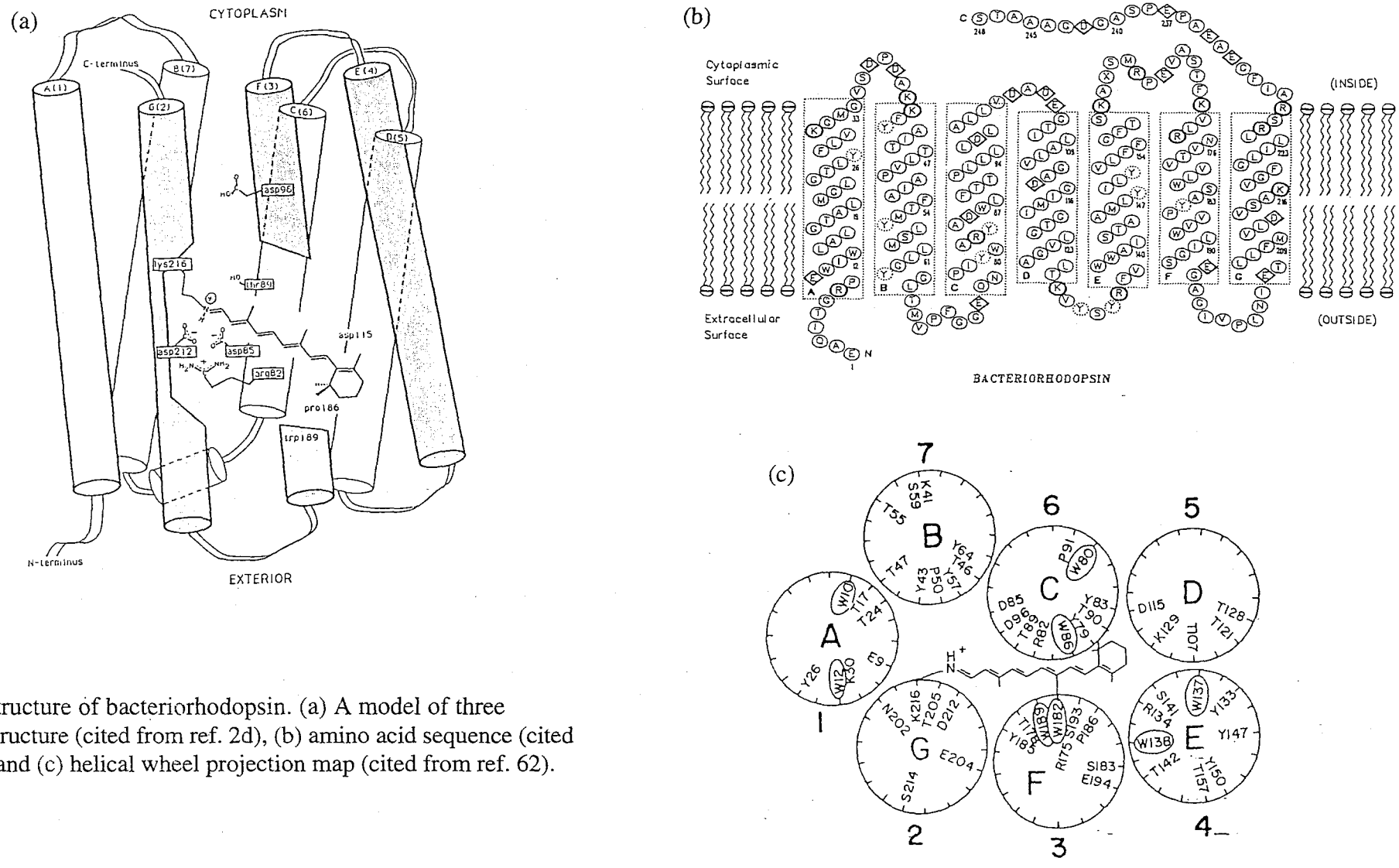

Figure 1.3 Structure of bacteriorhodopsin. (a) A model of three dimensional structure (cited from ref. 2d), (b) amino acid sequence (cited from ref. 2a), and (c) helical wheel projection map (cited from ref. 62).

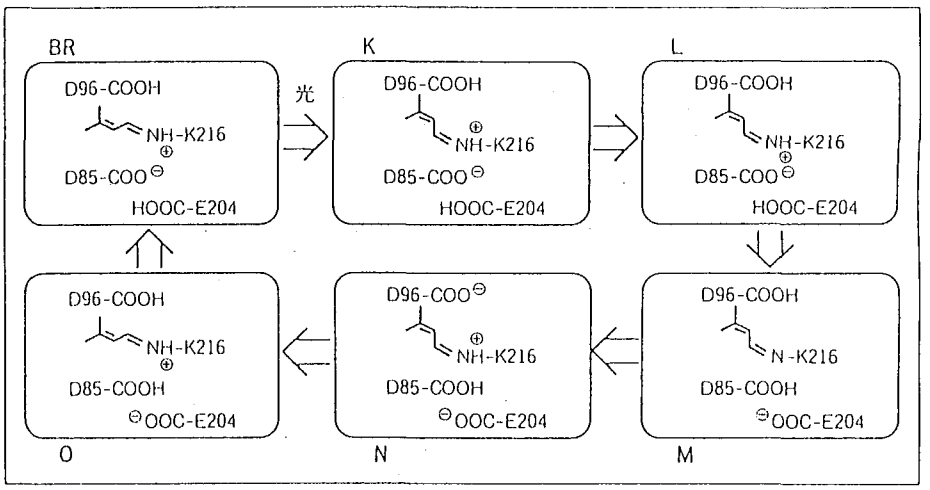

Figure 1.4 Change in ionization state of the protonated residues during the photoreaction cycle of bacteriorhodopsin. (cited from ref. 8).

technique, however, has some difficulties in determining the arrangements of dissociated residues, and hence the reliability is relatively low for the analyses of hydrogen bonding networks which may present in the chromophore-binding site.

Halorhodopsin (hR) and sensory rhodopsin (sR) are also known to be retinal proteins found in *halobacteria*. In contrast to bR, hR serves as a light-driven pump to transfer chloride ions across the membrane. Based on the fact that the residue corresponding to Asp85 in bR is replaced by threonine in hR, Sasaki et al. investigate the function of the D85T mutant of bR.[11] Although the amino acid sequences of bR and hR are only 30% identical, D85T was found to function as a chloride pump. It is surprising that only one residue is responsible for functional differentiation of the two proteins.

§1.2 The Origin of the Opsin Shift

A long standing question in retinal proteins is the mechanism by which different proteins tune the absorption spectrum of retinal. For example, the absorption maximum of Rh is 500 nm, while those of cone pigments are ranging from 420 to 560 nm.[3] By way of comparison, the chloride salt of protonated retinylidene Schiff base (PRSB) in methanol (λ_{max} = 440 nm) is often taken as the reference. The difference in absorption maxima between the protein and the reference is called opsin shift.[2]

The absorption maxima of the chromophore corresponds to its lowest π–π^* excitation energy. A positive charge is localized mainly on the Schiff base nitrogen in the ground state, and upon excitation it shifts toward the ionone ring (Figure 1.5).[12] Accordingly, any perturbations which can stabilize this charge delocalization leads to a smaller energy gap between the ground and excited states, resulting in a red shift of the absorption maximum. On the basis of this background, several mechanisms were proposed as summarized below.

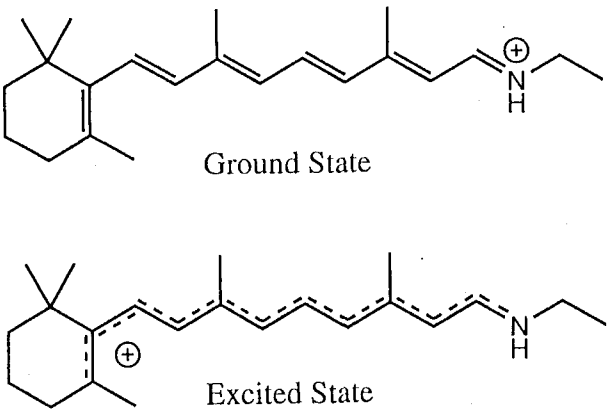

Figure 1.5 Electronic distribution of retinylidene Schiff base in the ground and the lowest π–π* excited states.

The first mechanism pays attention to the twisting about single bond. In bR, the chromophore was shown to take 6*s-trans* conformation,whereas PRSB takes skewed 6*s-cis* form in solution.[13-16] Such a conformational change causes an elongation of the π-conjugated system, resulting in a red shift.

The second mechanism concerns the fact that the counterion of PRSB causes a positive charge to localize near the Schiff base linkage, leading to a blue shift. Blatz et al.[17] studied the counterion-dependence of the absorption maximum of PRSB in various solvents. According to their results, the HCl, HBr, and HI salts of the Schiff base exhibited the absorption maxima at 437, 448, and 457 nm, respectively. This spectral change correlates with the distance between the counterion and the PRSB moiety. Namely, as the counterion goes away from PRSB, the absorption maxima shift to red-side.

The third mechanism is called "external point charge model",[2e,18,19] where a negatively charged (or polar) residue placed along the polyene chain is expected to cause a charge delocalization (Figure 1.6). The location of the external charge was investigated by using a variety of analogue chromophores, where some of the double bonds in the conjugated chain are saturated.[20-23] By interrupting the π-conjugation at different positions, one can find the region where the chromophore mainly receives the perturbation. In bovine Rh the major perturbation appears to be near C12 and C14. The later study using two-photon spectroscopy, however, indicated that the retinal-binding site is electrically neutral, suggesting the absence of the external charge.[24] For bR, although it was predicted that there was a perturbation near the β-ionone ring, this model has been supported neither from the crystal structure analyses[9] nor from the site-directed mutagenetic studies.[25]

Finally, the forth mechanism stresses the contribution of polarizable groups which may be located along with the conjugated chain.[26,27] Such polarizable groups could stabilize the excited state by compensatory electronic movement

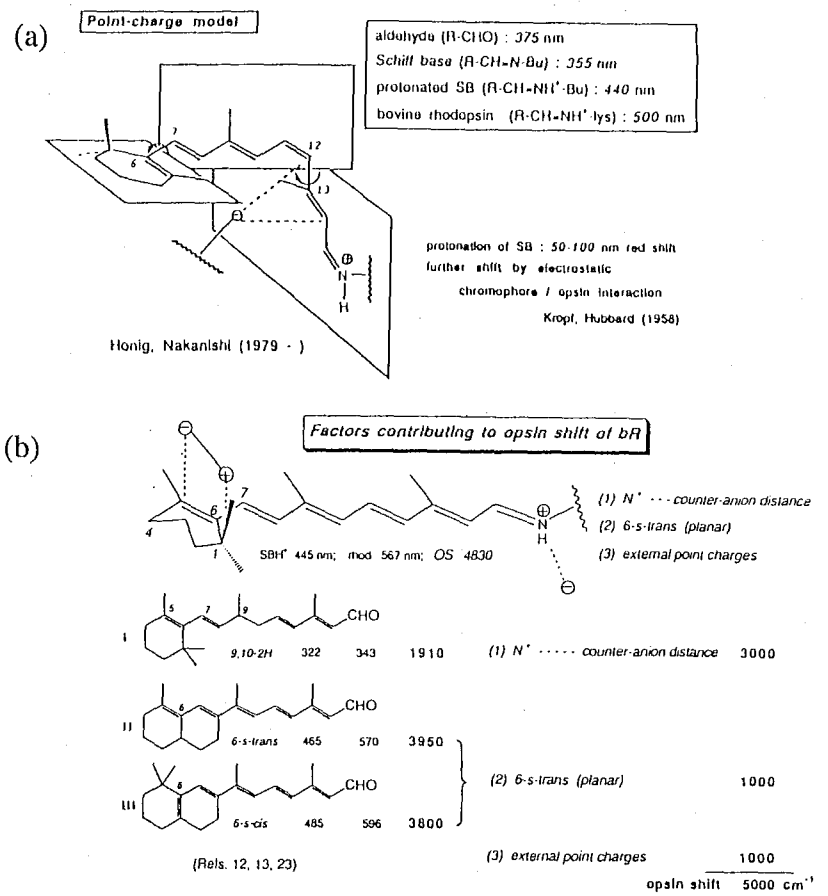

Fig.7. Factors contributing to the opsin shift in bacteriorhodopsin.

Figure 1.6 External point charge model for the opsin shift. (a) the case of rhodopsin, and (b) bacteriorhodopsin (cited from ref. 2e).

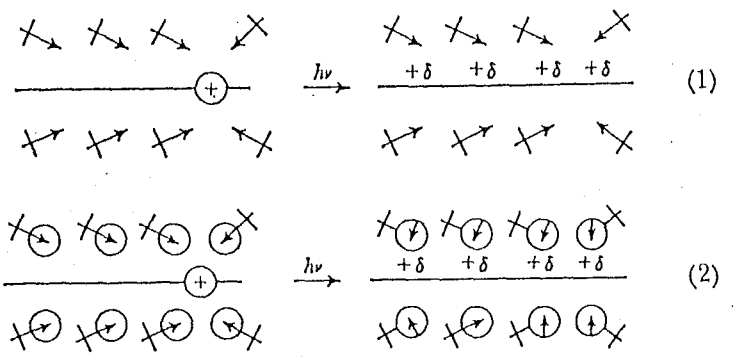

Figure 1.7 Schematic representation of the sequence by which polarizable solvents stabilizes the excited state of retinylidene Schiff base. (cited from ref. 26a).

(Figure 1.7). This mechanism was supported by the fact that the absorption maximum of PRSB in ethanol shifts to red by addition of phenol, indole, etc.[28] In proteins, aromatic residues (phenylalanine, tyrosine, and tryptophan) would play a role similar to such polarizable solvents.

§1.3 Solid–State NMR Studies

High-Resolution Solid State NMR (nuclear magnetic resonance) technique may be one of the most powerful means to elucidate the origin of the spectral tuning because ^{13}C chemical shifts of the chromophore bound to opsin involve invaluable information on perturbations from the surrounding protein environment and on the structural properties of the chromophore.

1.3.1 High-Resolution Solid State NMR Studies of Rhodopsin

The ^{13}C labeled experiments for the chromophore of Rh have been successfully performed by Smith et al.[29,30] and Mollevanger et al..[31] At present, thus, the ^{13}C chemical shift values for all the unsaturated carbons of the chromophore of Rh in the binding state are known. Smith et al. also applied ^{13}C labeled experiments to isorhodopsin (9-*cis* chromophore), and bathorhodopsin (*all-trans* chromophore).[30,32,33]

Tables 1.2 and 1.3 summarize the isotropic chemical shifts (σ_{iso}) and chemical shift principal values (σ_{11}, σ_{22}, σ_{33}) of rhodopsins and retinal model compounds. The σ_{11} element, perpendicular to the conjugated plane, reflects steric interactions while the σ_{22} and σ_{33} elements on the conjugated plane are sensitive to a change in the electronic structure.

X-ray crystallography revealed that most retinal derivatives crystallize in a skewed 6*s-cis* conformation, with an angle of 40-65° between the ionone ring and the conjugated chain (ϕ_{6-7}), while some derivatives have been found to be a planar

6*s-trans* form (ϕ_{6-7}=165-180°).[34-38] Retinoic acid takes two crystalline states: triclinic 6*s-cis* form (ϕ_{6-7}=42°) and monoclinic 6*s-trans* form (ϕ_{6-7}=165).[36] Harbison et al. found that the most remarkable difference in chemical shifts between the two forms of retinoic acid are observed for the C5 and C8.[15] The C5 and C8 resonances for 6*s-cis* retinoic acid appear at 128.8 and 138.9 ppm, respectively, while those for 6*s-trans* form at 135.9 and 130.9 ppm, respectively.[15] In the case of Rh, the C5 and C8 resonances are observed at 130.3 (130.5) ppm and 139.2 ppm, respectively, both of which are closer to the data for 6*s-cis* retinoic acid.[29-31] Furthermore, Harbison et al. reported that the 6*s-cis* to 6*s-trans* isomerization in retinoic acid mainly affects the σ_{33} element and hardly perturbs the σ_{11} and σ_{22} elements.[15] The principal values for the C5 shielding of 6*s-cis* retinoic acid are 28, 141, 217 ppm, respectively, while those for the 6*s-trans* form are 27, 143, 237 ppm, respectively.[15] The σ_{33} value for C5 in Rh is 215 (210±6) ppm, also supporting the presence of a 6*s-cis* conformation.

Next, the author surveys studies of environmental effects on the ^{13}C chemical shifts of PRSB. Table 1.3 contains chemical shift data for chloride salt of *N*-(11-*cis* retinylidene)-*n*-propylamine[39] and perchlorate salt of *N*-(11-*cis*-retinylidene)-*tert*-butylamine.[30] The interaction between the Schiff base and its counterion is expected to be weaker in the perchlorate salt because perchlorate ion is more bulky than chloride. Comparison of the C15 chemical shift in Rh with those of these 11-*cis* model compounds indicates that the C15 resonance in Rh shifts to downfield 1.5 ppm relative to that of the chloride salt.[30] The direction of this shift is opposite to that expected from a weakening of the Schiff base-counterion interaction. Additionally, the chemical shift of C14 in Rh (121.2 ppm) is close to that for the chloride salt (121.3 ppm).[30] On the basis of these results, Smith et al. concluded that the Schiff base in Rh is strongly hydrogen-bonded to the counterion.[30] This conclusion seems to be consistent with results of a resonance Raman study,which

demonstrate that the C=N stretching frequency in Rh appears at 1657 cm^{-1}, closer to that (1658 cm^{-1})[40] in the chloride salt rather than that (1636 cm^{-1}) in the perchlorate salt (*all-trans* isomer).[30]

The C13 resonance in Rh exhibits a large downfield shift (6.5 ppm) relative to that in *N*-(11-*cis*-retinlylidene)-*n*-propylamine, accompanied by a slight downfield shift of the C12 signal (3.1-4.5 ppm).[30,31] These results may support the validity of the external point charge model where two negative charges are presumed to be located equally apart from the C12 and C14 carbons. Thus, if this is the case, nearly the same amounts of positive charges would be induced on both C12 and C14 carbons. As a result, the nearly equal amount of downfield shift should be observed at the C12 and C14 positions.[2e] However, this prediction is inconsistent with the fact that no significant difference is observed between the chemical shift of C14 in Rh and the corresponding value of the model compounds.

1.3.2 High resolution Solid State NMR of Bacteriorhodopsin

The ^{13}C labeled experiments for the chromophore of bR (bR_{568}, bR_{555}, and M intermediate) have been successfully performed by Harbison et al. and Smith et al..[14,41-44] As indicated in Tables 1.2 and 1.3, the C5 (144.8 ppm) and C8 (132.7 ppm) shieldings of bR are close to those of 6*s*-*trans*-retinoic acid (σ_{C5} = 135.9, σ_{C8} = 130.9), respectively, rather than 6*s*-*cis* form (σ_{C5} = 128.8, σ_{C8} = 138.9). Thus, in contrast to the case of Rh, bR (bR_{568}) is considered to have a planar 6*s*-*trans* conformation.[14,44] One should notice that the σ_{22} element of C5 in bR shifts to downfield ca. 30 ppm relative to those in both types of retinoic acid (Table 1.2 and 1.3). Harbison et al. suggested that an origin of this downfield shift is an external point charge located near the ionone ring: the negative charge located near C5 may induce a positive charge on C5, leading to a significant amount of downfield shift.[14] However, on the basis of ^{13}C NMR studies of model compounds

Table 1.2 Isotropic ^{13}C chemical shifts[a] of the unsaturated carbons of the chromophore bound to rhodopsin and bacteriorhodopsin and their photointermediates

	Rh	isoRh	bathoRh[e]	bR_{568}[f]	bR_{555}	M_{412}[j]
C5	130.3[b] 130.5[c]	130.5[b]		144.8	144.8[g]	139.8
C6	137.7[b]	137.0[b]		135.4	134.9[g]	
C7	132.3[b]	128.2[b]		129.5	130.7[g]	
C8	139.2[b]	131.1[b]	136.6	132.7	131.6[g]	
C9	148.5[b]	147.5[b]		146.4	148.4[h]	
C10	127.8[b]	130.8[b]	132.0	133.0	129.7[h]	
C11	141.6[b]	139.3[b]	140.0	139.1	135.4[h]	
C12	132.1[b] 133.5[c]	133.9[b]	137.7	134.3	124.4[f]	128.1
C13	168.9[b]	169.2[b] 169.0[d]	168.5	164.8	168.7[f]	146.7
C14	121.2[b]	119.0[b]	120.0	122.0	110.5[i]	125.7
C15	163.9[b]	166.5[b] 166.7[d]	163.4	163.2	163.2[g]	162.5

a) given in ppm measured from TMS
b) Smith, S. O., et al., *Biochemistry* **1990**, *29*, 8158.
c) Mollevanger, L. C. P. J., et al., *Eur. J. Biochem.* **1987**, *163*, 9.
d) Smith, S. O., et al., *Photochem. Photobiol* **1992**, *56*, 1035.
e) Smith, S. O., et al., *Biochemistry* **1991**, *30*, 7409.
f) Smith, S. O., et al., *Biochemistry* **1989**, *28*, 8897.
g) Harbison, G. S., *Biochemistry* **1985**, *24*, 6955.
h) Harbison, G. S., *Biochemistry* **1984**, *23*, 2662.
i) Harbison, G. S., *Proc. Natl. Acad. Sci. USA* **1985**, *81*, 1706.
j) Smith, S. O., et al., *Biochemistry* **1989**, *28*, 237.

Table 1.3 Isotropic and principal values[a] of ^{13}C shielding tensor for the chromophores in rhodopsin and bacteriorhodopsin and retinal derivatives.

	σ_{iso}	σ_{11}	σ_{22}	σ_{33}
C5				
Rh[b]	130.3	26±6	134±6	210±6
Rh[c]	130.5	33	143	215
bR_{568}/bR_{555}[d]	144.8	27±3	170±1	237±2
M_{412}[e]	139.4	26	161	232
all-trans-6*s*-*cis*-retinoic acid[f]	128.8	28	141	217
all-trans-6*s*-*trans*-retinoic acid[f]	135.9	27	143	237
all-trans-PRSB (*n*-Bu, Cl^-)[f]	128.8			
all-trans-retinal[f]	128.5	30.9	141.1	215.9
all-trans 6*s*-*cis*-RSB[f]	126	33.0	143.2	202.2
C8				
Rh[b]	139.2			
bR_{568}[d]	132.7	49±6	131±2	216±5
bR_{555}[d]	131.6			
all-trans-6*s*-*cis*-retinoic acid[f]	138.9			
all-trans-6*s*-*trans*-retinoic acid[f]	130.9			
all-trans-PRSB (*n*-Bu, Cl^-)[f]	140.8			
all-trans-retinal[f]	135.15	59.2	144.4	215.9
all-trans-RSB[f]	140	62.7	132.2	224.1
C12				
Rh[b]	132.1			
Rh[c]	133.5	41	149	209
bR_{568}[g]	134.3	56	130	211
bR_{555}[g]	124.2	35	132	206
all-trans-retinal[f]	134.0	55.2	130.9	215.6
13-*cis*-retinal[f]	127.9	39.0	132.7	212.1
11-*cis*-PRSB (*n*-Pr, Cl^-)[f]	129.0			
all-trans-PRSB (n-Bu, Cl^-)[h]	135.0	58	133	212

Table 1.3 (continued)

	σ_{iso}	σ_{11}	σ_{22}	σ_{33}
C13				
Rh[h]	168.9			
bR_{568}[g]	164.8	22	209	264
bR_{555}[b]	168.7	26	217	262
M_{412}[e]	146.7	30	169	240
all-trans-PRSB (Cl^-)[f]	161.8	29	189	267
11-*cis*-PRSB (*n*-Pr, Cl-)[f]	162.7			
all-trans-retinal[f]	155.5	31.2	187.6	249.9
all-trans-6*s*-*cis*-RSB[f]	144	28.7±7.5	165.8±4.8	237.0±7.4
C14				
Rh[b]	121.2	47±2	127±3	185±6
bR_{568}[g]	122.0	50	134	182
bR_{555}[g]	110.5	45	107	179
all-trans-retinal	129.8	60.9	131.0	200.7
all-trans-RSB[f]	131	63.9±3.0	124.7±4.1	204.9±1.7
all-trans-PRSB (*n*-Bu, Cl^-)[f]	122.6			
C15				
Rh[h]	165.4			
bR_{568}[g]	160.0	76	170	236
bR_{555}[g]	163.2	51	182	256
all-trans-retinal[f]	189.4	97.6	212.9	259.9
all-trans-6*s*-*cis*-RSB[f]	161	85.7±6.1	154.2±6.9	241.6±5.1
11-*cis*-PRSB (*tert*-Bu, ClO_4^-)[i]	160.0			
11-*cis*-PRSB (*n*-Pr, Cl^-)[i]	163.9			

a) given in ppm measured from TMS
b) Smith, S. O., et al., *Biochemistry* **1987**, *26*, 1606.
c) Mollevanger, L. C. P. J., et al., *Eur. J. Biochem.* **1987**, *163*, 9.
d) Harbison, G. S., *Biochemistry* **1985**, *24*, 6955.
e) Smith, S. O., et al., *J. Am. Chem. Soc.* **1989**, *28*, 237.
f) Harbison, G. S., *J. Am. Chem. Soc.* **1985**, *107*, 4809.
g) Smith, S. O., et al., *Biochemistry* **1989**, *28*, 8897.
h) Smith, S. O., et al., *Biochemistry* **1990**, *29*, 8158.
i) Shriver, J. W., et al., *Biochemistry* **1979**, *18*, 4785.

for bR, Albeck et al. indicated that both the absorption maximum of bR and its C5 chemical shift could be simultaneously reproduced without requiring such a nonconjugated negative charge in the vicinity of the ionone ring.[45] A similar conclusion was also obtained by Hu, et al..[46]

A significant difference between bR_{568} (*all-trans*) and bR_{555} (13-*cis*) has been observed for the C14 shielding. The C14 shielding of bR_{555} shifts 11.5 ppm upfield relative to that of bR_{568} (Table 1.2).[41] The origin of this upfield shift has been attributed to the *syn-anti* isomerization about the C=N double bond: the C14 resonance depends on the steric interaction, so-called γ-effect, between the H14 of the retinal moiety and the δ-hydrogens of Lys216. On the basis of these results, the retinal moieties in bR_{568} and bR_{555} are identified as the *all-trans*-15-*anti* and 13-*cis*-15-*syn* isomers, respectively.[41] Rhodopsin, isoRh and bathoRh are thought to take the 15-*anti* configuration because their C14 shieldings are close to that of bR_{568} rather than that of bR_{555} (Table 1.2).[47]

The M_{412} intermediate is the key state directly relating to the proton pumping function of bR, since the proton release occurs in the L_{550} to M_{412} transition. The evidence that the M_{412} intermediate has unprotonated Schiff base is deduced from results of NMR measurements. The C13 resonance of the M_{412} intermediate is observed at 146.7 ppm, which is characteristic of unprotonated Schiff bases, and it shifts by 20-25 ppm to upfield relative to those of Rh, bR_{568} and bR_{555} and PRSBs.[44] Furthermore, the data for C14 imply that the M_{412} intermediate has the 15-*anti* configuration.[47] It should be noted that the C5 shielding of the M_{412} intermediate shifts 5 ppm upfield relative to those of bR_{568} and bR_{555}.[41,43,44] This upfield shift may be partly due to the change in location of the negative charge near the ionone ring, induced by structural changes of the protein and the chromophore.

The C5 and C8 resonances for bR_{568} shift downfield and upfield, respectively, relative to the corresponding data for the chloride salt of *N*-(*all-trans*-retinylidene)-

n-butylamine. Most of these shifts are induced as a result of 6*s*-*cis* to 6*s*-*trans* isomerization. However, the anomalous amount (16.0 ppm) of downfield shift observed for C5 seems not to be fully explained by this isomerization. Such an anomalous shift may originate from a synergistic effect of isomerization around the C6-C7 bond and weakening of the Schiff base-counterion interaction, or imply the existence of a negative charge (or dipole) near the ionone ring.

The downfield shift for the C5 resonance and the upfield shift for the C8 resonance observed for bR_{555} may be also induced as a result of 6*s*-*cis* to 6*s*-*trans* isomerization. The downfield shift observed for C13 in bR_{555} is 6.5 ppm, which is 3.5 ppm larger than that for bR_{568}.[43] The origin of such an added downfield shifts should not be due to the weakening of the Schiff base-counterion interaction, because this interpretation is inconsistent with the fact that the absorption maximum of bR_{555} blue shifts relative to that of bR_{568}. Any reasonable explanation for this phenomenon has not been given so far. As mentioned above, a large upfield shift observed for C14 may be due to the *syn-anti* isomerization about the C=N bond.

§1.4 Structure–Function Relationships

Studies on the structure–function relationships in retinal proteins have remarkably progressed since the establishment of the site-directed mutagenesis technique.[2c,48-50] Using this technique, various kinds of artificial mutants were prepared, and their physical and biological properties were investigated.

1.4.1 Amino Acid Replacement in Visual Pigments

Among all the artificial mutants of rhodopsin in which an ionizable residue was replaced by a neutral residue, only the replacement of Glu113 exhibited a significant change in absorption wavelength.[51-53] The absorption maximum of E113Q in neutral pH was 380 nm, indicating the deprotonation of the chromophore.

With a lowering of pH, the absorption maximum shifted up to 490 nm, indicating the protonation of Schiff base. In E113D, where the length of the side chain is one methylene unit shorter than that in the wild-type, a red shift of 5~7 nm was observed.[51,52] By addition of HCl, HBr, and HI to E113Q, the absorption maxima appeared at 495, 498, 505 nm, respectively,[53b] consistent with Blatz's results[17] for PRSB in solutions. These results strongly suggest that Glu113 serves as the counterion of the chromophore.

Table 1.4 summarizes the absorption maxima of mutants where the ionizable residues were substituted.[54-57] The primary purpose of these mutation experiments was to explore the residue(s) responsible for the wavelength regulation, but this was not achieved. Except for Glu113, only the replacement of Glu122 moderately affected the absorption maxima. The absorption maxima of E122Q and E122D, respectively, appear at 480 and 475 nm,[51] while that of E122I did at a wavelength similar to that of the wild-type.[52] Thus, the effect of Glu122 was considered to originate in steric interactions. Both D83N/E122Q and M86E/E122Q, which have sequences similar to the blue and red pigments of human, respectively, show their absorption maxima at 480 nm,[52] suggesting that Glu122 is not a dominant factor for regulating the absorption wavelength. Recently, Imai et al. reported that Glu122 is a functional determinant of rod and cone visual pigments.[5] The E122Q and E122I mutants have a sequence similar to the green and red pigments of chicken, respectively. According to their report, the mutant rhodopsins E122Q and E122I exhibited a rapid decay of meta II as similar to the cases of the green and red pigments, respectively, while the Q122E mutant of the green pigment exhibited a slow decay as similar to that observed for Rh.

The artificial Rh reconstituted from the K216A mutant and the ethylimine of retinal absorbs maximally at 495 nm, and activates the G protein.[58] This indicates that in this pigment, the chromophore is correctly located to lead to a

Table 1.4 Absorption maxima (given in nm) of mutant rhodopsins (substitution of ionizable residue(s))

	λmax	ref.
Native	498	2
WT	500	70
WT	498	53a
single mutation		
E5Q	495	53b
E25Q	496	53b
E33Q	495	53b
D83G	501	53a
D83N	492	53a
D83N	492	57
D83N	495	54
D83N	498	59a
D83N	492	53b
M86E	498	53a
G90D	483	65
G90D	484	71
G90D	484	70
E113D	506	55
E113D	507	52
E113D	505	51
E113D	509	70
E113Q	380/490	51
E113Q *	380	51
E113Q	380 (pH6)	52

Table 1.4 (continued)

	λmax	ref.
E113Q	490 (pH>6)	52
A117D	475	56
E122A	476	59a
E122A	475	52
E122D	476	59a
E122D	475	51
E122I	497	53a
E122L	495	57
E122Q	480	51
E122Q	480	54
E122Q	479	53a
E122Q	482	59a
E122Q	479	53b
E122Q	480	52
E134D	498	57
E134D	500	51
E134L	495	53a
E134Q	496	53a
E134Q	500	51
E134Q	495	53b
E134R	498	57
R135L	498	53a
R135Q	500	51
E150Q	497	53b

Table 1.4 (continued)

	λmax	ref.
E181Q	502	53b
D190N	495	53b
E196Q	499	53b
E197Q	494	53b
E201Q	495	53b
E201Q	500	52
E232Q	495	53b
E239Q	496	53b
E247Q	501	53b
E249Q	496	53b
D282N	500	53b
A292D	488	59a
K296A †	493	58
K296G ‡	486	58
E341Q	497	53b

	λmax	ref.
double mutation		
D83G/E122I	497	53a
D83N/E122Q	480	52
D83N/E122Q	475	54
M86E/E122I	492	53a
G90D/E113A	474	71
G90D/E113Q	472	65
E113A/A117E	493 (pH6)	60
E113A/A117E	490	70
E113Q/A117D	493	56
E113Q/E122Q	372	52
E113Q/E122Q	380/470	51
E134A/R135A	500	51
E134L/R135L	498	53a
E134R/R135E	496	53a
E134R/R135E	500	51

*reconstituted with *all-trans*-retinal
† reconstituted with ethylamine Schiff base of retinal
‡ reconstituted with propylamine Schiff base of retinal

correct function in the absence of the Schiff base linkage with the protein. This implies some steric interactions between the chromophore and the surrounding residues. From a cross-linking study of photoaffinity labeling of retinal and site-directed mutagenesis, Nakayama et al.[59] identified residues present in the vicinity of the chromophore. They indicated that the substitutions of Trp265 or Glu122 induced a blue shift of 20~30 nm, and that the regeneration ratio of the chromophore is significantly lowered in W265A. By the substitutions of Ala117, Trp265, and Ala292, the bleach process was appreciably changed. By the substitutions of Trp265, Glu122, Trp126, Pro267, and Tyr268, the activity for a G protein was lowered. On the basis of these results, they concluded that Trp265, Glu122, Trp126, and Tyr268 are interacting with the chromophore.

The interaction of tryptophan residues with the chromophore was investigated from measurements of UV absorption of the indole ring.[60] It was suggested that the interaction of Trp265 and Trp126 with the chromophore is coupled with a structural change of the protein, induced by the transition to meta II. Trp265, Trp126, and Tyr268 are known to be well conserved among the visual pigments of many animals.[61,62] Table 1.5 summarizes the absorption maxima of the mutants of Rh where non-ionizable residues are substituted. It can be seen from this table that the substitutions of tryptophan into a less polarizable residue causes a significant amount of blue shift. This implies that non-ionizable residues, especially aromatic residues, play an important role in regulating the wavelength of Rh.

There are some reports to clarify the relationship between an amino acid replacement and the resulting absorption maximum from the viewpoint of molecular phylogenetic trees. Yokoyama prepared a phylogenetic tree for 28 kinds of visual pigments, and picked up 55 residues responsible for the wavelength regulation.[63] Neitz et al., based on the analysis of the amino acid sequences of long- and mid-wavelength-sensitive pigments of primates, found that the difference

Table 1.5 Absorption maxima (given in nm) of mutant rhodopsins (substitution of non-ionizable residue)

	λmax	ref.
W35F	500	60
W126A	486	59a
W126F	500	60
W126F	498	59a
W126L	490	59a
W161L	495	59a
W161F	500	60
W175F	500	60
H211C	493	53a
H211F	495	53a
W265A	470	59a
W265F	481	60
W265F	480	59a
W265Y	485	60
W265Y	483	59a
P267A	500	59a
P267G	498	59a
P267N	495	59a
P267S	495	59a
Y268F	493	59a
Y274F	498	59a

Table 1.5 (Continued)

in absorption maxima between red and green pigments originated from the replacements of only a few residues (Figure 1.8).[64] For the human cone pigments, Ala180, Phe277, and Ala285 in the red pigment is replaced by Ser180, Tyr277, and Thr285 in the green pigment, suggesting that hydroxy group-containing residues induce a red shift.

Amino acid replacements of Rh are naturally occurring in two human retinal diseases: autosomal dominant retinitis pigmentosa (ADRP) and congenital night blindness. There are about 40 kinds of mutations to cause these diseases.[65] L125R, P23H, and G188R (mutations on the loop site) cause ADRP, the origin of which is attributed to the mis-folding of the protein.[66,67] K216G and K296M both can not be bound to a chromophore, but are "constitutively active" for a G protein.[68,69] Consequently, these mutants bring about the excitation of the optic nerve even if light is absent. This might arise from the fact that these mutants cannot form the salt-bridge between Lys216 and Glu113, necessary to keep the protein inactive in the wild-type Rh. A292E and G90D mutants, which cause congenital night blindness, are constitutively active as well, due to the breakdown of the salt-bridge.[69-72] This provides the evidence that Ala292 (in helix G) and Gly90 (in helix B) are in the vicinity of the chromophore-binding site.

1.4.2 Amino Acid Replacement in Bacteriorhodopsin

As already described, the residues Asp85, Asp96, Asp212, Arg82, and Glu204 play important roles in translocating a proton in their respective ways. These residues were the major targets of site-directed mutagenetic studies.

Table 1.6 summarizes the absorption maxima of several mutants of bR where ionizable residues are replaced. By the substitution of Asp85 into asparagine, the absorption maximum red shifts up to ~600 nm,[73-76] suggesting the occurrence of interaction between this residue and the chromophore in the native bR. The D85N

Table 1.6 Absorption maxima (given in nm) of mutant bacteriorhodopsins[a] (substitution of ionizable residue)

	(DA) λmax	(LA) λmax	ref.
Native	558	568	2
WT	549	559	83
WT	560	570	79
WT	548		75
WT	550	560	94
R7Q	549	558	83
D36N	550	561	25a
D38N	553	563	25a
E74C	551		72
N76C	552		72
Y79C	525		72
R82A	572		74
R82C	574		72
R82Q		590	77
R82Q	575	580	83
R82Q	548	553	73
R82Q	567		74
R82Q	585		75
D85A		610	73
D85A	599		74
D85C	590		72
D85E	604		73
D85E	584		74
D85E	556	560	25a
D85N	589		74
D85N	596		75
D85N		610	77
D85N	587	594	25a

Table 1.6 (Continued)

	(DA) λmax	(LA) λmax	ref.
D85N		590	73
D96A	554		74
D96C	551		72
D96E	553	561	25a
D96N	556		75
D96N	553	560	25a
D96N	554		74
D102N	553	563	25a
D104N	550	560	25a
D115E	541	543	25a
D115E	541		74
D115N	544		74
D115N	545	544	25a
R134Q	551	557	83
R164Q	553	562	83
R175Q	550	562	83
D212A	540	unstable	25a
D212A	537		74
D212E	556	566	73
D212E	580		74
D212E	584	581	25a
D212N	545		74
D212N	560	548	25a
D212N		585	76
D212N		569	76
R225Q	553	560	83
R227Q	552		74
R227Q	551	563	83

a) DA and LA indicate the dark-adapted and the light-adapted states, respectively.

Table 1.7 Absorption maxima (given in nm) of mutant bacteriorhodopsins[a] (substitution of non-ionizable residue)

	(DA) λmax	(LA) λmax	ref.
W10F	548	558	62
W12F	551	561	62
Y26F	551	561	94
Y43F	551	561	94
T46V	550		74
Y57F	536	548	94
Y64F	551	561	94
Y79F	547	556	94
W80F	549	558	62
Y83F	533	540	94
W86F	534	547	93
W86F	530		74
W86F	529	539	62
T89A	545		74
T89D	556		74
T89N	563	582	79
A98C	551		72
V101C	551		72
A103C	552		72
Q105C	551		72
L109C	552		72
Y131F	551	561	94
Y133F	546	560	94

Table 1.7 (Continued)

	(DA) λmax	(LA) λmax	ref.
W137C	546	550	62
W137F	532	541	62
W138C	543	547	62
W138C	531		74
W138F	551	561	62
S141A	540		74
S141C	466		74
Y147F	551	561	94
Y150F	548	560	94
W182F	548		91
W182F	477	491	62
W182F	465		74
Y185A	554		74
Y185F	556	573	94
Y185F		600	73
Y185F	556		74
Y185F	548	563	73
P186G	472		74
W189F	570		91
W189F	513	521	62
W189F	526		74
T205V	550		74
S226A	551		74

a) DA and LA indicate the dark-adapted and the light-adapted states, respectively.

Species	Spectral peak	Amino acid position																				
		A							B	C						D	E		F		G	
		61	65	111	115	116	173	174	180	230	233	236	274	275	276	277	279	285	298	309	320
*Rhesus monkey	LWS												I	F	A	Y	V	T	A	Y	I
Human deuteranope	561	I	T	I	V	S	I	A	S	I	A	M	I	F	A	Y	V	T	A	Y	V
Squirrel monkey	561	I	T	I	V	S	V	A	S	I	A	M	I	M	A	Y	V	T	A	Y	I
Tamarin	562	L	V	V	V	Y	V	A	S	I	A	M	I	V	A	Y	V	T	A	Y	I
Tamarin	556	L	V	V	V	Y	I	A	A	I	A	M	I	A	A	Y	V	T	A	Y	I
Squirrel monkey	547	I	T	V	V	Y	V	V	A	I	A	M	I	L	T	F	I	T	A	Y	I
Tamarin	541	L	V	V	I	Y	I	A	A	I	A	M	I	L	A	Y	V	A	A	Y	I
Squirrel monkey	532	I	T	I	V	S	V	A	A	T	S	V	I	V	T	F	I	A	A	Y	I
Human protanope	530	I	T	I	V	S	I	A	A	T	S	V	V	L	A	F	F	A	P	F	V
*Rhesus monkey	MWS												F	L	A	F	F	A	A	Y	I

Figure 1.8 Differences in deduced amino acid sequences of eight visual pigments sensitive to middle to long wavelength. Results from partial sequences of cone pigments from rhesus monkey are included for comparison. Boxes indicate residues identified as those involved in spectral tuning. (cited from ref. 64).

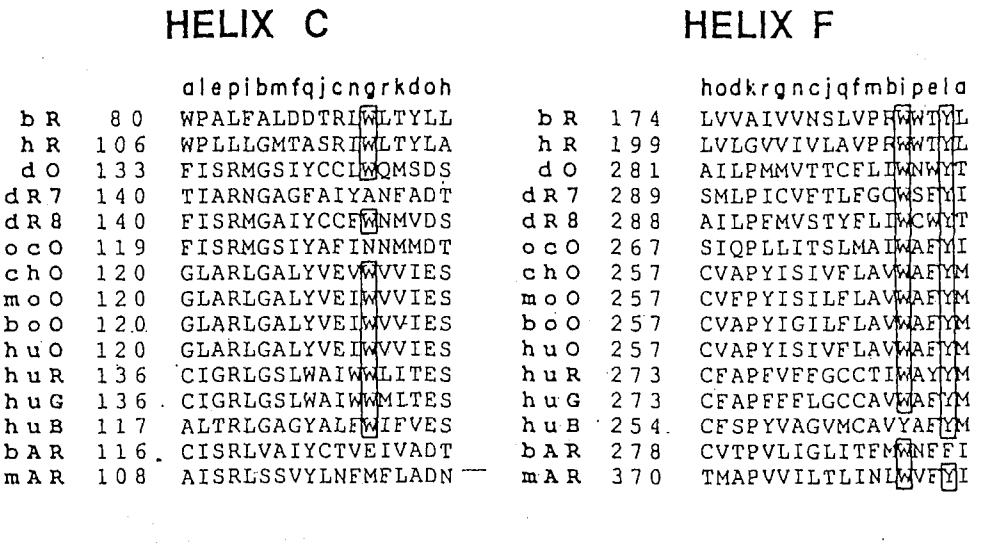

Figure 1.9 Alignment of surface residues of helices C and F of bacteriorhodopsin (bR) with the corresponding segments of halorhodopsin, opsin family proteins, and signal receptors. (cited from ref. 62).

mutant shows no proton pump activity.[77] In the ground state of D85N, three states, similar to M, N, O intermediates in the wild-type bR, are kept in equilibrium,[78] where the chromophore is present as a mixture of *all-trans* and 13-*cis* form.[79] These results indicate that the protonation and deprotonation of Asp85 acts as a molecular switch in the proton pump process. According to a report on the mutant where every aspartic acid were substituted by asparagine residue, no support was obtained for the external point charge model for the opsin shift.[25a]

Asp212 is also a residue whose substitution largely affects the absorption maximum. As similar to D85N, the D212N mutant, where the chromophore takes *all-trans* or 13-*cis* form, exhibits an irregular photoreaction cycle.[77] When pH is larger than 7, D212N shows a photoreaction cycle similar to acidic bR.[76] When pH is less then 7, D212N undergoes transformation into the M intermediate, and partially shows the proton pump function.[76] These results suggest that Asp212, together with Asp85, serves as a counterion of the chromophore. In addition, Thr89 and Tyr185 are considered to take part in a hydrogen bonding network including the protonated Schiff base linkage.[79,80]

In bR, the side chain of Arg82 is protonated. When pH<6, the R82Q mutant, where the positive charge of Arg82 is neutralized, shows a red shift of ~20 nm relative to that of the wild-type.[81,82] When pH>7.5, its absorption maximum is nearly identical to that of the wild-type.[83] The generation of this long-wavelength species corresponds to the purple to blue transition observed for the wild-type bR under acidic conditions.[73] It was found that the neutralization of Arg82 displaced the pH of the transition mid-point toward the alkaline side. There exists a calcium ion near the Schiff base linkage,[84] and that the removal of this ion causes the purple to blue transition as well (i.e., deionized bR).[85] In view of the fact that both acidic and deionized bRs have protonated Asp85, both Arg82 and calcium ion are likely to regulate the pKa's of Asp85 and Asp212.[81,83]

In addition to Arg82, the substitutions of Arg134 and Arg227 into glutamine lead to the anomaly of the proton pump function.[83] Under the condition of pH>4, the decay of the M intermediate of R227Q is about ten times slower than that observed for the wild-type.[81] It is reasonable to assume that Arg227 forms a salt bridge with Asp96, which releases a proton during the M→N process.[83]

Asp96 takes in a proton from the intracellar side. The D96N mutant exhibits a slow decay of the M intermediate,[74,86] and its pump function is lower than 10% of the corresponding decay rate for the wild-type.[25a] It was reported that Asp96 and Thr46 form a hydrogen bonding network including one water molecule.[87] Although T46D and T46D/D96 have the proton pump function, the life time of the N intermediates are very long. Accordingly, it was suggested that the Asp96-Thr46 interaction plays a role in promoting the reprotonation of Asp96 during the N→O process.[86] In addition, it was reported that the interaction between these two residues is coupled with structural changes of the protein during the photocycle.[88,89]

Many works have focussed their attention not only on the ionizable residues described above, but also on the effects of non-ionizable residues. Table 1.7 summarizes the absorption maxima of the mutants of bR, where non-ionizable residues were substituted. Leu93 is considered to be located in the proximity of the 13-Me group of the chromophore. In L93A, the rate of the photoreaction cycle is 250 times slower than that of the wild-type. The rate determining step is believed to be the 13-*cis*→*all-trans* re-isomerization process, which may be influenced by the interaction between Leu93 and the 13-Me group.[90]

Since the aromatic residues corresponding to Trp86, Trp182, and Tyr185 are well conserved across many retinal proteins (Figure 1.9), they seem to play an important role in maintaining the functions and structures of the proteins. The substitutions of some tryptophan residues largely affect the absorption maximum

and the pump function of bR. The W182F mutant shows relatively slow decay from L to M.[91] Trp182 is located in the vicinity of the 9-Me group of the chromophore. In the bR analogue reconstituted with 9-desmethylretinal, its kinetics for the primary part of the photoreaction is similar to that for W182A. This suggests that the interaction between Trp182 and the 9-Me group plays a role in determining the rate of the L→M process.[91,92]

On substitution of Trp86 into phenylalanine, appreciable changes in the arrangement of water molecule(s) were observed.[93] The changes were similar to those observed in the L and M intermediates of the wild-type bR. This result implies that Trp86, together with Asp85, is bound to the water molecule and contributes to preventing the formation of some photo-induced side-products.

The substitutions of tyrosine into phenylalanine do not significantly affect the pump function.[94] In Y57F, Y83F, and Y185F, however, the rate of the reconstitution of the chromophore was reduced, and the absorption maxima significantly shifted. These observations imply the presence of direct interactions between these tyrosine residues and the chromophore. Particularly, Tyr185 is supposed to form a hydrogen bond with Asp212, and is responsible for the pKa control of Asp85 and Asp212.[80]

§1.5 Aim of This Dissertation

As described above, a variety of experiments have provided a great deal of information about the structures and functions of Rh and bR at the molecular level. However, there remain several ambiguous points about the chromophore-protein interaction. Particularly, the molecular mechanism of the opsin shift is still controversial. To construct a precise molecular model of the active site of the proteins, two problems need to be solved: molecular structure of the chromophore itself in the protein, and interactions between the chromophore and the protein

matrix surrounding it.

The analysis of ^{13}C chemical shielding tensor is helpful to solve the first problem because the tensor reflects the electronic structure of a carbon atom in question. Early quantum chemical studies of ^{13}C chemical shieldings for the chromophores of Rh and bR have been carried out on the assumption of linear correlation between ^{13}C chemical shift and π-electron density on the carbon of interest.[95,96] However, such an approach seems to have some difficulties in interpreting the NMR chemical shift data quantitatively, since chemical shieldings are the function not only of electron density, but also of the whole density matrix and excitation energy, namely a second-order property in the perturbation theory.

At present, there are various methodologies of *ab initio* NMR shielding calculations which allow us to predict more accurately the shielding constants of molecules.[97-99] By means of *ab initio* NMR shielding calculation, Sakurai et al. successfully indicated that the chromophore of bR takes 6*s-trans* conformation.[16] Furthermore, they succeeded in reproducing the chemical shifts observed for the chromophore of bR.[100] It is thus expected that the *ab initio* shielding calculation enables us to interpret exactly the behavior of ^{13}C chemical shifts of polyene compounds in conjunction with their electronic structures.

The second problem, that is, the chromophore-protein interactions will be revealed by the analysis of absorption spectra of Rh and bR. Quantum chemical calculations have been also applied to the problem of the opsin shifts of Rh and bR. Due to the limitation of computational resources, most of those calculations were performed for model systems including only the chromophore and some residues that were likely to affect the electronic state of the chromophore. However, in order to explain the complicated functions of the proteins, the contributions of all the constituting atoms should be taken into account.

One possible method capable of incorporating the environmental effect of the

protein into quantum chemical calculation is a self-consistent reaction field (SCRF) method combined with a polarizable continuum model (PCM). In this method, a protein matrix will be approximated as a continuum medium, which represents the dielectric property of the protein. Utilizing the boundary element method, Sakurai et al. developed an SCRF-PCM theory.[101] A great success in applying this method to various ground-state solvation problems including chemical and biological phenomena[102] makes us expect to provide good perspective for excited-states solvation phenomena as well.

Another approach is to use the so-called linear scale molecular orbital (MO) methods recently developed by several groups. In a usual molecular orbital calculation, its computational time increases in proportion to the third power of the number of atoms in a system. Thus, its application is limited to relatively small molecules, even if a semiempirical approximation is used. Recently, however, Stewart has developed a new quantum chemical method with an algorithm using localized molecular orbital.[103] In this method, the CPU time increases only linearly against the number of atoms. This enables us to calculate the wave function of a whole protein within reasonable computational time and resources. Such a sophisticated method is expected to provide invaluable information about the chromophore-protein interactions in Rh and bR.

The aim of this dissertation is to investigate the chromophore-protein interactions in Rh and bR by means of various quantum chemical methods, including *ab initio* shielding calculation, SCRF-PCM calculation, and linear scale MO calculation. The author's main concern is to understand how the ^{13}C chemical shifts and absorption maxima of retinal and its Schiff bases are influenced by perturbations from their environments. On the basis of such information, the author will elucidate the origin of abnormal behavior of these spectroscopic parameters observed for Rh and bR, and finally propose a new molecular model of

the opsin shift.

In Chapter 2, *ab initio* shielding calculations are performed for ten linear π-conjugated compounds that are selected as models of the chromophore of Rh and bR. Conformation-dependence of the principal values of chemical shielding tensor for each unsaturated carbon is analyzed in detail. From those results, the author obtains universal rules for the effects of substitution, isomerization, and electronic perturbation, and for the additivity among these effects. Utilizing the results for model compounds, the author analyzes the chemical shifts of the chromophore in Rh. Finally, from the results for the C12 shielding, the author estimates the conformation around the C12-C13 single bond.

In Chapter 3, based on a self-consistent reaction field theory, the author formulates a new method to evaluate the medium effects on the absorption spectra of molecular solutes. In this method, the effects of orientational and electronic polarizations of the medium are explicitly taken into account through simple functions of its dielectric constant and refractive index, respectively. The expression for the excitation energy of the whole system including the medium is derived by allowing for electronic polarization in the medium, caused by excitation of a solute molecule. The excitation energy is obtained by the singly-excitation configuration interaction (CI) method incorporated into a semiempirical MO program. It is shown that the test calculation for a merocyanine dye well reproduces the observed solvatochromic shifts.

In Chapter 4, the method developed in Chapter 3 is applied to retinal and its Schiff bases. The reliability of the method is confirmed by comparison between the observed and calculated absorption spectra of several retinal derivatives. It is shown that the absorption maxima of these compounds significantly red shift with an increase in refractive index of solvents. An effective refractive index of bR is estimated, and is used for the calculations of the opsin shifts. As a result, the opsin

shifts of both bR_{568} and M_{412} are consistently explained. In addition, the cooperative action between the counterion of the chromophore and the medium effects is discussed.

In Chapter 5, in order to investigate the effect of the electronic polarization of the protein on the absorption maximum, the author newly formulates a method for incorporating this effect into a full-atomic calculation. In this method, each bond constituting the protein is regarded as a cylindrical stick made of dielectric. It is shown that this method, combined with the full-atomic quantum chemical calculation developed by Stewart, well reproduces the opsin shift of bR. From analysis of electrostatic potential maps for the ground and excited states, the residues dominating the opsin shift are identified.

In Chapter 6, the main conclusions of this dissertation are summarized and some prospects are remarked.

References

(1) Newton, I. in "Optics: or a treatise of the reflections, refractions, inflections, and colours of light." (1704).

(2) See for reviews: (a) Birge, R. R. *Annu. Rev. Phys. Chem.* **1990**, *41*, 683. (b) Lanyi, J. K. *Biochim. Biophys. Acta* **1993**, *1183*, 241. (c) Khorana, H. G. *Annu. N. Y. Acad.Sci. USA* **1986**, *471*, 272. (d) Mathies, R. A.; Lin, S. W.; Ames, J. B.; Pollard, W. T. *Annu. Rev. Biophys. BioPhys. Chem.* **1991**, *20*, 491. (e) Nakanishi, K. *Pure & Appl. Chem.* **1991**, *63*, 161. (f) Ottolenghi, M.; Sheves, M. *J. Membrane Biol.* **1989**, *112*, 193. (g) Kandori, H. *Chemistry & Industry* **1995**, *Sep. 18*, 735.

(3) Nathans, J. *Biochemistry* **1992**, *31*, 4923.

(4) Kandori, H.; Sasabe, H.; Nakanishi, K.; Yoshizawa, T.; Mizukami, T.; Shichida, Y. *J. Am. Chem. Soc.* **1996**, *118*, 1002.

(5) Imai, H.; Kojima, D.; Oura, T.; Tachibanaki, S.; Terakita, A.; Shichida, Y. *Proc. Natl. Acad. Sci. USA* **1997**, *94*, 2322.

(6) (a) Oesterhelt, D.; Stoeckenius, W. *Nature New. Biol.* **1971**, *233*, 149. (b) Kimura, Y.; Ikegami, A.; Stoeckenius, W. *Photochem. Photobiol.* **1984**, *40*, 641.

(7) Lozier, R.; Bogomolni, R. A.; Stoeckenius, W. *Biophys. J.* **1975**, *15*, 955.

(8) see for review: Kandori, H.; Maeda, A. *Protein Nucleic acid and Enzyme* **1997**, *42*, 101.

(9) Brown, L. S.; Sasaki, J.; Kandori, H.; Maeda, A.; Needleman, R.; Lanyi, J. K. *J. Biol. Chem.* **1995**, *270*, 27122.

(10) Grigorief, N.; Ceska, T. A.; Downing, K. H.; Baldwin, J. M.; Henderson, R. *J. Mol. Biol.* **1996**, *259*, 393.

(11) Sasaki, J.; Brown, L. S.; Chon, Y-S.; Kandori, H.; Maeda, A.; Nedleman, R.; Lanyi, J. K. *Science* **1995**, *269*, 73.

(12) Mathies, R. A.; Stryer, L. *Proc. Natl. Acad. Sci. USA* **1976**, *73*, 2169.

(13) van der Steen, R. ; Biesheuvel, P. L.; Mathies, R. A.; Lugtenburg, J. *J. Am. Chem. Soc.* **1986**, *108*, 6410.

(14) Harbison, G. S.; Smith, S. O.; Pardoen, J. A.; Courtin, J. M. L.; Lugtenburg, J.; Herzfeld, J.; Mathies, R. A.; Griffin, R. G. *Biochemistry* **1985**, *24*, 6955.

(15) Harbison, G. S.; Mulder, P. P. J.; Pardoen, H.; Lugtenburg, J.; Herzfeld, J.; Griffin, R. G. J*J. Am. Chem. Soc.* **1985**, *107*, 4809.

(16) Wada, M. ; Sakurai, M.; Inoue, Y.; Tamura, Y.; Watanabe, Y. *J. Am. Chem. Soc.* **1994**, *116*, 1537.

(17) Blatz, P. E.; Mohler, J. H.; Navangul, H. V. *Biochemistry* **1972**, *11*, 848.

(18) Honig, B.; Green berg, A. G.; Dinur, U.; Ebrey, T. G. *Biochemistry* **1976**, *15*, 4593.

(19) (a) Arnaboldi, M.; Motto, M. G.; Tsujimoto, K.; Balogh-Nair, V.; Nakanishi, K. J*J. Am. Chem. Soc.* **1979**, *101*, 7082. (b) Honig, B.; Dinur, U.; Nakanishi, K.; Balogh-Nair, V.; Gawinowicz, M. A.; Arnaboldi, M.; Motto, M. G. *J. Am. Chem. Soc.* **1979**, *101*, 7084. (c) Sheves, M.; Nakanishi, K.; Honig, B. *J. Am. Chem. Soc.* **1979**, *101*, 7086.

(20) (a) Nakanishi, K.; Balogh-Nair, V.; Arnaboldi, M.; Tsujimoto, K.; Honig, B. J. Am. Chem. Soc **1980**, *102*, 7945. (b) Motto, M. G.; Sheves, M.; Tsujimoto, K.; Balogh-Nair, V.; Nakanishi, K. *J. Am. Chem. Soc.* **1980**, *102*, 7947.

(21) Mao, B.; Govindjee, R.; Ebrey, T. G.; Arnaboldi, M.; Balogh-Nair, V.; Nakanishi, K.; Crouch, R. *Biochemistry* **1981**, *20*, 428.

(22) Spudich, J. L.; McCain, D. A.; Nakanishi, K.; Okabe, M.; Shimizu, N.; Rodman, H.; Honig, B.; Bogomolni, R. A. *BioPhys. J.* **1986**, *49*, 479.

(23) Koutalos, Y.; Ebrey, T. G.; Tsuda, M.; Odashima, K.; Lien, T.; Park, M. H.; Shimizu, N.; Derguini, F.; Nakanishi, K.; Gilson, H. R.; Honig, B. *Biochemistry* **1989**, *28*, 2732.

(24) Birge, R. R.; Muray, L. P.; Pierce, B. M.; Akita, H.; Balogh-Nair, V.; Findsen, L. A.; Nakanishi, K. P*Proc. Natl. Acad. Sci. USA* **1985**, *82*, 4117.

(25) (a) Mogi, T.; Stern, L. J.; Marti, T.; Chao, B. H.; Khorana, H. G. *Proc. Natl. Acad. Sci. USA* **1988**, *85*, 4148. (b) Mogi, T. *Biophysics* **1989**, *29*, 33.

(26) (a) Irving, C. S.; Byers, G. W.; Leermakers, P. A. *J. Am. Chem. Soc.* **1969**, *91*, 2141. (b) Irving, C. S.; Byers, G. W.; Leermakers, P. A. *Biochemistry* **1970**, *9*, 858.

(27) Suzuki, T.; Kito, Y. *Photochem. Photobiol.* **1972**, *15*, 275.

(28) (a) Kliger, D. S.; Milder, S. J.; Dratz, E. A. *Photochem. Photobiol.* **1977**, *25*, 277. (b) Milder, S. J.; Kliger, D. S. *Photochem. Photobiol.* **1977**, *25*, 287.

(29) Smith, S. O.; Palings, I.; Copie, V.; Raleigh, D. P.; Courtin, J.; Pardoen, J. A.; Lugtenburg, J.; Mathies, R. M.; griffin, R. G. *Biochemistry* **1987**, *26*, 1611.

(30) Smith, S. O.; Palings, I.; Miley, M. E.; Courtin, J.; de Groot, H.; Lugtenburg, J.; Mathies, R. A.; Griffin, R. G. *Biochemistry* **1990**, *29*, 8158.

(31) Mollevanger, L. C. P. J.; Kentgens, A. P. M.; Pardoen, J. A.; Courtin, J. M. L.; Veeman, W. S.; Lugtenburg, J.; de Grip, W. *J. Eur. J. Biochem.* **1987**, *63*, 9.

(32) Smith, S. O.; Courtin, J.; de Groot, H.; Gebhard, R.; Lugtenburg, J. *Biochemistry* **1991**, *30*, 7409.

(33) Smith, S. O.; de Groot, H.; Gebhard, R.; Lugtenburg, J. *Photochem. Photobiol.* **1992**, *56*, 1035.

(34) Hamanaka, T.; Mitsui, T.; Ashida, T.; Kakudo, M. *Acta Cryst.* **1972**, *B28*, 214.

(35) Giradi, R.; Karle, I. L.; Karle, J. *Acta Cryst.* **1972**, *B28*, 2605.

(36) Stam, C. H.; *Acta Cryst.* **1981**, *B28*, 2936.

(37) Simmons, C. J.; Liu, R. S.; Denny, M.; Seff, K. *Acta Cryst.* **1981**, *B37*, 2197.

(38) Santersiero, B.; James, M.; Mahendran, M.; Childs, R. *J. Am. Chem. Soc.* **1990**, *112*, 9416.

(39) Shriver, J. W.; Mateescu, G.; Fager, R.; Torchia, D.; Abrahamson, E. W. *Biochemistry* **1979**, *18*, 4785.

(40) Palings, I.; Pardoen, J. A.; van der Berg, E.; Winkel, C.; Lugtenburg, J.; Mathies, R. A. *Biochemistry* **1987**, *26*, 2544.

(41) Harbison, G. S.; Smith, S. O.; Pardoen, J. A.; Winkel, C.; Lugtenburg, J.; Herzfeld, J.; Mathies, R. A.; Griffin, R. G. *Proc. Natl. Acad. Sci. USA* **1984**, *81*, 1706.

(42) Harbison, G. S.; Smith, S. O.; Pardoen, J. A.; Mulder, P. P. J.; Lugtenburg, J.; Herzfeld, J.; Mathies, R. A.; Griffin, R. G. *Biochemistry* **1984**, *23*, 2662.

(43) Smith, S. O.; de Groot, H. J. M.; Gebhard, R.; Courtin, J. M. L.; Lugtenburg, J.; Herzfeld, J.;

Griffin, R. G. *Biochemistry* **1989**, *28*, 8897.

(44) Smith, S. O.; Courtin, J.; van den Berg, E.; Winkel, C.; Lugtenburg, J.; Herzfeld, J.; Griffin, R. G. *Biochemistry* **1989**, *28*, 237.

(45) Albeck. A.; Livnah, N.; Gottlieb, H.; Sheves, M. *J. Am. Chem. Soc.* **1992**, *114*, 2400.

(46) Hu, J.; Griffin, R. G.; Herzfeld, J. *Proc. Natl. Acad. Sci. USA*, **1994**, *91*, 8880.

(47) Farrar, M. R.; Laksshmi, K.; Smith, S. O.; Stephen Brown, R.; Raap, J.; Lugtenburg, J.; Griffin, R. G.; Herzfeld, J. *BioPhys. J.* **1993**, *65*, 310.

(48) Reeves, P. J.; Thurmond, R. L.; Khorana, H. G. *Proc. Natl. Acad. Sci. USA* **1996**, *93*, 11487.

(49) Mollaaghababa, R.; Davidson, F.; Kaiser, C.; Khorana, H. G. *Proc. Natl. Acad. Sci. USA* **1996**, *93*, 11482.

(50) Shand, R. F.; Miercke, L. J. W.; Mitra, A. K.; Fong, S. K.; Stroud, R. M.; Betlach, M. C. *Biochemistry* **1991**, *30*, 3082.

(51) Sakmar, T. P.; Franke, R. R.; Khorana, H. G. *Proc. Natl. Acad. Sci. USA* **1989**, *86*, 8309.

(52) Zhukovsky, E. A.; Oprian, D. D. *Science* **1989**, *246*, 928.

(53) (a) Nathans, J. *Biochemistry* **1990**, *29*, 937. (b) Nathans, J. *Biochemistry* **1990**, *29*, 9746.

(54) Farmy, K.; Jäger, F.; Beck, M.; Zvyaga, T. A.; Sakmar, T. P.; Siebert, F. *Proc. Natl. Acad. Sci. USA* **1993**, *90*, 10206.

(55) Jäger, F.; Fahmy, K.; Sakmar, T. P.; Siebert, F. *Biochemistry* **1994**, *33*, 10878.

(56) Zhukovsky, E. A.; Robinson, P. R.; Oprian, D. D. *Biochemistry* **1992**, *31*, 10400.

(57) DeCaluwé, G. L.; Bovee-Geurts, P. H.; Rath, P.; Rothschild, K. J.; de Grip, W. J. *BioPhys. Chem.* **1995**, *56*, 79.

(58) Zhukovsky, E. A.; Robinson, P. R.; Oprian, D. D. *Science* **1991**, *251*, 558.

(59) (a) Nakayama, T.; Khorana, H. G. *J. Biol. Chem.* **1991**, *266*, 4269. (b) Nakayama, T. *Biophysics* **1991**, *31*, 7.

(60) Lin, S. W.; Sakmar, T. P. *Biochemistry* **1996**, *35*, 11149.

(61) Hisatomi, O.; Kayada, S.; Aoki, Y.; Iwasa, T.; Tokunaga, F. *Vision Res.* **1994**, *34*, 3097.

(62) Mogi, T.; Marti, T.; Khorana, H. G. *J. Biol. Chem.* **1989**, *264*, 14197.

(63) Yokoyama, S. *Mol. Biol. Evol.* **1995**, *12*, 53.

(64) Neitz, M.; Neitz, J.; Jacobs, G. H. *Science* **1991**, *252*, 971.

(65) Rao, V. R.; Cohen, G. B.; Oprian, D. D. *Nature* **1994**, *367*, 639.

(66) Garriga, P.; Liu, X.; Khorana, H. G. *Proc. Natl. Acad. Sci. USA* **1996**, *93*, 4560.

(67) Liu, X.; Garriga, P.; Khorana, H. G. *Proc. Natl. Acad. Sci. USA* **1996**, *93*, 4554.

(68) Cohen, G. B.; Oprian, D. D.; Robinson, P. R. *Biochemistry* **1992**, *31*, 12592.

(69) Rao, V. R.; Oprian, D. D. *Annu. Rev. Biophys. Biomol. Struct.* **1996**, *25*, 287.

(70) Jäger, S.; Lewis, J. W.; Zvyaga, T. A.; Szundi, I.; Sakmar, T. P.; Kliger, D. S. *Biochemistry* **1997**, *36* 1999.

(71) (a) Zvyaga, T. A.; Fahmy, K.; Siebert, F.; Sakmar, T. P. *Biochemistry* **1996**, *35*, 7536. (b) Farmy, K.; Zvyaga, T. A.; Sakmar, T .P.; Siebert, F. *Biochemistry* **1996**, *35*, 15065.

(72) Greenhalgh, D. A.; Altenbach, C.; Hubbel, W. L.; Khorana, H. G. *Proc. Natl. Acad. Sci. USA* **1991**, *88*, 8626.

(73) Duñach, M.; Marti, T.; Khorana, H. G.; Rothschild, K. J. *Proc. Natl. Acad. Sci. USA* **1990**, *87*, 9873.

(74) Subramaniam, S.; Marti, S. T.; Rösselet, J.; Rothschild, K. J.; Khorana, H. G. *Proc. Natl. Acad. Sci. USA* **1991**, *88*, 2583.

(75) Miercke, L. J. W.; Betlach, M. C.; Mitra, A. K.; Shad, R. E.; Fon, S. K.; Stroud, R. M. *Biochemistry* **1991**, *30*, 3088.

(76) Needleman, R.; Chang, M.; Ni, B.; Váró G.; Fornés, J.; White, S. H.; Lanyi, J. K. *J. Biol. Chem.* **1991**, *266*, 11478.

(77) Logunov, S. L.; El-Sayed, M. A.; Song, L.; Lanyi, J. K. *J. Phys. Chem.* **1996**, *100*, 2391.

(78) Turner, G. J.; Miercke, L. J. W.; Thorgeirsson, T. E.; Kliger, D. S.; Betlach, M. C.; Stroud, R. M. *Biochemistry* **1993**, *32*, 1332.

(79) Russel, T. S.; Coleman, M.; Rath, P.; Nilsson, A.; Rothschild, K. J. *Biochemistry* **1997**, 36, 7490.

(80) Sonar, S.; Krebs, M. P.; Khorana, H. G.; Rothschild, K. J. *Biochemistry* **1993**, *32*, 2263.

(81) Drachev, L. A.; Kaulen, A. D.; Khorna, H. G.; Mogi, T.; Postanogova, N. V.; Skulachev, V. P.; Stern, L. J. *Photochem. Photobiol.* **1992**, *55*, 741.

(82) Misra, S.; Ebrey, T. G.; Crouch, R. K.; Menick, D. R. *Photochem. Photobiol.* **1997**, *65*, 1309.

(83) Stern, L. J.; Khorana, H. G. *J. Biol. Chem.* **1989**, *264*, 14202.

(84) Stuart, J. A.; Vought, B. W.; Zhang, C-H.; Birge, R. R. *Biospectroscopy* **1995**, *1*, 9.

(85) Zhag, Y. N.; El-Sayed, M. A.; Bonet, M. L.; Lanyi, J. K.; Chang, M.; Ni, B.; Needleman, R. *Proc. Natl. Acad. Sci. USA* **1993**, *90*, 1445.

(86) Coleman, M.; Nilsson, A.; Russell, T. S.; Rath, P.; Pandey, R.; Rothschild, K. J. *Biochemistry* **1995**, *34*, 15599.

(87) Yamazaki, Y.; Hatanaka, M.; Kandori, H.; Sasaki, J.; Karstens, W. F. J.; Raap, J.; Lugtenburg, J.; Bizounok, M.; Herzfeld, J.; Needleman, R.; Lanyi, J. K.; Maeda, A. *Biochemistry* **1995**, *34*, 7088.

(88) Harms, G. S.; Johnson, C. K. *Photochem. Photobiol.* **1997**, *66*, 133.

(89) Gergely, C.; Ganea, C.; Groma, G.; Váró, G. *BioPhys. J.* **1993**, *65*, 2478.

(90) Delaney, J. K.; Schweiger, U.; Subramaniam, S. *Proc. Natl. Acad. Sci. USA* **1995**, *92*, 11120.

(91) Yamazaki, Y.; Sasaki, J.; Hatanaka, M.; Kandori, H.; Maeda, A.; Needleman, R.; Shinada, T.; Yoshihara, K.; Brown, L. S.; Lanyi, J. K. *Biochemistry* **1995**, *34*, 577.

(92) Weidlich, O.; Sohalt, B.; Friedman, N.; Sheves, M.; Lanyi, J. K.; Brown, L. S.; Siebert, F. *Biochemistry* **1996**, *35*, 10807.

(93) Hatanaka, M.; Kashima, R.; Kandori, H.; Friedman, N.; Shees, M.; Needleman, R.; Lanyi, J. K.; Maeda, A. *Biochemistry* **1997**, *36*, 5493.

(94) Mogi, T.; Stern, L. J.; Hackett, N. R.; Khorana, H. G. *Proc. Natl. Acad. Sci. USA* **1987**, *84*, 5595.

(95) Rodman Gilson, H. S.; Honig, B. H. *J. Am. Chem. Soc.* **1988**, *110*, 1943.

(96) (a) Han, M.; DeDecker, B. S.; Smith, S. O. *BioPhys. J.* **1993**, *65*, 899. (b) Han, M.; Simith, S. O. *Biochemistry* **1995**, *34*, 1425.

(97) (a) Kutzelnigg, W. *Isr. J. Chem.* **1980**, *19*, 193. (b) Schindler, M.; Kutzelnigg, W. *J. Chem. Phys.* **1982**, *76*, 1919. (c) Schindler, M.; Kutzelnigg, W. *J. Am. Chem. Soc.* **1983**, *105*, 1360. (d) Schindler, M.; Kutzelnigg, W. *Mol. Phys.* **1983**, *48*, 781.

(98) Ditchfield, R. *Mol. Phys.* **1974**, *27*, 789. (b) Wokinski, K.; Hilton, J. F.; Pulay, P. JJ. *Am. Chem. Soc.* **1990**, *112*, 8251.

(99) (a) Hansen, A. E.; Bouman, T. D. *J. Chem. Phys.* **1985**, *82*, 5035. (b) Bouman, T. D.; Hansen, A. E. *Chem. Phys. Lett.* **1988**, *149*, 510. (c) Facelli, J. C.; Grant, D. M.; Bouman, T. D.; Hansen, A. E. *J. Comput. Chem.* **1990**, *11*, 32.

(100) Wada, M.; Sakurai, M.; Inoue, Y.; Tamura, Y.; Watanabe, Y. *J. Phys. Chem.* **1996**, *100*, 1957.

(101) (a) Hoshi, H.; Sakurai, M.; Inoue, Y.; Chûjô, R. *J. Chem. Phys.* **1987**, *87*, 1107. (b) Hoshi, H.; Sakurai, M.; Inoue, Y.; Chûjô, R. *J. Mol. Struct. (Theochem)* **1988**, *180*, 267.

(102) (a) Furuki, T.; Hosokawa, H.; Sakurai, M.; Inoue, Y.; Chûjô, R. *J. Am. Chem. Soc.* **1993**, *115*, 2903. (b) Furuki, T.; Sakurai, M.; Inoue, Y. *J. Phys. Chem.* **1995**, *99*, 12047. (c) Sakurai, M.; Furuki, T.; Inoue, Y. JJ. *Phys. Chem.* **1995**, *99*, 17789.

(103) Stewart, J. J. P. *Int. J. Quant. Chem.* **1996**, *58*, 133.

Chapter 2. Conformational Analysis of the Chromophore of Rhodopsin Based on Ab Initio Shielding Calculation

§2.1 Introduction

The photo-receptive proteins, rhodopsin (Rh) and bacteriorhodopsin (bR), possess retinal isomers bound to a lysine residue via the protonated Schiff base linkage.[1] In both proteins, the conformation of retinal moiety closely is related to the appearance of the biological function, especially to the regulation of their absorption maxima. For example, in bR_{568} the C6-C7 bond is likely to be planar *s-trans*,[2] which essentially contributes to the fact that this absorbs yellow green light.

At present, a diffraction method such as electron microscopy[3,4] seems to be insufficient in resolution to elucidate the conformational state of the chromophore in the proteins. Instead, structural information has been obtained mainly by means of spectroscopic studies. Among them, the observation of ^{13}C NMR chemical shifts for the chromophore provides a good insight not only into its conformation, but also into the interaction of the chromophore with the surrounding protein matrix. The solid-state NMR technique has been applied to Rh,[5-7] bR,[8-10] and their photo-intermediates.[11-13] Consequently, it was revealed that the chemical shifts for the chromophore are significantly different from those for free protonated retinal Schiff base. As for bR, the chemical shifts of C5 and C8 are displaced significantly to downfield and upfield, respectively, relative to those of model compounds.[9] Recent *ab initio* studies[14,15] have successfully provided a rigorous theoretical interpretation for the origin of such chemical shift displacements.

As for the chromophore of Rh, the ^{13}C chemical shifts from C8 to C13 show significant downfield shifts compared with those for protonated 11-*cis*-retinylidene Schiff base in solution.[6] Recently, Han and Smith[16,17] have attempted to explain this chemical shift difference by assuming that a carboxylate anion exists nearby

C12, a model which is based on the so-called external-charge model.[1f,18] Their molecular orbital calculation indicated that both of the chemical shift and absorption data for Rh could be consistently explained by this model. However, there seem to be some ambiguities in their analysis of the chemical shift data, because a linear correlation was assumed between chemical shielding and atomic charge density. Although the validity of such a correlation has been widely accepted,[19] this may not necessarily hold when the π-conjugation breaks due to the torsion of a single bond. In fact, the author's preliminary *ab initio* calculation[20] has demonstrated that the isotropic shielding for C12 of 11-*cis*-retinal changes with rotation of the C12-C13 bond by nearly 6 ppm, which is comparable to the chemical shift difference between the free and protein-bound states. It is thus of great necessity to unambiguously determine the conformation around the C12-C13 bond before attempting to build a molecular model of chromophore-protein interaction.

In order to deduce decisive information on the conformational state of the chromophore from its chemical shift data, basic data are required to inform us how chemical shieldings are influenced by substituents, *trans-cis* isomerization, inductive effects, and so on. As for saturated cyclic or acyclic hydrocarbons[21-24] and polypeptides,[25-27] *ab initio* shielding calculation has been extensively carried out to examine the relationship between the chemical shieldings and molecular conformations. The calculation successfully reproduced empirical rules known as α-, β-, γ-, or δ-substituent effects. A recent study using the solid-state NMR measurements and *ab initio* calculations has elucidated which component of a shielding tensor dominates the steric effects.[28] However, those data accumulated for aliphatic compounds alone may be insufficient to interpret the chemical shift data for conjugated compounds, because the conformation dependence of conjugated carbon shieldings would be influenced with changing π-electronic state, induced by

rotation of a single-bond. Therefore, a systematic study is newly required for conjugated systems.

The major part of this chapter is targeted on the search of some empirical rules held between the chemical shifts of conjugated systems and their conformation. For this purpose, *ab initio* shielding calculation is applied to ten diene derivatives with various conformational states. First, the auhor provide a rigorous theoretical interpretation for shielding changes arising from the modification of π-electronic state. Next, several types of steric effects and an inductive effect are analyzed in conjunction with the data for electronic structures of the conjugated chains. It will be found that the additivity is fulfilled among these effects. Through such a systematic analysis, it is shown how a conformational change of conjugated systems influences the principal values of the shielding tensor for each unsaturated carbon. On the basis of this information, the author successfully determine the C12-C13 conformation of the chromophore in Rh.

§2.2 Calculations

Figure 2.1 shows ten diene derivatives examined here: (*E,E*)-hexa-2,4-diene (HEX), (*E,E*)-3-methylhexa-2,4-diene (3MET), (*E,Z*)-hexa-2,4-diene (1CIS), (*E,Z*)-3-methylhexa-2,4-diene (1C3M), (*E*)-2-methylhexa-2,4-diene (4MET), (*E*)-2,3-dimethylhexa-2,4-diene (34DME), (*E,E*)-3-*tert*-butylhexa-2,4-diene (3TBU), (*E*)-2-methyl-3-*tert*-butylhexa-2,4-diene (3TB4M), (*E,E*)-hexa-2,4-dienal (HEXAL), and (*E,Z*)-3-methylhexa-2,4-dienal (1C3MAL). These compounds are selected as minimal analogues of partial structures of 11-*cis*-retinal. Here the numbering of the carbon atoms and the abbreviations (in parenthesis) of these dienes are given so as to easily compare the chemical shifts of corresponding carbons between different compounds.

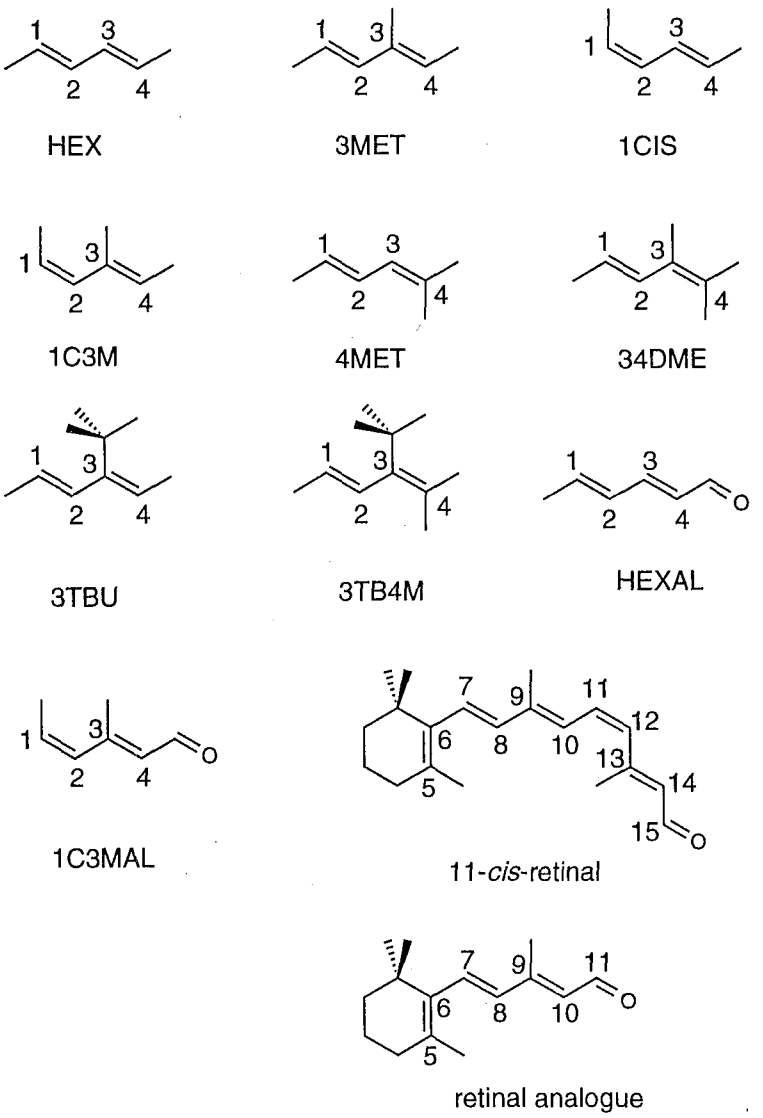

Figure 2.1 Molecular structures of the linear π-conjugated compounds studied.

The geometries of the compounds are fully optimized except for the dihedral angle of C1-C2-C3-C4, which was fixed at every 30° from 0° to 180°. 3TBU and 3TB4M are models of a molecular fragment of retinal including the C1 , C5, C6, C7 and C8 carbons. Two methyl groups of the *tert*-butyl moiety of each model correspond to the two methyl groups attached to C1 of retinal. Thus, by reference to the optimized structure of retinal,[29] the orientation of the *tert*-butyl group was determined. One of the C-Me bonds of the *tert*-butyl group was rotated by 15° from eclipsed form against the C3-C4 double bond and fixed at this orientation during geometry optimization. Such a geometrical constraint is required to reflect the rigidity of the cyclohexene ring of retinal.

The full geometry optimization of 11-*cis*-retinal (Figure 2.1) was executed by using the X-ray data[30] as an initial structure. Restricted geometry optimization was carried out with the dihedral angle of C11-C12-C13-C14 fixed at every 30° from 0° to 180°.

The geometry optimization and Mulliken population analysis were carried out using the GAUSSIAN92 program.[31b] Due to the CPU limitation of available computer facilities, the shielding calculations were carried out using two different programs, RPAC 9.0 and GAUSSIAN94, which were installed on Cray computers at Eagan, Minnesota, USA and an IBM SP2 cluster system at Institute for Molecular Science, Okazaki, Japan, respectively. The shielding calculation coded in GAUSSIAN94[31c] follows the so-called GIAO (gauge-invariant atomic orbital) theory,[32] while the program RPAC9.0[33] is based on Hansen and Bouman's theory[34,35] for LORG (localized orbital/local origin) shielding calculations, interfacing to the GAUSSIAN90 program.[31a] All the shielding calculations were performed at Hartree-Fock level. The shielding calculation for 11-*cis* retinal was performed using the RPAC9.0 program, while that for the model compounds

mentioned above was done using the GAUSSIAN 94 program. PM3 (Parametric Method 3) calculation[36] were performed using the program MOPAC6.01.[37]

Wada et al. have already reported a detailed study of the basis set dependence of chemical shieldings of conjugated carbons.[38] According to the results of that study, the 4-31G and 6-31G* basis sets were used for 11-*cis*-retinal and the diene derivatives, respectively.[39] In the latter case, the basis sets of 4-31G and 6-31G**, which gave essentially identical results with those from the 6-31G* were tested.

The calculated shieldings were converted to TMS reference, and the positive sign indicates deshielding. The shieldings of TMS are calculated as a 2.1 ppm downfield from methane[19] whose shieldings obtained from the LORG/4-31G and GIAO/6-31G* methods are 222.4 ppm and 201.0 ppm, respectively.

§2.3 Results

2.3.1 Conformation-Dependent Shifts in HEX

Throughout the former part of this chapter, the author focuses on how the ^{13}C shieldings of the conjugated carbons of the diene derivatives are influenced by rotation of their central single bonds. First, the data for HEX, which provides the most fundamental information on this subject, are described. Figure 2.2(a) shows the calculated ^{13}C shieldings for the unsaturated carbons of HEX as a function of $\varphi_{2\text{-}3}$, defined as the dihedral angle of C1-C2-C3-C4. The angle $\varphi_{2\text{-}3}$ of 180° means *s-trans* form with respect to the C2-C3 bond. The values of σ_{iso} is the isotropic chemical shielding of each carbon atom and those of σ_{11}, σ_{22}, and σ_{33} are the principal values of the corresponding shielding tensor. For all the conjugated carbons, the principal axis for σ_{11} is almost perpendicular to the conjugated plane, whereas both of σ_{22} and σ_{33} are the in-plane elements and the former's axis is almost parallel to each double bond. During the rotation the direction of each principal axis was almost kept constant within 5° (data not shown).

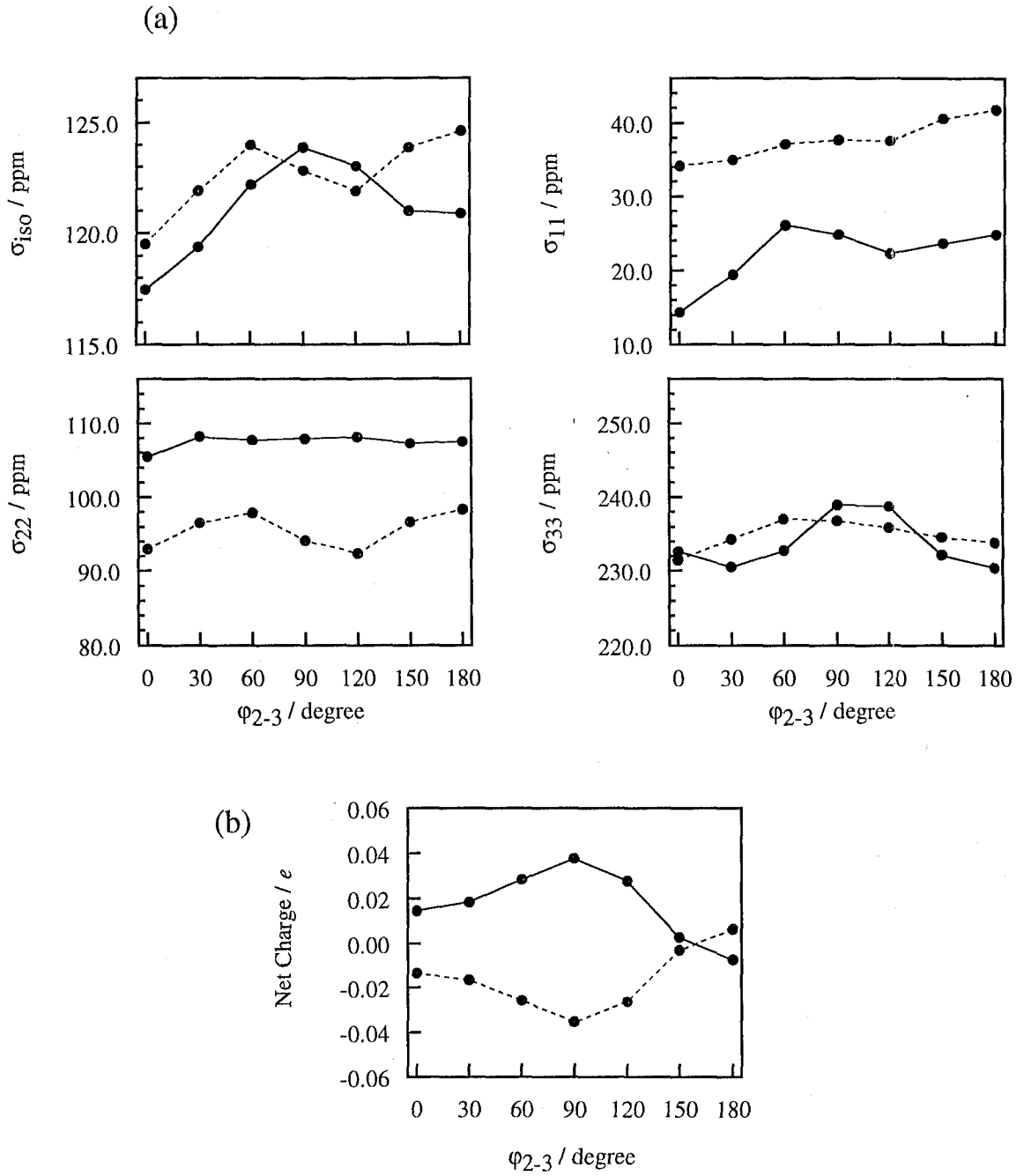

Figure 2.2 Conformation dependence of the shielding parameters and net charges for the conjugated carbon of HEX. (a) The data for the isotropic shielding and the principal values of the shielding tensor for each unsaturated carbon. (b) The data for net charges which mean the total charge on the corresponding methine (CH) group. In both (a) and (b), the data for C1 (equivalent to C4) and C2 (equivalent to C3) are represented by solid and dashed lines, respectively.

As shown in Figure 2.2(a), the σ_{iso} of C1 (equivalent to C4) exhibits the most deshielded value at $\varphi_{2\text{-}3} = 90°$, and the most shielded value at $\varphi_{2\text{-}3} = 0°$, resulting in a span of 6.4 ppm in chemical shielding. Such a profile of the C1 shieldings arises mainly from the behavior of σ_{11} and σ_{33}: σ_{11} shifts steeply to upfield on going from $\varphi_{2\text{-}3} = 0°$ to 60°, and σ_{33} exhibits a convex-type profile with a maximum around $\varphi_{2\text{-}3} = 90°$. Figure 2.2(b) shows the net charge of each C-H unit, the value of which was obtained from Mulliken population analysis. The change in σ_{33} appears to be synchronizing with the change in charge density. Thus, the angular dependence of the C1 shielding could be explained by considering the effect of charge distribution and another factor dominating the behavior of σ_{11}, which will be described later in detail.

The σ_{iso} of C2 (equivalent to C3) shows a different profile from that of C1: it has a maximum at $\varphi_{2\text{-}3} = 60°$ and a minimum at $\varphi_{2\text{-}3} = 120°$. Clearly, there is no apparent correlation between the angular dependencies of the shielding and charge density. In particular, it should be noted that σ_{33} shifts in the direction opposite to that predicted from the change in charge density. Such unusual behavior is thought to be a common phenomenon to the shieldings of carbons forming a rotating bond. It is thus of interest to provide a rigorous theoretical interpretation for its origin.

2.3.2 π-orbital modification effect

Any perturbations which modify π-orbitals of the conjugated system should more largely affect the paramagnetic shielding term than the diamagnetic one. According to Ramsey's formalism,[40] the paramagnetic shielding term depends on two factors: namely the matrix element of angular momentum and excitation energy. In planar conjugated systems, the π–π* transition is not responsible for the shieldings because the matrix element of angular momentum vanishes between π-bonding atomic orbitals.[41] However, rotation of a single bond distorts the π-

orbitals, generating some amount of angular momentum. In addition, the π–π* transition energy would increase accompanied by the rotation, because the bond alternation is strengthened due to the breaking of conjugation. The generation of angular momentum contributes to causing a downfield shift for the shielding of the conjugated carbons, while the increase in transition energy does causing an upfield shift. Thus, the fact that the σ_{33} for C2 of HEX shifts to the downfield with rotation of the C2-C3 bond (Figure 2.2) can not be interpreted without explicit theoretical analysis.

In the framework of molecular orbital theory , by setting the gauge origin at the center of atom n, the $\alpha\alpha$ component ($\alpha = x$, y, or z) of the paramagnetic term is represented as follows:

$$\sigma_{\alpha\alpha}^{\mathrm{para}}(n) = \frac{1}{c^2}\sum_{l}^{\mathrm{occ}}\sum_{m}^{\mathrm{vac}}\Delta E_{lm}^{-1} \times\left\{\langle\psi_l|L_\alpha^{(n)}|\psi_m\rangle\langle\psi_m|\frac{L_\alpha^{(n)}}{r^{-3}}|\psi_l\rangle + \text{complex conjugate}\right\} \qquad (2.1)$$

where ψ_l and ψ_m are lth occupied (occ) and mth virtual (vac) molecular orbitals, respectively, and ΔE_{lm} is the difference in orbital energy between them. $L^{(n)}$ is the local angular momentum defined as

$$L^{(n)} = L - R_n \times p \qquad (2.2)$$

where R_n is a positional vector measured from the atom n.[35]

Here, a four π-electron system like diene is considered. For the sake of convenience, we let the x, y, and z axes coincide with the direction of the principal axes for σ_{33}, σ_{22}, and σ_{11} of dienes, respectively. The dependence of the orbital

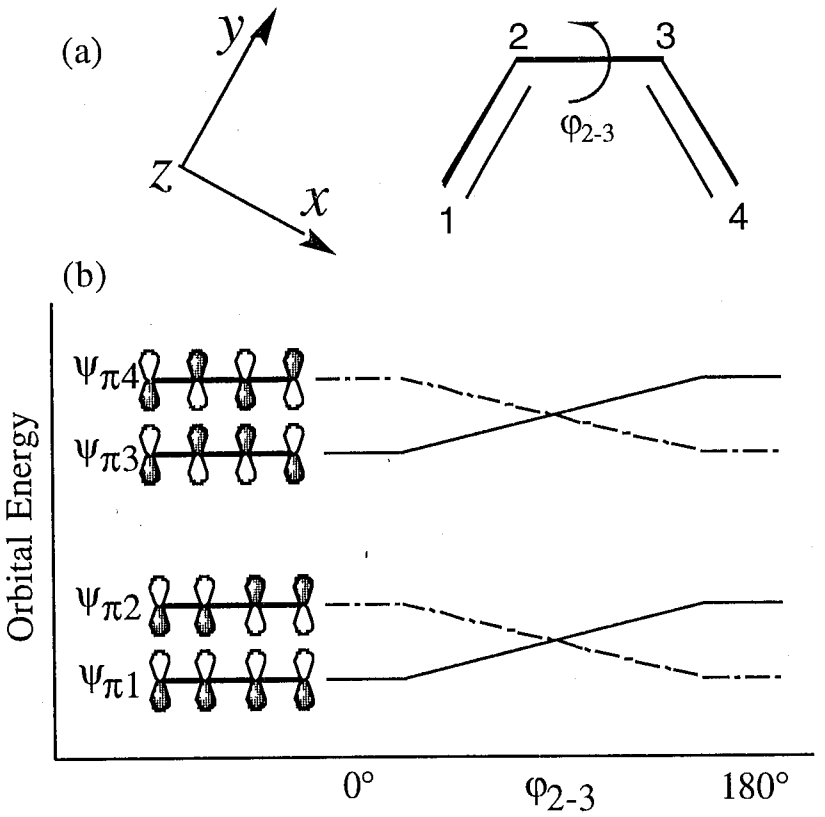

Figure 2.3 Schematic representations for explaining the π-orbital modification effect in diene. (a) The coordinate system assumed in the formulation (see text). (b) The conformation dependence of π-orbital energy.

Table 2.1 The orbital energies of the four π-orbitals of butadiene as a function of the dihedral angle C1-C2-C3-C4 (in eV)

	0°	30°	60°	90°	120°	150°	180°
$\psi_{\pi 4}$	2.12	1.97	1.59	1.12	1.58	1.98	2.15
$\psi_{\pi 3}$	0.29	0.39	0.68	1.10	0.67	0.37	0.27
$\psi_{\pi 2}$	-9.50	-9.59	-9.86	-10.33	-9.86	-9.56	-9.47
$\psi_{\pi 1}$	-11.97	-11.59	-10.97	-10.35	-10.95	-11.58	-12.00

energy on $\varphi_{2\text{-}3}$ are schematically illustrated in Figure 2.3. The scheme indicates that the energy of the orbital with an antibonding character with respect to the central single bond is lowered when rotation of the single bond occurs, and that of the orbital with a bonding character is raised. The validity of this scheme is proved by the result from PM3 molecular orbital calculation for butadiene shown in Table 2.1. It can be assumed that the p_z orbitals of the carbons which form the rotating single bond are perturbed from each other when the bond rotates. This perturbation causes a distortion of the p-orbital, which is represented by the mixing of the p_z orbital with the $p_{x\text{-}y}$ orbital defined as

$$p_{x-y} = \frac{1}{2}\left(p_x - \sqrt{3}\, p_y\right) \tag{2.3}$$

whose direction is perpendicular to both z-axis and the single bond. Using a mixing parameter λ, the distortion can be described as follows:

$$p_z \rightarrow \frac{1}{\sqrt{1+\lambda^2}}\left(p_z \pm \lambda p_{x-y}\right) \tag{2.4}$$

where the double sign takes plus for $\psi_{\pi 1}$ and $\psi_{\pi 3}$, and takes minus for $\psi_{\pi 2}$ and $\psi_{\pi 4}$, depending on the symmetry of the molecular orbitals. As for the C2 carbon, the matrix elements of angular momentum, for example, $\langle \psi_{\pi 1} | L_x^{(2)} | \psi_{\pi 3} \rangle$ is calculated as

$$\begin{aligned}\left\langle \psi_{\pi 1} \middle| L_x^{(n)} \middle| \psi_{\pi 3} \right\rangle = -\frac{1}{4(1+\lambda^2)} \{ & \left\langle p_z(2) \middle| L_x^{(2)} \middle| p_z(2) \right\rangle \\ & + \lambda^2 \left\langle p_{x-y}(2) \middle| L_x^{(2)} \middle| p_{x-y}(2) \right\rangle \\ & + \lambda \left\langle p_z(2) \middle| L_x^{(2)} \middle| p_{x-y}(2) \right\rangle \\ & + \lambda \left\langle p_{x-y}(2) \middle| L_x^{(2)} \middle| p_z(2) \right\rangle \}\end{aligned}$$

$$= -\frac{i\lambda}{8(1+\lambda^2)} \int dr\, z\phi\{(xy\frac{\partial\phi}{\partial z} - zx\frac{\partial\phi}{\partial y}) + \sqrt{3}\,(y^2\frac{\partial\phi}{\partial z} - z\phi - yz\frac{\partial\phi}{\partial y})\}$$
$$+(x-\sqrt{3}\,y)\phi(y\phi + yz\frac{\partial\phi}{\partial z} - z^2\frac{\partial\phi}{\partial y})$$

$$= \frac{\sqrt{3}\,i\lambda}{4(1+\lambda^2)} \tag{2.5}$$

where the function ϕ represents the radial part of p-orbital and the following approximation was used:

$$L_\alpha^{(n)}|p_\beta(m)\rangle = L_\alpha^{(n)}|p_\beta(n)\rangle\delta_{mn} \tag{2.6}$$

The approximation of Eq. 2.6 means that the angular momentum of a different-centered p-electron from the atom of interest is neglected. Consequently we can obtain the following equations:

$$\langle\psi_{\pi 1}|L_x^{(2)}|\psi_{\pi 4}\rangle = \langle\psi_{\pi 2}|L_x^{(2)}|\psi_{\pi 3}\rangle = 0$$
$$\langle\psi_{\pi 1}|L_x^{(2)}|\psi_{\pi 3}\rangle = \langle\psi_{\pi 2}|L_x^{(2)}|\psi_{\pi 4}\rangle = \frac{\sqrt{3}\,i\lambda}{4(1+\lambda^2)} \tag{2.7}$$

It should be noted that the energy difference ΔE_{13} and ΔE_{24} are nearly equal and remains almost unchanged through the bond rotation (see Figure 2.3). This means that the factor of transition energy does not contribute to the change in shielding. In other words, the conformation-dependent change of the shielding tensor is dominated by the change in the matrix element of angular momentum.

On the basis of the these results, we can write the paramagnetic term as follows:

$$\sigma_{xx}^{para}(2) = -\frac{1}{c^2}\Delta E^{-1}\langle r^{-3}\rangle\frac{3\lambda^2}{4(1+\lambda^2)} \qquad (2.8)$$

,where we put $\Delta E_{13} = \Delta E_{24} = \Delta E$, and regarded the average of r^{-3} as a constant. Similarly the expressions of the other components can be obtained as follows:

$$\sigma_{yy}^{para}(2) = -\frac{1}{c^2}\Delta E^{-1}\langle r^{-3}\rangle\frac{\lambda^2}{4(1+\lambda^2)}$$
$$\sigma_{zz}^{para}(2) = 0 \qquad (2.9)$$

According to eqs. 2.8 and 2.9, the π-orbital modification induced by rotation of the single bond affects mainly the terms of σ_{xx} and σ_{yy}, namely σ_{33} and σ_{22} in the diene system. Since the value of λ increases with rotation of the bond, an appreciable amount of downfield shift should be induced for these tensor components. This indicates that the shieldings of carbons forming a rotating bond do not necessarily follow the profile of charge density. Therefore, the present formalism is helpful to understand the unusual behavior of the C2 shielding of HEX, especially of its σ_{33} component.

2.3.3 γ-Steric Effect

As well known, the ^{13}C shielding of a aliphatic carbon significantly shifts to upfield when a methyl group is introduced at the γ-position relative to the carbon of interest, usually called γ-steric effect. The γ-steric effect appears most remarkably when the carbon atom of interest stays in eclipsed conformation with respect to the γ-methyl group.

Accordingly, if a methyl group is introduced at the C3 position of HEX, an upfield shift is expected to be induced for the C1 carbon. Figure 2.4 shows the calculated results obtained by subtracting the values for HEX from those for 3MET, indicated as Δ3MET. Certainly, an appreciable amount of an upfield shift occurs in the isotropic shielding of C1 when the angle of $\varphi_{2\text{-}3}$ is around 180°, supporting the above conventional picture.

A theoretically more interesting finding is that such an upfield shift predominantly comes from a large upfield shift of σ_{11}. This agrees with the experimental result[42] that in the case of sp^2 carbon, the γ-steric effect is reflected on the principal value whose direction is perpendicular to the conjugated plane. It is also consistent with a recent report indicating that in the case of sp^3 carbon a significant change occurs in the principal value whose direction is perpendicular to the plane in which the interaction forces operate.[28] Thus, the behavior of σ_{11} can be used to judge whether conformation-dependent changes in ^{13}C shielding of a given carbon are due to the γ-steric effect or not.

Next, along with the above criteria, the author examines the data for C1 of 1C3M, the shielding of which is shown as a difference (Δ1C3M) measured from that of HEX in Figure 2.4. In this case, the isotropic shielding also shifts to upfield when the angle of $\varphi_{2\text{-}3}$ is around 180°, but the σ_{11} component does not. This indicates that the change in the isotropic shielding cannot be ascribed to the γ-steric effect from the C3 methyl group. As can be seen from Figure 2.4, the conformation dependence of σ_{11} value for the C1 shielding is very similar to that for the C1 carbon of 1CIS. Thus, the C1 shielding of 1C3M is predominantly influenced by the *trans-cis* isomerization of the C1=C2 double bond. On the basis of these results, a theorem for the γ-steric effect can be deduced: the shielding of a C-H carbon of interest receives the γ-steric effect only when the C-H group directs

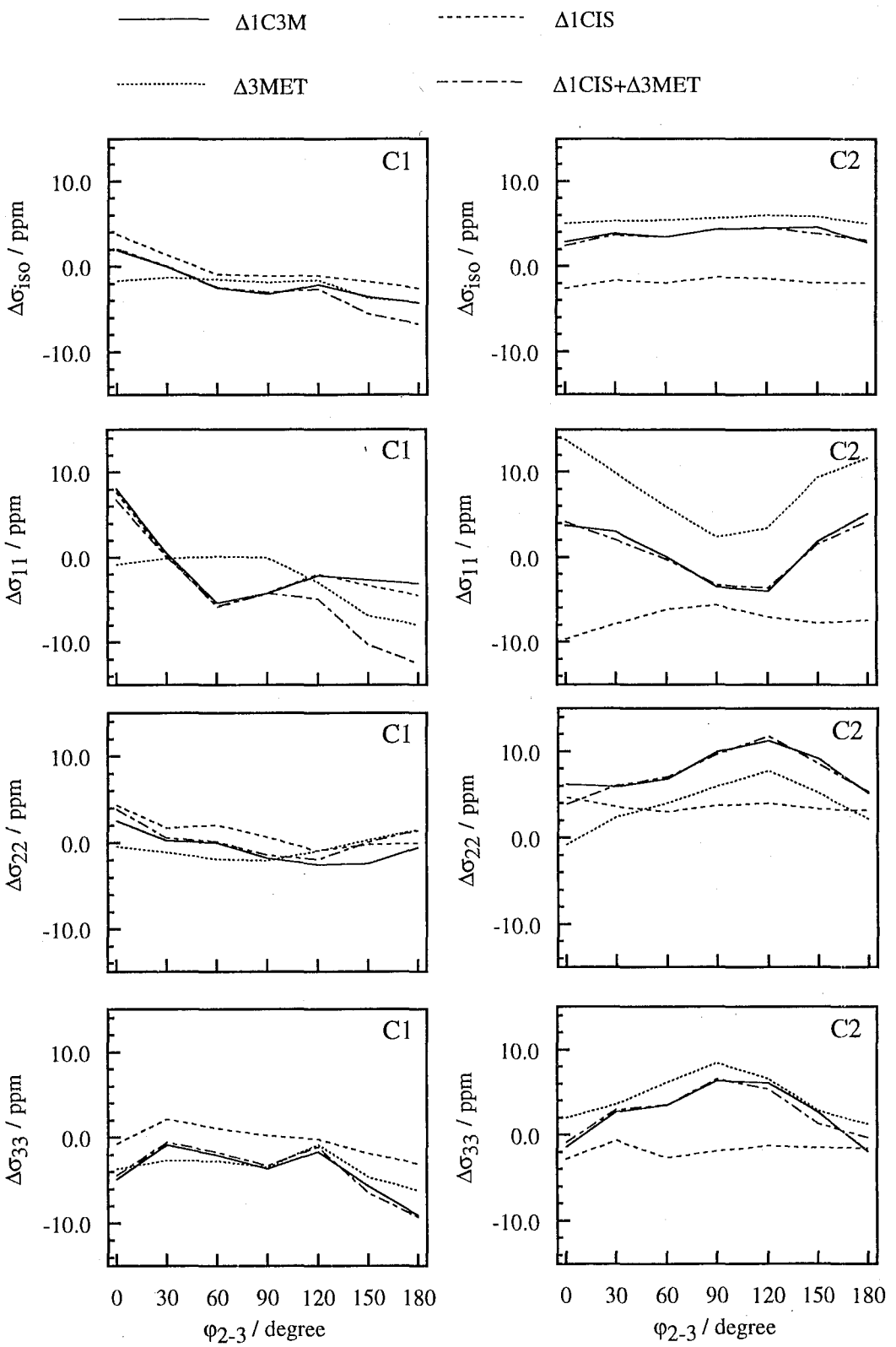

Figure 2.4 Conformation dependence of the shielding parameters of the conjugated carbons in 3MET, 1CIS, and 1C3M. The value of each shielding parameter is given as the difference from that for the corresponding carbon of HEX with the same angle of $\varphi_{2\text{-}3}$.

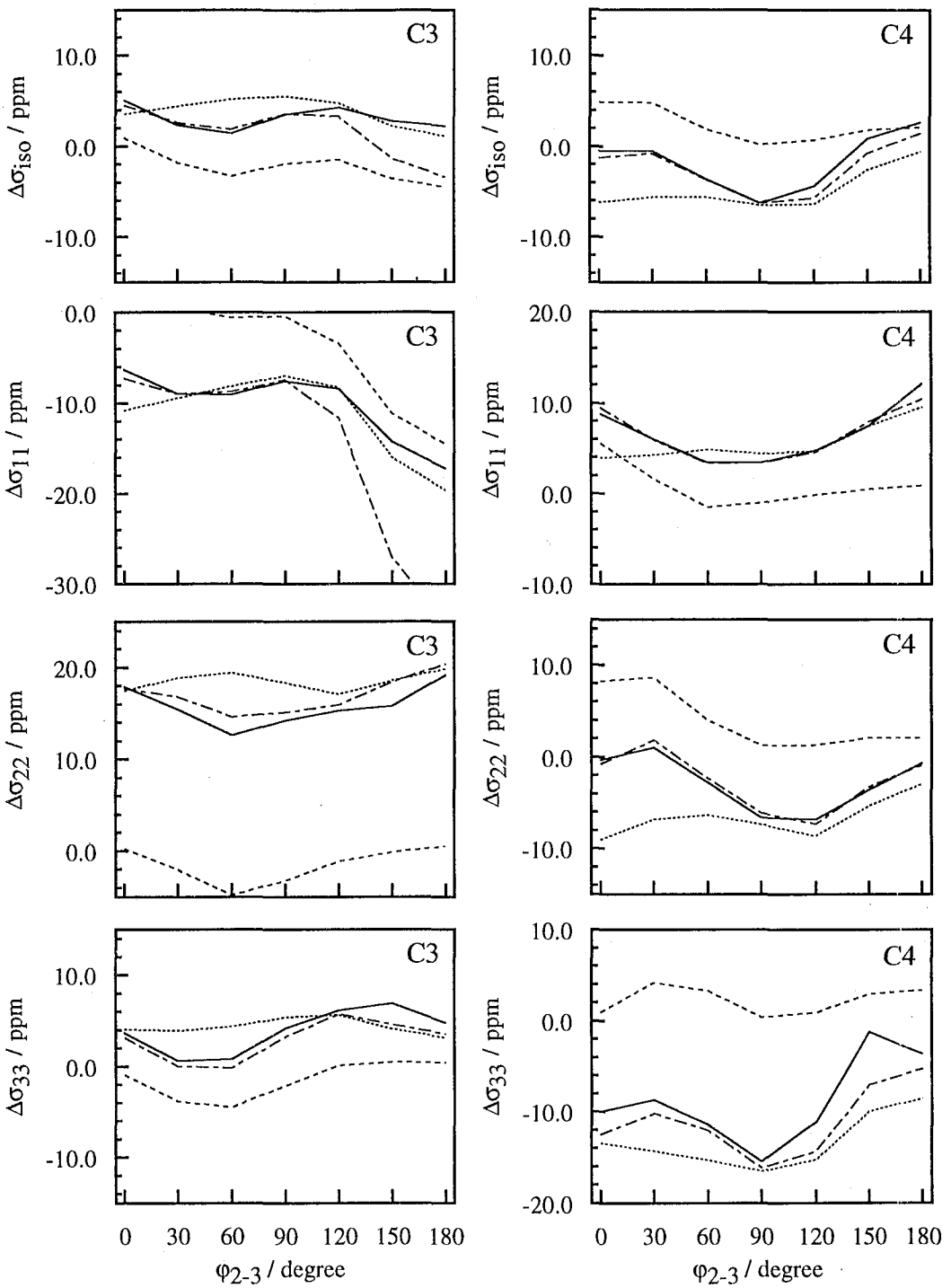

Figure 2.4 (continued)

towards the same side as that of the γ-methyl group. This theorem implicitly states that a quaternary carbon (nonprotonated carbon) is insensitive to the γ-steric effect.

The σ_{11} shielding of C3 of 1CIS shows an upfield shift when the $\varphi_{2\text{-}3}$ is around 180°, indicating the γ-steric effect from the 1-methyl group. On the other hand, the behavior of σ_{11} of C3 of 1C3M nearly coincides with that for 3MET, supporting the above theorem that the quaternary C3 of 1C3M does not receive the γ-steric effect from the C1 methyl group.

In summary, the σ_{11} component of the shielding tensor can be used as a measure of the γ-steric effect. The maximal shift by the effect occurs at the rotation angle of 180°, that is, *s-trans* conformation. The σ_{11} of C1 of 3MET upfield shifts by 8.0 ppm, whereas that of C3 of 1CIS upfield shifts by 14.6 ppm. This difference may arise from the difference in the direction of steric force. In the former, the γ-methyl group exists nearly in the direction of σ_{33} axis which is almost perpendicular to the C1=C2 double bond. In the latter, the γ-methyl group exists nearly in the direction of σ_{22} which is almost parallel to the C3=C4 double bond.

2.3.4 Other Steric Effects

As described above, the most apparent effect due to the methyl substitution is the γ-effect, but the shieldings of carbon atoms having no γ-substituents also show a characteristic conformation dependence. It was confirmed that the σ_{11} component again reflects the steric effect due to the presence of β- and δ-substituents. Table 2.2 summarizes the change in the σ_{11} shielding induced by various substituents, as indicated in Figure 2.5. For example, the difference between the σ_{11} for C2 of 3MET in *s-trans* form and that of HEX is denoted as "β_3-steric" effect. Interestingly, an upfield shift is caused only by the γ-substituent, consistent with the results for aliphatic compounds.

Table 2.2 Effects of substituents on the σ_{11} component of the shielding tensor of a given carbon

Position[a)]	$\Delta\sigma_{11}$ / ppm[b)]
β_1	13.8
β_2	12.8±0.6
β_3	11.7
β_4	5.5±2.7
γ_1	-12.8±1.9
γ_2	-7.4±0.6
γ_3	2.9±0.7
δ_2	4.5±1.0

a) Position where a substituent is introduced (see Figure 2.5).
b) Net shielding change induced by a substituent. Plus sign indicates down field shift. The data except for β_1 and β_3 indicate the average value with standard deviation over several kinds of diene derivative.

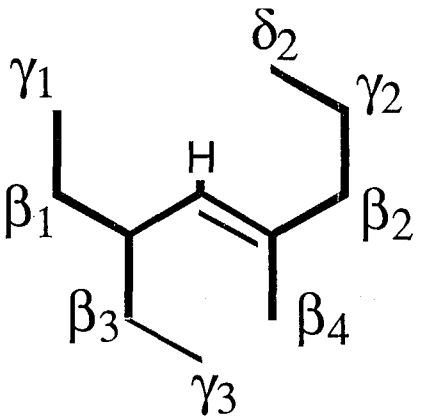

Figure 2.5 Conformation dependence of the shielding parameters and net charges for the conjugated carbon of HEX. (a) The data for the isotropic shielding and the principal values of the shielding tensor for each unsaturated carbon. (b) The data for net charges which mean the total charge on the corresponding methine (CH) group. In both (a) and (b), the data for C1 (equivalent to C4) and C2 (equivalent to C3) are represented by solid and dashed lines, respectively.

2.3.5 Inductive Effect

HEXAL was used to examine the effect of an electron inductive group on the conformation-dependent changes of the conjugated carbon shieldings. The value of ΔHEXAL was obtained by subtracting the chemical shifts of HEX from those of HEXAL. As shown in Figure 2.6, the data for ΔHEXAL have characteristic features. The shieldings of C1 and C4 exhibit concave and convex curves, respectively. On the other hand, the shieldings of C2 and C3 have less apparent profiles. Thus, as similar to the case of HEX, the carbons relevant to the rotating bond have intrinsically different properties from the other ones in chemical shielding.

It should be noted that the shielding changes of C1 and C4 are dominated by the behavior of σ_{33}. As shown in Figure 2.7, the σ_{33} values for C1 and C4 of ΔHEXAL change in the opposite sense to each other; that is, as the molecule distorts from the planar conformation, the shielding of C1 shifts to upfield, while that of C4 shifts to downfield. The net charge of each C-H unit of HEXAL, measured from that for HEX, is superposed upon Figure 2.7. In both carbons, the charge density and chemical shielding are synchronizing with each other. From this correlation, a shielding change of ~600 ppm is expected to occur per a change of unit charge. These data clearly indicate that the changes in the C1 and C4 shieldings are dominated by that in electronic distribution of the conjugated system. The behavior of the net charge is explained as follows. When the molecular structure is planar, positive charge should be induced on C1 and C3 due to the so-called resonance effect. When the conjugation is broken as a result of the rotation of the C2-C3 bond, the contribution of the resonance structure is reduced. Consequently the positive charge density on C1 decreases whereas that on C4 increases. This successfully explains that C1 exhibits concave-type curves in conformation dependence of both shielding and charge density, but C4 does convex curves.

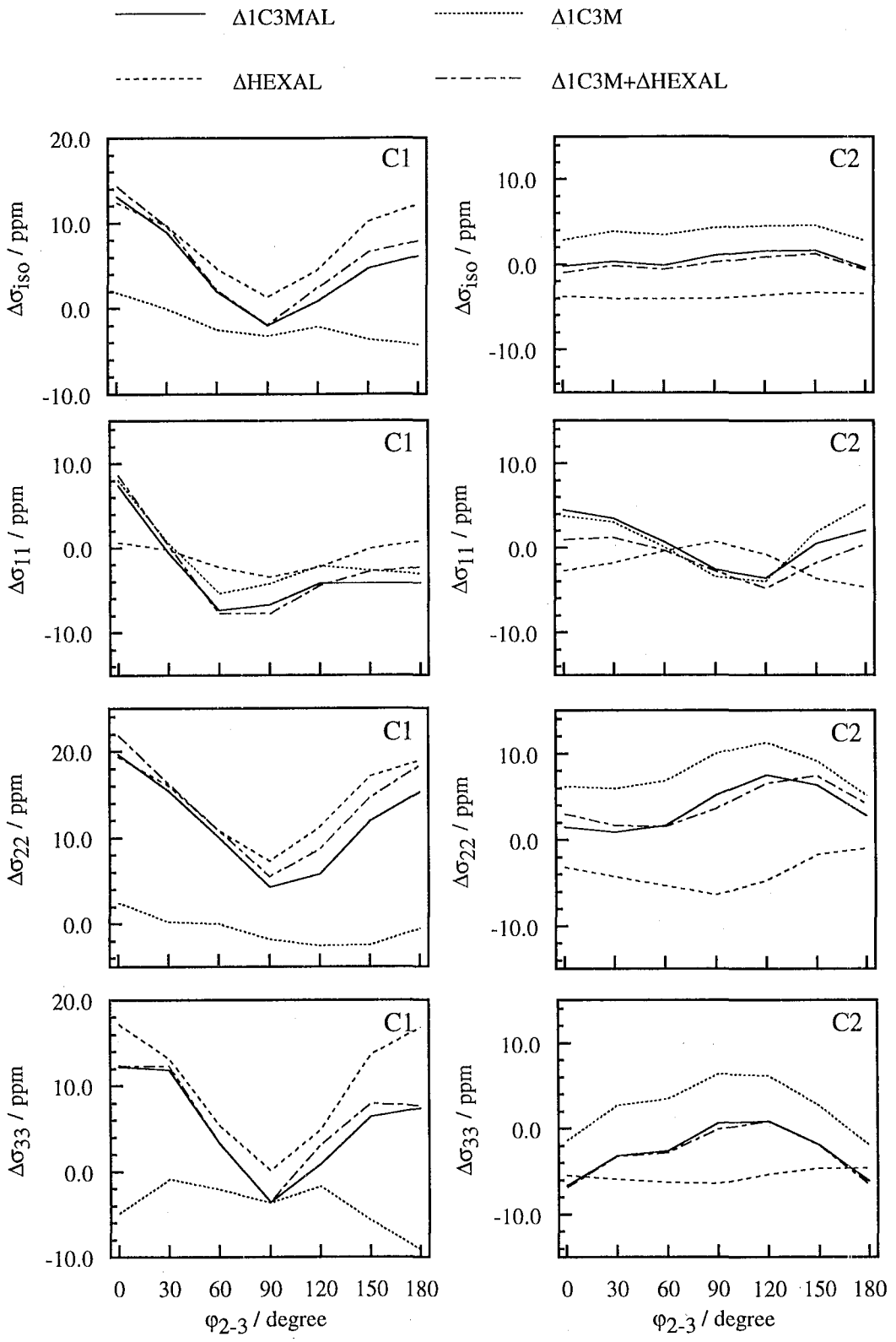

Figure 2.6 Conformation dependence of the shielding parameters of the conjugated carbons in 1C3M, HEXAL, and 1C3MAL. The value of each shielding parameter is given as the difference from that for the corresponding carbon of HEX with the same angle of $\varphi_{2\text{-}3}$.

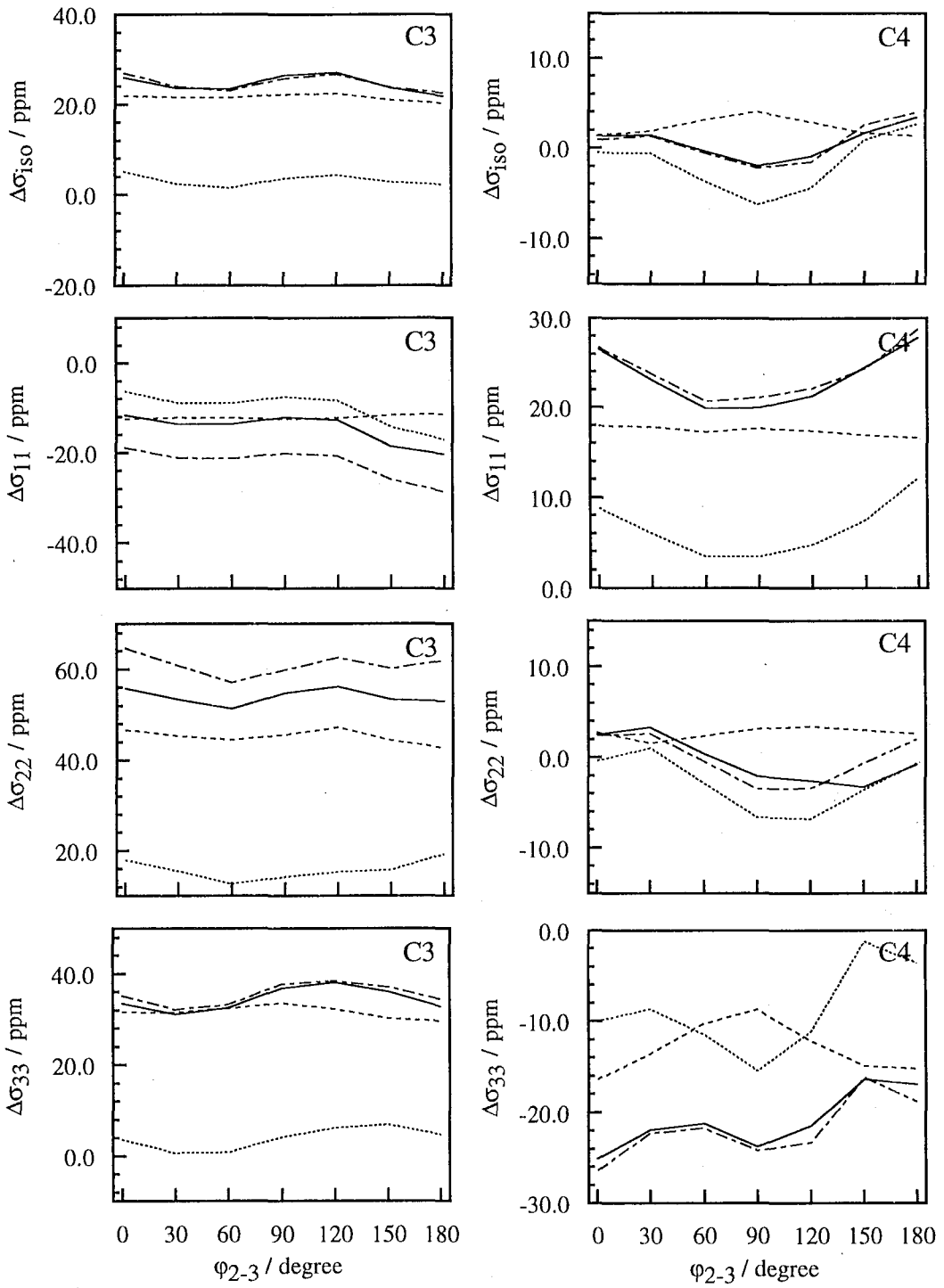

Figure 2.6 (continued)

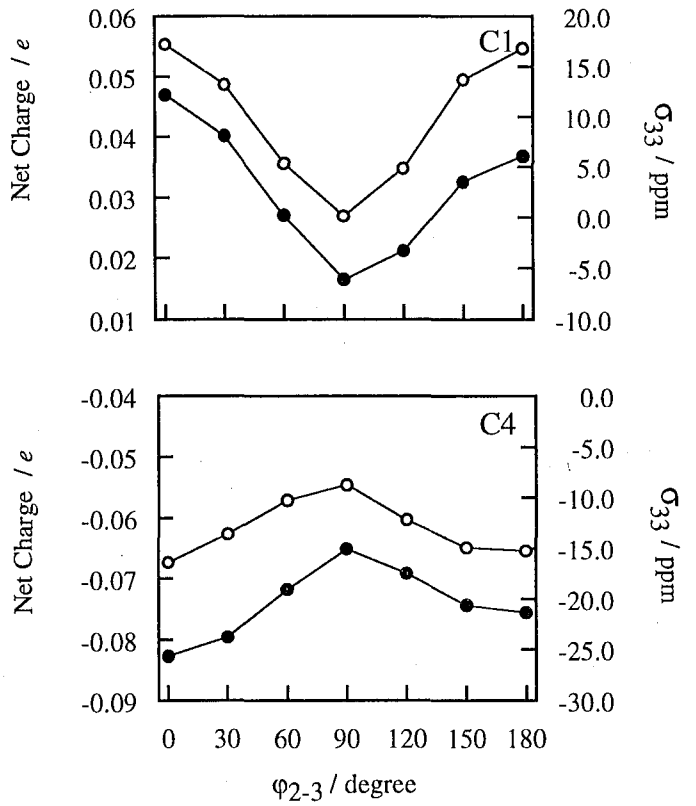

Figure 2.7 The conformation dependence of the σ_{33} component (O) and the net charge of the CH unit (●) for HEXAL. The value of each parameter is given as the difference from that for the corresponding carbon or CH unit of HEX with the same angle of $\varphi_{2\text{-}3}$. The upper and lower figures represent the data for C1 and C4, respectively.

As for C2 and C3 of HEXAL, there was no apparent correlation between the charge density and chemical shielding. As described above, the shieldings of these carbons should directly receive the π-orbital modification effect. It is thus reasonable that their behavior does not follow the simple correlation with charge density. Similarly, for C2 and C3 of HEX (Figure 2.2) the shieldings of σ_{22} and σ_{33} would be determined by a simultaneous contribution of both electronic distribution and π-orbital modification effects. It can be said that in general the shielding of the carbon on the both sides of the rotating single bond shows some complicated conformation dependence due to these two factors.

For all the other model compounds studied here, it was confirmed that the conformation dependence of charge density fairly coincides with that of σ_{33} (data not shown). Therefore, in contrast to the steric effect, the effect of charge density is reflected on σ_{33}. Since the behavior of σ_{22} resembles that of σ_{33}, it may be expected that σ_{22} also reflects the change in charge density. However, such a correlation was less apparently observed for σ_{22} than for σ_{33}.

2.3.6 Additivity of Miscellaneous Effects

Figure 2.4 shows the sum of Δ1CIS and Δ3MET, which is indicated as Δ1CIS+Δ3MET. As can be seen from this figure, each value of σ_{iso}, σ_{11}, σ_{22}, and σ_{33} of Δ1CIS+Δ3MET fairly coincides with that of Δ1C3M. This indicates that the methyl substituent effect acting in 3MET and the *trans-cis* isomerization effect in 1CIS are almost additive throughout the rotation. Exceptionally, a sizable deviation is observed between Δ1CIS+Δ3MET and Δ1C3M in σ_{11} of both C1 and C3 carbons in the range of $\varphi_{2\text{-}3}$ = 90° to 180°. In other words, such a breakdown of the additivity occurs while the γ-steric effect acts predominantly.

The results for 4MET, 3MET, and 34DME are shown in Figure 2.8. As for all carbons, the sum of Δ3MET and Δ4MET agrees with Δ34DME. Thus, the effects of the methyl substituent on C3 and C4 are also additive to each other.

As can be seen from Figure 2.9, Δ3TB4M agrees with the values of the sum of Δ3TBU and Δ4MET. This indicates that the additivity such as shown in Figure 2.8 is also maintained in the case of the *tert*-butyl group instead of the methyl group. Comparing Figures 2.8 with 2.9, it is shown that the profile of Δ3TBU is similar to that of Δ3MET. Thus, in the *tert*-butyl group the carbon which plays a role in exerting steric effect is not that of the outer methyl groups, but the central quaternary carbon. Exceptionally the outer methyl groups exert a γ-steric effect on the C2 shielding in the range of $\varphi_{2\text{-}3} = 0°\sim30°$.

Figure 2.6 shows that the values of Δ1C3M+ΔHEXAL agrees with those of Δ1C3MAL. This indicates that the effect of the aldehyde group is additive to the other effects included in the data of Δ1C3MAL such as methyl substitution or isomerization. This finding is quite natural because the charge density effect caused by the carbonyl group mainly affects the σ_{22} and σ_{33}, while the steric effect exerts on σ_{11}.

In summary, for most of the cases the effects of alkyl substitution, isomerization, and carbonyl substitution are additive to each other. Only one situation in which the additivity is disturbed is in the conformational range that the γ-effect is acting predominantly.

§2.4 Discussion

2.4.1 Features of the ^{13}C shielding of conjugated carbons

In the previous section, we obtained some basic data for conformation dependence of the ^{13}C shieldings of conjugated carbons. Clearly, the conjugated carbons are classified into two types according to the behavior of shielding changes.

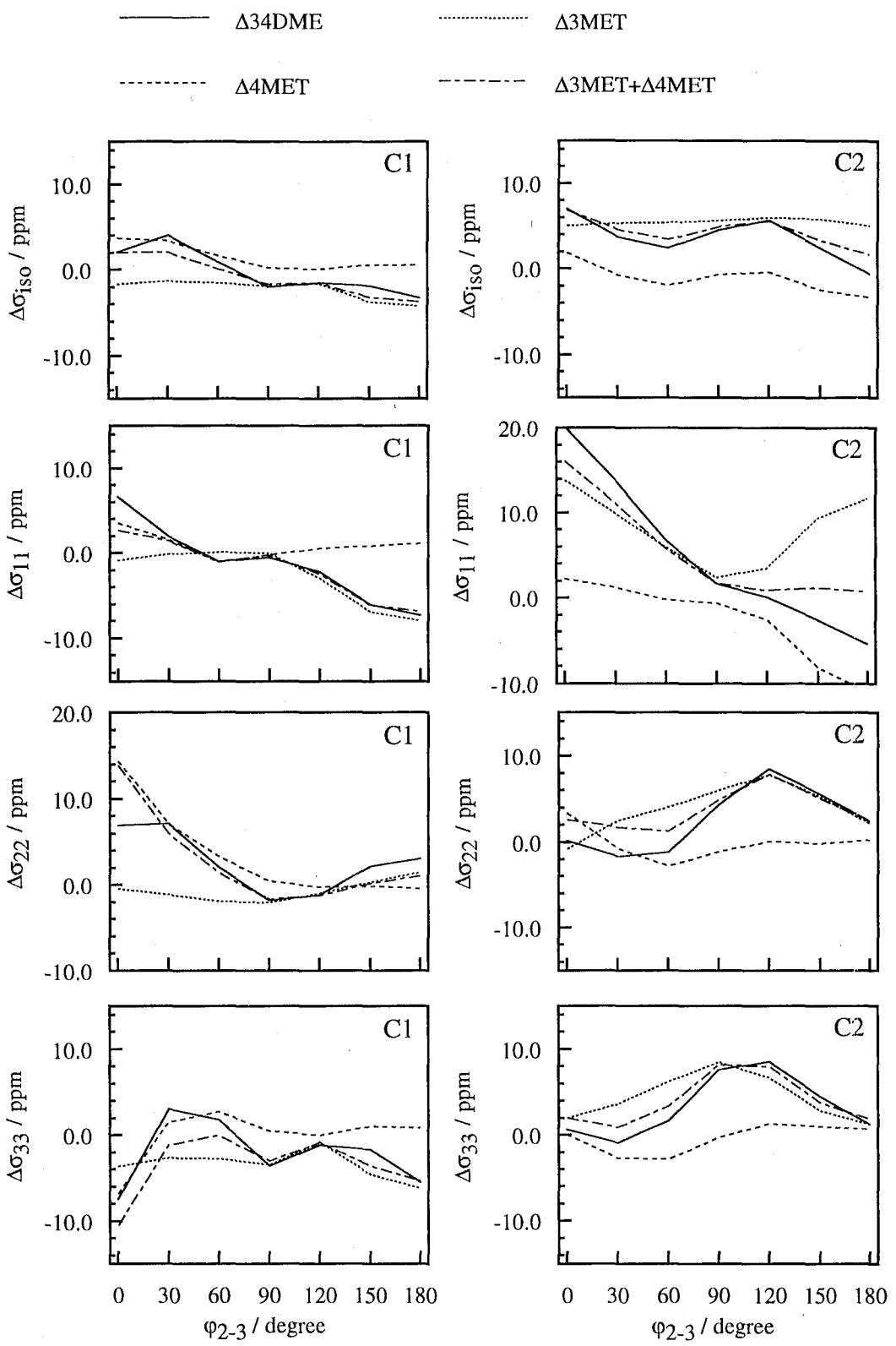

Figure 2.8 Conformation dependence of the shielding parameters of the conjugated carbons in 3MET, 4MET, and 34DME. The value of each shielding parameter is given as the difference from that for the corresponding carbon of HEX with the same angle of $\varphi_{2\text{-}3}$.

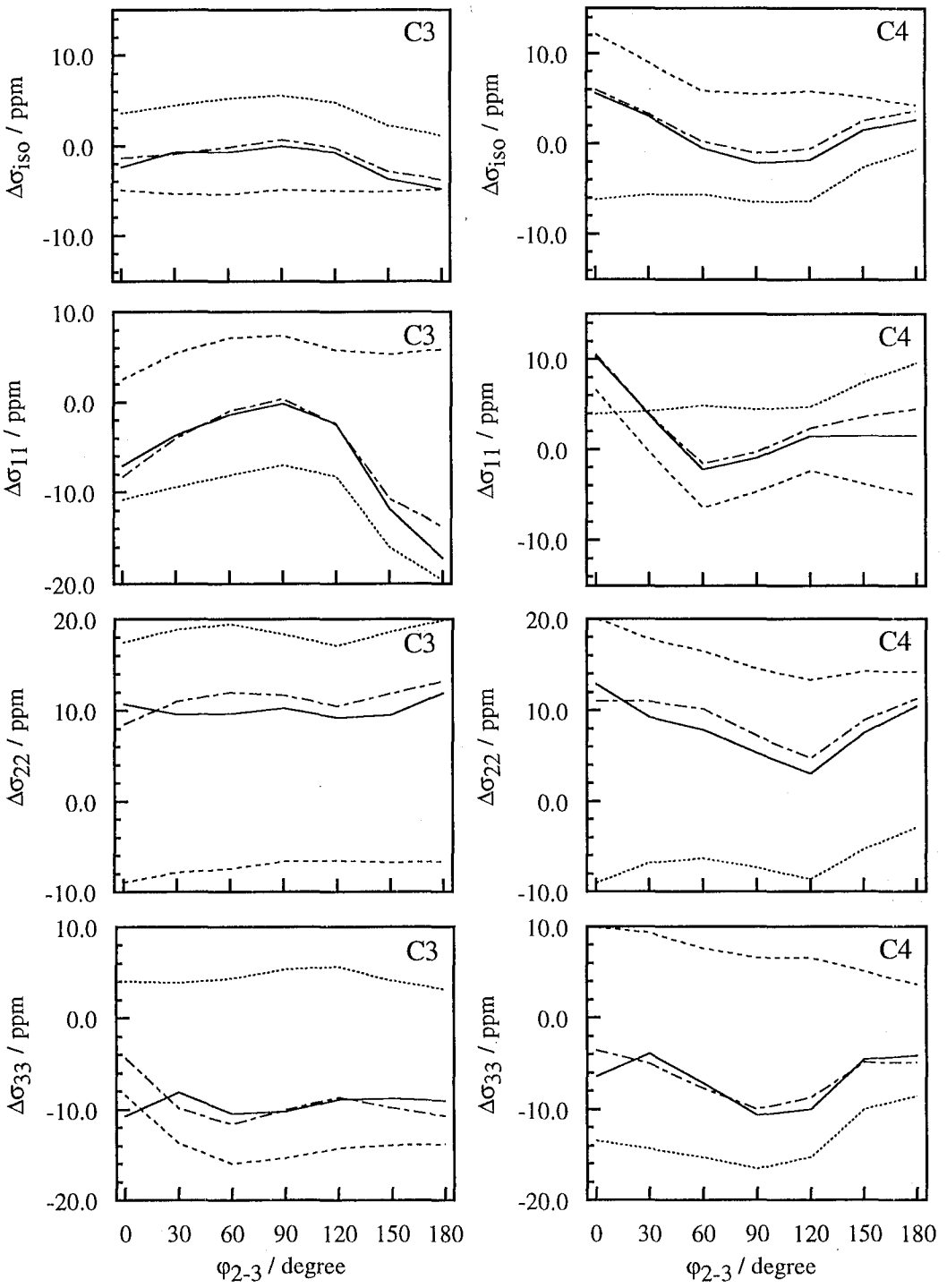

Figure 2.8 (continued)

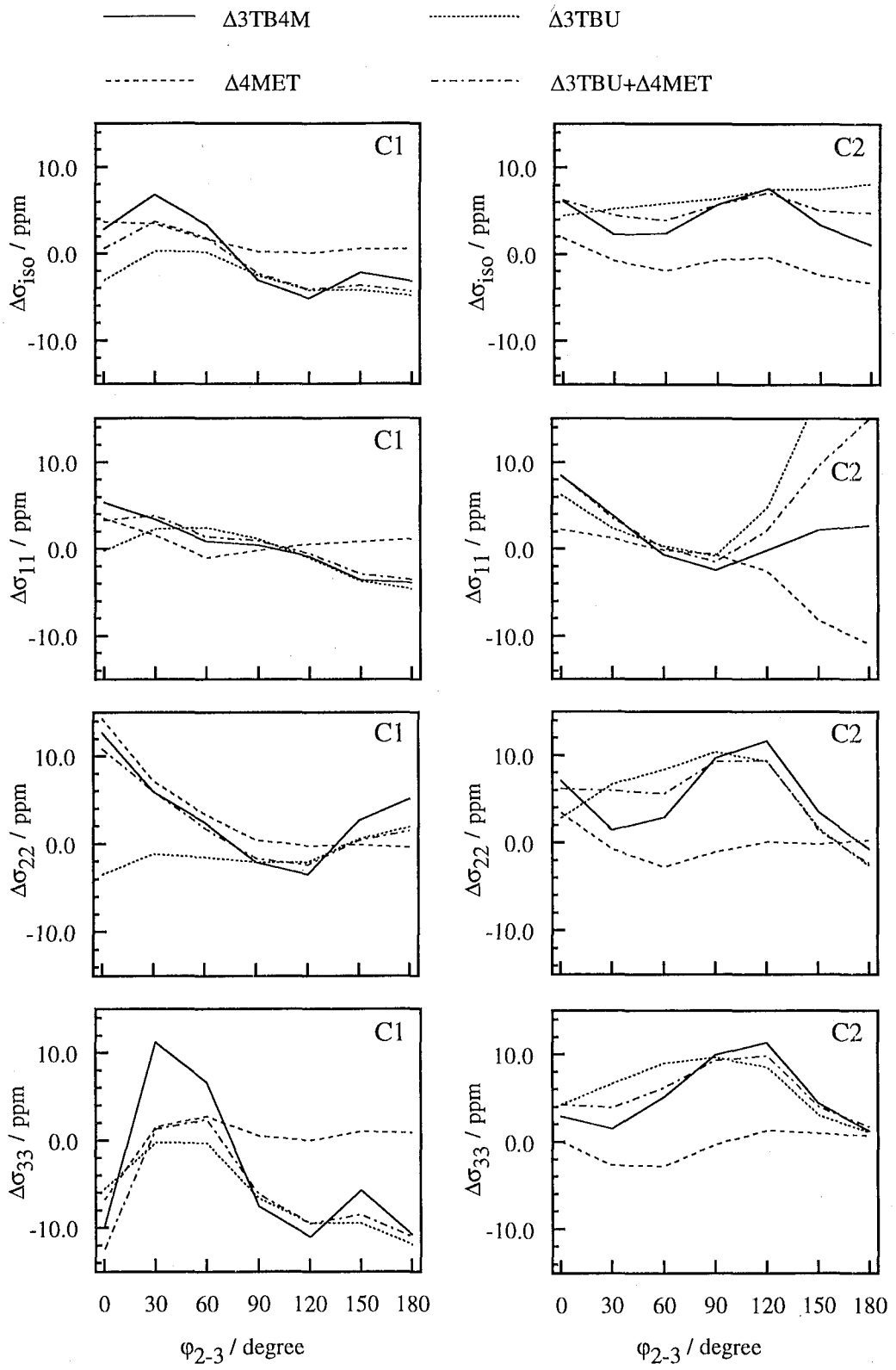

Figure 2.9 Conformation dependence of the shielding parameters of the conjugated carbons in 3TBU, 4MET, and 3TB4M. The value of each shielding parameter is given as the difference from that for the corresponding carbon of HEX with the same angle of $\varphi_{2\text{-}3}$.

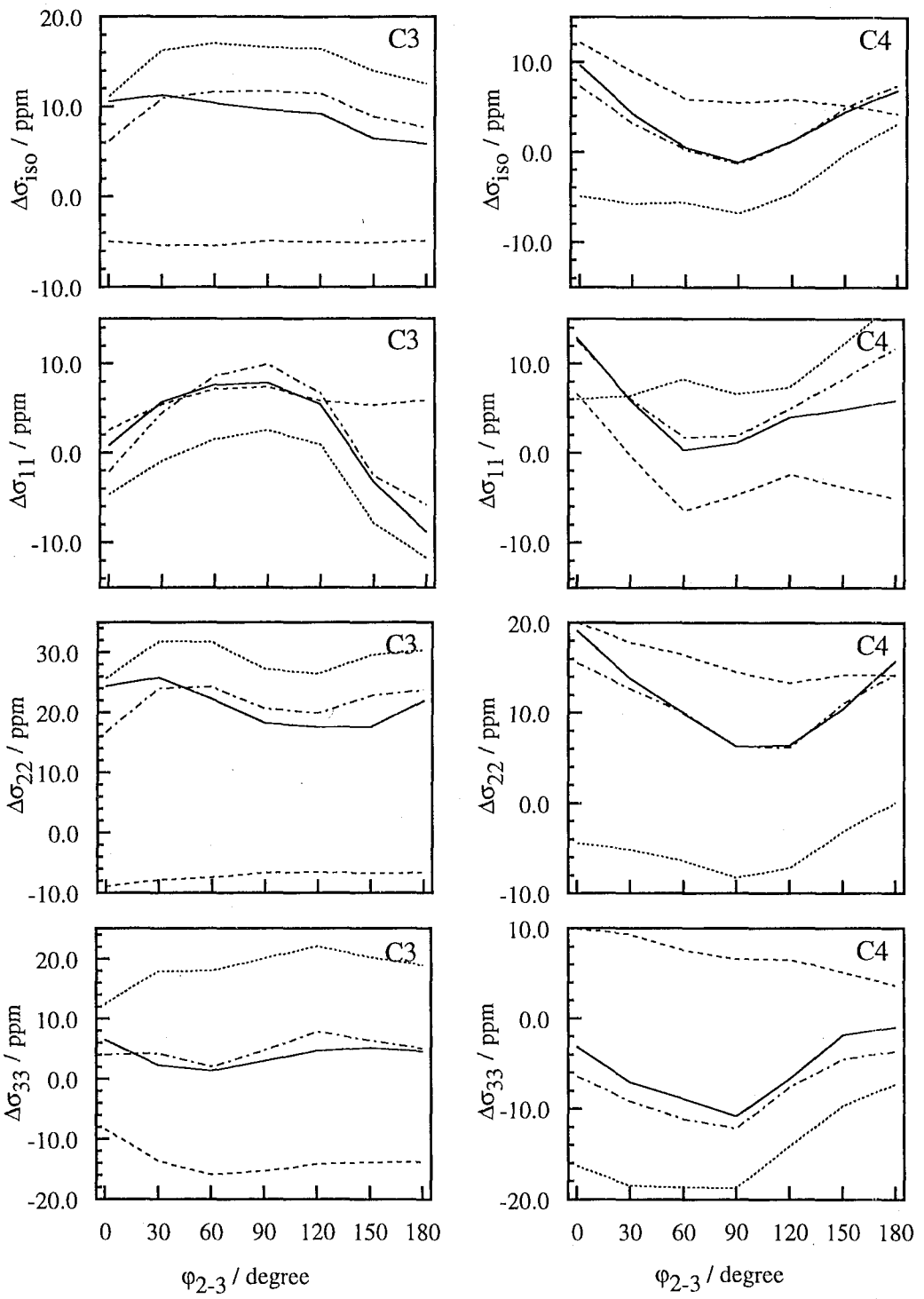

Figure 2.9 (continued)

As found in the data for HEX and HEXAL, the shieldings of the carbons forming the rotating bond exhibits complicated angular dependence. To understand the behavior, one must take into account the effect of π-orbital modification other than the steric and inductive (charge density) effects. Thus, the direct *ab initio* calculation would be required to predict the shielding of such a type of carbon. On the other hand, the shieldings of the other carbons essentially follows the well-known mechanisms including the steric and charge density effects, and so on. Thus, their angular dependence can be understood by using the additivity rule among them and the data for charge density obtained from Mulliken population analysis.

One of the most important findings is that the steric effects are reflected predominantly on the σ_{11} component, and the effects originated in electronic perturbation are on the σ_{22} and σ_{33}. This classification is hardly disturbed even when both types of effects simultaneously act during a conformational change. For example, the σ_{11} and σ_{33} components of C1 (and C4) of HEX are independent of each other. As previously described, the latter changes according to the charge density profile. The former exhibits a steep upfield shift of about 10 ppm on going from $\varphi_{2\text{-}3} = 0°$ to 30° (Figure 2.2). Clearly, this shift can be explained by the γ-steric effect between the C1 and C4 carbons.

These results suggest the possibility that by means of analysis of shielding tensor one may identify the origin of shielding change which is caused by unknown factors. In the final section, the author attempts to analyze the unusual shifts of retinal in Rh.

2.4.2 Availability of the diene data to retinal

To check the availability of the diene data to retinal and its derivatives, the author first selected 11-*cis*-retinal as a target molecule. The shielding calculation for 11-*cis*-retinal was executed for each conformer with a given rotation angle of

C12-C13, which is an angle crucial to interpretation of the chemical shift data for rhodopsin.[20] The angle of $\varphi_{12\text{-}13}$ was defined as the dihedral angle of C11-C12-C13-C14, the value of which is taken to be 180° when the C12-C13 conformation is *s-trans*. In Figure 2.10 the isotropic shieldings of C5 to C14 are plotted as a function of $\varphi_{12\text{-}13}$.

The chamical environment of the C11 carbon is similar to that of the C1 carbon of HEXAL. As can be seen from Figures 2.7 and 2.10, both carbon shieldings exhibit similar conformation dependence, characterized as a concave-type curve with minima located around $\varphi_{12\text{-}13} = 90°$. Similar patterns are also observed for the C9 and C7 shieldings of retinal, although the amplitude in shielding change becomes smaller with increasing distance from the rotating bond: C11>C9>C7>C5. These results imply that the conformation dependence of the C11, C9 , C7 and C5 shieldings follows the same mechanism as the C1 shieldings of HEXAL. Namely, the origin of occurrence of the concave-type curve is attributable to the breaking of the π-conjugation, leading to a reduction of the contribution of the resonance structure in distorted form. The C13 shielding exhibits a different pattern from those for the other odd-numbered carbons, because the carbon is involved in the rotating bond as similar to the C3 carbon of HEXAL.

Among the diene compounds studied, 1C3MAL is the most resemble model to the molecular fragment of 11-*cis*-retinal including C11, C12, C13, and C14 carbons. The calculated isotropic shifts for 1C3MAL are also shown in Figure 2.10. Clearly, the conformation-dependent profiles of the C1, C2, C3, and C4 shieldings of 1C3MAL coincides with those for C11, C12, C13 and C14 of 11-*cis*-retinal. In addition, the conformation dependence of the principal values are also reproduced well by the calculation for the model as shown in Figure 2.11, where the data for the C12 shielding are indicated as an example.

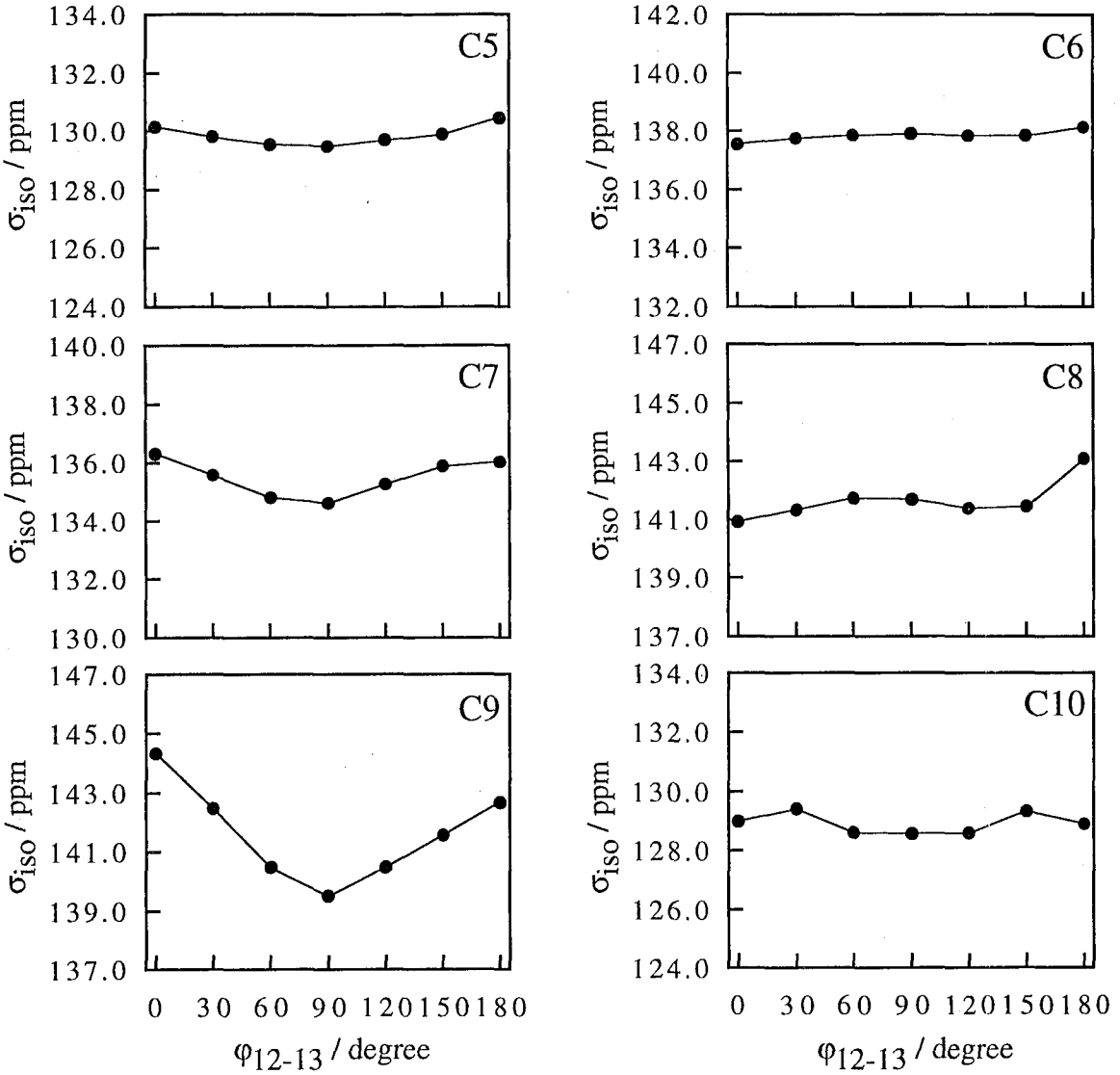

Figure 2.10 Conformation dependence of the isotropic shieldings of conjugated carbons of 11-*cis*-retinal. The data for C1, C2, C3, and C4 of 1C3MAL are also included in the figures for C11, C12, C13, and C14, respectively.

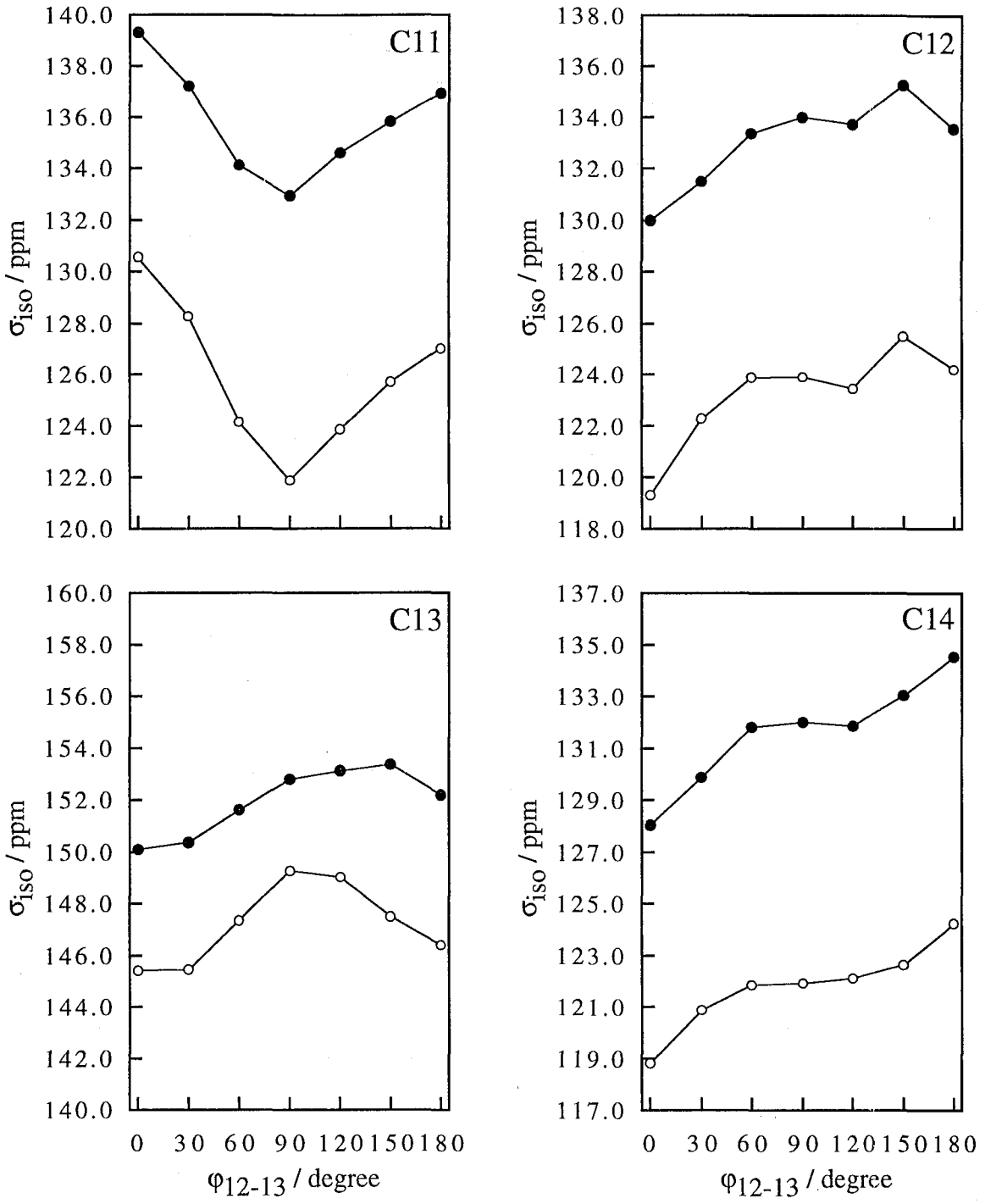

Figure 2.10 (continued)

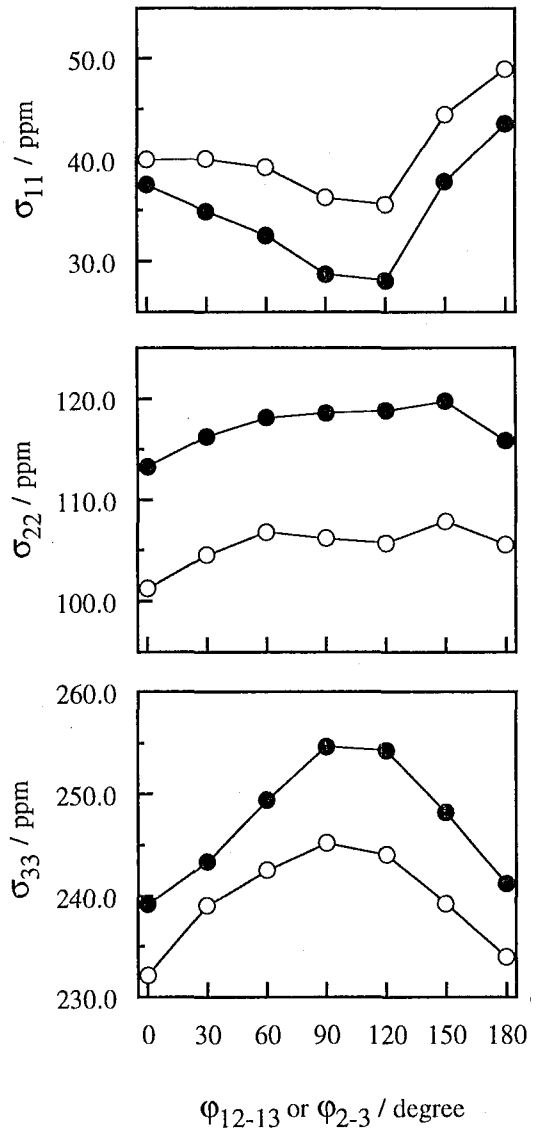

Figure 2.11 Comparison of the principal values for the C12 shielding of 11-*cis*-retinal (●) and those for the C2 shielding of 1C3M (○). The former and latter data are plotted against $\varphi_{12\text{-}13}$ and $\varphi_{2\text{-}3}$, respectively.

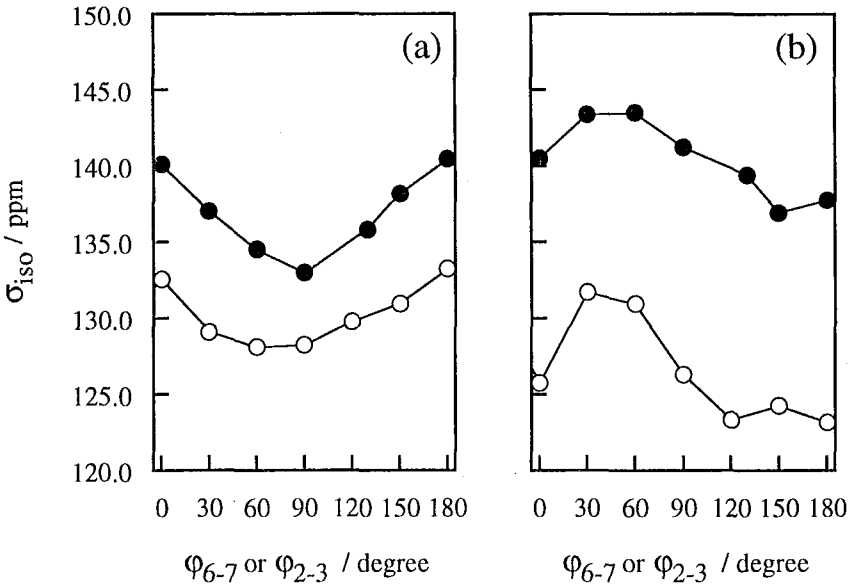

Figure 2.12 Comparison of the isotropic shieldings of conjugated carbons of the retinal analogue (●) and those for 3TB4M (○). The former data are cited from ref. 14. (a) The data for the C5 shielding of the retinal analogue and those for the C4 shielding of 3TB4M. (b) The data for the C8 shielding of the retinal analogue and those for the C1 shielding of 3TB4M. In both (a) and (b), the shielding data for the retinal analogue and 3TB4M are plotted against φ_{6-7} and φ_{2-3}, respectively.

In a previous study using an analogue compound (β-ionylideneacetaldehyde, see Figure 2.1),[14] Wada et al. investigated the change of carbon shieldings as a function of the C6-C7 torsion. In that paper, it was indicated that the C5 shielding shows a concave-type dependence while the C8 shielding does a convex-type. At first sight, such a behavior of C5 and C8 shielding seems to be strange because both carbons locate in the equivalent position to C1 of HEX whose shielding shows a convex-type profile (Figure 2.2). However it can be shown that these profiles represent intrinsic properties of the β-ionone ring moiety. The 3TB4M is an appropriate model, in which C4 and C1 are in similar chemical environments to C5 and C8 of retinal, respectively. As shown in Figure 2.12, the shieldings for C5 and C8 of the retinal analogue coincide with those for C4 and C1 of 3TB4M, respectively. This indicates again that the data for the dienes can be used to interpret the shieldings of carbons apart from the rotating bond.

From these results, the author believes that the data for the present model compounds are applicable to analyze the conformation dependence of chemical shifts of the conjugated carbons of retinal, even if the length of the conjugated chain is shorter than that of retinal's.

2.4.3 The C12-C13 Conformation of the chromophore of Rh

The isotropic shielding of C12 of the chromophore of Rh shows a ~3 ppm downfield shift relative to that of protonated 11-*cis*-retinylidene Schiff base in solution. It has been hypothesized that this shielding difference arises from the electrostatic interaction between the chromophore and charged amino acid(s) of the protein, a model which has been originally proposed by Nakanishi's group.[15] However, there is still no direct evidence for the hypothesis from either theoretical or experimental viewpoint. According to accumulated data for ^{13}C shieldings of conjugated compounds,[19] only a few ppm of shielding change could be also

explained by other factors including nonspecific interactions like solvent effects[43,44] and structural changes of molecules as studied here. Thus, the information on isotropic shielding alone is insufficient to identify the real origin of the above shielding difference. Here an attempt of interpretation of the isotropic shielding is abondoned. Instead, the author focuses on analysis of the principal values of the shielding tensor.

Unfortunately, the solid-state NMR data for 11-*cis*-retinal Schiff base have not been published. Thus, protonated all-*trans*-retinylidene Schiff base was used as a reference compound. There have been two reports which refer to the C12 shielding in the chromophore of Rh (see Table 2.3).[6,7] First, we consider along with Mollevanger's data.[7] Table 2.4 summarizes the differences in the principal values between the C12 shielding of the Rh chromophore and that for the reference. A notable feature is that the σ_{11} and σ_{22} components are largely shifted (-17 ppm and +16 ppm, respectively) as compared with those for the reference. On the basis of the present results for the dienes, σ_{11} reflects steric effects like γ-effect, while σ_{22} and σ_{33} does electronic perturbations to the conjugated systems. It may be thus concluded that the C12 shielding of the Rh chromophore receives both types of effects. Furthermore, the detailed analysis of steric effects, responsible for the change in σ_{11}, may enable us to speculate the conformation about the C12-C13 bond.

Table 2.4 summarizes the calculated values for shielding changes that would be induced on C12 as a result of *trans-cis* isomerization of the C11=C12 double bond and the rotation of the C12-C13 bond. The effect of these factors was estimated first by subtracting the C12 shielding of all-*trans*-retinal from that of 11-*cis*-retinal. When the angle $\varphi_{2\text{-}3}$ is kept to be 180°, the σ_{11} component shifts upfield by 2.7 ppm on going from all-*trans* to 11-*cis*-retinal. 3MET and 1C3M are the minimal models available for examining the effect of the *trans-cis*

Table 2.3 Experimental chemical shift of C12

	σ_{iso}	σ_{11}	σ_{22}	σ_{33}
all-trans PRSB	134.3[a)]	58	133	212
Rh [b)]	132.1	(56)	(131)	(210)
Rh [c)]	133.5	41	149	209

a) ($\sigma_{11}+\sigma_{22}+\sigma_{33}$) / 3
b) taken from ref.6. Each principal value shown in blackets was obtained by subtracting 2 from the corresponding value of *all-trans* PSB.
c) taken from ref.7.

Table 2.4 Comparison between the experimental and calculated data for the shielding parameters of C12

		σ_{iso}	σ_{11}	σ_{22}	σ_{33}
Exp.[a)]		-0.8	-17	+16	-3
Calcd.[b)]	$\varphi_{12\text{-}13} = 180°$	-4.2	-2.7	-2.7	-7.1
(full atom)	$\varphi_{12\text{-}13} = 120°$	-4.0	-18.1	+0.3	+5.9
Calcd.[c)]	$\varphi_{2\text{-}3} = 180°$	-2.2	-6.5	-3.0	-3.1
(model)	$\varphi_{2\text{-}3} = 120°$	-3.2	-19.9	+3.1	+7.0

a) Obtained by subtracting the data for protonated *all-trans*-retinylidene Schiff base (ref.6) from those for rhodopsin (ref.7) (positive sign denotes down field shift).
b) Obtained by subtracting the data for *all-trans*-retinal (ref.14) from those for 11-*cis*-retinal (positive sign denotes down field shift).
c) Obtained by subtracting the data for 3MET from those for 1C3M (positive sign denotes down field shift).

isomerization: C1, C2, C3 and C4 of the models correspond to C11, C12, C13 and C14 of retinal, respectively. As shown in Table 2.4, the σ_{11} component of C2 shifts upfield by 6.5 ppm on going from 3MET to 1C3M. These results indicate that the net effect of the *trans-cis* isomerization on the σ_{11} shielding is not more than several ppm, which is insufficient to explain the above experimental data for Rh.

As the C12-C13 bond of 11-*cis*-retinal is rotated from the *s-trans* form, the σ_{11} shielding gradually shifts upfield. As shown in Figure 2.11, the σ_{11} of C12 exhibits a concave-type profile with a minimum at $\varphi_{2\text{-}3}$ = 90°-120°. When $\varphi_{2\text{-}3}$ equals 120°, the σ_{11} shifts upfield by 18.1 ppm as measured from that of the all-*trans* isomer with $\varphi_{2\text{-}3}$ = 180°. A comparable amount of upfield shift (19.9 ppm) was also obtained from the calculation using the model compounds (Table 2.4). When the C12-C13 takes *s-trans* conformation, the C12 shielding should receive the β_3-steric effect from the C13 methyl. Similarly, the C2 shielding of 1C3M does the effect from the C3 methyl. As previously described in Table 2.2, the β_3-steric effect causes a large downfield shift to the σ_{11} shielding of a carbon of interest. The rotation of the C12-C13 or C2-C3 bond should decrease the β_3-steric effect on the C12 or C2 shielding, resulting in a large upfield shift. Thus, the occurrence of the concave-type profile as shown in Figure 2.11 can be regarded as an intrinsic property of molecules possessing the local structure like 1C3M.

In both cases of retinal and the models, the σ_{11} shielding changes on going from $\varphi_{12\text{-}13}$ ($\varphi_{2\text{-}3}$) = 180° to $\varphi_{12\text{-}13}$ ($\varphi_{2\text{-}3}$) = 120° are quite close to the experimental value for Rh. The uniqueness of such an agreement is assured from Figure 2.11. Therefore, on the basis of Mollevanger results,[7] it can be concluded that the chromophore of Rh takes skewed *s-trans* form around the C12-C13 bond.

Recently, Smith et al.[6] have reexamined the C12 shielding for Rh, and found that the principal values of the C12 shielding tensor are largely unperturbed in comparison with that of *all-trans* protonated retinylidene Schiff base chloride salt

(*all-trans*-PRSB), which is in quite contrast to Mollevanger's results.[7] According to this new finding, it may be reasonable to be concluded that the conformation about the C12-C13 bond is nearly planar trans. However, as can be seen from Table 2.3, an appreciable discrepancy arises in the isotropic shielding on the assumption that all the principal values of the C12 shielding equal between the Rh and *all-trans* PSB cases. Namely, the isotropic shielding (134.3 ppm) calculated from the principal values shifts to downfield about 2 ppm relative to the actually observed value (132.1 ppm) for Rh. Such a discrepancy may arise from the fact that *all-trans* isomer is used as a reference compound. To consistently explain both isotropic shielding and principal values for Rh, it is sufficient to be assumed that each of the principal values for Rh is actually about 2 ppm smaller than those for *all-trans* PSB: namely, σ_{11}, σ_{22}, and σ_{33} are 56, 131, 210 ppm, respectively. Such a modification does not bring about any change on the value of magnetic anisotropy and the NMR spectral pattern (shown in Figure 4 B of reference 6).

The present calculation provides information about what extent of shielding change is induced for the isotropic shielding of C12 purely as a result of *cis-trans* isomerization of the C11-C12 bond. As shown in Table 2.4, a 2-4 ppm of downfield shift is expected on going from *cis* to *trans* isomerization when the rotational angle about the C12-C13 bond is kept 180°. In addition, each of the principal values exhibits a similar amount of downfield shift, although the shielding change of σ_{33} for retinal and that of σ_{11} for the model are somewhat larger. Consequently, the major part of the above discrepancy between Rh and all-trans PSB could be ascribed to the difference in the configuration of the C11-C12 bond. Therefore, on the basis of the later NMR results given by Smith et al., it could be accepted that the C12-C13 conformation of the Rh chromophore takes nearly planar trans one, in agreement with that of *all-trans* PSB.

One of the main purposes in this study is to present a theoretical procedure by which a conformational structure of linear polyene is deduced from given experimental data for isotropic shieldings and the corresponding principal values. As described above, this was successfully achieved by using the chromophore of Rh as an example of linear polyene. A biologically significant finding is that the occurrence of 12-*s-trans* conformer alone is deduced from both of the two different sets of experimental data, although there is a difference in the rotational angle about the C12-C13 bond.

Throughout this section, the author focused mainly on the C12 shielding of the chromophore, because our attention was given to the conformational property about the C12-C13 bond. However, for a thorough understanding of interactions of the retinal chromophore with opsin, it is necessary to consistently explain the occurrence of the shielding differences extending over several carbon atoms from C5 to C14. A recent theoretical study[16,17] has successfully indicated that such shielding differences can be interpreted in terms of charge polarization effects on the conjugated system by the putative Glu side chain. In that study, the conformation of the C12-C13 bond was assumed to be *s-trans*, the validity of which is supported by the present calculation.

§2.5 Concluding Remarks

The results for the dienes can be summarized as follows: (1) The presence of effect uniquely occurring in the conjugated systems, called π-orbital modification effect, was evidenced with rigorous theoretical analysis; (2) Some characteristics of the steric and substituent effects in acting for the conjugated system were revealed with tensor analysis; (3) The additivity of all the effects studied was confirmed. In addition to these results, the direct *ab initio* shielding calculation of 11-*cis*-retinal

enabled us to determine the preferred conformation around the C12-C13 bond of the chromophore in Rh.

An earlier theoretical study[45] has indicated that there are two energy minima at skewed *s-trans* and skewed *s-cis* conformations around the C12-C13 bond of 11-*cis*-retinal. According to NMR studies of protonated 11-*cis*-retinal Schiff base, in solution the thermal equilibrium holds between the two conformers.[46] The C12-C13 conformation is a key factor to determine the orientation of the chromophore in the protein pocket, and thereby the chromophore-protein interaction. In spite of this, the C12-C13 conformation of the chromophore in Rh has not been determined yet, probably because there is no direct method available to determine the conformational population in the protein. This study is the first one to answer this problem.

References and Notes

(1) See for reviews: (a) Birge, R.R *Ann. Rev. Phys. Chem.*, **1990**, *41*, 683. (b) Lanyi, J.K.; *Biochem. Biophys. Acta.*, **1993**, 1183, 241. (c) Nathans, J. *Biochemistry*, **1992**, *31*, 4923. (d) Khorana, H.G *Ann. N. Y. Acad. Sci.*, **1986**, *471*, 272. (e) Mathies, R.A.; Lin, S.W.; Ames, J.B.; Pollard, W.T. *Ann. Rev. Biophys. Biophys. Chem.*, **1991**, *20*, 491. (f) Nakanishi, K. *Pure Appl. Chem.*, **1991**, *63*, 161. (g) Ottolenghi, M.; Sheves, M.; *J. Membrane Biol.*, **1989**, *112*, 193.

(2) van der Steen, R.; Biesheuvel, P.L.; Mathies, R.A.; Lugtenberg, J. *J. Am. Chem. Soc.*, **1986**, *108*, 6410.

(3) Henderson, R.; Baldwin, J.M.; Ceska, T.A.; Zemlin, F.; Beckmann, E.; Downing, K.H. *J. Mol. Biol.*, **1990**, *213*, 899.

(4) Unger, V.M.; Schertler, G.F.X. *Biophys. J.*, **1995**, *68*, 1776.

(5) Smith, S.O.; Palings, I.; Copié, V.; Raleigh, D.P.; Courtin, J; Pardoen, J.A.; Lugtenburg, J.; Mathies, R.A.; Griffin, R.G. *Biochemistry*, **1987**, *26*, 1606.

(6) Smith, S.O.; Palings, I.; Miley, M.E.; Courtin, J; de Groot, H.; Lugtenburg, J.; Mathies, R.A.; Griffin, R.G. *Biochemistry*, **1990**, *29*, 8158.

(7) Mollevanger, L.C.P.J.; Kentgens, A.P.M.; Pardoen, J.A.; Courtin, J.M.L.; Veeman, W.S.; Lugtenburg, J.; de Grip, W.J. *Eur. J. Biochem.*, **1987**, *163*, 9.

(8) Harbison, G.S.; Smith, S.O.; Pardoen, J.A.; Mulder, P.P.J.; Lugtenburg, J.; Hertzfeld, J.; Mathies, R.A.; Griffin, R.G. *Biochemistry*, **1984**, *23*, 2662.

(9) Harbison, G.S.; Smith, S.O.; Pardoen, J.A.; Courtin, J.M.L.; Lugtenburg, J.; Hertzfeld, J.; Mathies, R.A.; Griffin, R.G. *Biochemistry*, **1985**, *24*, 6955.

(10) Smith, S.O.; de Groot, H.J.M.; Gebhard, R.; Courtin, J.M.L.; Lugtenburg, J.; Hertzfeld, J.; Griffin, R.G. *Biochemistry*, **1989**, *28*, 8897.

(11) Smith, S.O.; Courtin, J.; de Groot, H.; Gebhard, R.; Lugtenburg, J. *Biochemistry*, **1991**, *30*, 7409.

(12) Smith, S.O.; de Groot, H.; Gebhard, R.; Lugtenburg, J. *Photochem. Photobiol.*, **1992**, *56*, 1035.

(13) Smith, S.O.; Courtin, J.; van den Berg, E.; Winkel, C.; Lugtenburg, J.; Hertzfeld, J.; Griffin, R.G. *Biochemistry*, **1989**, *28*, 237.

(14) Wada, M.; Sakurai, M.; Inoue, Y.; Tamura, Y; Watanabe, Y. *J. Am. Chem. Soc.*, **1994**, *116*, 1537.

(15) Wada, M.; Sakurai, M.; Inoue, Y.; Tamura, Y; Watanabe, Y. *J. Phys. Chem.*, **1996**, *100*, 1957.

(16) Han, M.; DeDecker, B.S.; Smith, S.O. *Biophys. J.*, **1993**, *65*, 899.

(17) Han, M.; Smith, S.O. *Biochemistry*, **1995**, *34*, 1425.

(18) Honig, B.; Dinur, U.; Nakanishi, K.; Balogh-Nair, V.; Gawinowicz, M.A.; Arnaboldi, M.; Motto, M.G. *J. Am. Chem. Soc.*, **1979**, *101*, 7084.

(19) Stothers, J.B. *Carbon-13 NMR Spectroscopy*; Academic Press: New York, 1972; pp 55-207.

(20) Houjou, H.; Sakurai, M.; Asakawa, N.; Inoue, Y.; Tamura, Y.; Watanabe, Y. *Chem. Lett.*, **1995**, 1039.

(21) Barfield, M.;Yamamura,S.H. *J. Am. Chem. Soc.*, **1990**, *112*, 4747.

(22) Barfield, M. *J. Am. Chem. Soc.*, **1993**, *115*, 6916.

(23) Barfield, M. *J. Am. Chem. Soc.*, **1995**, *117*, 2862.

(24) Kurosu, H.; Ando, I.; Webb, G.A. *Magn.Resn.Chem.*, **1993**, *31*, 399.

(25) Sulzbach, H.M.; Schleyer, Pv.R.; Schafer III, H.F. *J. Am. Chem. Soc.*, **1994**, *116*, 3967.

(26) de Dios, A.C.; Oldfield, E. *J. Am. Chem. Soc.*, **1994**, *116*, 5307.

(27) Jiao, D.; Barfield, M.; Combariza, J.E.; Hurby, V.J. *J. Am. Chem. Soc.*, **1992**, *114*, 3639.

(28) Soderquist, A.; Facelli, J.C.; Horton, W.J.; Grant, D.M. *J. Am. Chem. Soc.*, **1995**, *117*, 8441.

(29) The calculation in ref. 14 shows that the dihedral angle of C2-C1-C6-C5 of the retinal analogue maintains 10°-25° throughout the rotation of C6-C7.

(30) Gilardi, R.D.; Karle, I.L.; Karle, J. *Acta cryst.*, **1972**, *B28*, 2605.

(31) (a) Frisch, M.J.; Head-Gordon, M.; Trucks, G.W.; Foresman, J.B.; Schlegel, H.B.; Raghavachari, K.; Robb, M.; Binkley, J.S.; Gonzalez, C.; Defrees, D.J.; Fox, D.J.; Whitesie, R.A.; Seeger, R.; Merius, C.F.; Baker, J.; Martin, R.L.; Kahn, L.R.; Stewart, J.J.P.; Topiol, S.; Pople, J.A. GAUSSIAN90, Revision J; Gaussian, inc.: Pittsburgh, PA, 1990. (b)Frisch, M.J.; Trucks, G.W.; Head-Gordon, M.; Gill, P.M.W.; Wong, M.W.; Foresman, J.B.; Johnson, B.G.; Schlegel, H.B.; Robb, M.; Replogle, E.S.; Gomperts, R.; Andres, J.L.; Raghavachari, K.; Binkley, J.S.; Gonzalez, C.; Martin, R.L.; Fox, D.J.; Defrees, D.J.; Baker, J.; Stewart, J.J.P.; Pople, J.A. GAUSSIAN92, Revision B; Gaussian, inc.: Pittsburgh, PA, 1992. (c) Frisch, M.J.; Trucks, G.W.; Schlegel, H.B.; Gill, P.M.W.; Johnson, B.G.; Robb, M.A.; Cheeseman, J.R.; Keith, T.; Petersson, G.A.; Montgomery, J.A.; Raghavachari, K.; Al-Laham, M.A.; Zakrzewski, V.G.; Ortiz, J.V.; Foresman, J.B.; Cioslowski, J.; Stefanov, B.B.; Nanayakkara, A.; Challacombe, M.; Peng, C.Y.; Ayala, P.Y.; Chen, W.; Wong, M.W.; Andres, J.L.; Replogle, E.S.; Gomperts, R.; Martin, R.L.; Fox, D.J.; Binkley, J.S.; Defrees, D.J.; Baker, J.; Stewart, J.P.; Head-Gordon, M.; Gonzalez, C.; Pople, J.A. GAUSSIAN94, Revision B.2; Gaussian, inc.: Pittsburgh PA, 1995.

(32) Ditchfield, R.; Ellis, P.D. *Topics in Carbon-13 NMR Spectroscopy*; Levy, G.C. Ed., John Wiley & Sons: New York, 1974; pp18-34.

(33) Bouman, T.D.; Hansen, A.E. RPAC Ver. 9.0; 1991.

(34) Hansen, A.E.; Bouman, T.D. *J. Chem. Phys.*, **1985**, *82*, 5035.

(35) Facelli, J.C.; Grant, D.M.; Bouman, T.D.; Hansen, A.E. *J. Comput. Chem.*, **1990**, *11*, 32.

(36) Stewart, J.J.P. *Comput. Chem.*, **1989**, *10*, 209.

(37) Stewart, J.J.P.; Frank, J. MOPAC Ver.6.01; Seilar Reserch Laboratory, U.S.Air Force Academy:Colorado Springs, CO 80840-6528, 1989.

(38) Wada, M.; Sakurai, M.; Inoue, Y.; Tamura, Y; Watanabe, Y. *Magn. Reson. Chem.*, **1995**, *33*, 453.

(39) Hehre, W.J.; Radom, L.; Schleyer, P.v.R.; Pople, J.A. *Ab Initio Molecular Orbital Theory*; John Wiley & Sons: New York, 1986; pp 65-88.

(40) Ramsey, N. *Phys. Rev.*, **1952**, *86*, 243.

(41) Ebraheem, K.A.K.; Webb, G.A. *Prog. NMR Spectrosc.*, **1977**, *11*, 149.

(42) Harbison, G.S.; Mulder, P.J.J.; Perdon, H.; Lugtenberg, J.; Herzfeld, J.; Griffin, R.G. *J. Am. Chem. Soc.*, **1985**, *107*, 4809.

(43) Sakurai, M.; Hoshi, H.; Inoue, Y.; Chujo, R. *Bull. Chem. Soc. Jpn.*, **1990**, *63*, 1335.

(44) Sakurai, M.; Ando, I.; Inoue, Y.; Chujo, R. *Photochem. Photobiol.*, **1981**, *34*, 367.

(45) Honig, B.; Karplus, M. *Nature*, **1971**, *229*, 558.

(46) Shriver, J.W.; Mateescu, G.D.; Abrahamson, E.W. *Biochemistry*, **1979**, *18*, 4785.

Chapter 3. Formulation of a Method for Theoretical Evaluation of Medium Effects on Absorption Spectra

§3.1 Introduction

Theoretical evaluation of solvent effects on the absorption maxima of molecules is important not only from the viewpoint of pure quantum chemical interest but also from practical use for elucidating the mechanisms of solvatochromic shifts observed for organic and biological molecules. Several methods have been proposed for the calculation of solvent effects on optical properties of molecules in the framework of a continuum dielectric approach, including early models based on the perturbation theory[1,2] and the so-called self-consistent reaction field polarizable continuum model (SCRF-PCM) .[3-9] The latter allows for a very efficient implementation of solvation effects into the configuration interaction (CI) part of molecular orbital calculation, and hence it is expected to become a standard methodology at least for semi-quantitative analysis of excitation energies.

The SCRF-PCM itself has been successfully developed as a methodology applicable to ground-state solvation phenomena. However, in spite of much effort, the formalism for coupling it to the CI calculation seems to be insufficient. In order to clarify this point, the author briefly summarizes the fundamental scheme in which the SCRF-PCM is applied to molecular excitation. A solute molecule causes a polarization in the surrounding dielectric, leading to the generation of a reaction field. For the ground-state, the polarization of the dielectric is assumed to be composed of an orientational contribution and an inductive or electronic one of solvent molecules. Upon excitation, the solute molecule alters its charge distribution. Subsequently the rapid relaxation of the solvent polarization occurs so as to stabilizes the excited state. Considering vertical electronic excitation, the

relaxation is assumed to be induced only by a change in the electronic polarization of the solvent molecules with their orientations being frozen.

Therefore, the first necessary condition to correctly describe the solvation of excited molecules is that the solvent polarization is correctly partitioned into the orientational and electronic contributions. As pointed by Klamt,[6] several SCRF-PCMs were formulated on the erroneous assumption that the orientational and electronic polarization contributions are additive. Recently, correct formalisms have been given by Klamt[6] and Aguilar et al.,[5b] who constructed new theories based on the fact that electric susceptibility has an additive property. The second necessary condition is to clarify what physical meaning is given to the excitation energy obtained directly from the CI calculation. Karelson and Zerner have indicated that the solvent effect is incorporated "automatically" into the CI only by adding solute-solvent interaction term(s) to the Fock matrix elements for the *in vacuo* state, but the resulting excitation energy must be corrected for the electronic relaxation and for the costs required for the polarization of solvent (model A in ref.4). They obtained the final expression of the excitation energy as the sum of the term directly obtained from CI and these correction terms (eq.26a in ref.4). Similarly, Klamt derived the correction term corresponding to the electronic relaxation (denoted "electronic screening correction" in ref.6), and the diagonal correction in the CI matrix (see eq.10 in ref.6). The third necessary condition is to clarify how the CI matrix elements, including the off-diagonal elements, are modified by the solute-solvent interaction. Probably, one more condition is required for a better description of solvated molecules, although it is not limited to the case of excited molecules. That is, the shape of the cavity in which the solute molecule is embedded must be determined so as to fit its actual shape. In addition, the charge distribution of the solute is treated realistically without being approximated by the classical electrostatics such as multipole expansions.

As far as the author knows, there is no SCRF model simultaneously satisfying the above four conditions. For example, the studies by Klamt[6] and Aguilar et al.[5b] did not give the off-diagonal elements of the CI matrix. Instead, the model proposed by Karelson and Zerner has the limitation that the charge distribution of a solute molecule must be described in the framework of the classical electrostatics and the cavity shape taken to be spherical.

During the past decade, Sakurai's group have developed an SCRF method which is formulated by utilizing the boundary element method (BEM).[10,11] In this method, the solute charge distribution can be quantum-chemically treated and no limitation for the cavity shape is imposed, indicating that the fourth condition is satisfied. In addition, the solute-solvent interactions are rigorously given with matrix representation, facilitating the construction of the CI matrix including solvent effects. Recently, a method quite similar to Sakurai's has been reported by Tomasi's group, as a modified version of their original SCRF method.[5c] A great success in applying Sakurai's method to various ground-state solvation problems[12] makes me expect it to provide good perspective for excited-states solvation phenomena as well.

In this chapter, the author formulates a new theory of the SCRF-PCM satisfying the above four conditions in the framework of the single excitation CI method. In addition, the result of a test calculation for a merocyanine dye is described. It will be shown that the calculated solvatochromic shifts are in excellent agreement with available experimental data.

§3.2 Theory

3.2.1 Outline of the Ground-State Solvation Theory

Here, the author briefly describes the PCM method developed by Sakurai et al..[10] In this method, a solute molecule is represented by a charge distribution $\rho(r)$

in the cavity embedded in an infinite polarizable dielectric medium. The charge distribution induces the polarization of dielectrics, so that the reaction field is generated which acts back on the solute molecule. The Hamiltonian $\mathcal{H}$ of the solute is written by

$$\mathcal{H} = \mathcal{H}_0 + \mathcal{V} \tag{3.1}$$

where $\mathcal{H}_0$ is the Hamiltonian of the solute molecule *in vacuo* and $\mathcal{V}$ is the perturbation term representing the effect of the reaction field. The electronic state of the solute molecule is determined by solving the following Schrödinger equation

$$\mathcal{H}|\Psi\rangle = E|\Psi\rangle \tag{3.2}$$

The reaction field actually originates in the surface charges $\sigma(s)$ induced on the boundary by the polarization of dielectrics. The interaction $\mathcal{V}$ is then represented by

$$\mathcal{V} = \int dr\ \hat{\rho}(r) \int_\Gamma ds\ \frac{\sigma(s)}{|r - s|} \tag{3.3}$$

where the surface integral in the second term is taken over the entire boundary surface Γ. According to the type of particle pair that interacts with each other through the reaction field, the perturbation energy $\mathcal{V}$ can be divided into four parts: electron-electron term $\mathcal{V}_{ee}$, core-electron term $\mathcal{V}_{ce}$, electron-core term $\mathcal{V}_{ec}$, and core-core term $\mathcal{V}_{cc}$.

$$\mathcal{V} = \mathcal{V}_{ee} + \mathcal{V}_{ce} + \mathcal{V}_{ec} + \mathcal{V}_{cc} \tag{3.4}$$

The physical meanings of these terms are as follows. $\mathcal{V}_{ee}$ is the potential energy of electrons placed in the reaction field which is induced by the presence of the electrons themselves. $\mathcal{V}_{ce}$ is the potential energy of electrons placed in the reaction field which is induced by the presence of nuclei. $\mathcal{V}_{ec}$ is the potential energy of nuclei placed in the reaction field which is induced by the presence of electrons. $\mathcal{V}_{cc}$ is the potential energy of nuclei placed in the reaction field which is induced by the presence of the nuclei themselves.

The matrix expression of each term on the right hand side of eq. 3.4 is given for the ground state as follows:

$$\langle \Psi_0 | \mathcal{V}_{ee} | \Psi_0 \rangle = \mathbf{P}_0\mathbf{T}\mathbf{P}_0 \qquad (3.5a)$$

$$\langle \Psi_0 | \mathcal{V}_{ce} | \Psi_0 \rangle = \mathbf{P}_0\mathbf{J}_1 \qquad (3.5b)$$

$$\langle \Psi_0 | \mathcal{V}_{ec} | \Psi_0 \rangle = \mathbf{J}_2\mathbf{P}_0 \qquad (3.5c)$$

$$\langle \Psi_0 | \mathcal{V}_{cc} | \Psi_0 \rangle = \mathbf{B} \qquad (3.5d)$$

where P_0 is the electron density matrix of the solute in the ground state and $\mathbf{T}$, $\mathbf{J}_1$, $\mathbf{J}_2$, $\mathbf{B}$ are matrices whose elements depend only on the geometry of the solute, the dielectric constant of the medium and the shape of the cavity (see Appendix 3A). The matrix $\mathbf{T}$ has a role in mediating the interaction between the initial electronic distribution of the solute molecule and the reaction field originated in itself. The roles of $\mathbf{J}_1$, $\mathbf{J}_2$, $\mathbf{B}$ can be interpreted in a similar way. The physical meanings of these matrices are schematically represented in Figure 3.1(a).

Since the work required for the polarization of the dielectric, i.e. electrostatic energy among the surface charges, is given by 1/2 $\langle \Psi | \mathcal{V} | \Psi \rangle$, the Helmholtz free energy A of the whole system is given by

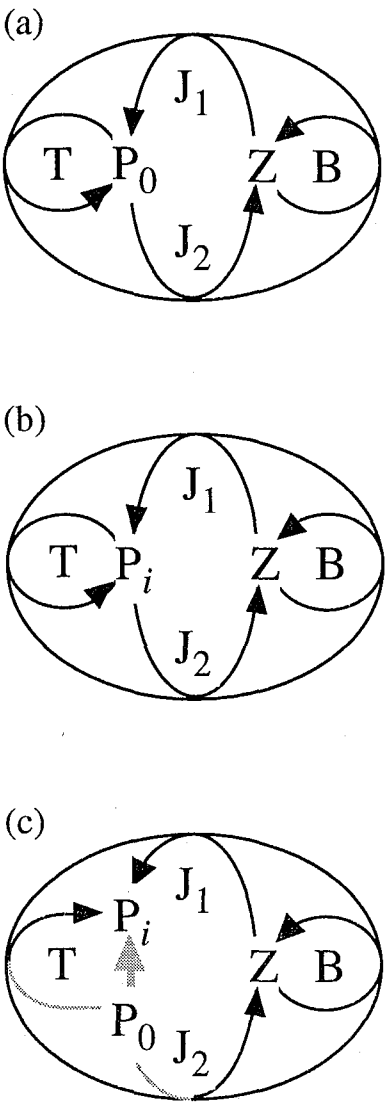

Figure 3.1 Schematic representation showing the physical meanings of the reaction field matrices.
Solid arrows indicate the routes connecting the source of a reaction field (P or Z) with the charge distribution (P or Z) finally interacting with it, where P and Z are the electronic and nuclear charge distribution of a solute molecule, respectively. (a) indicates all the modes of the interactions in the ground state. (b) and (c) correspond to the solvations of excited states on the assumption of infinitely-fast relaxation of the medium and of infinitely-slow relaxation, respectively. A shaded arrow in (c) denotes the rearrangement of the electronic distribution caused by excitation.

$$A = \langle\Psi|\,\mathcal{H}\,|\Psi\rangle - 1/2\,\langle\Psi|\,\mathcal{V}\,|\Psi\rangle$$
$$= \langle\Psi|\,\mathcal{H}_0\,|\Psi\rangle + 1/2\,\langle\Psi|\,\mathcal{V}\,|\Psi\rangle \qquad (3.6)$$

If we focus on the ground state Ψ_0, the Helmholtz energy is given by

$$A_0 = \langle\Psi_0|\,\mathcal{H}_0\,|\Psi_0\rangle + 1/2\,\langle\Psi_0|\,\mathcal{V}\,|\Psi_0\rangle$$
$$= E_0 + 1/2\,V_0 \qquad (3.7)$$

where E_0 is the energy of the solute itself and V_0 is the interaction energy between the solute and the medium. Combining the eqs. 3.4, 3.5 and 3.7, the energy V_0 is given by

$$V_0 = \mathbf{P}_0\mathbf{T}\mathbf{P}_0 + \mathbf{P}_0\mathbf{J}_1 + \mathbf{J}_2\mathbf{P}_0 + \mathbf{B} \qquad (3.8)$$

3.2.2 Solvation Effects on Excitation Energy

In this section the author attempts to extend the above theory so as to be applicable to excited states. Upon excitation, the electronic distribution of the solute molecule is altered. The surface charges must be thus rearranged, corresponding to the relaxation of solvent polarization. Here, we consider two extreme cases different in the rate of relaxation.

In the first case, the medium instantaneously re-polarizes following the change in the electronic distribution of the solute molecule. Then, the interaction energy V_i $(= \langle\Psi_i|\,\mathcal{V}\,|\Psi_i\rangle)$ between the solute and the medium is given as follows:

$$V_i^{\mathrm{f}} = \mathbf{P}_i\,\mathbf{T}\mathbf{P}_i + \mathbf{P}_i\,\mathbf{J}_1 + \mathbf{J}_2\,\mathbf{P}_i + \mathbf{B} \qquad (3.9)$$

where $\mathbf{P}_i$ is the density matrix for an excited state Ψ_i. In this case the excited

molecule receives the reaction field which originates in the charge distribution of its own (see Figure 3.1(b)). From eqs. 3.6, 3.8 and 3.9, the difference in the Helmholtz energy between the ground and the excited state is given by

$$\begin{aligned}\Delta A_i^{\mathrm{f}} &= A_i - A_0 \\ &= E_i - E_0 + 1/2\ \{\mathbf{P}_i\,\mathbf{T}\mathbf{P}_i\ - \mathbf{P}_0\mathbf{T}\mathbf{P}_0 \\ &\qquad + (\mathbf{P}_i\ - \mathbf{P}_0)\mathbf{J}_1 + \mathbf{J}_2\,(\mathbf{P}_i\ - \mathbf{P}_0)\}\end{aligned} \tag{3.10}$$

where E_i $(= \langle \Psi_i | \mathcal{H}_0 | \Psi_i \rangle)$ is the energy of the solute in the excited state Ψ_i. Equation 3.10 gives the excitation energy under the condition of extremely-fast relaxation.

In the second case, the polarization of the medium is unchanged during the excitation, that is, the relaxation is infinitely slow. Then the perturbation energy V_i^{s} is written by

$$V_i^{\mathrm{s}} = \mathbf{P}_i\,\mathbf{T}\mathbf{P}_0 + \mathbf{P}_i\,\mathbf{J}_1 + \mathbf{J}_2\,\mathbf{P}_0 + \mathbf{B} \tag{3.11}$$

This equation means that the excited molecule receives the reaction field generated from the charge distribution in the ground-state (see Figure 3.1(c)). Then from eqs. 3.6, 3.8 and 3.11, the excitation energy ΔA_i^{s} is given in a manner similar to the first case,

$$\Delta A_i^{\mathrm{s}} = E_i - E_0 + 1/2\ \{(\mathbf{P}_i\ - \mathbf{P}_0)\mathbf{T}\mathbf{P}_0 + (\mathbf{P}_i\ - \mathbf{P}_0)\mathbf{J}_1\} \tag{3.12}$$

The condition that each of the above extreme cases is realized is expressed using a frequency-dependent dielectric constant $\varepsilon(\omega)$ of solvent. Here, we denote $\varepsilon(0)$ as $\varepsilon_{\mathrm{stat}}$, indicating a static dielectric constant, and do $\varepsilon(\infty)$ as $\varepsilon_{\mathrm{opt}}$, the dielectric

constant for an infinitely high (optical) frequency. ε_{opt} is nearly equal to n^2, the square of the refractive index. The first case (eq. 3.10) is realized only when ε_{opt} is equal to ε_{stat}, while the second case (eq. 3.12) corresponds to the condition of $\varepsilon_{opt}=1$.

In actual solvents, ε_{stat} involves both contributions of orientational and electronic polarizations, and thereby their relaxation behavior should be expressed by correcting the effect of ε_{stat} for that of ε_{opt} corresponding to the electronic polarization. Therefore the perturbation energy is written by

$$V_i = \mathbf{P}_i \mathbf{T}_{stat}\mathbf{P}_0 + \mathbf{P}_i \mathbf{J}_{1stat} + \mathbf{J}_{2stat} \mathbf{P}_0 + \mathbf{B}_{stat} + \mathbf{P}_i\mathbf{T}_{opt} (\mathbf{P}_i - \mathbf{P}_0) + \mathbf{J}_{2opt} (\mathbf{P}_i - \mathbf{P}_0) \qquad (3.13)$$

where the subscripts "stat" and "opt" indicate that the corresponding matrix is a function of ε_{stat} and ε_{opt}, respectively The fifth and sixth terms on the right hand side of eq. 3.13 are the correction terms expressing the electronic part of relaxation. Then, from eqs. 3.6, 3.8 and 3.13, we can obtain the following expression for the excitation energy :

$$\Delta A_i = E_i - E_0 + 1/2 \{(\mathbf{P}_i - \mathbf{P}_0)\mathbf{T}_{stat}\mathbf{P}_0 + (\mathbf{P}_i - \mathbf{P}_0)\mathbf{J}_{1stat} + \mathbf{P}_i\mathbf{T}_{opt} (\mathbf{P}_i - \mathbf{P}_0) + \mathbf{J}_{2opt} (\mathbf{P}_i - \mathbf{P}_0)\} \qquad (3.14)$$

This equation is identical to eq. 3.10 when $\mathbf{J}_{2opt}$ and $\mathbf{T}_{opt}$ are equal to $\mathbf{J}_{2stat}$ and $\mathbf{T}_{stat}$, respectively, and identical to eq. 3.12 when both $\mathbf{J}_{2opt}$ and $\mathbf{T}_{opt}$ vanish.

3.2.3 Correction of the CI Matrix

The single excitation configuration interaction (CI) method is employed for the

calculation of excitation energy. Ψ_i is denoted as a singlet state configuration generated by one-electron transition from an occupied molecular orbital ψ_a to a vacant one ψ_r. Then, the diagonal element of the CI matrix for the *in vacuo* state is given as

$$\Delta E_i^{CI(0)} = \epsilon^\circ_r - \epsilon^\circ_a - J_{ar} + 2K_{ar} \tag{3.15}$$

where ϵ°_a is an orbital energy for ψ_a, and J_{ar} and K_{ar} are the coulomb and exchange integrals, respectively.

First, the author clarify how eq. 3.15 is modified as a result of incorporation of the solute-solvent interaction into the Fock operator. It is now assumed that the Fock operator is written as the sum of the "intra-solute" part (f°) and the "solute-solvent interaction" part (f').

$$f = f^\circ + f' \tag{3.16}$$

The orbital energy could be thus divided into the corresponding two parts.

$$\begin{aligned} \epsilon_x(\varepsilon_{stat}) &= \langle\psi_x | f | \psi_x\rangle = \langle\psi_x | f^\circ | \psi_x\rangle + \langle\psi_x | f' | \psi_x\rangle \\ &= \epsilon^\circ_x + \epsilon'_x \end{aligned} \tag{3.17}$$

where the subscript x indicates the numbering of a molecular orbital. If we expand ψ_x by a linear combination of atomic orbitals $\{\phi_\mu\}$ (eq. 3.18), ϵ'_x can be given by eq. 3.19.

$$\psi_x = \sum_\mu C_{\mu x}\phi_\mu \tag{3.18}$$

$$\epsilon'_x = \sum_{\mu\nu} C_{\mu x} C_{\nu x} \langle \phi_\mu | f' | \phi_\nu \rangle = \sum_{\mu\nu} C_{\mu x} C_{\nu x} F'_{\mu\nu}(\varepsilon_{stat}) \qquad (3.19)$$

As described in ref.10, the solute-solvent interaction part of the Fock matrix element is given by

$$F'_{\mu\nu}(\varepsilon_{stat}) = 1/2 \{(\mathbf{J}_{1stat}) + (\mathbf{J}_{2stat})\}_{\mu\nu} + (\mathbf{T}_{stat}\mathbf{P}_0)_{\mu\nu} \qquad (3.20)$$

Besides the density matrix for the excited state Ψ_i is

$$(\mathbf{P}_i)_{\mu\nu} = (\mathbf{P}_0)_{\mu\nu} + C_{\mu r} C_{\nu r} - C_{\mu a} C_{\nu a} \qquad (3.21)$$

Then, from eqs. 3.19, 3.20 and 3.21, we can obtain the contribution of the reaction field to the orbital energy difference as follows:

$$\epsilon'_r - \epsilon'_a = 1/2 \{2(\mathbf{P}_i - \mathbf{P}_0)\mathbf{T}_{stat}\mathbf{P}_0 + (\mathbf{P}_i - \mathbf{P}_0)\mathbf{J}_{1stat} + \mathbf{J}_{2stat}(\mathbf{P}_i - \mathbf{P}_0)\} \qquad (3.22)$$

Consequently, the CI calculation combined with the SCRF method gives the following excitation energy:

$$\Delta E_i^{CI(0)} = E_i - E_0 + 1/2 \{2(\mathbf{P}_i - \mathbf{P}_0)\mathbf{T}_{stat}\mathbf{P}_0 + (\mathbf{P}_i - \mathbf{P}_0)\mathbf{J}_{1stat} + \mathbf{J}_{2stat}(\mathbf{P}_i - \mathbf{P}_0)\} \qquad (3.23)$$

Clearly, the right hand side of eq. 3.23 is different from either extreme case of eq. 3.10 or 3.12, in which subscripts "stat" are omitted. This indicates that the simple SCRF-CI treatment does not yield the exact excitation energy.

Next, we attempt to find the correction terms for ΔE_i^{CI}. Comparing eq. 3.23

with eq. 3.14, the following relation is obtained:

$$\Delta A_i = \Delta E_i^{\mathrm{CI}(0)} - 1/2\ \{\mathbf{J}_{2\mathrm{stat}}(\mathbf{P}_i - \mathbf{P}_0) + \mathbf{P}_0\mathbf{T}_{\mathrm{stat}}(\mathbf{P}_i - \mathbf{P}_0)\} + 1/2\ \{\mathbf{J}_{2\mathrm{opt}}(\mathbf{P}_i - \mathbf{P}_0) + \mathbf{P}_i\mathbf{T}_{\mathrm{opt}}(\mathbf{P}_i - \mathbf{P}_0)\} \qquad (3.24)$$

Therefore the diagonal elements of the CI matrix should be rewritten as follows:

$$\Delta A_i^{(0)} = \langle\Psi_i|\ \mathcal{H}_0\ |\Psi_i\rangle + 1/2\ \langle\Psi_i|\ \mathcal{V}\ |\Psi_i\rangle - A_0 = \epsilon_r(\varepsilon_{\mathrm{stat}}) - \epsilon_a(\varepsilon_{\mathrm{stat}}) - J_{ar} + 2K_{ar} + 1/2\ \langle\Psi_i|\ \mathcal{V}'\ |\Psi_i\rangle \qquad (3.25)$$

where $\langle\Psi_i|\ \mathcal{V}'\ |\Psi_i\rangle$ is a state-dependent perturbation term defined as

$$\langle\Psi_i|\ \mathcal{V}'\ |\Psi_i\rangle = -\mathbf{J}_{2\mathrm{stat}}(\mathbf{P}_i - \mathbf{P}_0) - \mathbf{P}_0\mathbf{T}_{\mathrm{stat}}(\mathbf{P}_i - \mathbf{P}_0) + \mathbf{J}_{2\mathrm{opt}}(\mathbf{P}_i - \mathbf{P}_0) + \mathbf{P}_i\mathbf{T}_{\mathrm{opt}}(\mathbf{P}_i - \mathbf{P}_0) \qquad (3.26)$$

3.2.4 Derivation of the Off-Diagonal Elements of the CI matrix

In analogy with eq. 3.26, the off-diagonal elements $\langle\Psi_i|\ \mathcal{V}'\ |\Psi_j\rangle$ could be written by using the reaction field matrices $\mathbf{J}_2$ and $\mathbf{T}$. To find their relationship, we first search the relationship between the reaction field matrices and their operator form.

Once the geometry of the solute molecule (the nuclear coordinate) is given, $\mathcal{V}_{\mathrm{ce}}$, $\mathcal{V}_{\mathrm{ec}}$ and $\mathcal{V}_{\mathrm{ee}}$ appearing in eq. 3.4 become a function of the electron coordinate alone, and $\mathcal{V}_{\mathrm{cc}}$ is a constant, hereafter written by v_{cc}. Considering the physical meanings of $\mathcal{V}_{\mathrm{ce}}$, $\mathcal{V}_{\mathrm{ce}}$ and $\mathcal{V}_{\mathrm{ee}}$, it can be *a priori* assumed that $\mathcal{V}_{\mathrm{ce}}$ and $\mathcal{V}_{\mathrm{ec}}$ can be represented as a sum of one-electron operators, and that $\mathcal{V}_{\mathrm{ee}}$ can be represented as a sum of two-electron operators. Namely,

$$\mathcal{V}_{ce} = \sum_i v_{ce}(r_i) \tag{3.27a}$$

$$\mathcal{V}_{ec} = \sum_i v_{ec}(r_i) \tag{3.27b}$$

$$\mathcal{V}_{ee} = \sum_i \sum_j v_{ee}(r_i, r_j) \tag{3.27c}$$

$$\mathcal{V}_{cc} = v_{cc} \tag{3.27d}$$

where $v_{ec}(r_i)$ is an operator for the interaction energy through the reaction field between the ith electron and the nuclei, and $v_{ee}(r_i, r_j)$ is an operator for the interaction between the ith and jth electrons.

Now, we recall that the continuum model is based on the prerequisite that the electron exchange between the solute and the medium is negligible. In such a system, the medium "sees" the static charge distribution of the solute molecule. Thus, in the description of the solute-medium interaction, it is sufficient to use the Hartree product (eq. 3.28) for the solute wavefunction without considering the antisymmetric property for electron exchange.

$$|\Psi_0\rangle = \{\psi_a(1)\ \overline{\psi_a}(2)\ \psi_b(3) \cdots \overline{\psi_k}(n)\} \tag{3.28}$$

where $\psi_a(1) \cdots$ are molecular orbitals (upper bar means β spin) and are expanded in a similar manner as eq. 3.18. Then the first order perturbation term for $\mathcal{V}$ is readily obtained.

$$\langle\Psi_0|\ \mathcal{V}\ |\Psi_0\rangle = \sum_{\mu\nu} (\mathbf{P}_0)_{\mu\nu} \int dr_1\ \phi_\mu(r_1)\ \{v_{ce}(r_1) + v_{ec}(r_1)\}\phi_\nu(r_1)$$

$$+\sum_{\mu\nu}\sum_{\lambda\sigma}(\mathbf{P}_0)_{\mu\nu}(\mathbf{P}_0)_{\lambda\sigma}\int dr_1 dr_2\ \phi_\mu(r_1)\ \phi_\nu(r_1)$$

$$\times v_{ee}(r_1,r_2)\ \phi_\lambda(r_2)\ \phi_\sigma(r_2) + v_{cc} \qquad (3.29)$$

On comparing eq. 3.29 with eq. 3.8, the following relations are obtained:

$$\begin{aligned}
(\mathbf{J}_1)_{\mu\nu} &= \int dr_1\ \phi_\mu(r_1)\ v_{ce}(r_1)\ \phi_\nu(r_1) \\
(\mathbf{J}_2)_{\mu\nu} &= \int dr_1\ \phi_\mu(r_1)\ v_{ec}(r_1)\ \phi_\nu(r_1) \qquad (3.30) \\
(\mathbf{T})_{\mu\nu\lambda\sigma} &= \int dr_1 dr_2\ \phi_\mu(r_1)\ \phi_\nu(r_1)\ v_{ee}(r_1,r_2)\ \phi_\lambda(r_2)\ \phi_\sigma(r_2) \\
\mathbf{B} &= v_{cc}
\end{aligned}$$

Using these relationships, the expression of the CI matrix element, e.g., $\langle\Psi_a^r|\ \mathcal{V}_{ce}\ |\Psi_b^s\rangle$, is obtained as follows:

$$\langle\Psi_a^r|\ \mathcal{V}_{ce}\ |\Psi_b^s\rangle = 2\sum_c \langle\psi_c|\ v_{ce}\ |\psi_c\rangle\delta_{ab}\delta_{rs} - \langle\psi_a|\ v_{ce}\ |\psi_b\rangle\delta_{rs} + \langle\psi_r|\ v_{ce}\ |\psi_s\rangle\delta_{ab}$$

$$= \sum_{\mu\nu}\{(\mathbf{P}_0)_{\mu\nu}\delta_{ab}\delta_{rs} - C_{\mu a}C_{\nu b}\delta_{rs} + C_{\mu r}C_{\nu s}\delta_{ab}\}\ (\mathbf{J}_1)_{\mu\nu} \qquad (3.31)$$

where $|\Psi_a^r\rangle$ is a one-electron excitation configuration which is generated by a transition from an occupied MO ψ_a to virtual MO ψ_r.

Similarly, the elements for the two-electron part such as $\langle\Psi_a^r|\ \mathcal{V}_{ee}\ |\Psi_b^s\rangle$ are described as follows:

$$\langle\Psi_a^r|\ \mathcal{V}_{ee}\ |\Psi_a^r\rangle = \sum_{\mu\nu}\sum_{\lambda\sigma}\{(\mathbf{P}_0)_{\mu\nu}(\mathbf{P}_0)_{\lambda\sigma} - 2(\mathbf{P}_0)_{\lambda\sigma}C_{\mu a}C_{\nu a}$$

$$+ 2(\mathbf{P}_0)_{\lambda\sigma}C_{\mu r}C_{\nu r} - 2C_{\mu a}C_{\nu a}C_{\lambda r}C_{\sigma r}$$

$$+ C_{\mu a}C_{\nu a}C_{\lambda a}C_{\sigma a} + C_{\mu r}C_{\nu r}C_{\lambda r}C_{\sigma r}\}(\mathbf{T})_{\mu\nu\lambda\sigma} \quad (3.32a)$$

$$\langle \Psi_a^r | \mathcal{V}_{ee} | \Psi_a^s \rangle = \sum_{\mu\nu}\sum_{\lambda\sigma} \{(\mathbf{P}_0)_{\mu\nu}C_{\lambda r}C_{\sigma s} - C_{\mu a}C_{\nu a}C_{\lambda r}C_{\sigma s}$$

$$+ C_{\mu r}C_{\nu s}C_{\lambda r}C_{\sigma s}\}(\mathbf{T})_{\mu\nu\lambda\sigma} \quad (3.32b)$$

$$\langle \Psi_a^r | \mathcal{V}_{ee} | \Psi_b^r \rangle = -\sum_{\mu\nu}\sum_{\lambda\sigma} \{(\mathbf{P}_0)_{\mu\nu}C_{\lambda a}C_{\sigma b} - C_{\mu a}C_{\nu a}C_{\lambda a}C_{\sigma b}$$

$$- C_{\mu b}C_{\nu b}C_{\lambda a}C_{\sigma b} + C_{\mu a}C_{\nu b}C_{\lambda a}C_{\sigma b}$$

$$+ C_{\mu r}C_{\nu r}C_{\lambda a}C_{\sigma b}\}(\mathbf{T})_{\mu\nu\lambda\sigma} \quad (3.32c)$$

$$\langle \Psi_a^r | \mathcal{V}_{ee} | \Psi_b^s \rangle = C_{\mu a}C_{\nu r}C_{\lambda b}C_{\sigma s}\,(\mathbf{T})_{\mu\nu\lambda\sigma} \quad (3.32d)$$

Therefore, the expressions of the CI matrix elements are completely obtained.

§3.3 Computational Details

The computational procedure following the SCRF-PCM-CI method developed above can be summarized as follows. In the first step, for a given geometry of a solute molecule, the elements of the reaction field matrices $\mathbf{J}_1$, $\mathbf{J}_2$ and $\mathbf{T}$ are calculated under the condition of $\varepsilon = \varepsilon_{stat}$ (in eq. 3.A2), and are stored as $\mathbf{J}_{1stat}$, $\mathbf{J}_{2stat}$ and $\mathbf{T}_{stat}$. In the second step, the SCRF calculation with the Fock operator of eq. 3.16 is performed, giving the ground-state wavefunction. In the third step, the elements of $\mathbf{J}_1$, $\mathbf{J}_2$ and $\mathbf{T}$ are again evaluated under the condition of $\varepsilon = \varepsilon_{opt}$, and are stored as $\mathbf{J}_{1opt}$, $\mathbf{J}_{2opt}$ and $\mathbf{T}_{opt}$, respectively. By using the stored values of the elements concerning $\mathbf{J}_1$, $\mathbf{J}_2$ and $\mathbf{T}$, the correction terms for the CI matrix are calculated. Finally, the resulting CI matrix was diagonalized, giving a set of

excitation energy.

The above computational scheme was incorporated into the INDO/S molecular orbital program,[13] which can handle the single-excitation configuration interaction. The configurations whose zeroth-order transition energies are less than 10 eV were taken into account. The geometry of a solute molecule was optimized (under the *in vacuo* condition) with the PM3 method[14] using the MOPAC 6.01 program .[15] The geometry was assumed to be invariant during excitation.

Basically, the cavity in which the solute molecule was accommodated was prepared according to the previously-reported procedure:[16] (1) A van der Waals sphere was placed at each atomic center of the solute molecule; (2) The surface of each sphere was divided into longitude-latitude grids with a dividing angle of 18°; (3) Grid points placed in the overlapping region of the van der Waals spheres were deleted. Unfortunately, it was found that such a simple procedure often caused serious errors to the CI energies. This means that the accuracy of the excitation energy calculation more sensitively depends on the way of tessellation compared with the ground-state energy calculation. Here, the author added some modifications to the above procedure, especially for treatment of grids placed in the region where two van der Waals spheres are joining. The details of modification is described in Appendix 3C.

§3.4 Results and Discussion

3.4.1 Features of the Theory

According to the above formalism, excitation energies including solvatochromic shifts are evaluated by diagonalizing the CI matrix with the perturbation terms given in eqs. 3.25, 3.31 and 3.32. In other words, the values for all the singly-excited states considered in the CI calculation can be simultaneously obtained by once diagonalization. This is one of the most interesting features which

would discriminate the present SCRF-CI method from others.

The expression of the excitation energy including solvent effects (eq. 3.14) apparently consists of three portions: the term related to the solute molecule alone and two correction terms related to ε_{stat} and ε_{opt}. As described in ref.10, the reaction field potential changes as a function of $f(\varepsilon)$ defined as,

$$f(\varepsilon)=\frac{\varepsilon-1}{\varepsilon+1} \tag{3.33}$$

This means that the values of the matrix elements for $\mathbf{J}_1$, $\mathbf{J}_2$ and $\mathbf{T}$ are functions of $f(\varepsilon)$. As a result, the terms $(\mathbf{P}_i - \mathbf{P}_0)\mathbf{J}_{1stat}$ and $(\mathbf{P}_i - \mathbf{P}_0)\mathbf{T}_{stat}\mathbf{P}_0$ in eq. 3.14 are nearly proportional to $f(\varepsilon_{stat})$,while the terms $\mathbf{J}_{2opt}$ $(\mathbf{P}_i - \mathbf{P}_0)$ and $\mathbf{P}_i\mathbf{T}_{opt}$ $(\mathbf{P}_i - \mathbf{P}_0)$ are nearly proportional to $f(\varepsilon_{opt})$. Therefore, it is expected that the absorption maximum ν_{max} (given in energy unit) of the solute shifts approximately following the two-dimensional linear equation about $f(\varepsilon_{stat})$ and $f(\varepsilon_{opt})$:

$$\nu_{max} = A\, f(\varepsilon_{stat}) + B\, f(\varepsilon_{opt}) + C \tag{3.34}$$

where A, B and C are the parameters intrinsic to the given solute molecule, including its geometry and the shape of the cavity.

As described in the introductory remarks, some of the past SCRF models were based on the erroneous treatment about the polarization of solvent in response to excitation of a solute molecule. Namely, the partitioning of it into the orientational and electronic contributions was done on the assumption that the reaction field factor $f(\varepsilon)$ has an additive property. As pointed by Klamt,[6] it is only in electric susceptibility that additivity is truly held. The author reviewed this issue in more general form in Appendix 3B, where the problem of evaluating the solvent polarization is replaced by that of determining the charges σ_{ind} induced on the

surface of the dielectric. According to the analysis in Appendix 3B, the way of partitioning the induced charges σ_{ind} is not limited only to the conventional scheme, $\sigma_{ind} = \sigma_{or} + \sigma_{el}$, where σ_{or} and σ_{el} are the orientational and electronic parts of the induced charges, respectively. Alternatively, σ_{ind} can be written by the sum of a contribution (σ_{stat}) concerning ε_{stat} and a contribution (σ_{opt}) concerning ε_{opt}. The expressions for these quantity are given in eqs. 3.B9-11 in Appendix 3B. The formalism deriving eq. 3.14 follows this way of charge partitioning.

It is of interest to compare eq. 3.24 with eq. 26a of ref.4, which has been derived under the conditions that a solute molecule is approximated as a dipole and the cavity shape is taken to be spherical. In the latter, the correction term for the diagonal element of the CI matrix is given by $g(\varepsilon_{stat})\langle\psi_0|\mu|\psi_0\rangle(\langle\psi_i|\mu|\psi_i\rangle - \langle\psi_0|\mu|\psi_0\rangle)$, where $g(\varepsilon_{stat})$ is the reaction field factor for the dipole approximation and μ is the dipole operator. This is transformed into the more generalized form $\{\mathbf{J}_{2stat}(\mathbf{P}_i - \mathbf{P}_0) + \mathbf{P}_0\mathbf{T}_{stat}(\mathbf{P}_i - \mathbf{P}_0)\}$ given in eq. 3.24 when the formalism is extended to allow for an arbitrary charge distribution ($\mathbf{P}_i$ or $\mathbf{P}_0$) of a solute and for an arbitrarily-shaped cavity implemented in the matrices $\mathbf{J}_{2stat}$ and $\mathbf{T}_{stat}$. Equation 3.24 may also play a role similar to eq. 10 of ref. 6.

One of the most significant points in the present formalism is to derive the explicit matrix representation of the reaction field potential, enabling us to derive the off-diagonal elements of the CI matrix. In the reaction field model, a charged particle is implicitly assumed to interact with itself through the reaction field, because it receives the reaction field which partially originates from its own charge. Due to this unusual property, it is not easy to describe the operator as a simple one- or two-electron form. However, the author has found that as far as electron exchange is negligible between the solute and the medium, the problem becomes much simple. In this case, it is sufficient to describe the wavefunction of the solute as a Hartree product. Thus, the interaction of the particle with itself are naturally

taken into account. For example, in eq. 3.32a the terms such as $C_{\mu a}C_{\nu a}C_{\lambda a}C_{\sigma a}$ appear as a result of the use of the Hartree product. These terms constitute the integral $\int dr_1\ \psi_a(r_1)\ \psi_a(r_1)\ v_{ee}(r_1,r_1)\ \psi_a(r_1)\ \psi_a(r_1)$ responsible for the "self-interaction" of the electron occupying $\psi_a(r_1)$. If we used the Slater determinant as a wavefunction, such terms would vanish due to the antisymmetric character of the wavefunction.

Logically, the off-diagonal element of the CI matrix such as $\langle\Psi_0|\ \mathcal{V}'\ |\Psi_i\rangle$ never vanishes. This indicates that Brillouin's theorem is not strictly fulfilled. However, the value is actually not so large that the orthogonality condition between the ground and the excited states becomes meaningless. This was confirmed through test calculations as exemplified below. On the other hand, the off-diagonal elements such as $\langle\Psi_i|\ \mathcal{V}'\ |\Psi_j\rangle$ exert significant effects on the excitation energy, although their values are sufficiently small compared with those of the diagonal elements. They might be regarded as a coupling factor among the excited configurations through which each electronic state acquires optimum polarization in response to the instantaneous polarization of the medium.

3.4.2 Comparison with Experiment

Here, the solvatochromic shift of 4-[(4'-hydroxyphenyl)azo]-*N*-methylpyridine (**1**) was examined. This molecule has mesomeric structures shown in Figure 3.2. For this dye, Buncel et.al. have observed a large solvatochromic shift through UV-vis. measurements using 29 different solvents.[17] This molecule has been also studied by Rauhut et al.[8] in order to evaluate their solvent effect calculation.

Figure 3.3 summarizes the values of absorption maxima of **1** in 24 aprotic solvents whose values of dielectric constant ε and refractive index n are listed in Table 3.1. The horizontal axis is the regression values obtained from a two-dimensional minimum square fitting against eq. 3.34. The optimum values of

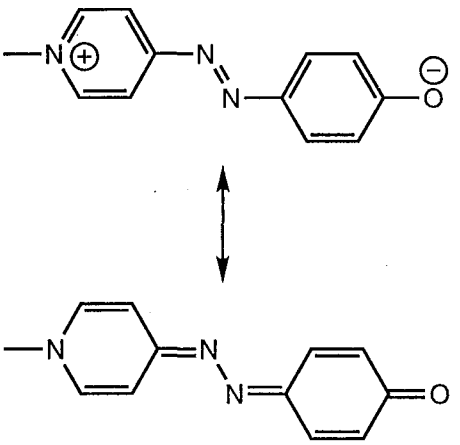

Figure 3.2 Mesomeric structures of 4-[(4'-hydroxyphenyl)azo]-*N*-methylpyridine (**1**).

Table 3.1 The list of aprotic solvents used for the observation of solvatochromic shifts of a merocyanine dye[a)]

No.	Solvent	Dielectric Constant[b)d)]	Refractive Index[c)d)]
1	hexane	1.89	1.375
2	cyclohexane	2.02	1.424
3	diethylether	4.34	1.350
4	1,4-dioxane	2.21	1.420
5	ethylacetate	6.02	1.373
6	monoglyme	7.20	1.378
7	methylacetate	6.68	1.361
8	dimethylacetoamide	37.8	1.436
9	dimethylformamide	36.7	1.429
10	dimethylsulfoxide	45.8	1.477
11	2-butanone	18.5	1.376
12	acetone	20.7	1.359
13	toluene	2.38	1.494
14	benzene	2.27	1.501
15	chlorobenzene	5.62	1.525
16	pyridine	12.3	1.523
17	nitrobenzene	34.8	1.550
18	benzonitrile	25.2	1.526
19	1,2-dichloroethane	10.4	1.442
20	chloroform	4.81	1.446
21	dichloromethane	8.90	1.424
22	HMPA	30.0	1.457
23	acetonitrile	37.5	1.346
24	nitromethane	35.9	1.380

a) Ref.17. b) At 25°C. c) For sodium (D) light at 25°C. d) Cited from "ORGANIC SOLVENTS 3rd Ed.", Weissberger, A. Ed., John Wiley & Sons, Inc. (New York) 1970.

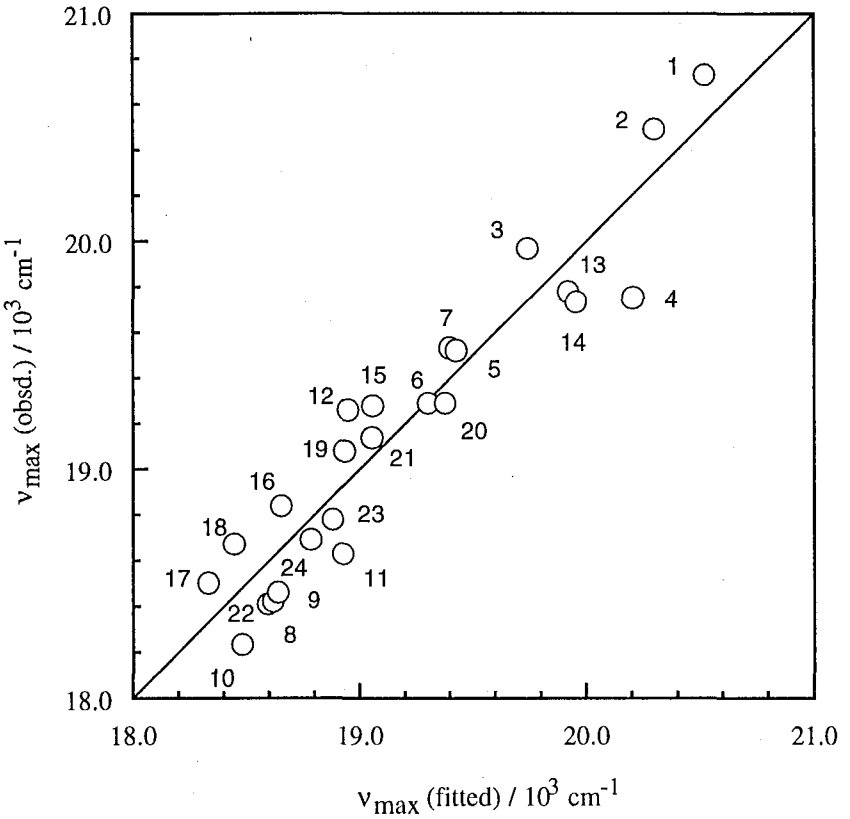

Figure 3.3 Correlation between the observed absorption maxima and their regression values based on eq. 3.34.

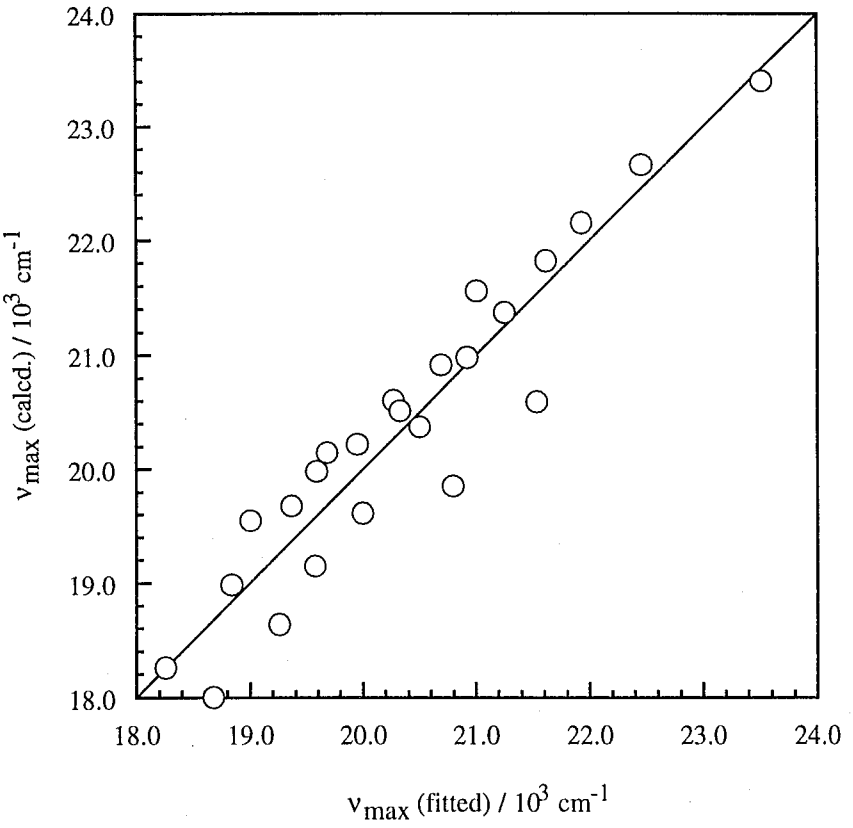

Figure 3.4 Correlation between the calculated π–π^* excitation energy and their regression values based on eq. 3.34.

Table 3.2 Comparison between the experimental and calculated results for the solvatochromic shift of a merocyanine dye

	Coefficients [a] / 10^3 cm^{-1}			r^2 [b]
	A	*B*	*C*	
Exptl.	-2.70	-4.54	22.75	0.901
Calcd.[c]	-3.17	-5.12	23.51	0.892
Calcd.[d]	2.07	1.92	22.19	0.582

a) Based on eq. 3.34. b) The square of the correlation coefficient. c) Results from the CI calculation with both diagonal and off-diagonal corrections. d) Results for the CI calculation without the off-diagonal correction.

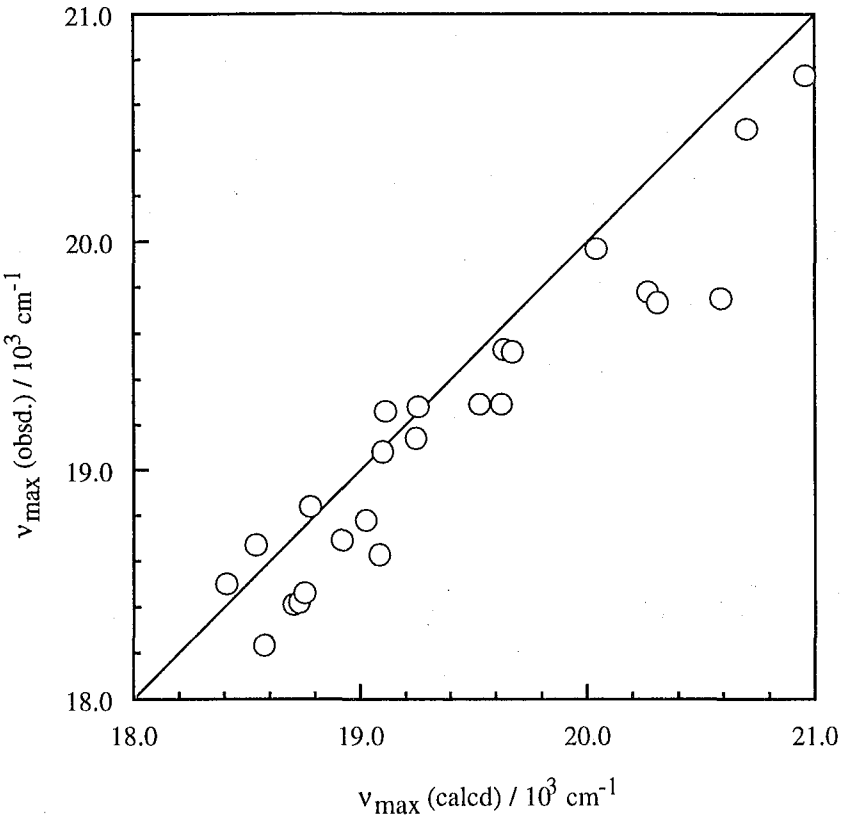

Figure 3.5 Correlation between the observed and calculated absorption maxima.

parameters A, B and C are summarized in Table 3.2. Figure 3.3 shows that there is good correlation between the experimental and regression values. This indicates that the solvatochromic shifts observed by Buncel are explained mainly by non-specific medium effects. In eq. 3.34, A and B are measures of sensitivity to ε and n^2, respectively, while C is the extrapolated value toward the vacuum state. As shown in Table 3.2, the coefficients A and B obtained from the experiment are negative values. This means that both effects of the orientational polarization and electronic polarizations cause a red shift. Additionally the sensitivity to n^2 is nearly twice larger than that to ε, indicating the importance of explicitly taking into account the effects of electronic polarization.

The calculations were performed for several sets of medium parameters ε and n whose values were taken to be 1~40 and 1.0~1.6, respectively. Figure 3.4 shows the calculated absorption maxima (corresponding to ΔA_i in eq. 3.24) for the lowest π-π* transition of **1**. The horizontal axis is again the regression values based on eq. 3.34. As expected, the calculated solvatochromic shifts behave according to eq. 3.34. The optimum values of the three parameters are listed in Table 3.2. They are in excellent agreement with the experimentally-determined values. Figure 3.5 shows the direct comparison between the experimental and calculated absorption maxima. The caluclated value for each solvent was obtained by substituting the actual values of ε and n into eq. 3.34 having the values of A, B and C in the second row of Table 3.2.

Table 3.2 also provides information about the effect of the off-diagonal correction (eqs. 3.32a-d) for the CI matrix. When the correction was neglected, the calculated absorption maxima considerably deviated from eq. 3.34 (the square of the correlation coefficient $r^2 = 0.582$) and the dependence on ε and n^2 exhibited quite an opposite tendency to the experimental results. This indicates that the off-diagonal correction is indispensable to the accurate description of the

solvatochromic shifts of molecules, as far as we stay in the SCRF-CI approach.

In conclusion, the validity of the methodology developed here was verified from both theoretical and computational viewpoints. This methodology can be easily implemented into the conventional programs of molecular orbital calculation, irrespective of its level of approximation, that is, semiempirical or *ab initio* method. Therefore, this is expected to be a standard method for predicting and interpreting solvatochromic shifts of organic molecules.

References and Notes

(1) MacRae, E. G. *J. Phys. Chem.* **1957**,*61*, 562.

(2) Ooshika, Y. *J. Phys. Soc. Japan* **1954**, *9*, 594.

(3) See for review: Tomasi, J.; Persico, M. *Chem. Rev.* **1994**, *94*, 2027.

(4) Karelson, M. M.; Zerner, M. C. *J. Phys. Chem.* 1992,*96*, 6949.

(5) (a) Bonaccorsi, R.; Cimiraglia, R.; Tomasi, J. *J. Comput.Chem.* **1983**, *4*, 567. (b) Aguilar, M. A.; Oliveres del Valle, F. J.; Tomasi, J. *J. Chem. Phys.* **1993**, *98*, 7375. (c) Cammi, R.; Tomasi, J. *J. Comput.Chem.* 1995, *16*, 1449.

(6) Klamt, A. *J. Phys. Chem.* **1996**, *100*, 3349.

(7) Fox, T.; Rösch, N.; Zauhar, R. J. *J. Comput. Chem.* **1993**, *14*, 253.

(8) Rauhut, G.; Clark, T.; Steinke, T. *J. Am. Chem. Soc.* **1993**, *115*, 9174.

(9) Zuccarello, F.; Raudino, A.; Buemi, G. *Chem. Phys.* **1984**, *84*, 209.

(10) Hoshi, H.; Sakurai, M.; Inoue, Y.; Chûjô, R. *J. Chem. Phys.* **1987**, *87*, 1107.

(11) Hoshi, H.; Sakurai, M.; Inoue, Y.; Chûjô, R. *J. Mol. Struct. (Theochem)* **1988**, *180*, 267.

(12) (a) Furuki, T.; Hosokawa, F.; Sakurai, M.; Inoue, Y.; Chûjô, R. *J. Am. Chem. Soc.* **1993**, *115*, 2903. (b) Furuki, T.; Sakurai, M.; Inoue, Y. *J. Phys. Chem.* **1995**, *99*, 12047. (c) Sakurai, M.; Furuki, T.; Inoue, Y. *J. Phys. Chem.* **1995**, *99*, 17789.

(13) (a) Krough-Jespersen, K.; Ratner, M. *J. Chem. Phys.* **1976**, *65*, 1305. In this study the β^0 value for oxygen was set to be -30eV according to (b) Faure, P. J. J.; Chalvet, O.; Jaffe, H. H. *J. Phys. Chem.*, **1981**, *85*, 473.

(14) Stewart, J. J. P. *J. Comput. Chem.* **1989**, *10*, 209.

(15) Stewart, J. J. P.; Frank, J. MOPAC Ver6.01, Seilar Reserch Laboratory, U.S.Airforce Academy, Colorado Springs, CO 80840-6528, 1989.

(16) Furuki, T.; Umeda, A.; Sakurai, M.; Inoue, Y.; Chûjô, R.; Harata, K. *J. Comput. Chem.* **1994**, *15*, 90.

(17) Buncel, E.; Rajagopal, S. *J. Org. Chem.* **1989**, *54*, 798.

Appendix: 3A: Supplementary Description of the Reaction Field Matrices

The reaction field matrices **T**, $\mathbf{J}_1$, $\mathbf{J}_2$ and **B** in eq. 3.5 are represented as the product of some matrices.[10]

$$\mathbf{T} = \mathbf{C}^t\mathbf{W}^{-1}\partial\tilde{}\mathbf{C} \qquad (3.A1a)$$

$$\mathbf{J}_1 = \mathbf{C}^t\mathbf{W}^{-1}\partial\tilde{}\mathbf{M}\mathbf{Z} \qquad (3.A1b)$$

$$\mathbf{J}_2 = \mathbf{Z}^t\mathbf{M}^t\mathbf{W}^{-1}\partial\tilde{}\mathbf{C} \qquad (3.A1c)$$

$$\mathbf{B} = \mathbf{Z}^t\mathbf{M}^t\mathbf{W}^{-1}\partial\tilde{}\mathbf{M}\mathbf{Z} \qquad (3.A1d)$$

In these equations, **C** and $\partial\tilde{}\mathbf{C}$ are the matrices representing the electrostatic potential and the electric field generated from the electronic distribution of a solute molecule, respectively. Similarly, **M** and $\partial\tilde{}\mathbf{M}$ are the matrices representing the electrostatic potential and the electric field generated from the nuclear charge distribution of the solute molecule, respectively. The diagonal element of the matrix **W** is inversely proportional to the reaction field factor $f(\varepsilon)$ (eq. 3.33).

$$W_{ii} \propto f(\varepsilon)^{-1} \qquad (3.A2)$$

As a result, **T**, $\mathbf{J}_1$, $\mathbf{J}_2$ and **B** are proportional to $f(\varepsilon)$.

Appendix 3B: Partition of the Induced Charge

Now, an external charge distribution ρ_{ext} is assumed to be present outside a dielectric. In the solute-solvent model focused here, the charge distribution of a solute molecule corresponds to ρ_{ext}. In response to ρ_{ext}, a charge distribution σ_{ind} is induced on the surface of the dielectric. According to the fundamental electrostatics, the relationship between ρ_{ext} and σ_{ind} is obtained as follows:

$$\sigma_{ind} = -\frac{\varepsilon - 1}{\varepsilon}\rho_{ext} \tag{3.B1}$$

$$\varepsilon = 1 + 4\pi\chi \tag{3.B2}$$

where ε and χ are the static dielectric constant and the electric susceptibility of the given dielectric, respectively. σ_{ind} is partitioned into the contributions of orientational and electronic polarizations:

$$\sigma_{ind} = \sigma_{or} + \sigma_{el} \tag{3.B3}$$

and similarly χ can be divided into the corresponding two parts:

$$\chi = \chi_{or} + \chi_{el} \tag{3.B4}$$

The partition of σ_{ind} into σ_{or} and σ_{el} is given by

$$\sigma_{or} = -\frac{\varepsilon - n^2}{\varepsilon}\rho_{ext} \tag{3.B5}$$

$$\sigma_{el} = -\frac{n^2 - 1}{\varepsilon}\rho_{ext} \tag{3.B6}$$

where n is the refractive index of the dielectric.

When an instantaneous change occurs in ρ_{ext}, i.e. $\rho_{ext} \rightarrow \rho_{ext} + \Delta\rho_{ext}$, only the σ_{el} part can change in response to it. Then, the σ_{or} part acts as a part of the external charge.

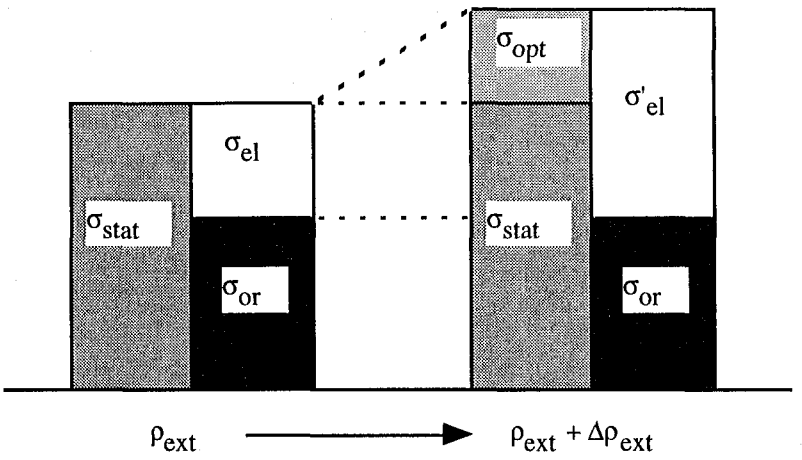

Figure 3.B1 Two ways of partitioning the induced charge. The conventional way is represented using sor and sel, and the new way proposed here is represented using σ_{stat} and σ_{opt}.

$$\sigma_{el} \rightarrow \sigma'_{el} = -\frac{n^2-1}{n^2}\left(\rho_{ext} + \Delta\rho_{ext} + \sigma_{or}\right) \tag{3.B7}$$

$$= \sigma_{el} - \frac{n^2-1}{n^2}\Delta\rho_{ext} \tag{3.B8}$$

The change in the total induced charge is thus given by

$$\sigma_{ind} \rightarrow \sigma'_{ind} = \sigma_{ind} - \frac{n^2-1}{n^2}\Delta\rho_{ext}$$

$$= -\frac{\varepsilon-1}{\varepsilon+1}\rho_{ext} - \frac{n^2-1}{n^2}\Delta\rho_{ext} \tag{3.B9}$$

Here σ_{stat} is defined as the induced charge distribution before the change of ρ_{ext} occurs, and σ_{opt} as the induced charge distribution appearing as a result of fast relaxation in the dielectric. Then, the total induced charge can be written by the sum of the following two terms:

$$\sigma_{stat} = \sigma_{or} + \sigma_{el} = -\frac{\varepsilon - 1}{\varepsilon}\rho_{ext} \tag{3.B10}$$

$$\sigma_{opt} = \sigma'_{el} - \sigma_{el} = -\frac{n^2-1}{n^2}\Delta\rho_{ext} \tag{3.B11}$$

This relationship is schematically indicated in Figure 3.B1. As understood from the above derivation, the final result is independent of which way of partition, 3.B5-6 or 3.B10-11, is chosen.

Appendix 3C: Overlap Correction for the Cavity Surface Elements

Any element on a cavity surface is identified by its area and the coordinate of a representative point taken in it, e.g., its centroid. Basically, the total area of the cavity surface is given by summing up the areas of all the elements. However, such

a simple calculation often leads to serious errors for final results for solvent energy, charge distribution, etc. Now we consider two elements, belonging to different van der Waals spheres centered on different atoms. When these elements are adjoining, there may arise an overlapping region between them. Then, if the overlapping area is sufficiently large, the above calculation overestimates the total surface area of the cavity. This causes errors for the charge densities of these elements, resulting in serious errors on the final results, including the ground- and excited-state energies.

In order to remove such numerical errors, the areas of all the overlapping elements must be corrected depending on the degree of overlap. For convenience of computer programming, an element is replaced by a circle with the same area as that of the original element. The center of the circle is taken to be coincident with the representative point of the element. Here it is assumed that two circles i and j, whose radii are r_i and r_j ($r_i > r_j$), respectively, are distant by d_{ij} (Figure 3.C1). From Figure 3.C1 the following relationships are found:

$$\cos\theta_i = (r_i^2 + d_{ij} - r_j^2)/2r_i d_{ij} \qquad (3.C1a)$$

$$\cos\theta_j = (r_j^2 + d_{ij} - r_i^2)/2r_j d_{ij} \qquad (3.C1b)$$

$$S_n^0 = \pi r_n^2 \qquad (3.C2)$$

$$P_n = S_n^0 - \theta_n r_n^2 + (1/2)r_n^2 \sin(2\theta_n) \qquad (3.C3)$$

where S_n^0 and P_n are the area of the element n ($n = i$ or j) before and after removal of the overlapping region, respectively.

The quantity, $d_{ij}/(r_i + r_j) = D_{ij}$ can be used as a measure of the degree of overlap. For mathematically reasonable correction of the total surface area, the following three-step criterion is necessary. Namely, when two values t_1 and t_2 ($t_1 > t_2$) are selected as thresholds of D_{ij}, the corrected areas of S_i and S_j are given as

follows:

if $D_{ij} > t_1$; $S_i = S_i^0$, $S_j = S_j^0$

if $t_1 > D_{ij} > t_2$; $S_i = P_i$, $S_j = P_j$

if $t_2 > D_{ij}$; $S_i = P_i + P_j$, $S_j = 0$

where $S_j = 0$ means the removal of the jth element. In this study, the values of t_1 and t_2 were set to be 0.6 and 0.3, respectively.

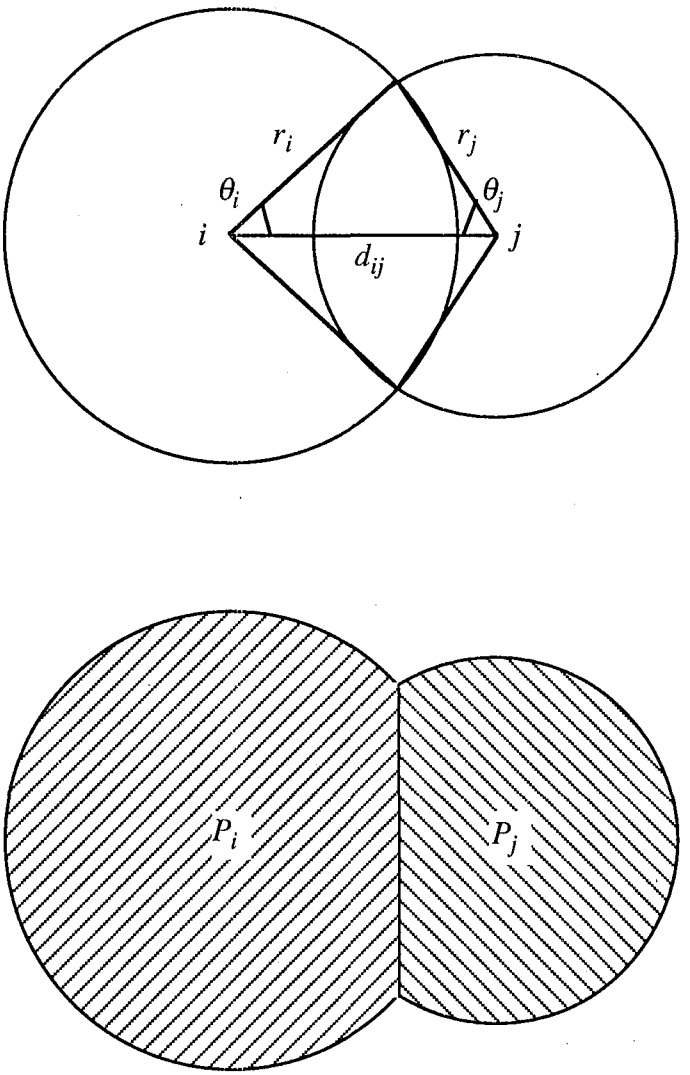

Figure 3.C1 A method for correcting the areas of overlapping elements. The areas after correction is given by P_i and P_j.

Chapter 4. Comprehensive Analysis of the Opsin Shift of Bacteriorhodospin Based on the Medium Effects Calculation

§4.1 Introduction

Bacteriorhodopsin (bR) is a retinal-bound protein and functions as a light-driven proton pump in the purple membrane of *Halobacterium halobium*.[1] Illumination of the light-adapted state bR_{568} initiates a sequential photoreaction cycle consisting of the spectroscopically-distinct intermediates K_{610}, L_{550}, M_{412}, N_{520}, and O_{640}.[2] The absorption maximum of bR_{568} is 568 nm, which is significantly red shifted in comparison with that of protonated retinylidene Schiff base (PRSB) measured in methanol solution (~440 nm). Being similar to bR_{568}, the absorption maximum of M_{412} is red shifted with respect to the corresponding solution data. Similar phenomena are also observed in visual pigments. Rhodopsin (Rh), the rod pigment of vertebrate, shows the absorption maximum at ~500nm.[1] Such protein-induced bathochromic shifts are known as opsin shift.[1] The elucidation of the mechanism of the opsin shift has been one of the most interesting issues in photochemistry of retinal-bound proteins for these decades.

The opsin shift is considered to arise mainly from following three factors: elongation of the π-conjugated system due to the ring/chain coplanarization, hereafter called mechanism (1),[3-6] π-electron delocalization due to weakening of the interaction between PRSB and its counterion (mechanism (2)),[7,8] and interaction of the chromophore with polar or polarizable residues in the protein. Among them, the molecular detail of the third factor remains unclear, although much effort has been made to identify the chromophore-protein interactions directly responsible for the opsin shift. There are two conceptual models for this factor. One is the so-called external point charge model (mechanism (3)) proposed by Nakanishi's

group.[9] The other model emphasizes the electronic polarization effect of aromatic residues (mechanism(4)).[10]

The location of the external charge has been intensively explored by a series of experiments using artificial pigments reconstituted with dehydro- or dihydroretinals.[9,11-15] For bR, a negatively charged or polar residue has been proposed to be present near the β-ionone ring.[12,16] Such a residue would largely delocalize the π-electrons of the chromophore, resulting in a significant amount of red shift. This mechanism was partially supported by experiments using model compounds which possess charged groups covalently bound to retinal itself.[7,17,18] However, there is room for argument against mechanism (3). First, this can not account for the spectral shift of M_{412}.[19] Second, from the crystal structure at 3.5 Å resolution,[20] such external charge(s) could not be identified. In addition, from a series of mutagenetic studies, it was shown that any ionizable residues do not contribute to the bathochromic shift observed in the wild type bR.[21] As for Rh, it has been also proposed that a second (i.e. other than the counterion of PRSB) negative charge is present near C12 and C14 of the chromophore (For the numbering of carbon atoms, see Figure 4.1).[9] Later, results from two-photon spectroscopy indicated that the chromophore-binding site is electrically neutral, suggesting the absence of the second negative charge.[22] Thus, the truthfulness of mechanism (3) is currently open to question.

According to mechanism (4),[10] the occurrence of the bathochromic shift is explained as follows. The dipole moment of PRSB in the lowest π–π^* excited state is larger than that in the ground state.[23] The surrounding solvent molecules could be electronically repolarized in response to the change in electronic distribution of the solute molecule. Such a solvent relaxation contributes to stabilizing the excited state, resulting in a red shift. In proteins, aromatic amino residues (phenylalanine, tyrosine and tryptophan) would play a role similar to polarizable solvents.[22,24]

This mechanism is supported by the fact that the absorption maximum of PRSB in ethanol shifts to red-side by addition of phenol, indole etc.[25]

In view of accumulated evidence, the whole opsin shift may not be reproduced only by the single action of any one of the four mechanisms. More current view of the spectral tuning mechanism stresses the necessity of concerted action of some of them. There were several attempts to decompose the opsin shift into a couple of contributions. Recently, Yan et al.[26] reported the results of experiments using 13,14-dihydro-analogues. The use of these analogues allows to exclude the contribution of PRSB-counterion interaction (mechanism (2)) to the entire bathochromic shift. They concluded that mechanisms (3) and/or (4) actually work in bR and their net contribution amounts to a red shift of 2030 cm^{-1}. On the other hand, according to a report of Hu et al.,[27] each of mechanisms (1) and (2) causes a red shift of about 2000 cm^{-1}. They proposed that the cooperative action of the models (1) and (2) causes an additional red shift (~1000 cm^{-1}), leading to full reproduction of the observed opsin shift without requiring mechanisms (3) and (4).

Therefore, the mechanism of the opsin shift is still controversial. For a comprehensive understanding of it, one must accurately evaluate the individual contributions of (1)-(4) and their cooperative action. Among them, (1)-(3) have been well investigated from both experimental and theoretical viewpoints.[28-30] However, the polarizable effect of the protein environment, i.e., the mechanism (4) has not been quantitatively studied so far.

Quantum chemical calculation is expected to provide a good insight into the above problem if a sophisticated solvent model is available. Self-consistent reaction field polarizable continuum model (SCRF-PCM)[31] is a reliable approximation to implement dielectric solvent effects into molecular orbital calculation. Raudino et al.[32] applied a SCRF-PCM to analysis of environmental effects on a PRSB-counterion system. However, due to methodological limitation in their SCRF

model, that report dealt with only two limiting cases: (i) dielectric constant equals the square of refractive index, and (ii) refractive index equals 1. The cases (i) and (ii) correspond to the conditions under which the relaxation of electronic polarization is infinitely fast and slow, respectively, while the actual situation lies between these two cases. In addition, they used a spherical cavity to accommodate the PRSB-counterion system. The use of a cavity which does not fit a molecular shape might lead an error in evaluating medium effects. Furthermore, the use of a cavity with a fixed shape and size could not allow to correctly follow effects of structural changes of the solute, including changing location of the counterion.

The evaluation of solvatochromic shifts of molecules is a topical subject of theoretical chemistry.[31] In Chapter 3, the author has developed a new SCRF-CI theory, capable of calculating medium effects with taking into account both orientational and electronic polarization effects of solvent.[33] This method can handle an arbitrarily shaped cavity, because its formulation was based on the boundary element method.[34] Therefore, this method has overcome the disadvantages of the previous solvent model, and hence is promising for unraveling the mechanism of the opsin shift.

In this chapter, the SCRF-CI method is applied to the problem of opsin shift. It is shown that the calculation excellently reproduce solvatochromic shifts observed for *all-trans*-retinal and its Schiff bases. By regression analysis, the author obtains an empirical equations to predict solvatochromic shifts of PRSB for an arbitrary set of dielectric constant and refractive index. On the other hand, on the basis of the crystal structure of bR and classical electrostatics, effective values of the medium parameters are estimated for the retinal-binding pocket. From combination of these results, the opsin shifts of both bR_{568} and M_{412} are successfully reproduced. Next, the calculated opsin shift is decomposed into the contributions of the above four mechanisms. It will be shown that mechanism (4) plays a decisive role in the

occurrence of the opsin shift. In addition, the author will also refer to the spectral tuning mechanism in Rh.

§4.2 Calculations

4.2.1 Modeling of Chromophores

The structure of molecules examined here are shown in Figure 4.1: *all-trans*-6*s*-*cis*-retinal (**1**), (*all-trans*-6*s*-*cis*-retinylidene)ethylamine (**2**), (*all-trans*-6*s*-*cis*-retinylidene)ethylammonium cation (**3a**), (*all-trans*-6*s*-*cis*-retinylidene) ethylammonium acetate (**3b**), (*all-trans*-6*s*-*trans*-retinylidene)ethylammonium cation (**4a**), (*all-trans*-6*s*-*trans*-retinylidene)ethylammonium acetate (**4b**), (13-*cis*-6*s*-*trans*-retinylidene)ethylamine (**5**), the model compounds of (11-*cis*-6*s*-*cis*-retinylidene)ethylammonium acetate (**6a-f**), 13,14-dihydro-*all-trans*-6*s*-*cis*-retinal (**7a**), (13,14-dihydro-*all-trans*-6*s*-*cis*-retinylidene)ethylammonium cation (**7b**), 13,14-dihydro-*all-trans*-6*s*-*trans*-retinal (**7c**), (13,14-dihydro-*all-trans*-6*s*-*trans*-retinylidene)ethylammonium cation (**7d**), 3,7,11-trimethyldodeca-4,6,8,10-tetraenal (**8a**), (3,7,11-trimethyldodeca-4,6,8,10-tetraenylidene)ethylammonium cation (**8b**), and (11-*cis*-6*s*-*cis*-retinylidene)ethylammonium acetate (**9**).

For all the molecules except **4b**, the geometrical parameters were optimized with the PM3 method[35] packed in the MOPAC 6.0 program.[36] The resulting geometry of **3b** was as follows: the O_1-C-O_2 plane of the acetate is almost contained in the conjugated plane of retinal, and the distances of O_1-N, O_2-N and C-N are 2.7, 3.4 and 3.5 Å, respectively (O_2 is closer to C14). As for **4a** and **5**, the dihedral angle of C5-C6-C7-C8 was fixed at 180°, while **1-3** have skewed *cis*-forms with respect to the C6-C7 bond. **4b** is a model of the complex of the chromophore retinal including the side chains of Lys216 and Asp85 residues, and their atomic coordinates were taken from the crystal structure of bR[20] deposited with the Protein Data Bank[48] as 2BRD. Since the crystal structure lacks the coordinates of

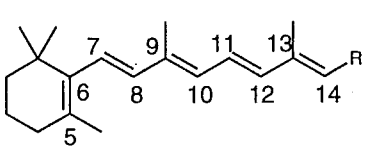

1 R: CH=O (6*s-cis*)
2 R: C=N–Et (6*s-cis*)
3a R: $C=N^{+}H–Et$ (6*s-cis*)
3b R: $C=N^{+}H–Et\cdot CH_3CO_2^{-}$ (6*s-cis*)
4a R: $C=N^{+}H–Et$ (6*s-trans*)
4b R: $C=N^{+}H–Et\cdot CH_3CO_2^{-}$ (6*s-trans*)

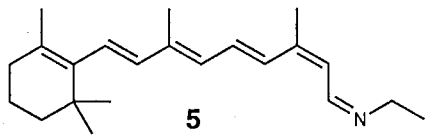

5

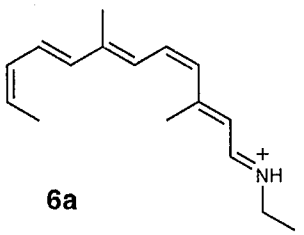

6a

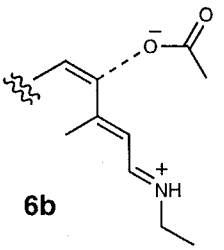

6b

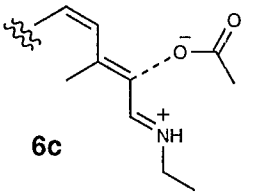

6c

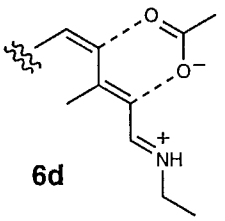

6d

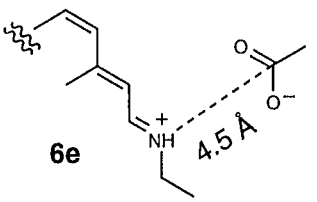

6e

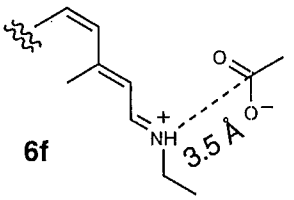

6f

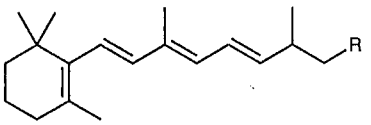

7a R: CH=O (6*s-cis*)
7b R: $C=N^{+}H–Et$ (6*s-cis*)
7c R: CH=O (6*s-trans*)
7d R: $C=N^{+}H–Et$ (6*s-trans*)

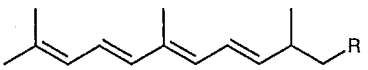

8a R: CH=O
8b R: $C=N^{+}H–Et$

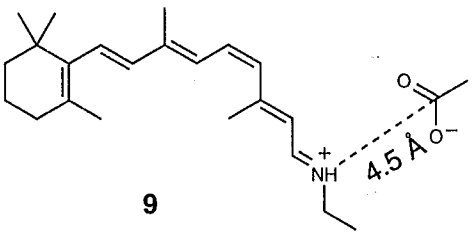

9

Figure 4.1 Molecular structures of *all-trans*-retinal and its related compounds.

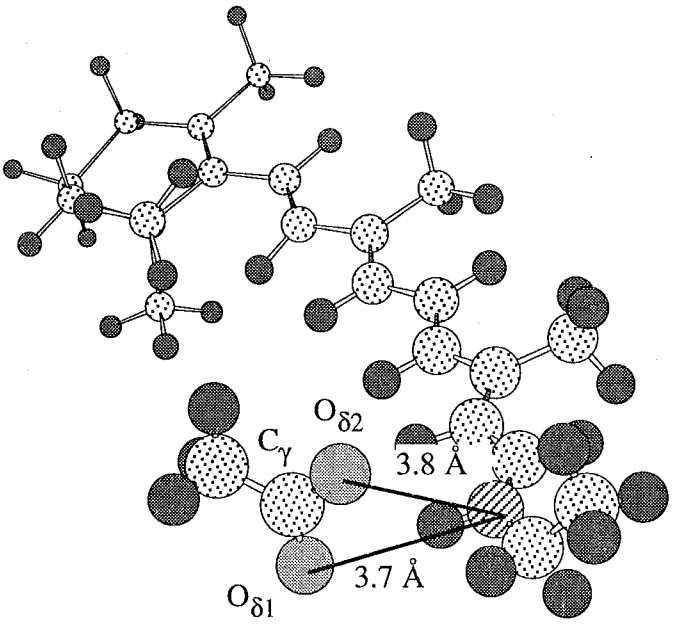

Figure 4.2 Molecular structure of the chromophore-counterion complex (**4b**) taken from the crystal structure of bR (ref. 20).

hydrogen atoms, hydrogen atoms were added by using LEaP module of the AMBER 4.1 program.[37] Figure 4.2 shows the structure of **4b**, where the $O_{\delta 1}$-C_{γ}-$O_{\delta 2}$ plane of the acetate group is almost perpendicular to the conjugated plane of retinal, and the $O_{\delta 1}$-N, $O_{\delta 2}$-N and C_{γ}-N distances are 3.7, 3.8 and 4.0 Å, respectively.

6b-f are models of the chromophore of Rh. They are different from each other in spacial arrangement of the counterion. The procedure of constructing **6a-f** was as follows. First, the geometries of **6a** and the acetate ion were separately optimized. Then, the dihedral angles of C5-C6-C7-C8 and C11-C12-C13-C14 of **6a** were fixed at 45° and -140°, respectively.[29] Next, in **6b**, one of the oxygen atoms of the carboxylate was placed at a distance of 3.0Å from C12 so as to make an angle O_1-C12-H12 of 60°. Such an arrangement of the counterion is similar to that assumed in Smith's report.[29] In **6c**, the counterion is placed near C14 in a fashion similar to **6b**. In **6d**, the acetate is arranged so that O_1-H14-C14 and O_2-H12-C12 make straight lines, with keeping distances of O_1-C14 and O_2-C12 to be 3.0 Å. In **6e** and **6f**, the acetate ion was placed so that the O_1-C-O_2 plane coincides with the conjugated plane of retinal and that N-H(N)-C(carbonyl) makes a straight line. The distance between N and C(carbonyl) for **6e** and **6f** were 4.5 and 3.5 Å, respectively. For **9**, the retinal moiety was at first optimized, and then acetate anion was added in the same way as **6e**.

4.2.2 Computational Details

The computational scheme based on the SCRF method described in Chapter 3 was incorporated into the INDO/S molecular orbital program,[38] which can handle a single-excitation configuration interaction (CI). The configurations whose zeroth order excitation energies were lower than 10 eV were taken into account. This threshold was confirmed to be sufficient in reproducing the experimental

absorption maxima of retinal derivatives. For each molecule, the lowest π–π^* excitation energy was regarded as the calculated absorption maximum.

The medium surrounding a solute is characterized by two non-specific parameters, i.e., static dielectric constant ε and refractive index n. The calculations of electronic transitions were performed for several sets of ε and n values. The values of ε were taken to be 1.0, 2.0, 4.0, 8.0 and 40.0, and those of n were to be 1.0, 1.2, 1.4 and 1.6.

Basically, the cavity in which the solute molecule was accommodated was prepared according to the following previously reported procedure;[39] (1) A van der Waals sphere was placed at each atomic center of the solute molecule; (2) the surface of each sphere was divided into longitude-latitude grids with a dividing angle of 10°; (3) grid points placed in the overlapping region of the van der Waals spheres were deleted. The van der Waals radii used are equal to the sum of solute and solvent van der Waals radii (H: 2.77Å, C: 3.16Å, N: 3.07Å, O: 2.97Å).

§4.3 Experimental

All-trans-retinal and (*all-trans*-retinylidene)butylamine (abbreviated as *all-trans*-RSB) were prepared according to a procedure described elsewhere.[40] Each compound was dissolved in each of the twenty aprotic solvents listed in Table 4.1. Protonated *all-trans*-retinal Schiff base (abbreviated as *all-trans*-PRSB) was prepared by adding an excess amount of dichroloacetic acid to each solution of *all-trans*-RSB. All photoactive compounds were handled in the dark. UV-VIS spectra were recorded on a Shimadzu UV-2100 spectrometer at room temperature.

§4.4 Results

4.4.1 *All-trans*-Retinal and *All-trans*-RSB

To assess the reliability of the SCRF method described above, the calculated

Table 4.1 The list of the aprotic solvents used for UV-VIS measurements

No.	solvent	Dielectric Constant (ε)	Refractive Index (*n*)
1	pentane	1.84	1.358
2	hexane	1.89	1.375
3	heptane	1.92	1.388
4	benzene	2.27	1.501
5	toluene	2.38	1.494
6	diethylether	4.34	1.350
7	diisopropylether	3.88	1.366
8	tetrahydrofrane	7.58	1.405
9	1,4-dioxane	2.21	1.420
10	ethylacetate	6.02	1.373
11	acetone	20.7	1.359
12	2-butanone	18.5	1.376
13	dimethylsurfoxide	45.8	1.477
14	acetonitrile	37.5	1.346
15	dimethylformamide	36.7	1.429
16	pyridine	12.3	1.523
17	carbontetrachloride	2.23	1.463
18	chloroform	4.81	1.446
19	dichloromethane	8.90	1.424
20	1,2-dichloroethane	10.4	1.442

results for **1** and **2** were first compared with the corresponding experimental data. As described in Chapter 3, the excitation energy depends on the medium parameters, ε_{stat} and ε_{opt}, according to eq. 3.34. Hereafter, the static dielectric constant ε_{stat} is simply denoted as ε, and the optical dielectric constant ε_{opt} as n^2. Then, eq. 3.34 is rewritten as follows:

$$\nu_{max} = A\, f(\varepsilon) + B\, f(n^2) + C \qquad (4.1)$$

In eq. 4.1, coefficients A and B can be regarded as measures of sensitivity to ε and n^2, respectively, while C is the extrapolated value of the excitation energy towards the *in vacuo* state. The first term involves both orientational and electronic polarization effects of solvents, while the second term does only the electronic effect. A way of assessing the accuracy of the calculation is to compare the values of these coefficients with the corresponding experimental values.

Figure 4.3 shows the absorption maxima of *all-trans*-retinal measured in various solvents. The horizontal axis indicates regression values, obtained from minimum square fitting against eq. 4.1. The optimum values of A, B and C are summarized in Table 4.2. There is good correlation between the observed and regression values. Thus, the solvatochromic shift of *all-trans*-retinal is well explained in terms of the continuum model, if the electronic polarization effects of solvents are exactly taken into account . A few exceptions are, however, found for the results in chroloform and dichrolomethane (solid circles), in which some specific interactions might work. These data points were excluded in the fitting calculation. The values of A and B are negative, indicating that the effects depending on ε and n both cause red shifts. It should be noted that the absolute value of B is considerably larger than that of A, indicating that the effect of electronic polarization of solvent more strongly affects the absorption maxima of

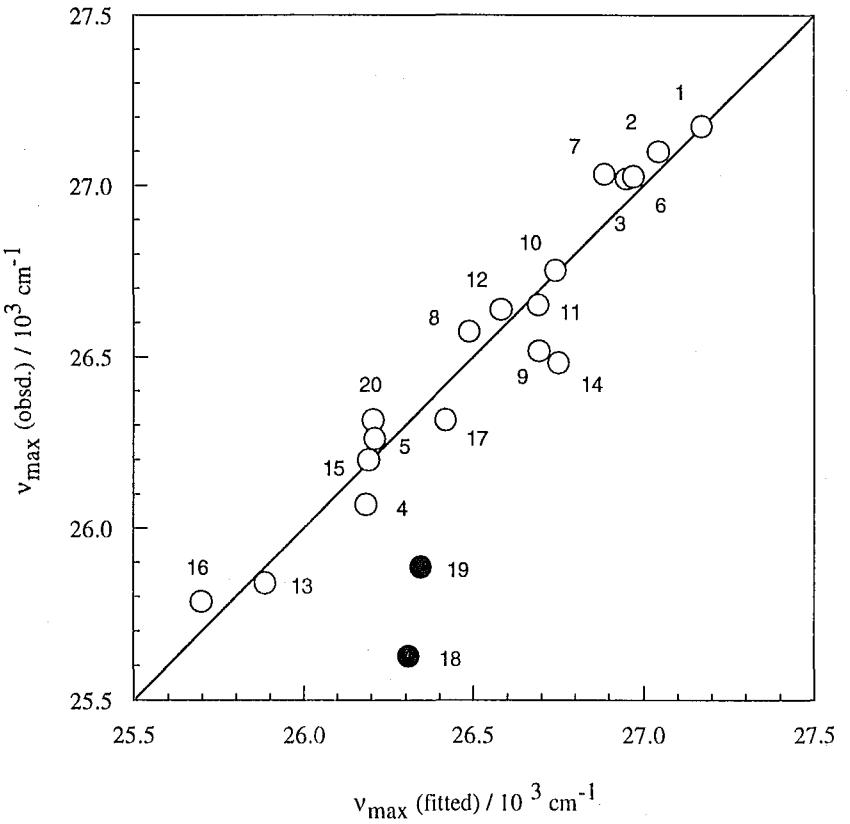

Figure 4.3 Correlation between the observed absorption maxima of *all-trans*-retinal and their regression values based on Eq. 4.1. Numbers respresent the solvents listed in Table 4.1. Solid symbols indicate the data excluded from the regression analysis.

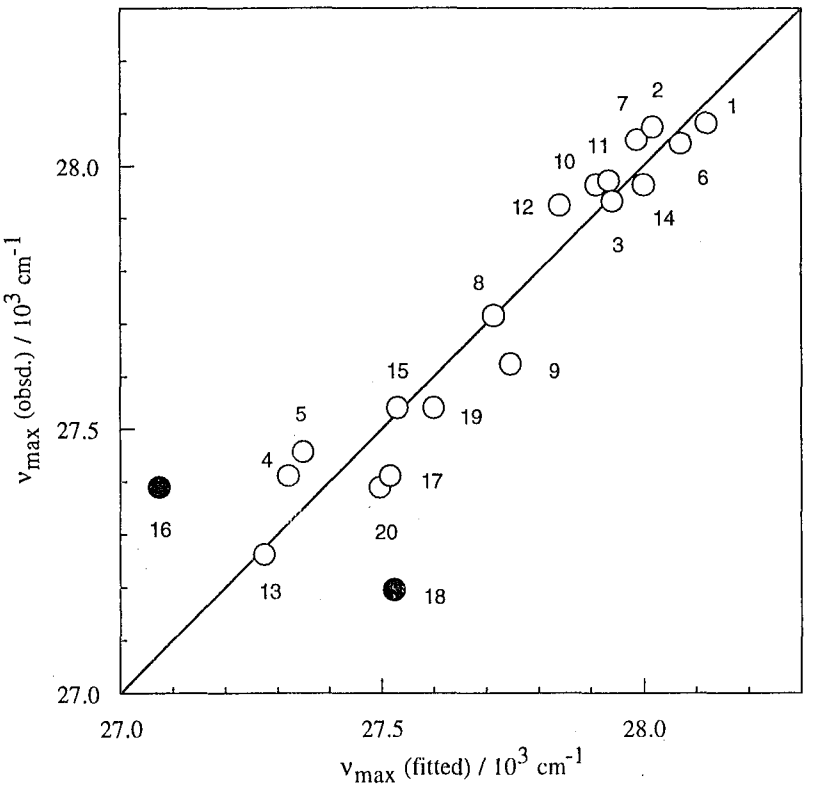

Figure 4.4 Correlation between the observed absorption maxima of *all-trans*RSB and their regression values based on Eq. 4.1. Numbers represent the solvents listed in Table 4.1. Solid symbols indicate the data excluded from the regression analysis.

Table 4.2 Comparison between experimental and calculated results of regression analysis for the absorption maxima of *all-trans*-retinal and *all-trans*-RSB

	Coefficients[a] / 10^3 cm^{-1}		
	A	*B*	*C*
		all-trans-retinal	
Exptl	-0.78	-10.35	30.5
Calcd	-0.46	-9.13	29.2
		all-trans-RSB	
Exptl	-0.29	-8.75	30.8
Calcd	-0.32	-4.68	29.7
		13-*cis*-RSB	
Calcd	-0.19	-8.12	27.8

a) Based on eq. 4.1.

b) Results for *all-trans*-retinylidenebutylamine

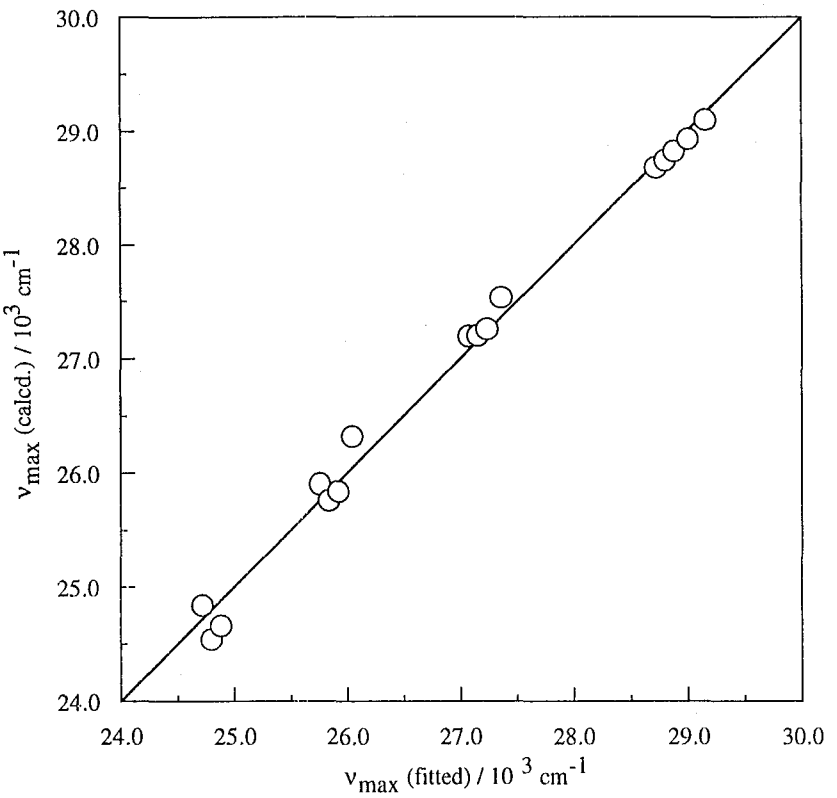

Figure 4.5 Correlation between the calculated absorption maxima of *all-trans*retinal and their regression values based on Eq. 4.1.

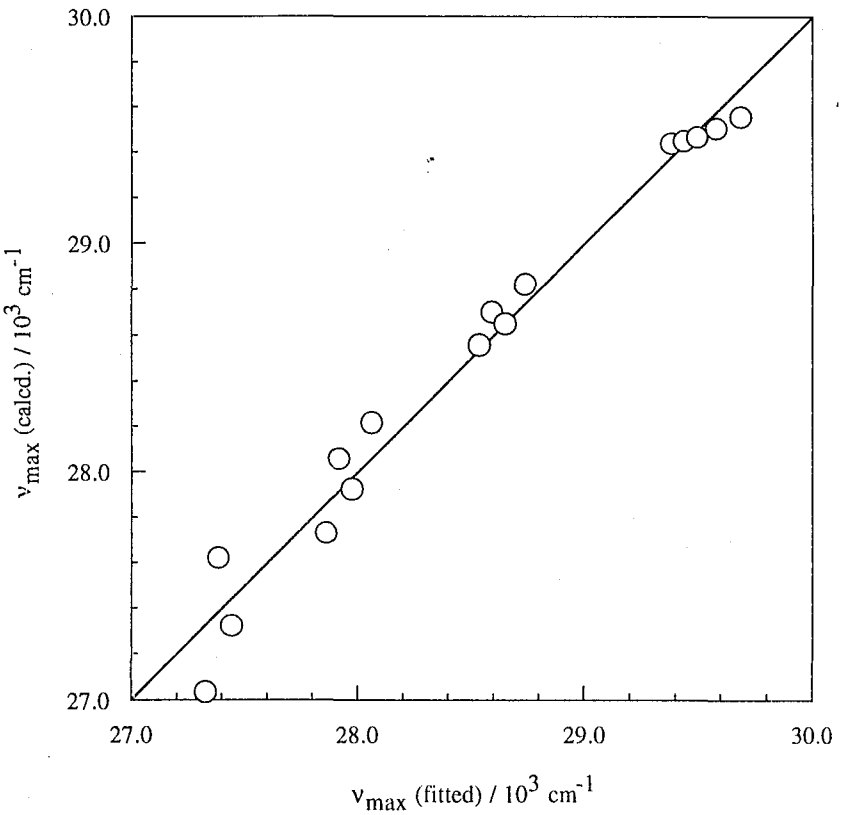

Figure 4.6 Correlation between the calculated absorption maxima of *all-trans*RSB and their regression values based on Eq. 4.1.

the solute than does that of orientational polarization.

The results for *all-trans*-RSB are shown in Figure 4.4 and also in Table 4.2. As shown in Figure 4.4, the experimental absorption maxima are in good agreement with their regression values. Thus, the solvatochromic shift of *all-trans*-RSB can be also described by the continuum approximation. There are also a few exceptions for the results in chroloform and pyridine. Table 4.2 shows that the ε- and n^2-dependent shifts of the absorption maximum of RSB occurs in a way similar to those for retinal, although the absolute values of the coefficients A and B are smaller.

Regression analysis is also necessary for processing primary data from the calculation because usually these are scattering due to numerical errors occurring in the solvent effect calculation, especially in the numerical evaluation of the reaction field. In addition, the determination of the coefficients A, B, and C allows to obtain the theoretical value for an arbitrary set of (ε, n). Figures 4.5 and 4.6 show the results of regression analysis. As similar to the case of experiments, the calculated values of the absorption maxima for **1** and **2** are well fitted to eq. 4.1. The results from the calculations summarized in Table 4.2 fairly coincide with those from the experiment, which assures us of the reliability of the present SCRF-CI method. For the sake of the subsequent discussion, in Table 4.2 the calculated results for 13-*cis*-RSB (**5**) are also listed.

4.4.2 Protonated Schiff Bases

In contrast to the cases of retinal and RSB, there are apparent deviations from eq. 4.1 in most of the *all-trans*-PRSB solutions studied here. This may imply the occurrence of specific interactions between the solute and solvent. As reported by Blatz et al.,[17] polar solvents such as alcohol and ether form hydrogen bond complexes with PRSB and hence they shield the electrostatic effect of a counterion.

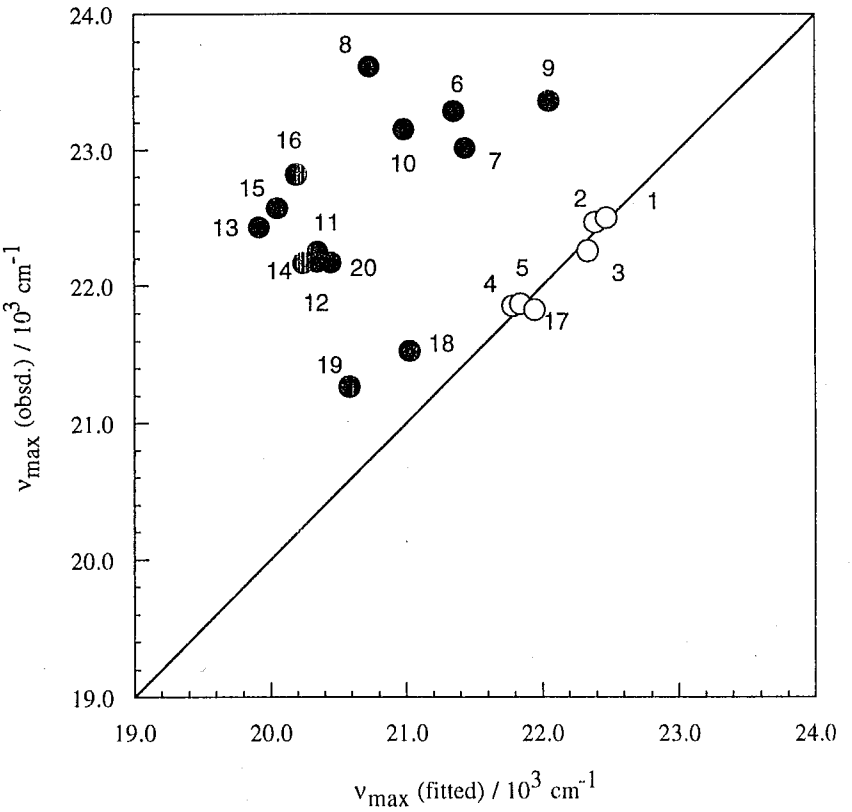

Figure 4.7 Correlation between the observed absorption maxima of *all-trans*PRSB and their regression values based on Eq.4.1. Numbers represent the solvents listed in Table 4.1. Solid symbols indicate the data excluded from the regression analysis.

Table 4.3 Results of regresion analysis for the absorption maxima of *all-trans*-PRSBs

	Coefficients[a] / 10^3 cm^{-1}		
	A	*B*	*C*
Exptl.[b]	-3.47	-3.57	24.6
3a	0.41	-2.90	20.9
3b	-0.09	-5.53	24.8
4a	0.50	-3.02	18.8
4b	-0.23	-6.58	21.1

a) Based on eq. 4.1

b) Results for *all-trans*-retinylidenebutylammonium dichloroacetate

It is known as "leveling effect". The fitting calculation was thus performed for solutions of non-polar and non-basic solvents, 1-5 and 17. The resulting coefficients *A*, *B* and *C* are summarized in Table 4.3. As shown in Figure 4.7, the absorption maxima observed for all the polar and basic solvents (solid circles) are blue shifted in comparison with the values predicted from the regression equation. Further analysis of them was not made, because the author's main interest is to extract the solvatochromic shifts following the linear response theory described in the section of theory .

The calculation was carried out for two types of PRSB: (*all-trans*-6*s*-*cis*-retinylidene)ethylammonium cation (**3a**) and (*all-trans*-6*s*-*cis*-retinylidene) ethylammonium acetate (**3b**) (for detail, see the calculation section). The results are summarized in Table 4.3. The value of *A* for **3a** is positive, suggesting that a blue shift occurs with an increase in ε, while that for **3b** is negative. In both cases, the absorption maxima are less sensitive to the static dielectric constant ε. The values of coefficient *B* for **3a** and **3b** both are relatively large negative values, indicating that a significant amount of red shift is induced with an increase in *n*. In addition, the *B* value of **3b** is about twice larger than that of **3a**.

Table 4.3 also lists the values of coefficients *A*, *B* and *C* for the solvatochromic shifts of **4a** and **4b**, both of which have 6*s*-*trans* conformation about the C6-C7 bond. The *A* value for the cationic species (**4a**) is positive, whereas that for a PRSB salt (**4b**) is negative. The *B* values for **4a** and **4b** both are negative, but the latter is about twice larger than the former. These relationships are quite similar to those found for **3a** and **3b**, indicating that the tendency of the solvatochromic shift is hardly influenced by the change of the ring/chain conformation.

All-trans-PRSB has 6*s*-*cis* conformation about the C6-C7 bond in solution.[5] In this regards, **3b** is a better model for the solution state of PRSB than **4b**. The *B* value for **3b** is -5.53×10^3 cm^{-1}, while the experimentally obtained *B* value for *all-*

trans-PRSB is -3.57×10^3 cm^{-1}. The calculated result is moderately encouraging. However, considering the fact that the regression analysis for the experimental values was performed with insufficient number of data points, further assessment would be needed.

The calculated values were compared with the results reported by Kliger et al.,[25a] who measured the absorption maxima of PRSB in phenol/ethanol solution. According to their results, the amount of red shift ($\Delta\nu$) of absorption maxima is in proportion to the concentration of phenol,

$$\Delta\nu = k\,[\text{phenol}] \tag{4.2}$$

where k is a constant and [phenol] is the concentration of phenol. In addition, it was interpreted that such a red shift arises from the increase in polarizability of solvent with an increase in phenol concentration. The polarizability of solvent was given by,

$$\alpha = \frac{3M}{4\pi N_a d}\left(\frac{n^2-1}{n^2+1}\right) \tag{4.3}$$

where N_a is Avogadro's number and α, M and d are the polarizability (11.0×10^{-24} cm^3), molecular weight and density of phenol, respectively. From eqs. 3.33, 4.2 and 4.3, we can obtain the following relationship between the amount of red shift and refractive index n.

$$\Delta\nu = k\left(\frac{3}{4\pi N_a \alpha}\right) f(n^2) \tag{4.4}$$

Comparing eq. 4.4 with eq. 4.1, we can see that the factor k ($3/4\pi N_a\alpha$) corresponds to the coefficient B. From Figure 4.1 of ref.13a, k is estimated to be 234 $cm^{-1}M^{-1}$. The B value can be estimated to be -6.5×10^3 cm^{-1}, which is very close to our calculated result. Therefore, it is expected that the present calculation can accurately predict the solvatochromic shifts of PRSB as well as those of retinal and RSB.

4.2.3 Details of the Counterion Effect

As already described, the C value corresponds to the absorption maxima *in vacuo*. Quite naturally, the C values obtained by this procedure well agree with the absorption maxima obtained from *in vacuo* SCF-CI calculations (data not shown). The difference in the C values between **3b** and **4b** is 3.7×10^3 cm^{-1}. This difference may arise from two geometrical factors: difference in the location of counterion, and difference in the conformation about the C6-C7 bond.

In order to investigate which factor is responsible for such a spectral difference, we calculated the absorption maxima for **3b** and **4b** with changing the location of the counterion. A unit negative charge was placed on the extended line of the N-H bond of PRSB, instead of explicitly treating the counterion (these models are denoted as **3b'** and **4b'**). According to an early work by Blatz et al.,[8b] the absorption maximum of PRSB red shifts with increasing size of the counterion, namely in the order of I^->Br^->Cl^-. And they indicated that the amount of red shift is nearly proportional to $1/d^2$. Here, a similar analysis are also applied to the calculated data for **3b'** and **4b'**.

In Figure 4.8 are the absorption maxima (filled symbols) of **3b'** and **4b'** plotted against $1/d^2$, where d is the distance between the N atom and the charge. The absorption maxima are certainly proportional to $1/d^2$ and the slopes ($\Delta C_{counterion}$) for **3b'** and **4b'** are nearly equal to each other (21.9× and 21.7×10^3

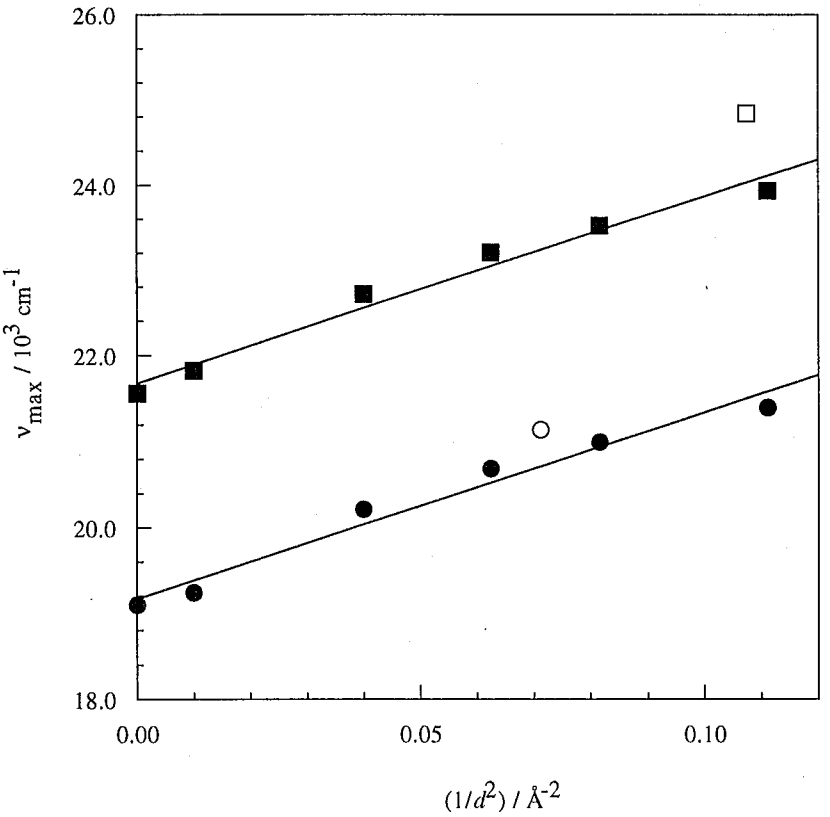

Figure 4.8 Calculated absorption maxima of 6*s-cis-all-trans*PRSB (■) and 6*s-trans-all-trans*PRSB (●) as a function of $1/d^2$, where d is the distance between the Schiff base nitrogen and a negative point charge. The absorption maxima of **3b** (□) and **4b** (○) are superposed.

$cm^{-1}Å^2$, respectively). These findings indicate that the *d*-dependence of the absorption maxima is hardly affected with the C6-C7 conformation. Figure 4.8 also shows the plots of the absorption maxima (open symbols) of **3b** and **4b** against $1/d^2$, where *d* is the average value of the distance O_1-N and O_2-N (d_{3b} = 3.1Å for **3b**, and d_{4b} = 3.8Å for **4b**). As can be seen, the data points for **3b** and **4b** are almost placed on the regression lines for **3b'** and **4b'**, respectively. This indicates that the blue shift induced on going from **3a** (**4a**) to **3b** (**4b**) is dominated by the electrostatic interaction between PRSB and its counterion. In Figure 4.8, the intercepts of the lines for **3b'** and **4b'** are distant by 2.5×10^3 cm^{-1} (denoted as $\Delta C_{C6\text{-}C7}$), which should correspond only to the contribution of the C6-C7 conformation change. This value almost agrees with the difference in the *C* value between **3a** and **4a** (2.1×10^3 cm^{-1}). These facts indicate that additivity is held between the shift induced by the counterion and that induced by a conformational change about the C6-C7 bond. Consequently, we can summarize the relation between the *in vacuo* absorption maxima of **3b** (C_{3b}) and **4b** (C_{4b}) as follows:

$$C_{4b} \fallingdotseq C_{3b} - \left(\frac{1}{(d_{4b})^2} - \frac{1}{(d_{3b})^2} \right) \times \Delta C_{\text{counterion}} - \Delta C_{C6-C7} \qquad (4.5)$$

where the second term originates from the difference in location of the counterion, and the third term from the ring/chain coplanarization. They contribute to red shifts of 1.2×10^3 cm^{-1} and 2.5×10^3 cm^{-1}, respectively.

Using **6a-f**, we investigated the dependence of the absorption maxima of PRSB on the spatial arrangement and orientation of a counterion. Figure 4.9(a) shows the calculated absorption maxima of **6a-f** as a function of $f(n^2)$ (ε was fixed to be four). When $f(n^2)$ = 0.0 (n = 1.0), the absorption maxima of **6a-f** are ranging from 19× to 23×10^3 cm^{-1}. With an increase in *n*, the absorption maxima of **6a-e**

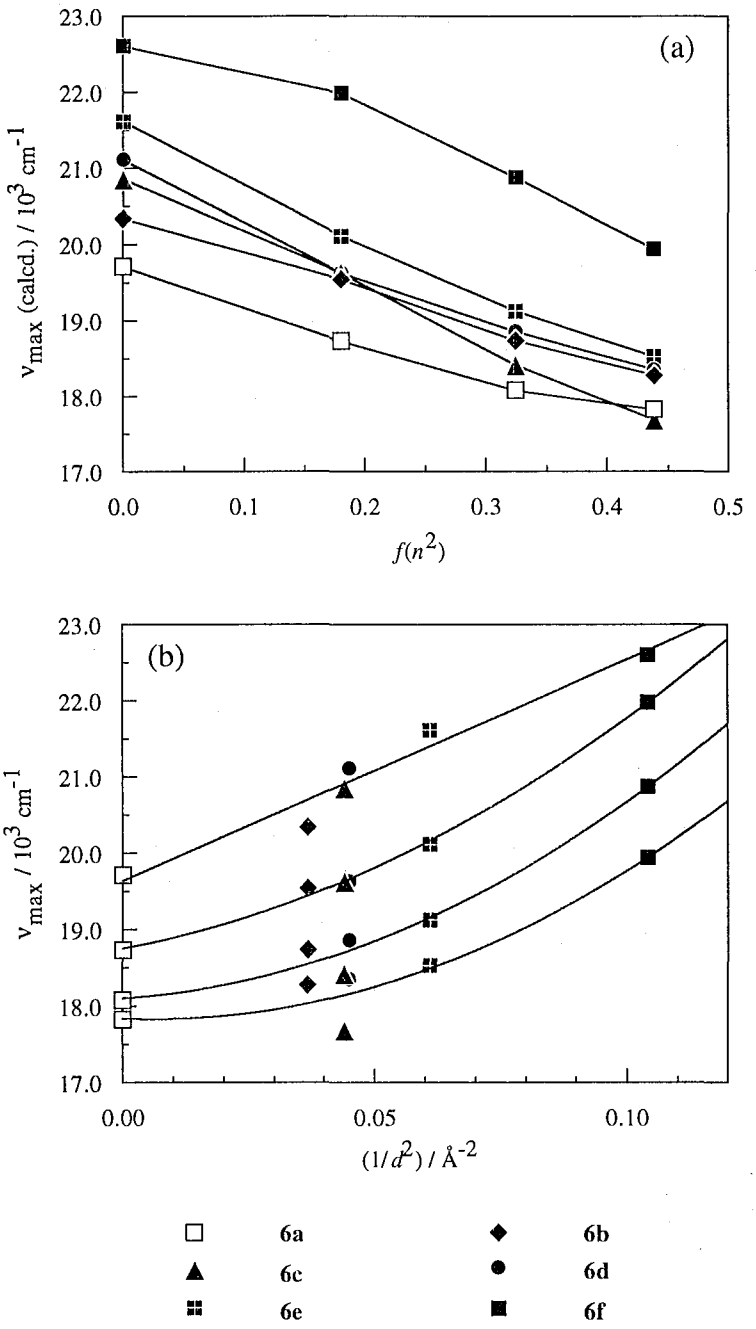

Figure 4.9 Absorption maxima of **6a-f** calculated under the condition of $\varepsilon = 4.0$. (a) The data are plotted as a function of $f(n^2)$. (b) The data are plotted as a function of $1/d^2$, where d is the average value of the distances between the Schiff base nitrogen and the oxygen atoms of carboxylate.

appears to converge, but the data for **6f** keeps away from the others. Next, for each n, the data are plotted against $1/d^2$, where d is the average value of the distances O_1-N and O_2-N (Figure 4.9(b)). The curves in this figure are drawn after the treatment of quadratic regression for each set of the data. When n=1.0, the absorption maxima almost change in proportion to $1/d^2$. This implies that the distance between PRSB and the counterion is the most important geometrical factor governing change of the absorption maxima, and that the effects of the orientation and arrangement of the counterion are less important. With an increase in n, the absorption maxima red shift, and the contribution of the quadratic component becomes remarkable. As a consequence, when n is 1.6, the difference in the absorption maxima among **6a-e** is very small compared to the case of n=1.0.

§4.5 Discussion

4.5.1 The Opsin Shift of Bacteriorhodopsin

The present calculations showed that the absorption maxima of PRSBs are significantly red shifted with an increase in the polarizability of solvent. This suggests the possibility that the major part of the opsin shift in bR is caused by the electronic polarization effect of the protein matrix. On the basis of the crystal structure of bR,[20] the amino acid residues around the chromophore can be identified. Here, the chromophore-binding pocket is defined as a region made by interlocking spheres, with a radius of 5Å, centered on each atom of the chromophore. In this region, the following seven aromatic residues were found: Tyr83, Trp86, Trp138, Trp182, Tyr185, Trp189, and Phe208 (Figure 4.10). The ratio of the number of these aromatic residues to that of the other residues in this region was 41%, in contrast to the ratio of only 14% for the whole protein. The assembly of these aromatic residues may act as a dielectric medium with a high refractive index. The effective refractive index of the binding pocket can be

estimated with the aid of a theory of electrostatics. In general, the averaged refractive index for a mixed solvent can be estimated using the modified Lorentz-Lorenz equation given by,

$$\frac{n^2 - 1}{n^2 + 2} = \frac{4\pi N_a}{3} \sum_i \frac{\rho_i \alpha_i}{M_i} \qquad (4.6)$$

where ρ_i, α_i and M_i are density (given in gcm^{-1}), polarizability and molecular weight of the component *i*. Table 4.4 lists the polarizabilities of benzene, phenol and indole, which were calculated from the data for atomic contribution to molar refraction.[41] By utilizing the present program, which can be used to evaluate the surface area of a molecular cavity,[42] the volume of the chromophore-binding pocket was estimated to be 1300 $Å^3$. In this region, there are four Trp side chains (indole), two Tyr side chains (phenol), and one Phe side chain (benzene). Consequently, the densities of indole, phenol and benzene moieties are given by 0.60, 0.24 and 0.10 gcm^{-3}, respectively (Table 4.4). The average refractive index for the chromophore-binding pocket is thus determined to be 1.51.

To define the opsin shift $\Delta\nu$, we adopt the absorption maximum of *all-trans*-PRSB in hexane as a reference. Namely, $\Delta\nu = \nu_{\text{in hexane}} - \nu_{\text{in protein}}$. As described in the section 4.4.2, the absorption maxima of PRSB are interpreted in terms of the continuum model only when non-polar and non-basic solvents are used. In view of this, it is reasonable to choose hexane as the reference rather than methanol, which was often used in the previous studies.[9] Using the observed values of 17.6×10^3 cm^{-1} for bR_{568} and 22.5×10^3 cm^{-1} for the reference, one can obtain 4.9×10^3 cm^{-1} as the opsin shift (Table 4.5). For theoretical evaluation of the opsin shift, **3b** was used as a model of *all-trans*-PRSB and **4b** as a model of the bR chromophore. The calculated absorption maxima of **3b** and **4b** are summarized in Table 4.5. The absorption maxima (23.1×10^3 cm^{-1}) for **3b** in hexane was obtained by substituting

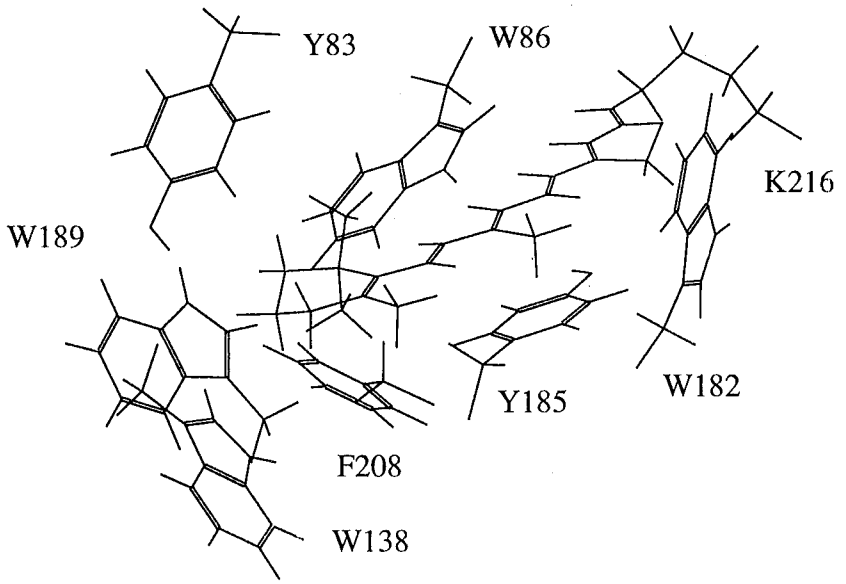

Figure 4.10 The molecular structure of the chromophore and the aromatic residues present within the chromophore-binding pocket. The coordinates of the heavy atoms were taken from the crystal structure (ref. 20) deposited with the Protein Data Bank (ref. 48). Hydrogen atoms were added in the way as described in the section of "Modeling of Chromophores".

Table 4.4 Polarizability and density of some aromatic compounds

	polarizability $4\pi\alpha$ / 10^{-24} cm^3	density[a] ρ / g cm^{-3}
benzene[b]	131.1	0.10
phenol[c]	138.7	0.24
indole[d]	187.2	0.60

a) Density in the region of 5Å-vicinity of the chromophore (see text)
b) A model of the side chain of Phe
c) A model of the side chain of Tyr
d) A model of the side chain of Trp

Table 4.5 Comparison between experimental and calculated opsin shifts for bR_{568}, M_{412}, and Rh_{500}

	ν_{max} in hexane / 10^3 cm^{-1}	ν_{max} in protein / 10^3 cm^{-1}	opsin shift $\Delta\nu$ / 10^3 cm^{-1}
		bR_{568}	
Exptl.	22.5	17.6	4.9
Calcd.	23.1	18.4	4.7
		M_{412}	
Exptl.	28.1	24.3	3.8
Calcd.	28.2	24.5	3.7
		Rh_{500}	
Exptl.	22.5	20.0	2.5
Calcd.	23.1	20.5	2.6

the values of the coefficients A, B and C (given in Table 4.3) and the medium parameters for hexane ($\varepsilon = 1.89$, $n = 1.375$) into eq. 4.1. For **4b**, the value of 1.51 was used as the refractive index of bR, as obtained above. Here the value of ε was taken to be 4.0, according to recent studies using the Poisson-Boltzmann electrostatics.[43,44] Then, the absorption maximum of **4b** in the bR-mimic environment is evaluated to be 18.4×10^3 cm^{-1}. As a consequence, the opsin shift is evaluated to be 4.7×10^3 cm^{-1}, in excellent agreement with the observed value.

Similarly, the author also analyzed the spectral shift observed for M_{412}. The chromophore of M_{412} is unprotonated 13-*cis* retinal Schiff base. The absorption maxima of *all-trans*-RSB in hexane was taken as a reference. Then, the observed opsin shift for M_{412} is 3.8×10^3 cm^{-1}. In calculation, **2** was used as a model of *all-trans*-RSB, and **5** as a model of the chromophore of M_{412}. As shown in Table 4.5, the calculated absorption maxima of **2** and **5** are 28.2×10^3 and $24.5\times10^3 cm^{-1}$, respectively. The resulting opsin shift is 3.7×10^3 cm^{-1}, again in excellent agreement with the observed value.

In summary, the opsin shifts of both bR_{568} and M_{412} can be explained by explicitly taking into account the polarizable medium effect of the aromatic residues surrounding the chromophore. It is known that most of the aromatic residues appearing in the retinal-binding pocket of bR are conserved across many retinal-bound proteins.[45] For example, Phe261, Trp265 and Tyr269 in bovine rhodopsin correspond to Trp182,Tyr185 and Trp189 in bR, respectively.[46] In fact, site-directed mutagenesis studies have shown that the replacement of these residues causes a significant amount of blue shift in both of bR and Rh.[45,47] For example, in the W182F mutant of bR the main absorption band appears at 491 nm. Now the author attempts to calculate the opsin shift for Rh. For this purpose, compound **9** was selected as a model of the chromophore in Rh. Since there is no available data

for the tertiary structure of Rh, the values of the medium parameters were assumed to be the same as determined for bR, namely $\varepsilon = 4.0$, $n = 1.51$. The results are summarized in Table 4.5. As expected, the calculated opsin shift (2.6×10^3 cm^{-1}) is in good agreement with the observed value (2.5×10^3 cm^{-1}). The above results strongly suggest that the polarizable medium effect, mechanism (4), is a common origin of the opsin shifts observed for retinal proteins.

4.5.2 Decomposition of the Opsin Shift

The calculated opsin shift of bR_{568} (4.7×10^3 cm^{-1}) can be decomposed into at least three kinds of contributions (Table 4.6). The first is the effect of 6*s-cis*→6*s-trans* conformational change (mechanism (1)), and the second is the weakening of the interaction of PRSB with its counterion in bR (mechanism (2)). These have been already estimated in the derivation of eq 4.5: namely, mechanisms (1) and (2) cause red shifts of 2.5×10^3 and 1.2×10^3 cm^{-1}, respectively. Then, the residual shift is 1.0×10^3 cm^{-1}, which should be attributed to the polarizable medium effect of the protein (mechanism (4)). In what follows, the author will compare these results with available experimental data.

Hu et al.[27] pointed out the importance of cooperative effect of mechanisms (1) and (2). According to their experimental results, the former causes a red shift of ~2×10^3 cm^{-1} and the latter also does that of ~2×10^3 cm^{-1} (Table 4.6). A unique point of their hypothesis is that the combined action of (1) and (2) generates an additional red shift of ~1×10^3 cm^{-1}. However, according to our results (Figure 4.8), such a phenomenon is not observed. In Hu's experiments, butylamine Schiff base was used as 6*s-cis*-PRSB, while aniline Schiff base as 6s-*trans*-PRSB. Generally speaking, the use of models with different imine structures may suffer from a potential disadvantage in investigating the spectral tuning mechanism, because the absorption maximum of PRSB is very sensitive to a subtle difference in

Table 4.6 Results for decomposition of the opsin shift[a)]

	mechanism					
	(1)	(2)	(3)	(4)	(1)+(2)[b)]	total
This work	2.5	1.2	–	1.0	–	4.7
Hu, et al.[c)]	~2	~2	0	0	~1	~5
Yan, et al.[d)]	2.0	–	(2.1)[e)]	(2.1)[e)]	–	4.1

a) Each contribution is given in 10^3 cm^{-1}
b) Concerted effect of mechanisms (1) and (2)
c) Taken from ref. 27
d) Taken from ref. 26
e) The total contributions from mechanisms (3) and (4) is 2.1×10^3 cm^{-1}

Table 4.7 Calculated and observed absorption maxima of 13,14-dihydro-retinal and its analogues[a)]

	in methanol (ε=33,n=1.327)		in protein (ε=4,n=1.51)		Opsin shift[b)]	
	Calcd.	Exptl.[c)]	Calcd.	Exptl.[c)]	Calcd.	Exptl.[c)]
7a	36.8	34.6	35.5			
7b	35.4		35.3			
7c	32.3		32.3			
7d	32.1		31.9	30.5	4.9	4.1
8a	32.1	32.6	32.0			
8b	31.4		30.7	31.2	1.4	1.4

a) Given in 10^3 cm^{-1}
b) Obtained by subtracting the absorption maxima of the chromophore (**7d** and **8b**) in protein from those of the corresponding aldehyde (**7a** and **8a**) in methanol
c) Taken from ref. 26

the Schiff base-counterion distance. Due to more bulkiness of the aniline group, the distance might be longer in the aniline Schiff base than in the butylamine Schiff base. If so, their observed data could be interpreted without considering a synergy between the two effects.

13,14-dihydro-retinal (**7a**) is a better probe capable of escaping from the counterion effects, because its conjugated system is not linked to the Schiff base linkage. Considering this fact, Yan et al.[26] evaluated the opsin shifts for **7a** and its analogue (**8a**) as the change in absorption maximum on going from **7a** (or **8a**) in methanol to that in bR. Namely, in the reference state the chromophore is aldehyde, not Schiff base: this point is different from the conventional definition of the opsin shift. As shown in Table 4.7, the resulting opsin shifts for **7a** and **8a** were 4.1 and 1.4×10^3 cm^{-1}, respectively. The present calculated results, following Yan's definition, are 4.9× and 1.4×10^3 cm^{-1} for **7a** and **8a**, respectively, in good agreement with the observed values.

8a has *s-trans* conformation about the C6-C7 bond because of lack of ionone ring, and thereby mechanism (1) does not operate on binding to the protein. In addition, the absence of such a bulky group has an advantage that there would be no significant steric interaction between the chromophore and the protein in the binding state. As a result, the opsin shift for **8a** is expected to more purely reflect the polarizable effect of the protein matrix than that for **7a**. This seems to be the main reason why the calculated value is in better agreement with the experimental value of **8a** than with that of **7a**. However, it should be noted that the opsin shift for **8a** involves not only the effect of the protein matrix, but also the effect of the terminal structure on the Schiff base side, even if the terminal C=N double bond is not linked directly to the conjugated system. In order to examine the latter effect, the author calculated the absorption maximum of **8b** in the methanol-like environment, namely ε=32.7 and n=1.327. As shown in Table 4.7, the structural

conversion, on going from aldehyde to Schiff base, causes a red shift of 0.7×10^3 cm^{-1}. Thus, the net contribution of the protein matrix occupying in the opsin shift for **8a** is estimated to be about 0.7×10^3 cm^{-1}. This value is somewhat smaller than the value (1.0×10^3 cm^{-1}) previously obtained from the analysis of the opsin shift for the native pigment. This is quite a reasonable result, considering the symmetric nature of the conjugated system of **8a**. Namely, unlike PRSB, the conjugated system of **8a** has no apparent dipole moment in the excited state, where an excessive stabilization would not be induced by interaction with solvent. Thus, the use of **7a** or **8a** tends to underestimate the polarizable effect of the protein matrix.

The calculated opsin shift for **7a** is larger than that for **8a** by 3.5×10^3 cm^{-1}. It is reasonable to say that the major part of this difference arises from the coplanarization effect (mechanism (1)). In fact, the 6s-*cis*→*trans* conversion from **7b** to **7d** causes a red shift of 3.3×10^3 cm^{-1}. On the other hand, the difference in the observed opsin shift between **7a** and **8a** is 2.7×10^3 cm^{-1} , which is somewhat smaller than the calculated value. The difference between the calculated and observed values would be chiefly due to the occurrence in a steric interaction between **7a** and the protein. The analysis of such a phenomenon is beyond the scope of the present study.

The difference in the observed absorption maxima between **7a** and **8a** is 2.0×10^3 cm^{-1} in methanol, a value which corresponds to the contribution of the ring/chain coplanarization. By subtracting this contribution from the total opsin shift for **7a** (4.1×10^3 cm^{-1}), Yan et al. concluded that the net contribution of the protein environment was a red shift of 2.1×10^3 cm^{-1}. This value is significantly larger than the above result (1.4×10^3 cm^{-1}) deduced from the opsin shift for **8a**. For more complete argument against such a difference, it is necessary to obtain experimental data for the absorption maxima of **7b-7d** and **8b**, and for the steric effect mentioned above.

In summary, the polarizable effect of the protein matrix actually works for the spectral tuning of bR. Its contribution is not less than 1.0×10^3 cm^{-1} for the native chromophore.

4.5.3 Cooperative Action between Counterion Effect and Polarizable Medium Effect

As far as the protein matrix works as a polarizable medium, the opsin shift is reproducible even when an external charge is absent. This is understood from the possibility that the medium behaves like a counterion or an external charge. In the ground state, the positive charge of PRSB is localized on the -CH=NH- moiety, and hence the medium polarizes so as to maximally stabilize such a distribution of positive charge. In other words, solvent molecules cooperatively behaves like a counterion of PRSB. Upon excitation, the positive charge of PRSB is delocalized towards the β-ionone ring,[23] immediately followed by the electronic part of polarization of the medium. Then, the polarizable medium acts as if it were a mobile counterion. The result from such an action is similar to that expected for the external charge proposed by Nakanishi et al.[12]

In order to provide a rigid physical basis for the above interpretation, the author examined the dependence of the energy levels of the ground and lowest π–π* excited states on the medium parameters. The energies of these states of **3a** and those for **3b** are plotted as a function of $f(\varepsilon)$ (n is fixed to be 1.4) in Figures 4.11(a) and (b), where the excited-state energy is the sum of the ground-state energy and the excitation energy obtained by the CI calculation. As for **3a** (Figure 4.11(a)), the increase in ε lowers the energy of the ground state. This effect corresponds just to that of the counterion of PRSB. On the other hand, for the case of **3b** (see Figure 4.11(b)), the effect of the static dielectric constant is less important, because the acetate anion already serves as a counterion. In both **3a** and

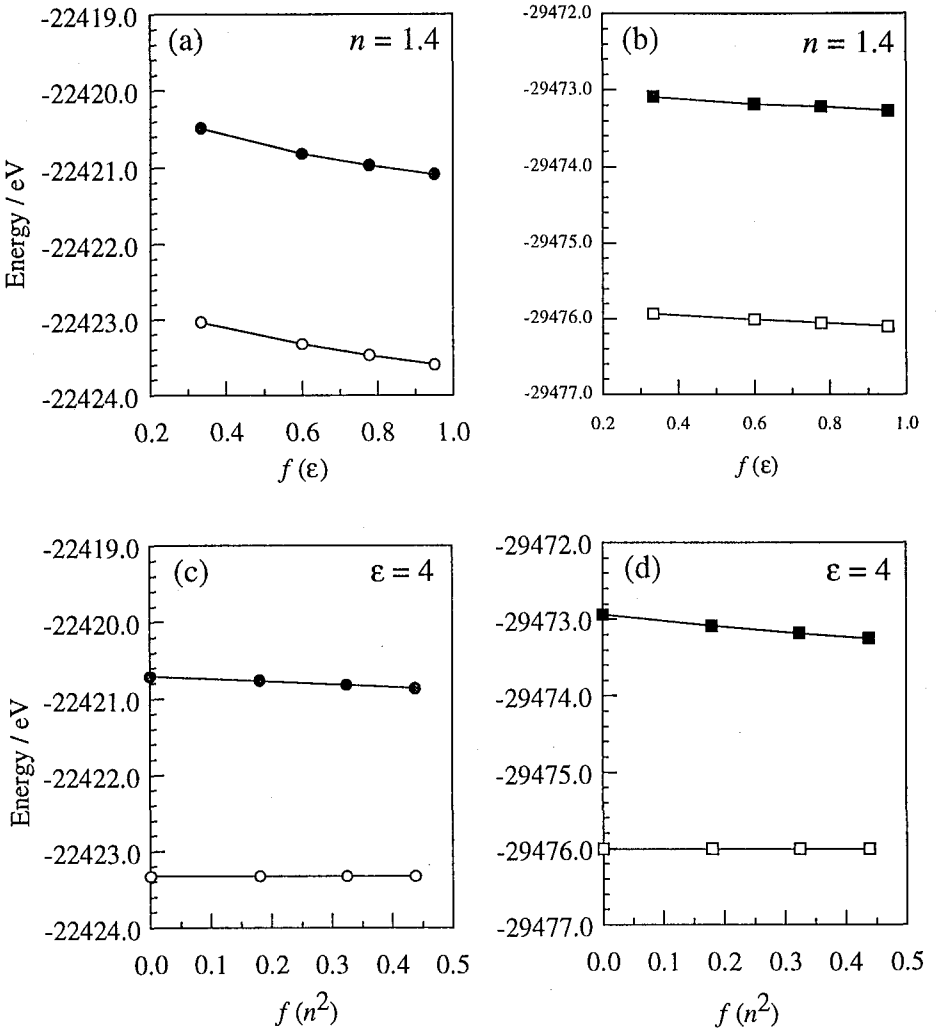

Figure 4.11 Energies of the ground state (O, □) and the π–π* excited state (●, ■) as a function of medium parameters. (a) and (c) are for **3a** (O, ●), and (b) and (d) are for **3b** (□, ■).

3b, the increase in ε causes a lowering of the excited-state energy as well, but the amount of energy change is comparable to the solvation energy in the ground state. As a result, the slow relaxation of solvent, depending on static dielectric constant ε, hardly affects the excitation energy in both cases of **3a** and **3b**. This supports the fact that in the PRSBs studied here the A values are much smaller than the B values.

In Figures 4.11(c) and (d) the electronic energies of the ground- and π–π^* excited-states of **3a** and those of **3b** are plotted as a function of $f(n^2)$ (ε is fixed to be 4.0). As far as ε is kept constant, the increase in n exerts no apparent influence on the ground-state energy. On the other hand, in both **3a** and **3b**, the increase in n causes a significant lowering of the excited-state energy, resulting in a red shift. This is just due to the external charge-like effect of the polarizable medium. In addition, these figures show that the lowering of the excited-state energy is remarkable in **3b**, which means that the polarizable medium operates more effectively for PRSB with a counterion (**3b**) than for the cationic form (**3a**). This explains why the B value for **3b** is larger than that for **3a** (Table 4.3).

According to the above analysis, the presence of counterion hardly affects the A value for PRSB, while it significantly increases the absolute value of B. These facts imply that the coefficients A, B and C in eq. 4.1 depend on the distance d, regarded as a measure of the counterion effect, in their respective ways. Now the author attempts to find a functional form representing the d-dependence of these coefficients, namely $A(d)$, $B(d)$ and $C(d)$. For this purpose, it is sufficient to know how the absorption maximum of PRSB is influenced by the change of d for a given set of (ε, n). Such information is obtained from the data for **6a-f**, which have different d values. As shown in Figure 4.9(b), the absorption maxima of **6a-f** well fit the quadratic regression curve against $1/d^2$, when the medium parameters are specified. Thus, the following relationship should be satisfied,

$$X(d) = \beta(1/d^2)^2 + \gamma(1/d^2) + \alpha \qquad (4.7)$$

where X is A, B or C, and α, β, and γ are constants. Although it is not easy to determine the values of α, β, and γ , it is possible to obtain the first order approximation of eq. 4.7 for each of A, B and C. For the coefficient C, we have already derived eq. 4.13, which clearly indicates that the leading term of the right-hand side is $\gamma(1/d^2)$. For the coefficient A, the d-dependence is nearly negligible, because the A value is hardly affected according to whether PRSB has a counterion or not. Thus, the term α is the leading term for A. Finally, in order to reproduce the quadratic nature of curves shown in Figure 4.9(b), the coefficient B must exhibit a quadratic dependence on $1/d^2$. In other words, the leading term for B is $\beta(1/d^2)^2$, which is qualitatively consistent with the fact that the B value is most remarkably affected by the presence of a counterion. These relationships are useful for understanding the gross tendency of the concerted effect of counterion and medium.

A phenomenological feature of the above concerted effect becomes noticeable in media with high refractive indices. When n = 1.4-1.6, the blue shift induced by the counterion effect and the red shift induced by the medium effect are almost compensated for each other in the region of 0.00-0.05 of $1/d^2$ (i.e., d>4.5). Therefore, the absorption maxima of **6a-e** hardly depends on the location of their counterion in high-refractive index environments. According to the estimation based on eq. 4.6, the retinal-binding pocket of bR, probably of Rh as well, satisfies this condition. **6b** is similar to the active center model of Rh proposed by Smith et al.,[29] who attempted to determine the spatial arrangement of a carboxylate group so as to reproduce the observed absorption maxima of this protein. To one's regret, the model was deduced from the calculation that did not involve the polarizable medium effect of the protein. The use of the *in vacuo* calculation may be

inappropriate for a precise modelling of the protein.

The absorption maximum of **6f** keeps blue-shifted relative to those of **6a-6e**. This implies that its solvatochromic shift is dominated by the contribution of C, namely the term proportional to $1/d^2$. Such an anomaly results from the fact that the distance d (3.5 Å) of **6f** is significantly shorter than those of the others.

§4.6 Concluding Remarks

The present study demonstrated that the SCRF-CI method developed in Chapter3 is a powerful tool for interpreting the solvatochromic shifts of *all-trans*-retinal, *all-trans*-RSB and *all-trans*-PRSB. With the aid of this method, the author succeeded in quantitatively reproducing the opsin shifts of bR_{568} and M_{412}. The calculation also revealed the contributions of all the mechanisms which had been believed to cause the opsin shift: namely, (1) ring/chain coplanarization, (2) weak interaction between PRSB and its counterion, (3) the external charge effect, and (4) the polarizable medium effect of the protein matrix. Although mechanism (4) has been accepted only as a conceptual model, the present study provides a realistic picture on it. Explicit treatment of mechanism (4) enables us to reproduce not only the opsin shifts for bR_{568} and M_{412}, but also the data for the artificial pigments and Rh. In conclusion, the aromatic residues forming the retinal-binding pocket plays a decisive role in causing the opsin shift. Finally, the author must emphasize that such an unambiguous conclusion comes from the fact that the hexane solution of PRSB was chosen as the reference state to measure the opsin shift.

References and Notes

(1) See for reviews: (a) Birge, R. R. *Annu. Rev. Phys. Chem.* **1990**, *41*, 683. (b) Lanyi, J. K. *Biochim. Biophys. Acta.* **1993**, *1183*, 241. (c) Nathans, J. *Biochemistry* **1992**, *31*, 4923. (d) Khorana, H. G. *Ann. N. Y. Acad. Sci.* **1986**, *471*, 272. (e) Mathies, R. A.; Lin, S. W.; Ames, J. B.; Pollard, W. T. *Ann. Rev. Biophys. Biophys. Chem.* **1991**, *20*, 491. (f) Nakanishi, K. *Pure Appl. Chem.* **1991**, *63*, 161. (g) Ottolenghi, M.; Sheves, M. *J. Menbr. Biol.* **1989**, *112*, 193.

(2) Lozier, R.; Bogomolni, R. A.; Stoeckenius, W. *Biophys. J.* **1975**, *15*, 955.

(3) van der Steen, R.; Biesheuvel, P. L.; Mathies, M. A.; Lugtenburg, J. *J. Am. Chem. Soc.* **1986**, *108*, 6410.

(4) Harbison, G. S.; Smith, S. O.; Pardoen, J. A.; Courtin, J. M. L.; Lugtenburg, J.; Herzfeld, J.; Mathies, R. A.; Griffin, R. G. Biochemistry **1985**, *24*, 6955.

(5) Harbison, G. S.; Mulder, P. P. J.; Pardoen, H.; Lugtenburg, J.; Herzfeld, J.; Griffin, R. G. *J. Am. Chem. Soc.* **1985**, *107*, 4809.

(6) Wada, M.; Sakurai, M.; Inoue, Y.; Tamura, Y.; Watanabe, Y. *J. Am. Chem. Soc.* **1994**, *116*, 1537.

(7) Bassov, T.; Sheves, M. *J. Am. Chem. Soc.* **1985**, *107*, 7524.

(8) (a) Blatz, P. E.; Johnson, R. H.; Mohler, J. H.; Al-Dilaimi, S. K.; Dewhurst, S.; Erickson, J. O. *Photochem. Photobiol.* **1971**, *13*, 237. (b) Blatz, P. E.; Mohler, J. H.; Navanglu, H. V. *Biochemistry* **1972**, *11*, 848. (c) Blatz, P. E.; Mohler, J. H. *Biochemistry* **1972**, *11*, 3240. (d) Blatz, P. E.; Mohler, J. H. *Biochemistry*, **1975**, *14*, 2340.

(9) (a) Arnaboldi, M.; Motto, M.G.; Tsujimoto, K.; Balogh-Nair, V.; Nakanishi, K. *J. Am. Chem. Soc.* **1979**, *101*, 7082. (b) Honig, B.; Dinur, U.; Nakanishi, K.; Balogh-Nair, V.; Gawinowics, M. A.; Arnaboldi, M.; Motto, M. G. *J. Am. Chem. Soc.* **1979**, *101*, 7084. (c) Sheves, M.; Nakanishi, K.; Honig, B. *J. Am. Chem. Soc.* **1979**, *101*, 7086.

(10) (a) Irving, C. S.; Byers, G. W.; Leermakers, P. A. *J. Am. Chem. Soc.* **1969**, *91*, 2141. (b) Irving, C. S.; Byers, G. W.; Leermakers, P. A. *Biochemistry* **1970**, *9*, 858.

(11) Honig, B.; Greenberg, A. D.; Dinur, U.; Ebrey, T.G. *Biochemistry* **1976**, *15*, 4593.

(12) (a) Nakanishi, K.; Balogh-Nair, V.; Arnaboldi, M.; Tsujimoto, K.; Honig, B. *J. Am. Chem. Soc.* **1980**, *102*, 7945. (b) Motto, M. G.; Sheves, M.; Tsujimoto, K.; Balogh-Nair, V.; Nakanishi, K. *J. Am. Chem. Soc.* **1980**, *102*, 7947.

(13) Mao, B.; Govindjee, R.; Ebrey, T.; Arnaboldi, M.; Balogh-Nair, V.; Nakanishi, K *Biochemistry* **1981**, *20*, 428.

(14) Spudich, J. L.; McCain, D. A.; Nakanishi, K.; Okabe, M.; Shimizu, N.; Rodman, H.; Honig, B.; Bogomolni, A. *Biophys. J.* **1986**, *49*, 479.

(15) Koutalos, Y.; Ebrey, T. G.; Tsuda, M.; Odashima, K.; Lien, T.; Park, M. H.; Shimizu, N.; Derguini, F.; Nakanishi, K.; Gilson, H. R.; Honig, B. *Biochemistry* **1989**, 28, 2732.

(16) Lugtenburg, J.; Muradin-Szweykowska, M.; Heeremans, C.; Pardoen, J. A.; Griffin, R. G.; Smith, S. O.; Mathies, R. A. *J. Am. Chem. Soc.* **1986**, *108*, 3104.

(17) Sheves, M.; Nakanishi, K. *J. Am. Chem. Soc.* **1983**, *105*, 4033.

(18) Derguini, F.; Caldwell, C. G.; Motto, M. G.; Balogh-Nair, v.; Nakanishi, K. *J. Am. Chem. Soc.* **1983**, *105*, 646.

(19) Gat, Y.; Sheves, M. *Photochem. Photobiol.* **1994**, *59*, 371.

(20) Grigorieff, T.; Ceska, K.; Downing, K. H.; Baldwin, J. M.; Henderson, R.; *J. Mol. Biol.* **1996**, *259*, 393.

(21) Mogi, T.; Stern, L. J.; Marti, T.; Chao, B. H.; Khorana, H. G. *Proc. Natl. Acad. Sci. USA* **1988**, *85*, 4148.

(22) Birge, R. R.; Murray, L. P.; Pierce, B. M.; Akita, H.; Balogh-Nair, V.; Findsen, L. A.; Nakanishi, K. *Proc. Natl. Acad. Sci. USA* **1985**, 82, 4117.

(23) Mathies, R.; Stryer, L. *Proc. Natl. Acad. Sci. USA* **1976**, *73*, 2169.

(24) Suzuki, T.; Kito, Y. *Photochem. Photobiol.*, **1972**, *15*, 275.

(25) (a) Kliger, D. S.; Milder, S. J.; Dratz, E. A. *Photochem. Photobiol.* 1977, 25, 277. (b) Milder, S. J.; Kliger, D. S. *Photochem. Photobiol.* **1977**, *25*, 287.

(26) Yan, B.; Spudich, J. L.; Mazur, P.; Vunnam, S.; Dergini, F.; Nakanishi, K. *J. Biol. Chem.*

1995, *270*, 29668.

(27) Hu, J.; Griffin, R. G.; Herzfeld, *J. Proc. Natl. Acad. Sci. U.S.A.* **1994**, *91*, 8880.

(28) For example, (a) Muthukumar, M.; Weimann, L. *J. Chem. Phys. Lett.* **1978**, *53*, 436. (b) Kakitani, H.; Kakitani, T.; Rodman, H.; Honig, B. *Photochem. Photobiol.* **1985**, *41*, 471. (c) Beppu, Y.; Kakitani, T. *Photochem. Photobiol.* **1994**, *59*, 660. (d) Tallent, J. R.; Hyde, E. W.; Findsen, L. A.; Fox, G. C.; Birge, R. R. *J. Am. Chem. Soc.* **1992**, *114*, 1581. (d) Gilson, H. S. R.; Honig, B. H; *J. Am. Chem. Soc.* **1988**, *110*, 1943.

(29) Han, M.; DeDecker, B. S.; Smith, S. O. *Biophys. J.* **1993**, *65*, 899.

(30) (a) Han, M.; Smith, S. O. Biochemistry, 1995, 34, 1425. (b) Han, M.; Smith, S. O. *Biophys. Chem.* **1995**, *56*, 23.

(31)See for review: Tomasi, J.; Perisico, M. *Chem. Rev.* **1994**, *94*, 2027.

(32) (a) Raudino, A.; Zuccarello, F.; Buemi, G. *J. Chem. Soc., Faraday Trans. 2* **1983**, *79*, 1759. (b) Zuccarello, F.; Raudino, A.; Buemi, G. *J. Mol. Struct. (Theochem)* **1984**, *107*, 215.

(33) Houjou, H.; Sakurai, M.; Inoue, Y. *J. Chem. Phys.* **1997**, *107*, 5652.

(34) (a) Hoshi, H.; Sakurai, M.; Inoue, Y.; Chûjô, R. *J. Chem. Phys.* **1987**, *87*, 1107. (b) Hoshi, H.; Sakurai, M.; Inoue, Y.; Chûjô, R. *J. Mol. Struct. (Theochem)* **1988**, *180*, 267.

(35) Stewart, J. J. P. *J. Comput. Chem.* **1989**, *10*, 209.

(36) Stewart, J. J. P.; Frank, J. MOPAC Ver6.01, Seilar Reserch Laboratory, U.S.Airforece Academy, Colorado Springs, CO 80840-6528, 1989.

(37) Pearlman, D. A.; Case, D. A.; Caldwel, J. W.; Ross, W. S.; Cheatham III, T. E.; Ferguson, D. M.; Seibel, G. L.; ChandraSingh, U.; Weiner, P. K.; Kollman,P. A. (1995) AMBER ver. 4.1, University of Calfornia, San Francisco.

(38) (a) Krough-Jespersen, K.; Ratner, M. *J. Chem. Phys.* **1976**, *65*, 1305. We adopted the β^0 value of -30eV for oxygen according to (b) Faure, P. J. J.; Chalvet, O.; Jaffe, H. H. *J. Phys. Chem.* **1981**,*85*, 473. (c) Rajzmann, M.; Francois, P. QCPE 11 **1979**, 382.

(39) Furuki, T.; Umeda, A.; Sakurai, M.; Inoue, Y.; Chûjô, R.; Harata, K. *J. Comput. Chem.* **1994**, *15*, 90.

(40) Inoue, Y.; Tokitô, Y.; Chûjô, R.; Miyoshi, Y. *J. Am. Chem. Soc.* **1977**, *99*, 5592.

(41) "LANGE'S HANDBOOK OF CHEMISTRY 11th Ed.", Dean, J. A. Ed., McGraw-Hill (New York) 1973.

(42) The volume of the binding pocket defined in the text was calculated as follows: (i) calculate the surface area (S) of the interlocking spheres whose radii are R=5Å; (ii) calculate the surface area (s) of the interlocking spheres whose radii are van der Waals radii (r) of each atom; (iii) the volume of the region enclosed by these two interlocking spheres is estimated by (1/3)(RS - rs).

(43) Bashold, B.; Gerwert, K, *J. Mol. Biol.* **1992**, *224*, 473.

(44) According to ref.43, the pKa values of the ionizable residues in bR were consistently reproduced on the assumption that the dielectric constant of the protein interior was 4.0.

(45) Mogi, T.; Marti, T.; Khorana, H. G. *J. Biol. Chem.* **1989**, *264*, 14197.

(46) Hisatomi, O.; Kayada, S.; Aoki, Y.; Iwasa, T.; Tokunaga, F. *Vision Res.* **1994**, *34*, 3097.

(47) Nakayama, T.; Khorana, H. G. *J. Biol. Chem.* **1991**, *266*, 4269.

(48) (a) Abola, E. E.; Bernstein, F. C.; Koetzle, T. F.; Weng, J Protein Data Bank, in Crystallographic Databases-Information Content, Software Systems, Scientific Applications, F. H. Allen, G. Bergerhoff, and R. Siebers, eds., Data Commission of the International Union of Crystallography, Bonn/Cambridge/Chester (1987) pp. 107-132. (b) Bernstein, F. C.; Koetzle, T. F.; Williams, G. J. B.; Meyer, Jr., E. F.; Brice, M. D.; Rodgers, J. R.; Kennard, O.; Shimonouchi, T.; Tasumi, M. The Protein Data Bank: a Computer-based Archival File for Macromolecular Structures, *J. Mol. Biol.* **1977**, *112*, 535.

Chapter 5. Analysis of the Opsin Shift of Bacteriorhodopsin Based on Full-atomic Calculation Involving Electronic Polarization Effect

§5.1 Introduction

Bacteriorhodopsin (bR) is a retinal protein that functions as a light-driven proton pump in the purple membrane of *Halobacterium halobium*.[1] Illumination of the light-adapted state (bR_{568}) initiates a sequential photoreaction cycle consisting of spectroscopically distinct intermediates K, L, M, N, and O.[2] The chromophore *all-trans* retinal is bound to Lys216 via protonated Schiff base linkage. The absorption maximum (568 nm) in the light-adapted state is shifted to red by ~130 nm with respect to that (~440 nm) for protonated retinylidene Schiff base (PRSB) in methanol solution.[1] Such a protein-induced bathochromic shift is known as opsin shift. The elucidation of its mechanism has been one of the most interesting issues in photochemistry of retinal proteins for these decades.

The absorption maximum of the chromophore corresponds to its lowest π–π^* excitation energy. In the ground state, a positive charge is localized mainly on the Schiff base nitrogen, and upon excitation, it shifts toward the ionone ring.[3] Accordingly, any perturbations which stabilize this charge delocalization lead to a smaller energy gap between the ground and excited states, resulting in a red shift of the absorption maxima. On the basis of this background, several mechanisms for the opsin shift of bR were proposed as follows: (1) elongation of the π-conjugated system due to the ring/chain coplanarization,[4-7] (2) π-electron delocalization due to weakening of the interaction between PRSB and its counterion,[8,9] and (3) interaction of the chromophore with polar or polarizable residues in the protein. Among them, the third mechanism is needed to be investigated in more detail for the construction of a reliable molecular model of the opsin shift.

Several studies have pointed out the importance of polarizable nature of the protein matrix. Polarizable amino acids could stabilize the excited state of the chromophore by compensatory electronic movement, if they are located near the chromophore.[10,11] This model is supported by the fact that the absorption maximum of PRSB in ethanol shows red shift by addition of phenol, indole, etc.[12] In proteins, aromatic residues (phenylalanine, tyrosine, and tryptophan) would play a role similar to such polarizable solvents.

Quantum chemical calculation is a powerful tool to examine the validity of the above model and to construct a precise molecular model of the active site. In Chapter 3, the author has developed a self-consistent reaction field (SCRF) theory based on a polarizable continuum model (PCM),[13,14] where a protein was treated as a continuous and homogeneous dielectric medium. In this theory, the effect of electronic polarization of the protein is represented as a function of refractive index. In Chapter 4, the theoretical results indicated that the absorption maxima of PRSB significantly red shift with an increase in the refractive index of the surrounding medium, consistent with corresponding experimental data. In addition, the author identified seven aromatic residues in the chromophore-binding pocket: Trp86, Trp138, Trp182, Trp189, Tyr83, Tyr185, and Phe208. According to the calculation, the opsin shift of bR_{568} and M_{412} both are quantitatively reproduced if these residues cooperatively act as a medium with a refractive index of 1.51. However, the PCM approximation equalizes polarizability over the whole protein, and hence is not capable of appreciating the contribution of individual residues. In order to clarify the molecular detail of the opsin shift following the above mechanism, a computational method that can explicitly take into account both molecular structure and electronic polarization effects of the protein is required.

Combined methods of quantum mechanics and molecular mechanics (QM/MM)[15] allow for the calculation of large systems. In those methods, the region of

interest is calculated quantum chemically, and the remainder of the system is treated using molecular mechanics. In order that QM/MM methods are applied to problems of molecular excitation, they must be formulated so as to allow electronic rearrangement in the MM region, caused by excitation of the QM region. The so-called Langevin dipole (LD) approximation[16] has been developed for this purpose.

Molecular orbital (MO) calculation may be the best way to investigate chromophore-protein interactions in photoreceptor proteins, if all the constituting atoms are explicitly taken into account. Recently, Stewart[17] developed an MO calculation program, called MOZYME,[18] capable of performing semiempirical MO calculations for large molecules such as proteins. This program allows us to obtain the ground-state wavefunction for the whole system of bR, because CPU time increases only linearly against the number of atoms. Once the ground-state wave function is obtained, the excitation energy may be evaluated by configuration interaction (CI) calculation. However, the direct use of the CI calculation for the whole protein is actually difficult, because the CPU time increases in proportion to more than the square of the number of atoms. At present, it is impractical to employ the CI method for the full-atomic system of a protein due to the limitation of the computational time and resources.

In this chapter, the author develops a new method capable of calculating the absorption spectra of large molecules under the approximation nearly equivalent to full-atomic representation. This is based on a modified CI method, coupled with "polarizable mosaic model" approximation, which allows us to evaluate the electronic rearrangement of proteins in the excited state. In this method, each bond constituting a protein is approximated as a cylindrical stick made of dielectric. By using the information about the ground-state wave function obtained from the MOZYME calculation,[17] the new method well reproduces the opsin shift of bR. From analysis of electrostatic potential map for the ground and excited states, the

author clarifies the contributions from the fixed charges and electronic polarization of the protein to the opsin shift. Furthermore, the calculations for several site-directed mutants will reveal a role of each residue in the wavelength regulation of bR. Based on these results, the author proposes a new model of the chromophore-protein interactions responsible for the opsin shift.

§5.2 Theory

5.2.1 Expression of Excitation Energy for a Large Molecular System

Firstly, the author describes a theory for evaluating the excitation energy of a protein system composed of a chromophore and apoprotein. In the present formulation, the system is partitioned into two regions: (I) a region which includes the chromophore, and (II) the remainder of the protein (Figure 5.1). In what follows, it is assumed that (1) during excitation, the geometry of the protein is unchanged, and that (2) the region II itself is inactive to excitation light. Then, Hamiltonian of the system can be divided into three terms as follows:

$$\mathcal{H} = \mathcal{H}^{\mathrm{I}} + \mathcal{H}^{\mathrm{II}} + \mathcal{V} \qquad (5.1)$$

where $\mathcal{H}^{\mathrm{I}}$ and $\mathcal{H}^{\mathrm{II}}$ are the Hamiltonian operators for the regions I and II, respectively, and $\mathcal{V}$ indicates the interaction between the regions I and II.

The wave function Ψ_n for the whole system is obtained by solving the Schrödinger equation given by,

$$\mathcal{H}\,|\Psi_n\rangle = E_n\,|\Psi_n\rangle \qquad (5.2)$$

If the electron exchange between the regions I and II is negligible, Ψ_n is represented

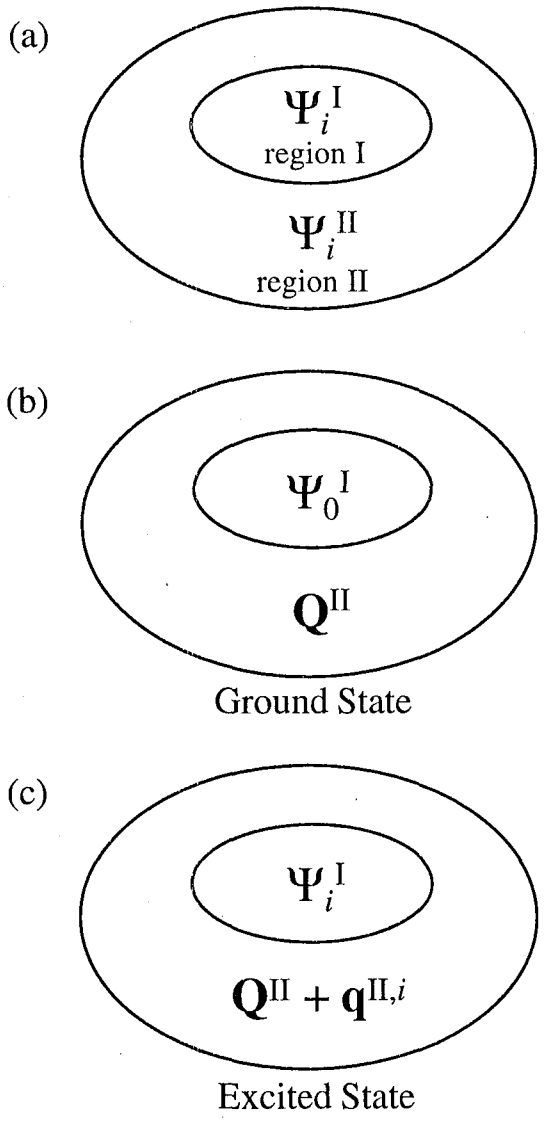

Figure 5.1 Conceptual framework of the new methodology formulated in this study. (a) The whole protein is divided into the regions I and II, whose wave functions are represented by Ψ_i^{I} and Ψ_i^{II}, respectively. The wave function of the whole system is assumed to be represented by $\Psi_i^{I}\Psi_i^{II}$. (b) In the ground-state caclulation, the charge distribution of the region II is replaced by the atomic charges. (c) In the excited-state calculation, the charge distribution of the region II is changed according to the electronic rearrangement induced by the excitation of the region I.

by the product of Ψ_n^{I} and Ψ_n^{II}, which are the wave functions for the regions I and II, respectively. As a consequence, the total energy E_n is described as follows:

$$E_n = \langle \Psi_n^{\mathrm{I}} \mid \mathcal{H}^{\mathrm{I}} + \mathcal{V}[\Psi_n^{\mathrm{II}}] \mid \Psi_n^{\mathrm{I}} \rangle + \langle \Psi_n^{\mathrm{II}} \mid \mathcal{H}^{\mathrm{II}} \mid \Psi_n^{\mathrm{II}} \rangle \qquad (5.3)$$

where $\mathcal{V}[\Psi_n^{\mathrm{II}}]$ is the Coulomb potential generated from the charge distribution in the regions II.

$$\mathcal{V}\left[\Psi_n^{\mathrm{II}}\right] = \left\langle \Psi_n^{\mathrm{II}}(r') \left| \frac{1}{|r-r'|} \right| \Psi_n^{\mathrm{II}}(r') \right\rangle \qquad (5.4)$$

If we focus on the ground state, the energy E_0 is given by,

$$\begin{aligned} E_0 &= \langle \Psi_0^{\mathrm{I}} \mid \mathcal{H}^{\mathrm{I}} + \mathcal{V}[\Psi_0^{\mathrm{II}}] \mid \Psi_0^{\mathrm{I}} \rangle + \langle \Psi_0^{\mathrm{II}} \mid \mathcal{H}^{\mathrm{II}} \mid \Psi_0^{\mathrm{II}} \rangle \\ &= \langle \Psi_0^{\mathrm{I}} \mid \mathcal{H}^{\mathrm{I}} \mid \Psi_0^{\mathrm{I}} \rangle + \langle \Psi_0^{\mathrm{I}} \mid \mathcal{V}[\Psi_0^{\mathrm{II}}] \mid \Psi_0^{\mathrm{I}} \rangle + \langle \Psi_0^{\mathrm{II}} \mid \mathcal{H}^{\mathrm{II}} \mid \Psi_0^{\mathrm{II}} \rangle \\ &= E_0^{\mathrm{I}} + \langle \Psi_0^{\mathrm{I}} \mid \mathcal{V}[\Psi_0^{\mathrm{II}}] \mid \Psi_0^{\mathrm{I}} \rangle + E_0^{\mathrm{II}} \end{aligned} \qquad (5.5)$$

Similarly, for the ith excited state, the energy E_i is given by,

$$E_i = E_i^{\mathrm{I}} + \langle \Psi_i^{\mathrm{I}} \mid \mathcal{V}[\Psi_i^{\mathrm{II}}] \mid \Psi_i^{\mathrm{I}} \rangle + E_i^{\mathrm{II}} \qquad (5.6)$$

Consequently, the excitation energy ΔE_i ($= E_i - E_0$) is represented as follows:

$$\begin{aligned} \Delta E_i = E_i^{\mathrm{I}} - E_0^{\mathrm{I}} &+ \langle \Psi_i^{\mathrm{I}} \mid \mathcal{V}[\Psi_i^{\mathrm{II}}] \mid \Psi_i^{\mathrm{I}} \rangle \\ &- \langle \Psi_0^{\mathrm{I}} \mid \mathcal{V}[\Psi_0^{\mathrm{II}}] \mid \Psi_0^{\mathrm{I}} \rangle + E_i^{\mathrm{II}} - E_0^{\mathrm{II}} \end{aligned} \qquad (5.7)$$

Hereafter, the interactions between the regions I and II (the third and forth terms in eq. 5.7), and the interactions inside the region II (the fifth and sixth term

in eq. 5.7) are treated by quasi-classical electrostatics. In the ground state, the ath atom in the region I is regarded as a point charge whose value is ${Q_a}^{\mathrm{I}}$, while the mth atom in the region II as a point charge with a value of ${Q_m}^{\mathrm{II}}$. The atomic charges in the regions I and II are collected in column vectors $\mathbf{Q}^{\mathrm{I}}$ and $\mathbf{Q}^{\mathrm{II}}$. For example, ${Q_a}^{\mathrm{I}}$ is defined as,

$$(\mathbf{Q}^{\mathrm{I}})_a = {Q_a}^{\mathrm{I}} \tag{5.8}$$

Upon excitation, the values of ${Q_a}^{\mathrm{I}}$ and ${Q_m}^{\mathrm{II}}$ both are changed. If we express the induced charges for the excited state Ψ_i as ${q_a}^{\mathrm{I},i}$ and ${q_m}^{\mathrm{II},i}$, the atomic charge distributions are given by $\mathbf{Q}^{\mathrm{I}}+\mathbf{q}^{\mathrm{I},i}$ and $\mathbf{Q}^{\mathrm{II}}+\mathbf{q}^{\mathrm{II},i}$ for the region I and II, respectively. Unless otherwise noted, the superscript i for $\mathbf{q}^{\mathrm{I},i}$ and $\mathbf{q}^{\mathrm{II},i}$ will be omitted in the subsequent derivation.

To describe the interaction between atoms a and m (a and m belong to the regions I and II, respectively), we introduce a new matrix $\mathbf{G}$, whose (a, m) component is defined as follows.

$$G_{am} = \frac{1}{|r_a - r_m|} \tag{5.9}$$

Then, using eqs. 5.4, 5.8, and 5.9, we can obtain the following expressions:

$$\langle \Psi_0^{\mathrm{I}} | \mathcal{V}[\Psi_0^{\mathrm{II}}] | \Psi_0^{\mathrm{I}} \rangle = \mathbf{Q}^{\mathrm{I}}\mathbf{G}\mathbf{Q}^{\mathrm{II}} \tag{5.10}$$

$$\langle \Psi_i^{\mathrm{I}} | \mathcal{V}[\Psi_i^{\mathrm{II}}] | \Psi_i^{\mathrm{I}} \rangle = (\mathbf{Q}^{\mathrm{I}} + \mathbf{q}^{\mathrm{I}})\mathbf{G}(\mathbf{Q}^{\mathrm{II}} + \mathbf{q}^{\mathrm{II}}) \tag{5.11}$$

Similarly, to describe the atom-atom pair interaction inside the region II (both m and n belong to the region II), we introduce a matrix $\mathbf{R}$, whose (m, n) component is defined as follows:

$$R_{mn} = \frac{1}{|r_m - r_n|} \quad (m \neq n) \tag{5.12a}$$

$$R_{mm} = 0 \tag{5.12b}$$

Then, the ground- and excited-state energies of the region II are approximately represented by

$$E_0^{II} = \frac{1}{2}\mathbf{Q}^{II}\mathbf{R}\mathbf{Q}^{II} + T^{II} \tag{5.13}$$

$$E_i^{II} = \frac{1}{2}(\mathbf{Q}^{II}+\mathbf{q}^{II})\mathbf{R}(\mathbf{Q}^{II}+\mathbf{q}^{II}) + T^{II} \tag{5.14}$$

where the first term represents the total Coulomb energy arising from the atom-atom pair interactions in the region II, and the second is the contribution from the other factors including kinetic energy of electrons and van der Waals interaction energy. In eqs. 5.13 and 5.14, T^{II} is assumed to be unchanged during excitation because the elements of $\mathbf{q}^{II}$ are expected to be sufficiently small.

Then, using eqs. 5.10, 5.11, 5.13, and 5.14, eq. 5.7 is rewritten as follows:

$$\begin{aligned}\Delta E_i = E_i^I - E_0^I + (\mathbf{Q}^I+\mathbf{q}^I)\mathbf{G}\mathbf{q}^{II} + \mathbf{q}^I\mathbf{G}\mathbf{Q}^{II} \\ +\frac{1}{2}\mathbf{q}^{II}\mathbf{R}\mathbf{q}^{II} + \mathbf{q}^{II}\mathbf{R}\mathbf{Q}^{II}\end{aligned} \tag{5.15}$$

This is the exact expression for the excitation energy on the assumption that the wave function of the protein can be described by the product of Ψ_n^I and Ψ_n^{II}.

In what follows, the author explores an approximate expression of ΔE_i in the framework of the configuration interaction (CI) method. The column vector $\mathbf{q}^I$

collects the excitation-induced atomic charges in the region I. Of course, these charges must be obtained under the condition that the perturbation from the region II is present. As understood from eq. 5.3, the wave function Ψ_n^{I} is obtained from the following Schrödinger equation:

$$(\mathcal{H}^{\mathrm{I}} + \mathcal{V}[\Psi_0^{\mathrm{II}}])\ |\Psi_n^{\mathrm{I}}\rangle = E'_n\ |\Psi_n^{\mathrm{I}}\rangle \tag{5.16}$$

where the electronic distribution of the region II is frozen as it is in the ground state. Then, if $\mathbf{Q}^{\mathrm{II}}$ is given in advance, the Fock matrix is modified in the following way:

$$F_{\mu\mu} = F^0{}_{\mu\mu} + (\mathbf{G}\mathbf{Q}^{\mathrm{II}})_l \quad (\phi_\mu \in \text{atom } l) \tag{5.17}$$

where ϕ_μ is the μth atomic orbital (AO), which belongs to the atom l. Under this condition, an SCF calculation gives the ground state energy written by,

$$E'_0 = E_0^{\mathrm{I}} + \mathbf{Q}^{\mathrm{I}}\mathbf{G}\mathbf{Q}^{\mathrm{II}} \tag{5.18}$$

where $\mathbf{Q}^{\mathrm{I}}$ can be obtained from the ground-state wave function Ψ_0^{I}. Since the charges of the region II are fixed, any excited states of the region I will receive the electrostatic potential originating from $\mathbf{Q}^{\mathrm{II}}$. After some mathematical manipulations according to the standard CI formalism, the ith diagonal term ($\Delta E'_i$) of the CI matrix is given by,

$$\Delta E'_i = E_i^{\mathrm{I}} - E_0^{\mathrm{I}} + \mathbf{q}^{\mathrm{I},i}\mathbf{G}\mathbf{Q}^{\mathrm{II}} \tag{5.19}$$

where $\mathbf{q}^{\mathrm{I},i}$ is the atomic charge alteration for the ith excited-state configuration.

After diagonalization of the CI matrix, a set of excitation energies close to $\Delta E'_i$'s will be obtained. Comparing eq. 5.19 with eq. 5.15, it is found that such simple CI treatment does not give the correct excitation energy. The excitation energy will be obtained by correcting $\Delta E'_i$ for the charge alteration in the region II, induced by excitation of the region I.

$$\Delta E_i = \Delta E'_i + (\mathbf{Q}^{\mathrm{I}}+\mathbf{q}^{\mathrm{I},i})\mathbf{G}\mathbf{q}^{\mathrm{II},i} + \frac{1}{2}\mathbf{q}^{\mathrm{II},i}\mathbf{R}\mathbf{q}^{\mathrm{II},i} + \mathbf{q}^{\mathrm{II},i}\mathbf{R}\mathbf{Q}^{\mathrm{II}} \qquad (5.20)$$

Therefore, the approximate value of ΔE_i can be obtained by only once diagonalizing the CI matrix, whose diagonal elements ($\Delta E'_i$) are modified according to eq. 5.20. This modification of the CI matrix corresponds to the replacement of $\mathcal{V}[\Psi_0^{\mathrm{II}}]$ in eq. 5.16 by $\mathcal{V}[\Psi_n^{\mathrm{II}}]$.

5.2.2 Charge Distribution of the Region II in the Ground State

As shown in eqs. 5.17-20, the values of $\mathbf{Q}^{\mathrm{II}}$ are need to be determined before the evaluation of ΔE_i. In standard QM/MM (quantum mechanics/molecular mechanics) methods, the charges corresponding to $\mathbf{Q}^{\mathrm{II}}$ are taken from molecular mechanics force field parameters or determined from results of molecular orbital calculations for small molecular fragments. In those methods, electron rearrangement is not allowed after the initial construction of a molecule. This may be a poor approximation for the charge distribution in a protein, because the electric fields from a charged chromophore or dissociated side chains significantly polarize the surrounding protein matrix. Therefore, for the ground state the author performed full-atomic quantum chemical calculation in order to obtain the self-consistent charge distribution over the whole protein. The charge distribution in the excited state was obtained using a new method described in the following section.

5.2.3 Polarizable Mosaic Model

At this stage, the values of q_m^{II} in eq. 5.18 is still unknown. The vector $\mathbf{q}^{II}$ represents the atomic charge rearrangements in the region II, induced by excitation of the region I. It is thus necessary to explore a method of calculating $\mathbf{q}^{II}$ from the information about the known quantity such as $\mathbf{q}^{I}$.

The author proposes a new methodology, hereafter called "polarizable mosaic model (PMM)", which allows us to explicitly treat the electronic polarization of a protein matrix. In PMM, every covalent bond in the region II is replaced by a cylindrical stick made of dielectric, whose permittivity depends on the nature of an original bond. As a consequence, a protein molecule is represented by a *mosaic* consisting of cylinders with various polarizabilities. For simplicity, first a diatomic molecule is taken as an example (Figure 5.2). Atoms m and n are distant by d_{mn}, and have charges of Q_m and Q_n, respectively. The cylindrical dielectric connecting these atoms has a polarizability of α_{mn}. When an electrostatic field $\mathbf{F}$ is applied to the dielectric, partial charges q_m and q_n (=$-q_m$) are induced on both edges of the cylinder, resulting in an induced dipole moment μ_{mn}. The magnitude of μ_{mn} is in proportion to the component of $\mathbf{F}$, F_{mn}, along the bond direction.

$$\mu_{mn} = q_m d_{mn} = \alpha_{mn} F_{mn} \tag{5.21}$$

In first order approximation, F_{mn} could be replaced by the difference in electrostatic potential between the atoms m and n.

$$F_{mn} = -\frac{\phi_n - \phi_m}{d_{mn}} \tag{5.22}$$

where ϕ_m is the electrostatic potential at the center of the atom m. Then, from eqs.

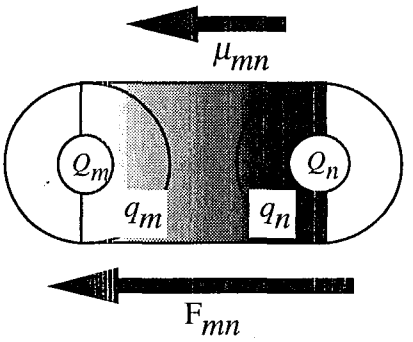

Figure 5.2 Schematic representation of the dielectric approximation of a polarizable bond. A bond is represented by a cylindrically-shaped dielectric. Initially, the atoms m and n have atomic charges of Q_m and Q_n, respectively. On applying an electric field F_{mn}, the cylindrical stick polarizes, resulting in an induced dipole moment μ_{mn}. The occurrence of μ_{mn} corresponds to the fact that the charges q_m and q_n are induced on the atoms m and n, respectively.

5.21 and 5.22, the following relationship is obtained:

$$q_m^{II} = \frac{\alpha_{mn}}{d_{mn}^2}(\phi_n - \phi_m) \tag{5.23}$$

This expression is easily extended to the case of multivalent atom.

$$q_m^{II} = \sum_n \frac{\alpha_{mn}}{d_{mn}^2}(\phi_n - \phi_m) \tag{5.24}$$

where n runs over all the atoms except for m. Here we define a matrix **A** and a column vector Φ, whose components are given by,

$$A_{mn} = \frac{\alpha_{mn}}{d_{mn}^2} \quad (m \neq n : \text{bonding}) \tag{5.25a}$$

$$A_{mn} = 0 \quad (m \neq n : \text{non-bonding}) \tag{5.25b}$$

$$A_{mm} = -\sum_n \frac{\alpha_{mn}}{d_{mn}^2} \tag{5.25c}$$

$$(\Phi)_n = \phi_n \tag{26}$$

Then eq. 5.21 can be rewritten in matrix form as follows:

$$\mathbf{q}^{II} = \mathbf{A}\Phi \tag{5.27}$$

Since $\mathbf{q}^{II}$ is induced in response to $\mathbf{q}^{I}$, the main source of the electrostatic potential in eq. 5.27 is the induced charges $\mathbf{q}^{I}$. In addition, $\mathbf{q}^{II}$ must be corrected for the mutual polarization among the $\mathbf{q}^{II}$ charges themselves. Namely, ϕ_m is determined by the induced charges and coordinates of all the particles other than the

atom m itself

$$\phi_m = \sum_a G_{am} q_a^{\mathrm{I}} + \sum_n R_{mn} q_n^{\mathrm{II}} \qquad (5.28)$$

Eq. 5.28 is also rewritten in matrix form.

$$\Phi = \mathbf{G}^t\mathbf{q}^{\mathrm{I}} + \mathbf{R}\mathbf{q}^{\mathrm{II}} \qquad (5.29)$$

By substituting eq. 5.29 into eq. 5.27, we obtain the following matrix equation:

$$\mathbf{q}^{\mathrm{II}} = \mathbf{A}(\mathbf{G}^t\mathbf{q}^{\mathrm{I}} + \mathbf{R}\mathbf{q}^{\mathrm{II}}) \qquad (5.30)$$

Consequently, the induced charge $\mathbf{q}^{\mathrm{II}}$ is given by,

$$\mathbf{q}^{\mathrm{II}} = (\mathbf{I} - \mathbf{A}\mathbf{R})^{-1}\mathbf{A}\mathbf{G}^t\mathbf{q}^{\mathrm{I}} \qquad (5.31)$$

where $\mathbf{I}$ is the unit matrix. Therefore, the charge alteration in the region II is uniquely determined from the charge alteration $\mathbf{q}^{\mathrm{I}}$, generated by excitation of the region I. Thus, we can obtain the vector $\mathbf{q}^{\mathrm{II}}$ necessary for evaluation of the excitation energy (eq. 5.20).

5.2.4 Parameterization of Bond Polarizability

To estimate the polarizability of an arbitrary bonding pair of atoms, we use an empirical rule that is satisfied for the refractive indices of molecules in the condensed phase. The refractive index n and isotropic polarizability α_{iso} of a molecule are related to each other according to the Lorentz-Lorenz equation,

$$\frac{n^2-1}{n^2+2}\frac{M}{\rho} = \frac{4\pi N_a \alpha_{iso}}{3} = P_M \qquad (5.32)$$

where M and ρ are molecular weight and the density in the liquid state, respectively, and N_a is Avogadro's number. P_M is molar refraction, which can be decomposed into atomic contributions (P_n) as follows:

$$P_M = \sum_n P_n \qquad (5.33)$$

Here we explore a way of decomposing the molar refraction into the contributions of individual bonds of a molecule. For an atomic pair (m, n), we newly define "molar bond refraction" (P_{m-n}) as follows:

$$P_{m-n} = \frac{P_m}{v_m} + \frac{P_n}{v_n} + P_\pi \qquad (5.34)$$

where v_m is the valence number counted only for σ-bonds of atom m. The third term in eq. 5.34 is added only when the atomic pair has a π-bond. In a π-conjugated system, the contribution of any π-bond is assumed to be equally shared to all the σ-bonds taking part in the conjugation. Then P_π is the net π-bond contribution per each bond.

For example, the molar bond refraction for indole is obtained as described below. According to literature data,[19] the contributions of H, C, and N(aromatic secondary amine) to the molar refraction are given by 1.100, 2.418, and 3.59 cm^3mol^{-1}, respectively. In addition, the contribution of one double bond is 1.733 cm^3mol^{-1}.[19] Then, the molar refraction P_M is calculated to be 37.57 cm^3mol^{-1}. According to eq. 34, P_{C-H} and P_{N-H} are given by 1.906 and 2.30 cm^3mol^{-1}, respectively. For indole, it can be supposed that four π-bonds are shared by eight C-C bonds and two C-N bonds. Thus, the π-bond contribution assigned to each

bond is 1.733×4/10 = 0.693 cm^3mol^{-1}. As a result, $P_{C\text{-}C}$ and $P_{C\text{-}N}$ are given by 2.305 and 2.70 cm^3mol^{-1}, respectively. The sum of the bond contributions is equal to 37.57 cm^3mol^{-1}, in agreement with the value of P_M. Table 5.1 summarizes the $P_{m\text{-}n}$ values for all the types of bonds that constitute a protein.

On going back to eq. 5.32, we can obtain the isotropic polarizability $\alpha_{mn,iso}$ for each *m*-*n* bond.

$$\alpha_{mn,iso} = \frac{3P_{m-n}}{4\pi N_a} \tag{5.35}$$

On the assumption that every bond has a cylindrical shape, the isotropic polarizability is given by,

$$\alpha_{iso} = \frac{\alpha_{\parallel} + 2\alpha_{\perp}}{3} \tag{5.36}$$

where $\alpha_{||}$ and $\alpha_{\perp}$ are the polarizabilities along the directions parallel and perpendicular to the bond, respectively. In general, the value of $\alpha_{\perp}$ is fully smaller than that of $\alpha_{||}$. Here, it is assumed that the value of $\alpha_{\perp}$ equals 0. Thus, $\alpha_{||} = 3\alpha_{iso}$. Consequently, the following expression is obtained:

$$\alpha_{mn,\parallel} = \frac{9P_{m-n}}{4\pi N_a} \tag{5.38}$$

Bond polarizabilities obtained from eq. 5.37 are used to evaluate the electrostatic interactions among the cylindrical dipoles. In view of the physical meaning of eq. 5.31, the **AR** part of the matrix $(\mathbf{I} - \mathbf{AR})^{-1}$ is responsible for the dipole-dipole interactions in the region II. On the other hand, the **AG** part in eq. 5.31 represents the charge-dipole interactions between the regions I and II. If the dipole-dipole interaction is much weaker than the charge-dipole interactions, (**I** –

Table 5.1 List of Molar Bonding Refraction (P_M / cm^3mol^{-1})

	H	C (sp3)	C (sp2)	C (benzene)	C (indole)	N (indole)	S
Single Bond							
H	2.20	1.70	1.91	1.91	1.91	2.30	4.95
C (sp3)	1.70	1.21	1.41	1.41	1.41		4.59
C (sp2)	1.91	1.41	1.61	1.62	1.62		4.79
N (prim.amine)	1.92	1.42	1.62				
N (prim.amide)	1.98		1.69				
N (sec.amine)	1.86	1.36	1.56				
N (tert.amide)		1.51	1.71				
O (alcohol)	1.86	1.37	1.57	1.57			
O (ester)	1.92	1.42	1.63				
S	4.95	4.59	4.79				8.11
Multiple Bond							
C (sp2)			3.34				
C (benzene)				2.48			
C (indole)					2.31	2.70	
N (imide)			4.43				
O (carbonyl)			4.75				
O (carboxyl)			3.19				

$\mathbf{AR})^{-1}$ is approximately equal to $\mathbf{I}$. Then, $(\mathbf{I} - \mathbf{AR})^{-1}\mathbf{A}$ in eq. 5.31 can be replaced by an effective polarizability matrix $\mathbf{A}_{\text{eff}}$.

$$\mathbf{q}^{\text{II}} = \mathbf{A}_{\text{eff}}\mathbf{G}^{\text{t}}\mathbf{q}^{\text{I}} \tag{5.38}$$

where the components of $\mathbf{A}_{\text{eff}}$ are given by substituting $\alpha_{mn,\|}$ into α_{mn} in eqs. 5.25a-c.

$$\left(\mathbf{A}_{\text{eff}}\right)_{mn} = \frac{\alpha_{mn,\|}}{d_{mn}^2} \qquad (\text{m} \neq \text{n: bonding}) \tag{5.39a}$$

$$(\mathbf{A}_{\text{eff}})_{mn} = 0 \qquad (m \neq n \text{ : non-bonding}) \tag{5.39b}$$

$$\left(\mathbf{A}_{\text{eff}}\right)_{mm} = -\sum_{n} \frac{\alpha_{mn,\|}}{d_{mn}^2} \tag{5.39c}$$

In this study, we use eq. 5.38 for evaluation of $\mathbf{q}^{\text{II}}$, instead of eq. 5.31.

§5.3 Calculation

The computational procedure is shown in Figure 5.3. First, by using the MOZYME program, the full atom MO calculation was performed for a given geometry of bR (see below). Next, the coordinate of the protein was divided into (*all-trans*-retinylidene)ethylammonium ion (region I) and bacterioopsin (apoprotein: region II) in which the side chain of Lys216 was removed. At this stage, all the atomic charges in the region II were stored in the vector $\mathbf{Q}^{\text{II}}$. Subsequently, Hartree-Fock calculation of the region I was performed with taking into account the electrostatic interaction with the external charges ($\mathbf{Q}^{\text{II}}$). For this calculation the author used an INDO/S program, whose Fock matrix elements were modified so as to include the electrostatic potential from the external charges (see

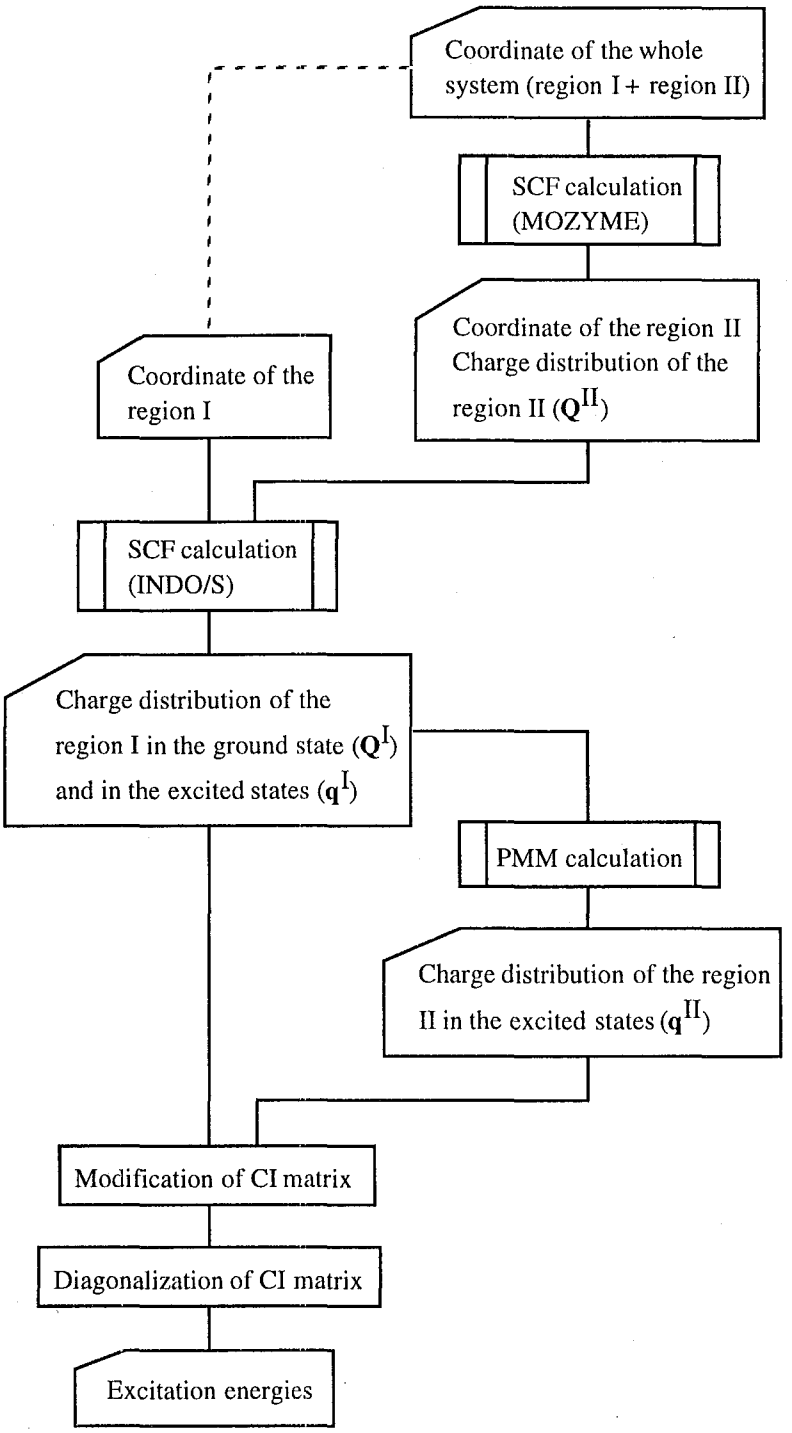

Figure 5.3 Flow chart of the whole computational procedure including the PMM calculation.

eq. 5.17). In addition, the diagonal elements of the CI matrix were also modified according to eq. 5.20. The elements of $\mathbf{A}_{\mathrm{eff}}$ were calculated by using the eqs. 5.34, 5.35 and 5.39, after the types of all the atoms were specified according to Table 5.1. Finally, the modified CI matrix was diagonalized, providing a set of the excitation energy including the effects of static and induced charges of the protein matrix.

The geometry of bR was originally taken from the protein data bank (2BRD) .[20-22] Hydrogen atoms were added to the skeleton by using the LEaP module of AMBER4.1 program,[23] and then their positions were optimized by the MOZYME program.[18] The resulting structure is hereafter abbreviated as "WT". Mutants of bR studied are W86A, W138A, W182A, W189A, Y83A, Y185A, F208A, W86A/ W182, W86A/Y185A, and W86A/W182A/Y185A. Their atomic coordinates were obtained by optimizing only the geometry of the methyl group (Ala side chain) at the mutated position. In a similar way, K216G mutant and the acidic form of bR (the carboxyl group of Asp85 is protonated: denoted as A-bR) were prepared. In all the MOZYME calculations, the AM1 Hamiltonian[24] was used and cut-off distance for short-range interactions (the keyword CUTOF2) was chosen to be 7.0 Å.

The electrostatic potential, i.e., eqs. 5.9 and 5.12a, was actually calculated using the Nishimoto-Mataga equation for two center Coulomb integral,[25] instead of the pure classical expression. Such a treatment was needed to smoothly extrapolate the results of the region I (quantum mechanical region) into those of the region II (classical region). In drawing electrostatic potential maps, a more simple expression, Qr^{-1} type potential, was used, where Q is a Mulliken charge obtained from MO calculations.

§5.4 Results

5.4.1 Electrostatic Potential Map for the Chromophore-Binding Pocket of bR

Figures 5.4(a) and (b) show the molecular coordinate system used for analysis of electrostatic potential maps for bR. This coordinate system was defined as follows: the C10 atom was set at the origin; the C10-C11 bond was set on the *x*-axis; an *x*-*y* plane is taken so as to include the atoms C9, C10, and C11. As a result, this plane (Figure 5.4(a)) almost coincides with the conjugated plane of PRSB. Figures 5.5(a) and (b) show electrostatic potential maps drawn by using the atomic charges obtained from the MOZYME calculation for WT. The potential in these figures (given in a.u.) involves only the contributions from the atomic charges of the region II. The features of the map on the conjugated plane (Figure 5.5(a)) are summarized as follows: the potential value is ranging from -0.3 to 0.0 a.u.; there are three apparent minima around (4.0, -7.0), (0.0, -4.0), and (3.0, 5.0); the region just including the chromophore has a relatively small absolute value of potential; the potential gradient is relatively small in that region, especially around the ionone ring. The deepest minimum around (4.0, -7.0) originates from the negative charge of ionized Asp85, which acts as the counterion of the chromophore. The minima around (0.0, -4.0) and (3.0, 5.0) originate from the presence of Trp86 and Trp182, respectively, which are arranged so as to surround the chromophore from its lateral sides. It is worth noting that the potential value gradually decreases on going from the ionone ring to the Schiff base linkage. The resulting potential gradient would localize the positive charge of the chromophore toward the Schiff base moiety. This is inconsistent with the well-known external charge model,[26] which states that the electrostatic effect of the protein would cause a delocalization of the positive charge toward the ionone ring.

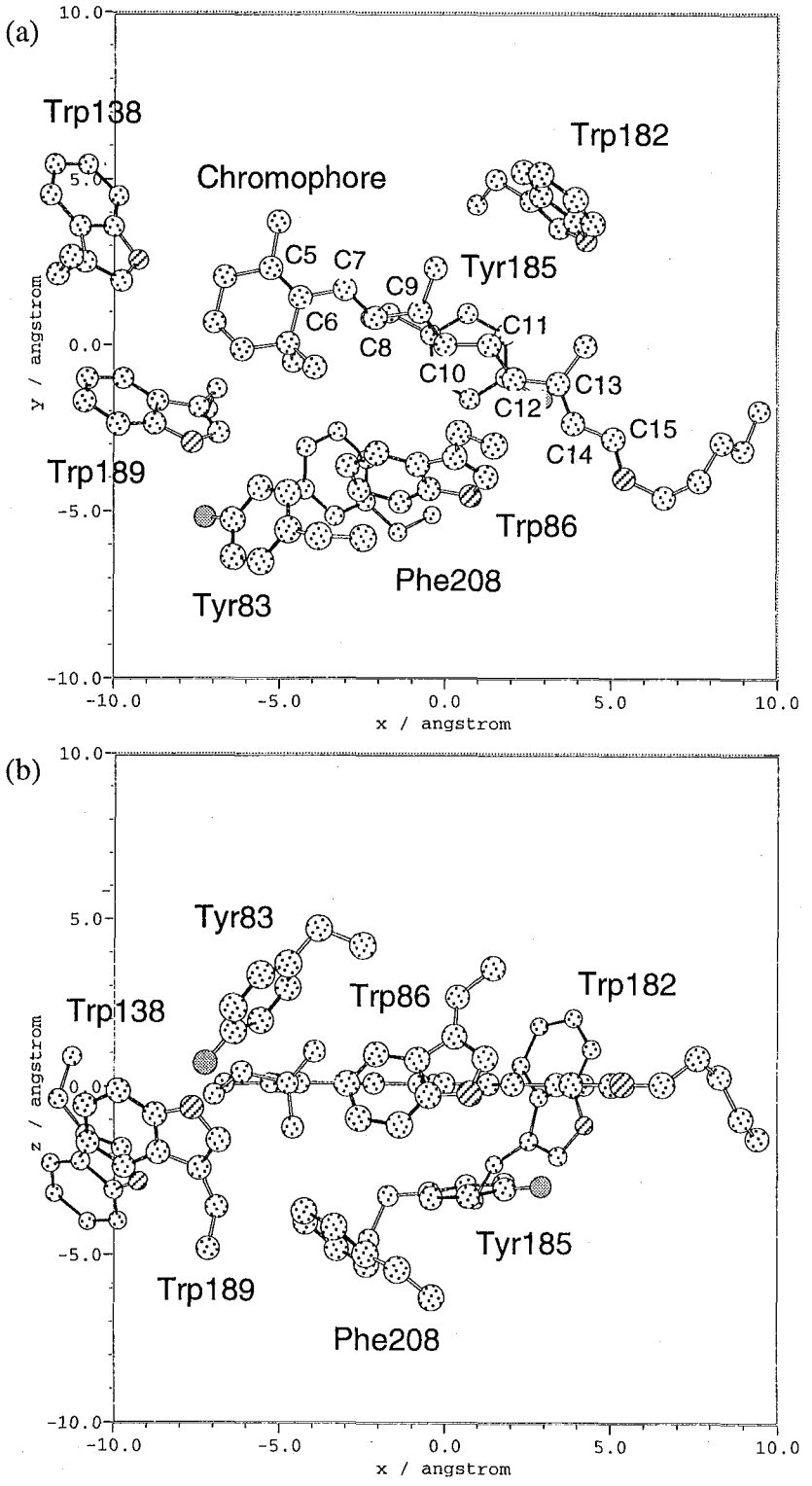

Figure 5.4 Molecular coordinate system used for analysis of electrostatic potential maps. The C10 atom was set at the origin; the C10-C11 bond was set on the *x*-axis; an *x*-*y* plane is taken so as to include the atoms C9, C10 and C11. (a) and (b) show the *x*-*y* and *x*-*z* planes, respectively. The aromatic residues present in the chromophore-binding pocket are also shown.

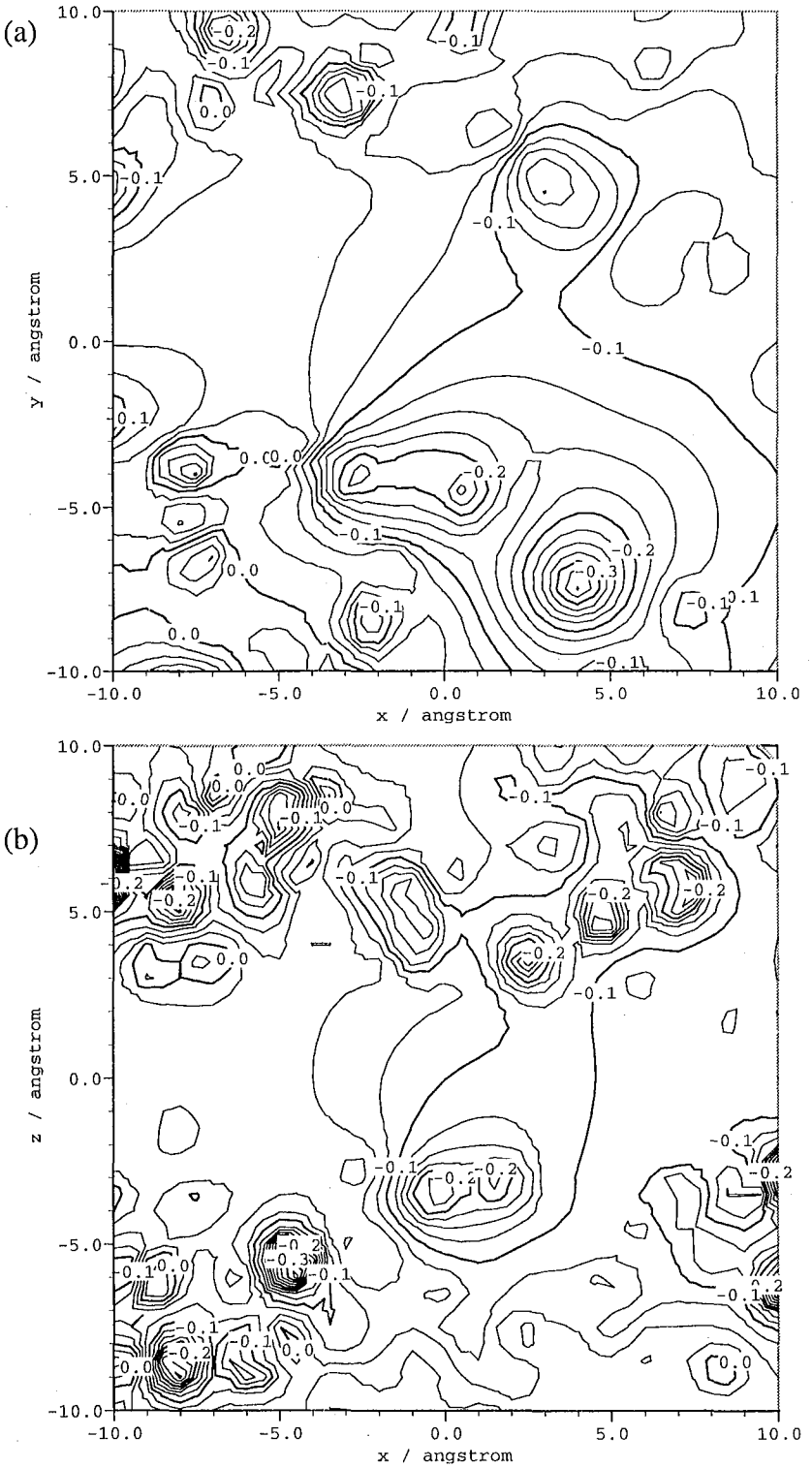

Figure 5.5 Electrostatic potential maps of the retinal-binding pocket in bR in the ground state. (a) and (b) were drawn on the plane shown in Figures 5.4(a) and 5.4(b), respectively.

5.4.2 Validity of the Polarizable Mosaic Model

To assess the reliability of the PMM approximation, it is sufficient to observe the response of a simple "mosaic" system to some fixed charges which correspond to $\mathbf{q}^{I}$ in the region I. First, we examine the charge distribution of a hypothetical system in Figure 5.6, where a unit positive charge (regarded as $\mathbf{q}^{I}$) induces the electronic polarization of an indole molecule which is approximated by PMM. The conjugated plane of the indole molecule was placed on an *x-y* plane. The unit positive charge was placed at the coordinate (5.0, 0.0, 0.0) or (0.0, 5.0, 0.0). These two cases are hereafter called cases 1 and 2, respectively.

The unit charge serves as $\mathbf{q}^{I}$ in eq. 5.38. After evaluation of the matrices $\mathbf{A}_{eff}$ and $\mathbf{G}$, we obtained the charge distribution corresponding to $\mathbf{q}^{II}$ from eq. 5.38. Figures 5.7(a) and (b) show maps of electrostatic potential (given in 10^{-3} a.u.) generated from $\mathbf{q}^{II}$ for the cases 1 and 2, respectively. In these figures, the maps are drawn on the plane of z = 5.0Å, and the position of the point charge is indicated as "*". These maps clearly show that the electrons of the indole molecule were withdrawn toward the positive charge.

These results were compared with those from explicit quantum chemical calculations for the same geometrical configurations as in Figure 5.6. The AM1 calculation was performed for the whole system and an isolated indole molecule, which was the reference to measure the charge rearrangement $\mathbf{q}^{II}$ induced by the point charge. Namely, the induced charge on each atom was obtained by subtracting the atomic charge of the isolated indole molecule from that of the indole-charge complex, and was used to draw an electrostatic potential map. Figures 5.7(c) and (d) show the results for the cases 1 and 2, respectively. As can be seen, Figures 5.7(c) and (d) are quite similar to Figures 5.7(a) and (b), respectively. This indicates that PMM is sufficiently accurate for evaluating the electronic polarization in a molecule, induced by an external electrostatic field.

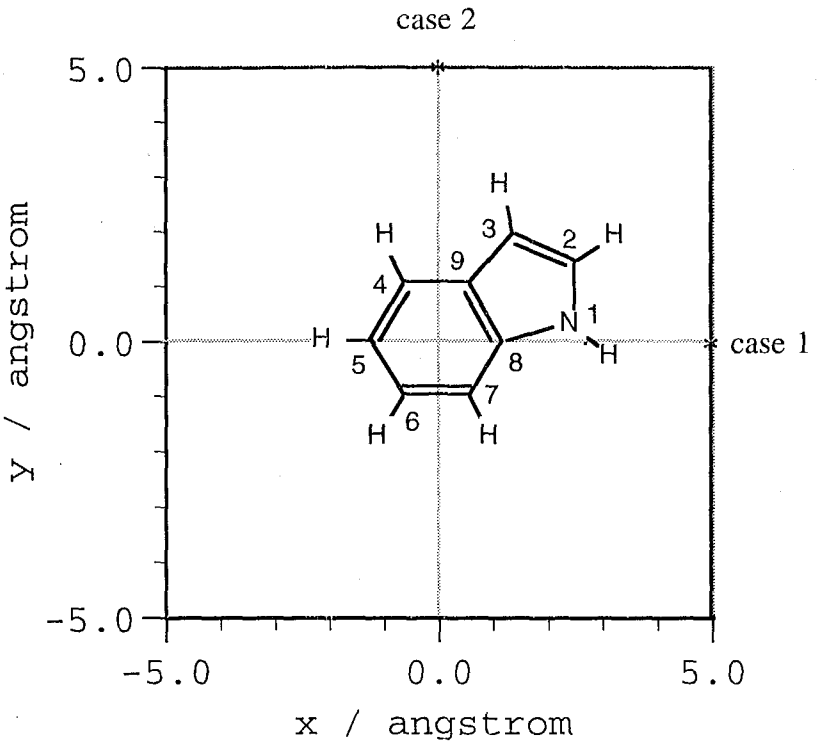

Figure 5.6 Molecular coordinate system for analysis of electrostatic potential map of the indole-point charge system. The mid-point of the C5 and C8 atoms were set at the origin; the C5 and C8 atoms were set on the *x*-axis; an *x*-*y* plane is taken so as to include atoms C4, C5 and C8. All the conjugated carbon and nitrogen atoms were placed on the plane of $z = 0.0$ Å. The position of the unit charges for cases 1 and 2 are indicated by "*".

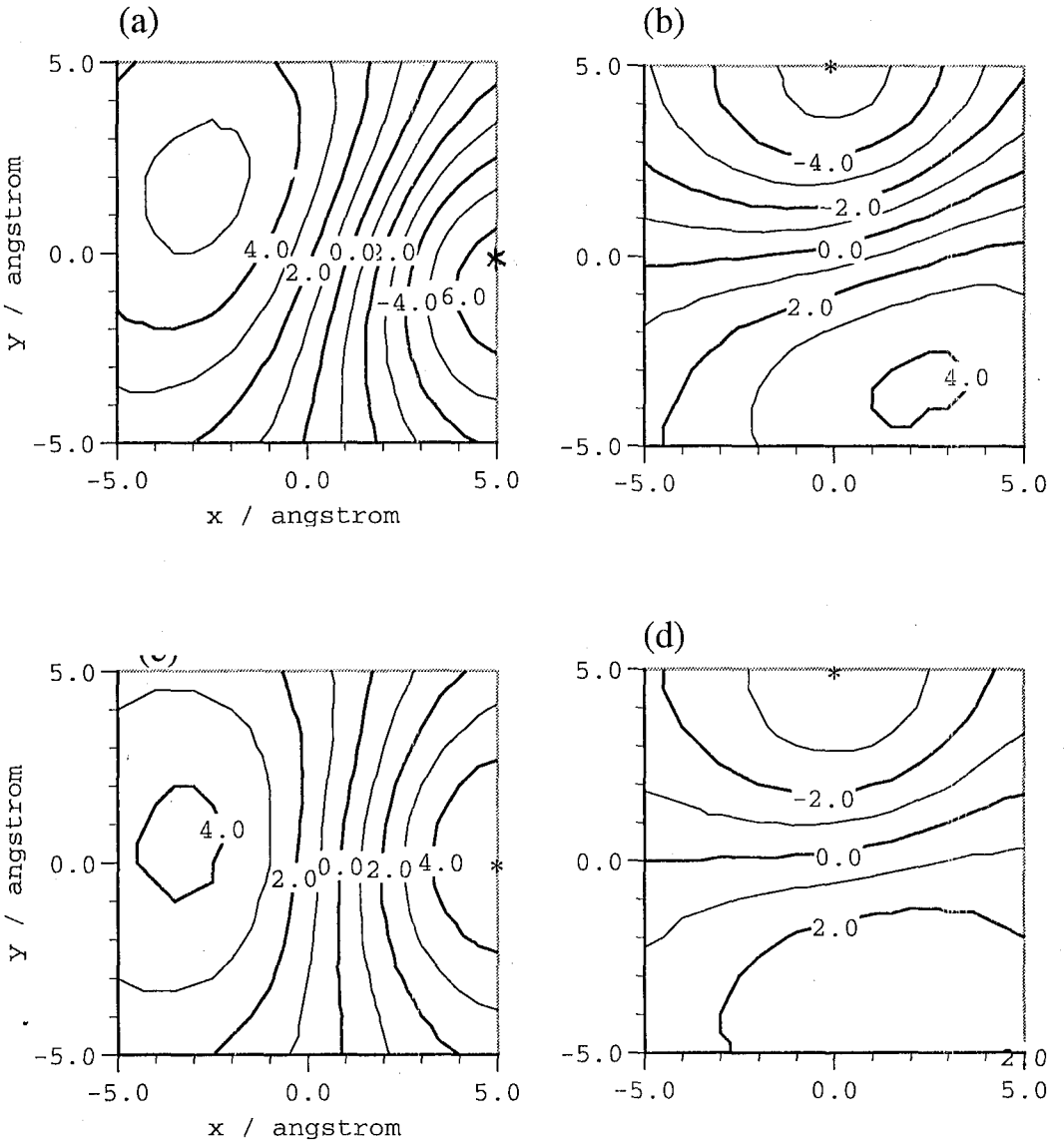

Figure 5.7 Electrostatic potentials generated from the induced charges of the indole molecule in the system of Figure 5.6. The position of the unit charge is indicated by "*". The induced charges used for drawing (a) and (b) were calculated by PMM approximation, and those for (c) and (d) were obtained by AM1 calculations. All the potential maps were drawn on the plane of z = 5.0 Å.

Next, we show results for bR, where the positive charges of the chromophore (region I) induces an electronic polarization of the protein. The atomic charges of the chromophore were regarded as $\mathbf{q}^{I}$ in eq. 5.38. These were obtained from the full-atomic calculation for WT. The matrix $\mathbf{A}_{eff}$ was again constructed by applying the PMM approximation to the apoprotein of WT. Figure 5.8(a) shows the electrostatic potential map drawn by using the resulting induced charges ($\mathbf{q}^{II}$). The map shows a broad minimum around (5.0, -5.0), where the protonated Schiff base linkage of the chromophore is placed. Clearly, this minimum arises from the positive charge of the chromophore.

This map was compared with the corresponding map obtained from the full-atomic quantum chemical calculation using MOZYME. The binding of the chromophore induces $\mathbf{q}^{II}$ charges, which can be obtained by subtracting the charge distribution of K216G mutant from that of WT. Figure 5.8(b) shows an electrostatic potential map drawn by using the induced charges in the region II. This figure is quite similar to Figure 5.8(a) in the landscape of the potential surface. However, a deviation of about 0.01 a.u. is found for the depth of the potential well between Figures 5.8(a) and (b). At any positions on the *x*-*y* plane, the deviation is not more than 10% of the potential value observed for WT (see Figure 5.5). These results greatly encourage us to apply the PMM approximation to large molecules.

The potential value shown in Figure 5.8(a) is ranging from -0.06 to 0.00 a.u.. The change of 0.06 a.u. nearly amounts to 30 % of the original potential observed for WT (see Figure 5.5). Therefore, the effect of electronic polarization of the protein is not negligible. This clearly shows the necessity of explicitly evaluating the electronic distribution in the ground state as described in the section of theory.

5.4.3 The Excitation Energy of bR and its Mutants

In the present formalism, two types of approximation are possible for

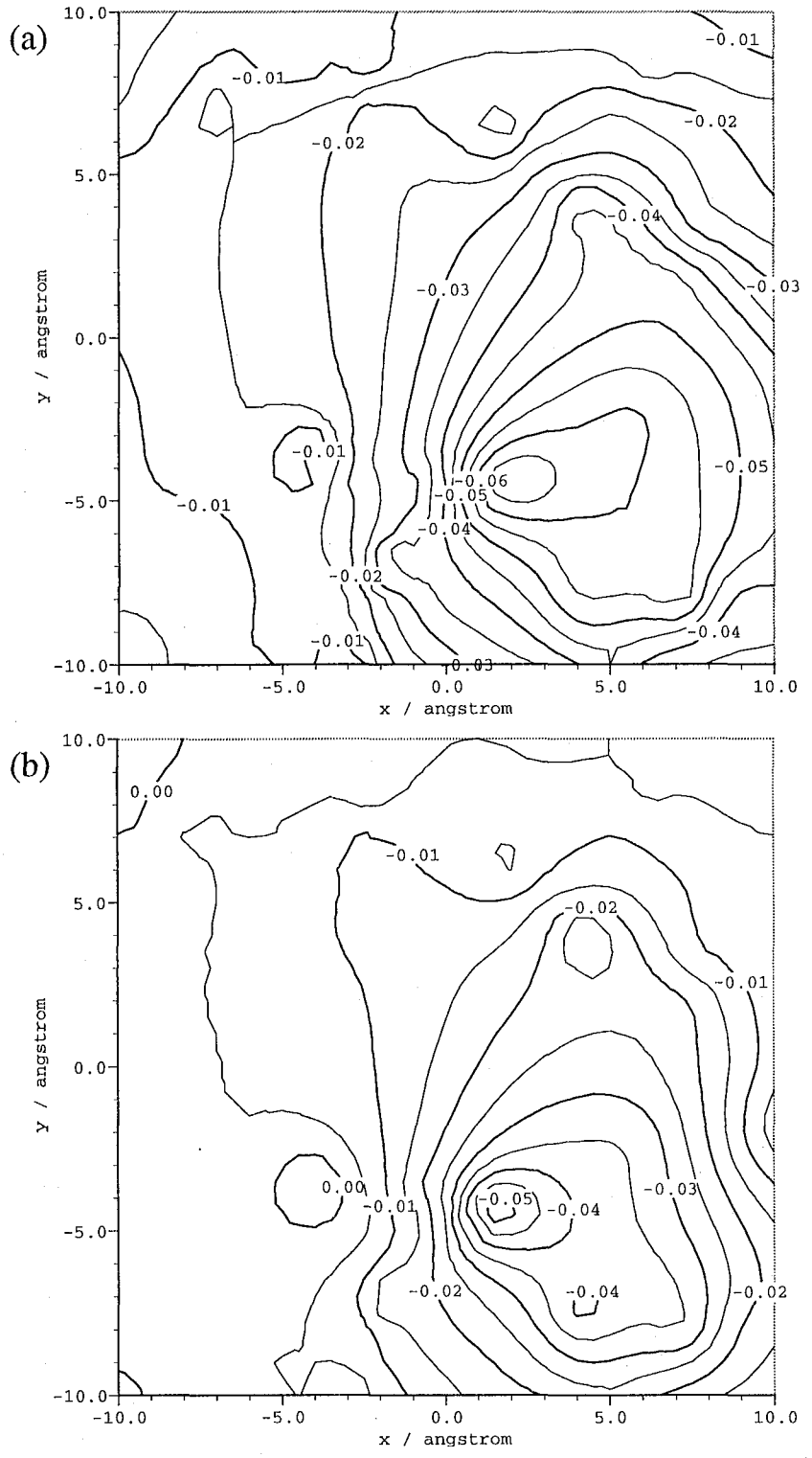

Figure 5.8 Electrostatic potentials generated from the charges induced in the region II of bR on binding of the chromophore. The induced charges used for drawing (a) were calculated by the PMM approximation, and those for (b) were obtained by AM1 calculation. These figures were drawn on the plane shown in Figures 5.4(a).

evaluating the excitation energy of a protein: (A) the atomic charges of an apoprotein are fixed during excitation (i.e., $\Delta E_i'$ eq. 19), and (B) they are altered according to eq. 5.34 (i.e., ΔE_i eq. 5.20). The calculated absorption maxima of WT are summarized in Table 5.2. The values from the approximations (A) and (B) were 465.3 and 534.9 nm, respectively. The latter is 69.6 nm longer than the former, which indicates that the electronic polarization effect of the apoprotein opsin induces a significant amount of red shift. Clearly, the calculation with the approximation (B) well reproduces the experimental absorption maximum (568 nm) of bR. Table 5.2 also shows the absorption maximum of the chromophore-Asp85 complex, where only the effect of counterion is taken into account. It is found that the counterion brings about a blue shift.

The vector $\mathbf{q}^{\mathrm{I}}$ indicates the charge rearrangements in the chromophore on going from the ground to the lowest π–π^* excited state, and is obtained by subtracting the atomic charges for the ground-state configuration from those for the excited-state configuration. The vector $\mathbf{q}^{\mathrm{II}}$ collects the charges induced in the protein matrix on excitation. An electrostatic potential map produced by using $\mathbf{q}^{\mathrm{II}}$ is shown in Figure 5.9(a), where the x-y plane is the same as shown in Figure 5.4(a). As can be seen from this figure, there are two sets of pairs of a maximum and a minimum: one is centered around (-1.0, -4.0) and the other around (3.0, 5.0). Such a pair-potential formation implies the generation of a dipole-like field. By comparison of Figure 5.9(a) with Figure 5.4(a), it is found that the C11-C15 atoms of PRSB exist in a region with positive potentials, while the C5-C10 atoms are in a region with negative potentials. Such a characteristic polarization in the protein matrix of course reflects a charge rearrangement in PRSB induced by its excitation. Figure 5.10 shows the value of $\mathbf{q}^{\mathrm{I}}$ for each of the conjugated carbons of the chromophore. Upon excitation, the charges on C11, C13, C15 largely decrease, while those on C5-C8, C10 and C12 increase. Consequently, in the excited state, the

Table 5.2 Absorption Maxima of PRSB Calculated under Various Conditions

	Calcd. λ_{max} / nm	Exptl. λ_{max} / nm
PRSB *in vacuo*	524.9	
PRSB + counterion	474.4[a]	465[b]
approximation (A)	465.3	
approximation (B)	534.9	568[c]

a) result for *all-trans-6s-trans*-retinal PSB.

b) result for *all-trans-6s-trans*-locked-retinal PSB. Taken from ref. 4

c) result for bR in the light-adapted state. Taken from ref. 1

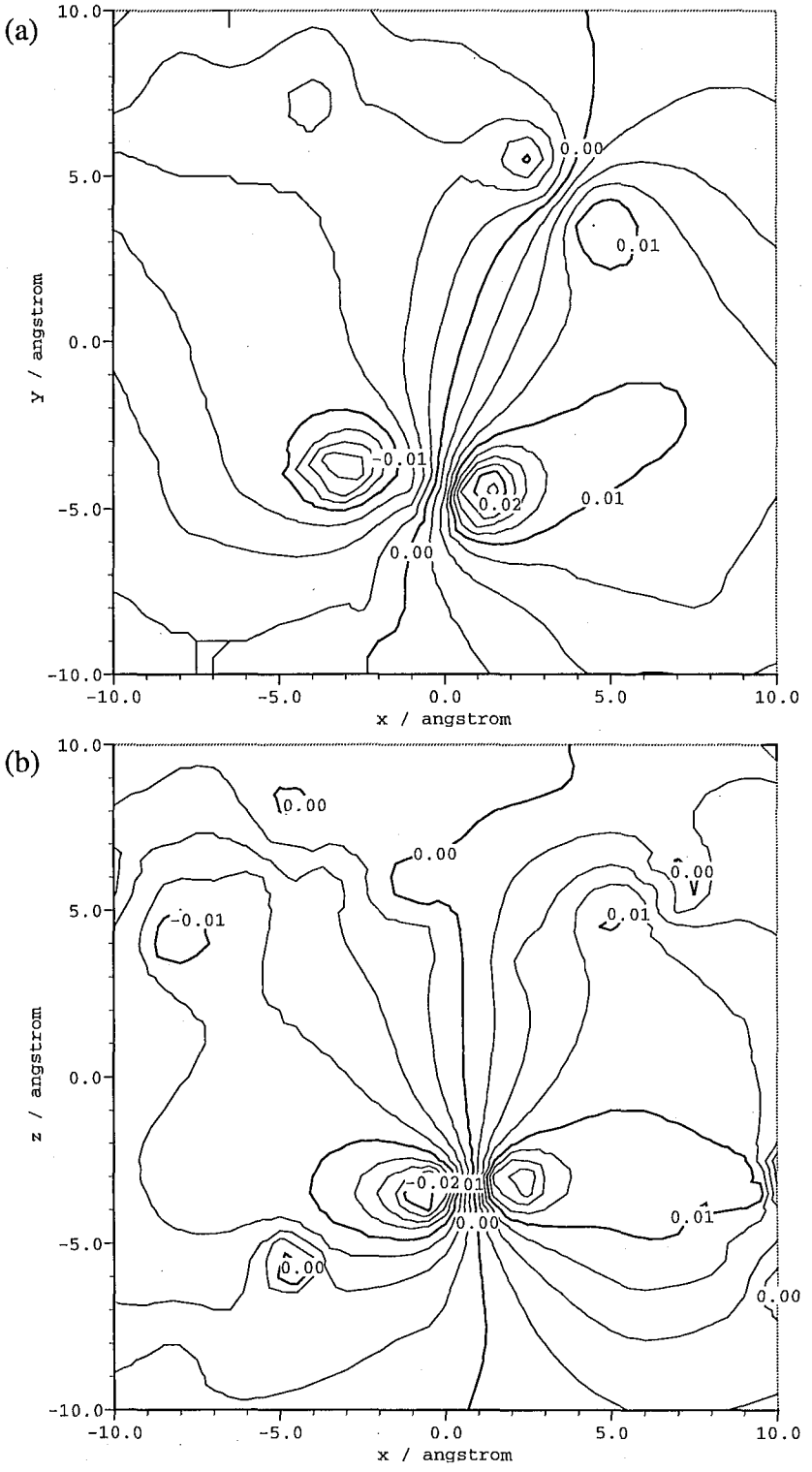

Figure 5.9 Electrostatic potentials generated from the charges ($\mathbf{q}^{II}$) induced by the π–π^* excitation of the chromophore. (a) and (b) were drawn on the plane shown in Figures 5.4(a) and 5.4(b), respectively.

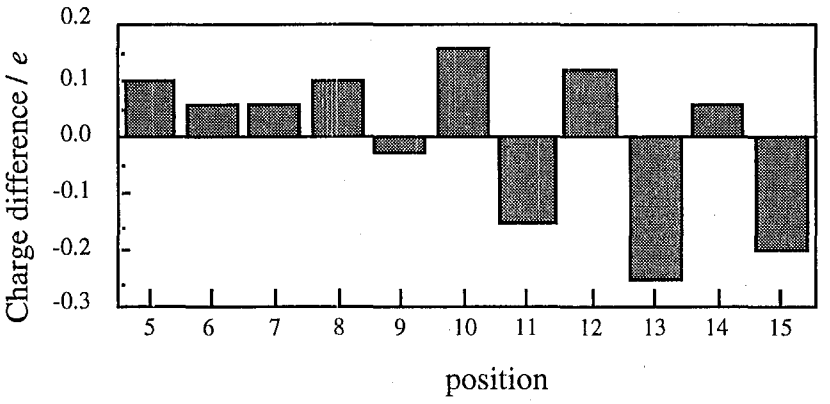

Figure 5.10 Change in atomic charges of the unsaturated carbons of the chromophore on going from the ground state to the π–π^* excited state.

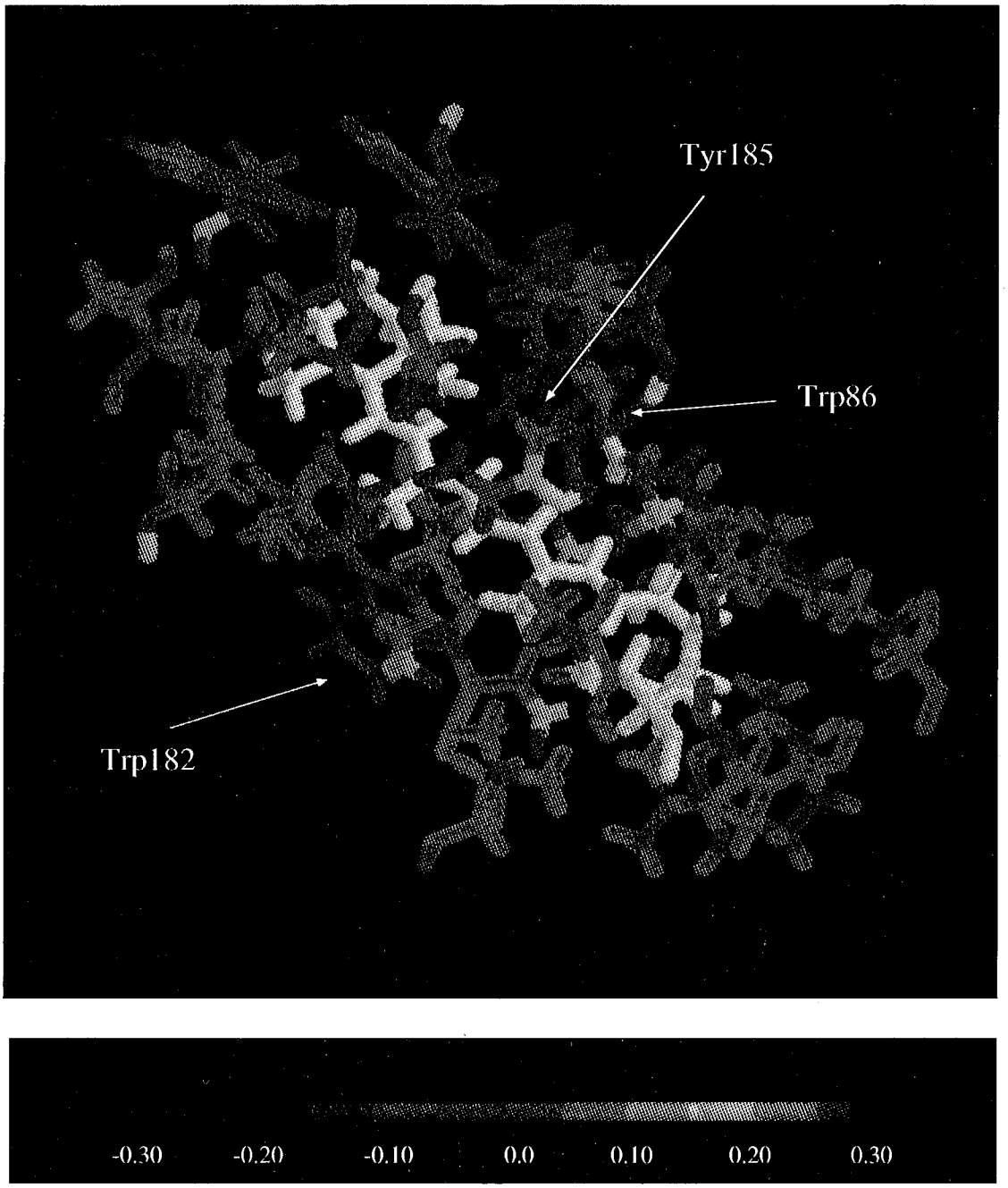

Figure 5.11 Distribution of the charges ($\mathbf{q}^{II}$) induced by the π–π^* excitation of the chromophore. The atoms are colored according to the vlues of $\mathbf{q}^{II}$ (see the scale bar). The chromophore and the side chain of Lys216 are drawn in white. This figure covers a region within 5.0 Å distant from the chromophore.

chromophore polarizes the surrounding protein matrix, resulting in the generation of a dipole-like field anti-parallel to the dipole moment of the chromophore itself. As a result, the excited-state of the chromophore is stabilized. This explains the reason why the absorption maximum based on the approximation (B) largely red shifted with respect to that based on the method (A).

By comparing Figure 5.9(a) with Figure 5.4(a), Trp86 and Trp182 are identified as the possible sources of the dipole-like potential in the protein. In addition, from the vertical cross-section of the map (see Figures 5.4(b) and 5.9(b)), Tyr185 also seems to contribute to the formation of the dipole-like potential. The contributions of these residues are more clearly understood by visualization of the distribution of $\mathbf{q}^{II}$. In Figure 5.11, the atoms of interest are colored according to the amount of induced charge. This figure covers a region within 5Å distant from the chromophore. This region is hereafter called the chromophore-binding pocket. It was confirmed that in the remainder of the protein, the magnitude of induced charge was negligibly small. In the chromophore-binding pocket, there are seven aromatic residues: Trp 86, Trp138, Trp182, Trp189, Tyr83, Tyr185, and Phe208. The side chains of these residues have relatively large electronic polarizabilities. It can be seen from Figure 5.11 that the residues Trp86, Trp182, and Tyr185 are remarkably polarized to make a significant contribution to the formation of the dipole-like field shown in Figure 5.9. The other aromatic residues exhibit no apparent polarization.

In order to appreciate the importance of the aromatic residues picked up above, we calculated the absorption maxima of a series of mutants: W86A, W138A, W182A, W189A, Y83A, Y185A, and F208A. The results are summarized in Table 5.3, where the second column contains the absorption maxima (λ^A) based on the approximation (A), and the fourth column does the absorption maxima (λ^B) based on the approximation (B). ΔE^A (ΔE^B) in this table also shows the change in $1/\lambda^A$ (

$1/\lambda^B$) on going from WT to each mutant. A significant amount of blue shift was observed in λ^B values of W86A and Y185A relative to that of WT, while the λ^A values for these mutants, especially for Y185A, exhibit relatively small blue shifts. These results indicate that the electronic polarization effect of Trp86 and Tyr185 greatly contributes to the opsin shift of bR. In contrast to expectation from the potential map, W182A causes only a slight amount of blue shift (24.5 cm^{-1}).

Furthermore, we examined the effects of double and triple mutations (Table 3). The ΔE^B value for W86A/Y185A is 1826.2 cm^{-1}, which is significantly larger than the simple sum of the ΔE^B values for W86A and Y185A (982.2 + 509.8 = 1492.0 cm^{-1}). This suggests that additivity does not hold among the ΔE^B values. The author attempted further analysis for the origin of the difference (1826.2 – 1492.0 = 334.2 cm^{-1}) in ΔE^B. The ΔE^B value for Y185A (509.8 cm^{-1}) indicates the shift induced by Tyr185 in the presence of Trp86. On the other hand, the difference in ΔE^B between W86A and W86A/Y185A is 844.0 cm^{-1}, corresponding to the contribution of Tyr185 in the absence of Trp86. Consequently, it costs 334.2 (= 844.0 - 509.8) cm^{-1} to simultaneously polarize Tyr185 and Trp86. This cost corresponds to the term $(1/2)\mathbf{q}^{II}\mathbf{R}\mathbf{q}^{II}$ in eq. 5.20, meaning work required for the mutual polarization among the residues in the region II. Figure 5.12 illustrates the energy diagram for these mutants. The collapse of additivity arises from the fact that the excited-state energy is influenced by two opposing factors: stabilization due to the attraction between the chromophore ($\mathbf{q}^I$) and the induced bond dipoles ($\mathbf{q}^{II}$), and work for the mutual polarization among the induced bond dipoles.

On the basis of the above results, the small blue shift observed for W182A can be explained. By comparing the result for W86A/Y185A and that for W86A/W182A/Y185A, the shift induced by Trp182 in the absence of both Trp86 and Tyr185 is estimated to be 195.5 (= 2021.7 – 1826.2) cm^{-1}. On the other hand, the ΔE^B value for W86A/W182A/Y185A is 2021.7 cm^{-1}, and the simple sum of the

Table 5.3 Calculated Absorption Maxima of Mutants of bR

	λ^A / nm	$\Delta E^{A\ a)}$/ cm^{-1}	λ^B / nm	$\Delta E^{B\ b)}$/ cm^{-1}
WT	465.3	(0.0)	534.9	(0.0)
W86A	456.3	423.9	508.2	982.2
Y185A	464.0	60.2	520.7	509.8
W189A	462.6	125.4	530.0	172.8
W182A	464.1	55.6	534.2	24.5
Y83A	464.9	18.5	536.4	-52.3
W138A	465.8	-23.1	537.4	-87.0
F208A	465.9	-27.7	539.9	-173.1
W86A/Y185A	454.5	510.7	487.3	1826.2
W86A/W182A	455.4	467.2	501.2	1257.0
W86A/W182A/Y185A	453.1	578.7	482.7	2021.7

a) The inverse of λ^A subtracted by that for WT

b) The inverse of λ^B subtracted by that for WT

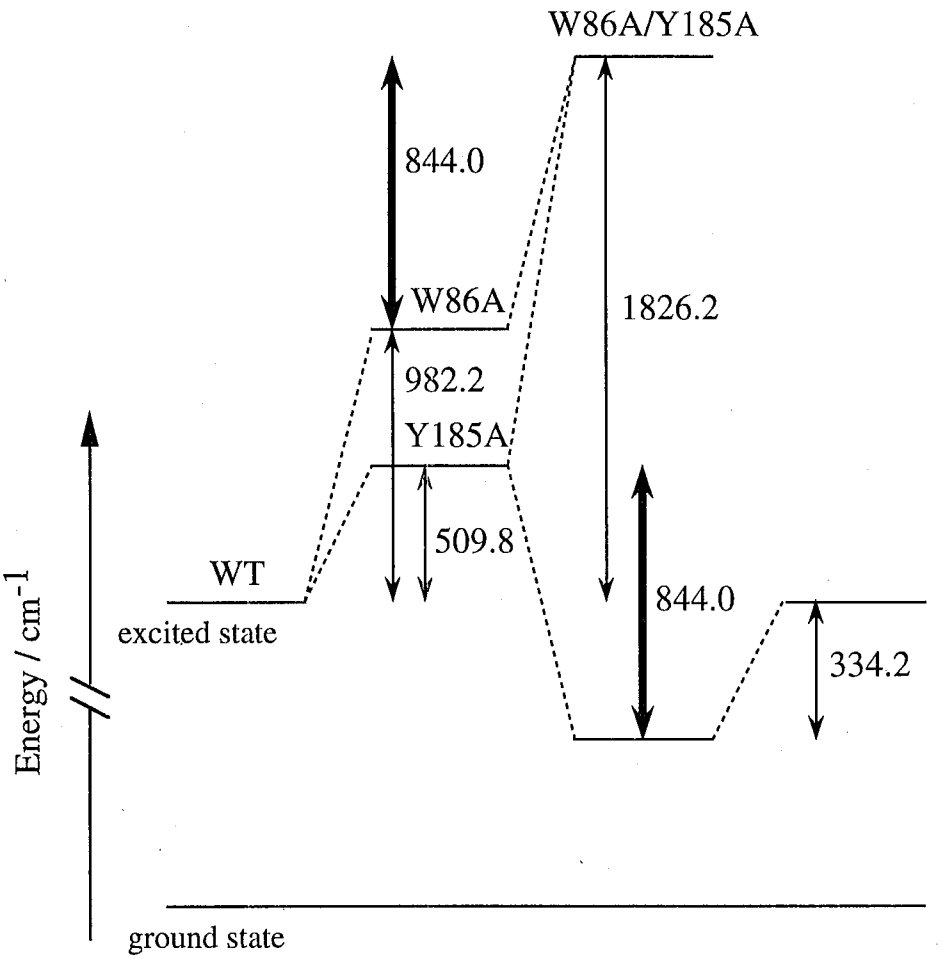

Figure 5.12 Energy diagram for WT, W86A, Y185A and W86A/Y185A. The energy is given in cm^{-1}. The difference (844.0 cm^{-1}) in the excited state energy between W86A/Y185A and W86A corresponds to the contribution of Tyr185 in the absence of Trp86. The subtraction of this value from the excited-state energy of T185A gives the excited-state energy lower than that of WT by 334.2 cm^{-1}, which corresponds to the cost of the mutual polarization of Trp86 and Tyr185.

ΔE^B values for W86A, W182A and Y185A is 1516.5 cm^{-1}. Namely, the cost required for simultaneous polarization of Trp86, Trp182 and Tyr185 is 2021.7 – 1516.5 = 505.2 cm^{-1}, which is larger than the cost (334.2 cm^{-1}) of double polarization of Trp86 and Tyr185 by 171.0 (= 505.2 – 334.2) cm^{-1}. In other words, the removal of Trp182 reduces the cost of the mutual polarization by 171.0 cm^{-1}. Consequently, the blue shift of 195.5 cm^{-1}, corresponding to the separate contribution of Trp182, is nearly canceled out by the work of the mutual polarization (171.0 cm^{-1}) between Trp182 and the neighboring residues of Trp86 and Tyr185, resulting in a relatively small blue shift (195.5 –171.0 = 24.5 cm^{-1}), in agreement with the difference in absorption maxima between WT and W182A.

If the absorption maxima of the chromophore-Asp85 complex (474.4 nm; see Table 5.2) is taken as a reference, the opsin shift of WT is evaluated to be 2384.2 cm^{-1}. On the other hand, the opsin shift of the W86A/W182A/Y185A mutant is 362.5 is cm^{-1}, corresponding to only 15 % of the opsin shift of WT. This indicates that the electronic polarization effect of Trp86, Trp182 and Tyr185 amounts to 85% of the total environmental effect of the protein. Thus, we can conclude that these residues dominates the opsin shift of bR. It should be noted that the λ^A values of all the mutants studied above blue shifts with respect to that of the chromophore-Asp85 complex. This indicates that the fixed charges of the protein induces a blue shift.

§5.5 Discussion

5.5.1 Insights from the Site-Directed Mutagenetic Studies

The present calculations demonstrated that the electronic polarization effect of several aromatic residues is responsile for the major part of the opsin shift. Inversely, the replacement of Trp86, Trp 182, and Tyr185 by alanine should induce a significant amount of blue shift. The importance of these residues in wavelength

regulation has been pointed out from a variety of mutagenetic studies.[27-31] Table 5.4 summarizes the experimental absorption maxima of mutants in which the aromatic residues of interest are replaced by Phe and Cys. The absorption maxima of these mutants are significantly blue shifted relative to that of the wild-type. These results can be qualitatively interpreted. In W86F, for example, the blue shift is attributed to the decrease in polarizability at the substituted position, since the polarizability (10.4×10^{-24} cm^{-1}) of benzene is smaller than that (14.9×10^{-24} cm^{-1}) of indole.[22] The blue shift observed for most of the mutants are explained by the same reason. Exceptionally, Y185F exhibits relatively a small blue or red shift, probably because the polarizabilities of tyrosine and phenylalanine nearly equal to each other.

The site-directed mutagenetic studies also revealed that the substitution of ionizable residues exerts no apparent influence on the absorption maxima of bR.[32] Exceptionally D85N, where the negative charge of Asp85 is neutralized, shows the absorption maxima around 600 nm (Table 5.5). This large red shift is similar to the phenomenon called purple-to-blue transition observed for acidic bR and deionized bR,[33] where the carboxyl group of Asp85 is protonated. In addition, the O intermediate, whose Asp85 is protonated, shows its absorption maxima at 640 nm.[1] These observations indicate that the naturalization of Asp85 induces a significant amount of red shift. In fact, the calculated absorption maxima of bR on protonation of Asp85 (denoted as A-bR) appears at 556.4 nm, which is red shifted by 721.4 cm^{-1} from that of WT (Table 5.5).

Based on the evidence from the experiments and our calculation, we propose a new molecular mechanism for the opsin shift of bR: the electronic polarization effects of Trp86, Trp182, and Tyr185 cooperatively stabilize the excited state of the chromophore, resulting in a red shift. This mechanism is illustrated in Figure 5.13.

Aromatic residues corresponding to Trp86, Trp182, and Tyr185 are

Table 5.4 Absorption Maxima Observed for Mutants of bR.

	Light-Adated state	Dark-Adapted state	
	λ_{max} / nm	λ_{max} / nm	ref.
wild-type	568	555	1
Y83F	540	533	28
W86F	547	534	29
W86F	539	529	27
W138C	547	543	27
W138F	561	551	27
W182F	491	477	27
Y185F	573	556	28
Y185F	563	548	31
Y185F		556	30
W189F	521	513	27

Table 5.5 The Absorption Maxima of bRs with Protonated Asp85.

	λ_{max} / nm	ΔE^a / cm^{-1}	ref.
D85N	610	1212	38
D85N	594	771	32
D85N	590	656	31
acidic bR	605	1077	33
deionized bR	605	1077	33
O-intermedite	640	1981	2
A-bR	556.4	722.4	This work

a) The amount of red shift measured from the absorption maximum of the corersponding wild-type bR.

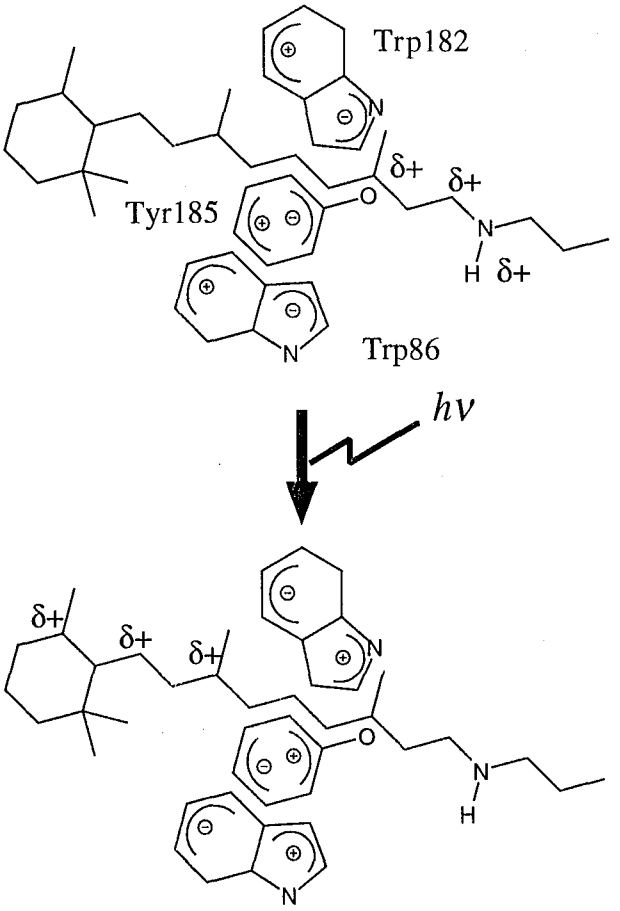

Figure 5.13 Schematic representation of the molecular model of the opsin shift. In the ground state, the positive charge of the chromophore is localized around the Schiff base nitrogen. Upon excitation, the positive charge moves toward the ionone ring, and the surrounding aromatic residues (Trp86, Trp182 and Tyr185) polarize so as to stabilize the excited-state.

conserved across many retinal-bound proteins.[27] As similar to the case of bR, several mutagenetic studies on rhodopsin (Rh) have pointed out the close relevance of aromatic residues to its wavelength regulation.[34,35] The mutants W126A, W265A, and Y268F shows their absorption maxima at 486, 470, and 493 nm, significantly blue shifted relative to that of the wild-type (500 nm).[34] It is thus evident that the residues Trp126, Trp265, and Tyr268 are responsible for the opsin shift. Therefore, there is the possibility that the opsin shifts of the retinal-bound proteins including visual pigments could be explained commonly in terms of the polarization effect of aromatic residues, although the tertiary structures of most of them have not been published.

5.5.2 Comparison with a Continuum Model

In Chapter 4, using a self-consistent reaction field (SCRF) calculation combined with the CI method, the author studied medium effects on the absorption maxima of retinal and its Schiff bases.[13,14] From regression analysis for experimental and calculated data, it was clarified that the solvatochromic shifts of these compounds are well-defined functions of physical parameters (i.e., dielectric constant (ε) and refractive index (n)) of the surrounding medium. In particular, the absorption maxima of PRSB significantly red shift with an increase in the refractive index of the medium. On the other hand, on the basis of the molecular structure of bR, the effective refractive index of the chromophore-binding pocket was estimated to be 1.51. On the assumpyion of this value for the refractive index and 4.0 for dielectric constant, the SCRF calculations quantitatively reproduced both opsin shifts of bR_{568} and M_{412}. From decomposition analysis of the calculated opsin shift (4700 cm^{-1}) of bR_{568}, the polarizable medium effects of the protein matrix are shown to be 1000 cm^{-1}.

The SCRF calculations in Chapter 4 is based on a polarizable continuum

Table 5.6 Absorption Maxima of PRSB Calculated by PMM and PCM Methods

	PMM	PCM
complex with Asp85	474.4	473.9
in hexane (ε, n) = (1.89, 1.375)	-	432.9
in bR (ε, n) = (4.00, 1.00)	-	477.1
in bR (ε, n) = (4.00, 1.51)	-	543.5
approximation (A)	465.3	-
approximation (B)	534.9	-

model, where the protein matrix is approximated as a dielectric. Table 5.6 compares the results from the continuum model (PCM) with those from the present calculations (PMM). In PMM, the approximation (A) takes into account only the fixed charge effect of the protein. This is similar to the situation that refractive index equals 1.0. On the other hand, the approximation (B) corresponds to the situation with refractive index of $n > 1.0$. In fact, the results from PMM is in excellent agreement with those from PCM, where refractive index is assumed to be 1.51. This indicates that the residues around the chromophore act as a dielectric medium with a high refractive index.

Next, the author discusses the equivalence between PMM and PCM from a theoretical viewpoint. In the SCRF-PCM method,[13] a solute molecule is placed in a cavity opened in a continuum dielectric. The dielectric is polarized in response to the charge distributions of the electrons (**P**) and the nuclei (**Z**) of the solute, and hence the charges ($\Gamma\sigma$) are induced on the cavity surface. According to our previous formulation,[36] the charge ($\Gamma\sigma$) is given by,

$$\Gamma\sigma = \mathbf{W}^{-1}\partial\mathbf{CP} + \mathbf{W}^{-1}\partial\mathbf{MZ} \qquad (5.40)$$

where ∂ is a diagonal matrix whose elements are $\partial/\partial\mathbf{n}_i$ (differential operator for the normal direction of the ith cavity element), and the matrices **C** and **M** have essentially the same physical meaning as **G** given by eq. 5.5, i.e., they are matrices which give Coulomb potential produced by charged particles. As a consequence, $\partial\mathbf{CP}$ and $\partial\mathbf{MZ}$ represent the electric fields originating from the electrons and the nuclei of the solute molecule, respectively.[37] $\mathbf{W}^{-1}$ can be approximately regarded as a diagonal matrix whose element is given by,

$$(\mathbf{W}^{-1})_{ii} = -\frac{\Delta_i}{2\pi}\frac{\varepsilon_i - 1}{\varepsilon_i + 1} \qquad (5.41)$$

where Δ_i and ε_i are the area and dielectric constant of the ith cavity element, respectively. The right-hand side of eq. 5.41 acts as the reaction field factor, which determines the degree of linear response of the medium.

$\Gamma\sigma$ and $(\mathbf{Z} - \mathbf{P})$ in eq. 5.41 correspond to $\mathbf{q}^{II}$ and $\mathbf{q}^{I}$ in eq. 5.39, respectively, while $\mathbf{C}$ and $\mathbf{M}$ do to $-\mathbf{G}$ and $\mathbf{G}$, respectively. Then, eq. 5.39 can be rewritten as follows:

$$\mathbf{q}^{II} = \mathbf{W}^{-1}\partial\mathbf{G}\mathbf{q}^{I} \tag{5.42}$$

Comparing eq. 5.42 with eq. 5.38, the following relationship can be derived:

$$\mathbf{W}^{-1}\partial = \mathbf{A}_{eff} \tag{5.43}$$

The equality in diagonal elements between the left- and right-hand sides of eq. 39 leads to an equation similar to the Lorentz-Lorenz equation given in eq. 5.32.

$$-\frac{\Delta_m}{2\pi}\frac{n_m^2 - 1}{n_m^2 + 1}\frac{\partial}{\partial \mathbf{n}_m} = -\sum_n \frac{\alpha_{mn,\parallel}}{d_{mn}^2} \tag{5.44}$$

This equation implies that each element of $\mathbf{A}_{eff}$ corresponds to a reaction field factor reflecting the polarizability of the whole protein. Therefore, the simplification of $(\mathbf{I} - \mathbf{AR})^{-1}\mathbf{A}$ in eq. 5.32 into $\mathbf{A}_{eff}$ is the approximation corresponding to the neglect of the non-diagonal elements of $\mathbf{W}^{-1}$ in PCM. It should be noted that α_{mn} in eq. 5.25 and $\alpha_{mn,\parallel}$ are different in their physical meanings: α_{mn} is a polarizability for an isolated bond, while $\alpha_{mn,\parallel}$ is that for a bond of a molecule in the condensed phase. In other words, $\alpha_{mn,\parallel}$ implicitly involves the electrostatic shielding effect originating from the mutual polarization of the bonds surrounding a bond in question. This would be the reason why the approximation

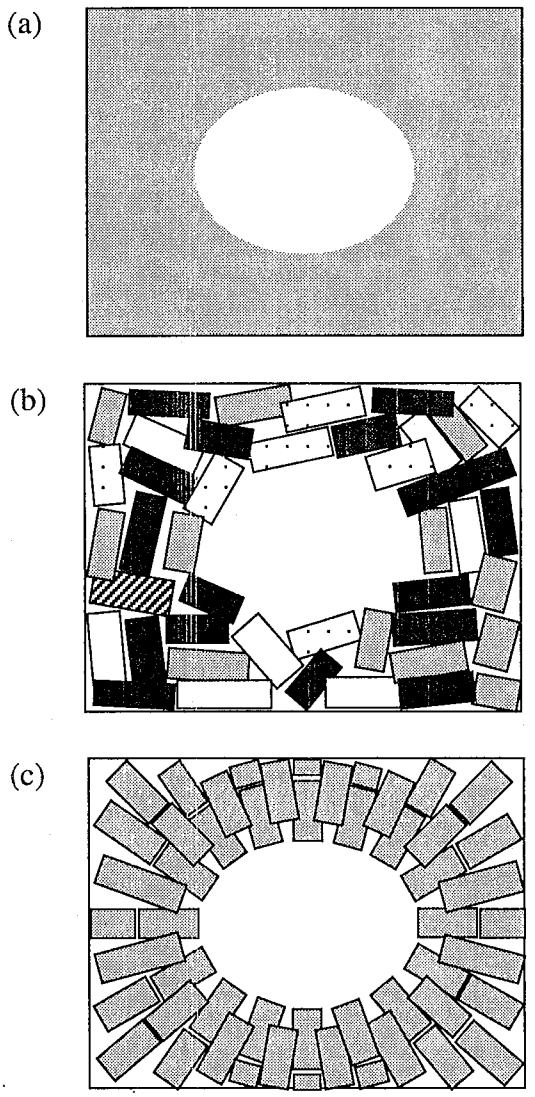

Figure 5.14 Comparison between PCM and PMM. (a) PCM is applicable to a homogenious and isotropic medium. (b) PMM is applicable to a heterogenious and anisotropic medium. (c) When polarizable bonds with identical polarizabilities are arranged so that their directions coincide wtih the normal vectors of a cavity surface, PMM is equivalent to PCM.

shown in eq. 5.38 appropriately works.

Equation 5.40 indicates that if we arrange the polarizable bonds so that their directions coincide with the normal vectors of the cavity surface, PMM becomes equivalent to PCM (Figure 5.14). From Figure 5.14, it is clear that PCM is a special case of PMM. It may be stated that PCM is applicable to a homogeneous and isotropic medium, whereas PMM is to a heterogeneous and anisotropic medium.

§5.6 Concluding Remarks

The polarizable mosaic model (PMM) approximation presented here proved to be a rapid and reliable method available for estimating the electronic polarization of large molecules such as protein. The PMM approximation, combined with a molecular orbital theory, is applicable to problems concerning the absorption maximum of a chromophore in a protein. The most valuable finding in this study is that the bathochromic shift observed for bR is dominated by several aromatic residues around the chromophore, i.e., Trp86, Trp182, and Tyr185. On the basis of these results, we propose a new molecular model for the opsin shift of bR: the electronic polarization of these aromatic residues stabilizes the excited state, resulting in a red shift. The present results also agreed with those from the calculations based on the continuum approximation. This assures us of the validity of the conclusion in Chapter 4 that the aromatic residues inside the chromophore-binding pocket serves as a polarizable medium.

References and Notes

(1) See for reviews: (a) Birge, R. R. *Annu. Rev. Phys. Chem.* **1990**, *41*, 683. (b) Lanyi, J. K. *Biochim. Biophys. Acta.* **1993**, *1183*, 241. (c) Khorana, H. G. *Ann. N. Y. Acad. Sci.* **1986**, *471*, 272. (d) Mathies, R. A.; Lin, S. W.; Ames, J. B.; Pollard, W. T. *Ann. Rev. Biophys. Biophys. Chem.* **1991**, *20*, 491.

(2) Lozier, R.; Bogomlni, R. A.; Stoeckenius, W. Biophys. J. **1975**, *15*, 955.

(3) Mathies, R.; Stryer, L. *Proc. Natl. Acad. Sci. USA* **1976**, *73*, 2169.

(4) van der Steen, R.; Biesheuvel, P. L.; Mathies, M. A.; Lugtenburg, J. *J. Am. Chem. Soc.*, **1986**, *108*, 6410.

(5) Harbison, G. S.; Smith, S. O.; Pardoen, J. A.; Courtin, J. M. L.; Lugtenburg, J.; Herzfeld, J.; Mathies, R. A.; Griffin, R. G. Biochemistry, **1985**, *24*, 6955.

(6) Harbison, G. S.; Mulder, P. P. J.; Pardoen, H.; Lugtenburg, J.; Herzfeld, J.; Griffin, R. G. *J. Am. Chem. Soc.*, **1985**, *107*, 4809.

(7) Wada, M.; Sakurai, M.; Inoue, Y.; Tamura, Y.; Watanabe, Y. *J. Am. Chem. Soc.* **1994**, *116*, 1537.

(8) Bassov, T.; Sheves, M. *J. Am. Chem. Soc.* **1985**, *107*, 7524.

(9) (a) Blatz, P. E.; Johnson, R. H.; Mohler, J. H.; Al-Dilaimi, S. K.; Dewhurst, S.; Erickson, J. O. *Photochem. Photobiol.*, **1971**, *13*, 237. (b) Blatz, P. E.; Mohler, J. H.; Navanglu, H. V. *Biochemistry*, **1972**, *11*, 848. (c) Blatz, P. E.; Mohler, J. H. *Biochemistry*, **1972**, *11*, 3240. (d) Blatz, P. E.; Mohler, J. H. *Biochemistry*, **1975**, *14*, 2340.

(10) (a) Irving, C. S.; Byers, G. W.; Leermakers, P. A. *J. Am. Chem. Soc.* **1969**, *91*, 2141. (b) Irving, C. S.; Byers, G. W.; Leermakers, P. A. *Biochemistry* **1970**, *9*, 858.

(11) Suzuki, T.; Kito, Y. *Photochem. Photobiol.*, **1972**, *15*, 275.

(12) (a) Kliger, D. S.; Milder, S. J.; Dratz, E. A. Photochem. Photobiol. 1977, 25, 277. (b) Milder, S. J.; Kliger, D. S. *Photochem. Photobiol.*, **1977**, *25*, 287.

(13) Houjou, H.; Sakurai, M.; Inoue, Y. *J. Chem. Phys.*, **1997**, *107*, 5652.

(14) Houjou, H.; Sakurai, M.; Inoue, Y. *J. Am. Chem. Soc.*, submitted.

(15) Gao, J. In *Reiews in Computational Chemistry*, K. B. Lipkowitx and D. B. Boyd, Eds., VCH, New York, 1995, pp. 119-185.

(16) Lutzhov, V.; Warshel, A. *J. Am. Chem. Soc.*, **1991**, *113*, 4491.

(17) Stewart, J. J. P. *Int. J. Quant. Chem.* **1996**, *58*, 133.

(18) Stewart, J. J. P. MOZYME version 2.3; Fujitsu Ltd.: Chiba, Japan, 1997.

(19) "LANGE'S HANDBOOK OF CHEMISTRY 11th Ed.", Dean, J. A. Ed., McGraw-Hill (New York) 1973.

(20) Grigorieff, T.; Ceska, K.; Downing, K. H.; Baldwin, J. M.; Henderson, R.; *J. Mol. Biol.*, **1996**, *259*, 393.

(21) Abola, E. E.; Bernstein, F. C.; Koetzle, T. F.; Weng, J Protein Data Bank, in Crystallographic Databases-Information Content, Software Systems, Scientific Applications, F. H. Allen, G. Bergerhoff, and R. Siebers, eds., Data Commission of the International Union of Crystallography, Bonn/Cambridge/Chester (1987) pp. 107-132.

(22) Bernstein, F. C.; Koetzle, T. F.; Williams, G. J. B.; Meyer, Jr., E. F.; Brice, M. D.; Rodgers, J. R.; Kennard, O.; Shimonouchi, T.; Tasumi, M. The Protein Data Bank: a Computer-based Archival File for Macromolecular Structures, *J. Mol. Biol.* **1977**, *112*, 535.

(23) Pearlman, D. A.; Case, D. A.; Caldwel, J. W.; Ross, W. S.; Cheatham III, T. E.; Ferguson, D. M.; Seibel, G. L.; ChandraSingh, U.; Weiner, P. K.; Kollman,P. A. (1995) AMBER ver. 4.1, University of Calfornia, San Francisco.

(24) Dewer, M. J. S.; Zoebisch, E. G.; Hearly, E. F.; Stewart, J. J. P. *J. Am. Chem. Soc.* **1985**, *107*, 3902.

(25) Mataga, N.; Nishimoto, K. *Z. Physik. Chem.*, **1957**, *13*, 140.

(26) Nakanishi, K. *Pure Appl. Chem.* **1991**, *63*, 161.

(27) Mogi, T.; Marti, T.; Khorana, H. G. *J. Biol. Chem.*, **1989**, *264*, 14197.

(28) Mogi, T.; Stern, L. J.; Hackett, N. R.; Khorana, H. G. *Proc. Natl. Acad. Sci. USA* **1987**, *84*, 5595.

(29) Hatanaka, M.; Kashima, R.; Kandori, H.; Friedman, N; Shees, M.; Needleman, R.; Lanyi, J.

K.; Maeda, A. *Biochemistry*, **1997**, *36*, 5493.

(30) Subramanium, S.; Marti, T.; Rösselet, S. J.; Rothchild, K. J.; Khorana, H. G. *Proc. Natl. Acad. Sci. USA* **1991**, *88*, 2583.

(31) Duñach, M.; Marti, T.; Khorana, H. G.; Rothchild, K. J. *Proc. Natl. Acad. Sci. USA* **1990**, *87*, 9873.

(32) Mogi, T.; Stern, L. J.; Marti, T.; Chao, B. H.; Khorana, H. G. *Proc. Natl. Acad. Sci. USA* **1988**, *85*, 4148.

(33) Zhag, Y. N.; El-Sayed, M. A.; Bonet, M. L.; Lanyi, J. K.; Chang, M.; Ni, B.; Needleman, R. *Proc. Natl. Acad. Sci. USA* **1993**, *90*, 1445.

(34) Nakayama, T.; Khorana, H. G. *J. Biol. Chem.*, **1991**, *266*, 4269.

(35) Lin, S. W.; Sakmar, T. P. *Biochemistry*, **1996**, *35*, 11149.

(36) Hoshi, H.; Sakurai, M.; Inoue, Y.; Chûjô, R. *J. Chem. Phys.*, **1987**, *87*, 1107.

(37) In the original formulation (ref. 36), the matrices $\partial\mathbf{C}$ and $\partial\mathbf{M}$ are represented by $\partial\tilde{}\mathbf{C}$ and $\partial\tilde{}\mathbf{M}$, whose components are $(\partial/\partial\mathbf{n}_i)C_{i\mu\nu}$, and $(\partial/\partial\mathbf{n}_i)M_{im}$, respectively. In this paper, we formally prepared the matrix ∂ for combinience.

(38) Logunov, S. L.; El-Sayed. M. A.; Song, L.; Lanyi, J. K. *J. Phys. Chem.* **1996**, *100*, 2391.

Chapter 6. Conclusions

In this dissertation, by means of various quantum chemical calculations, the author investigated how the ^{13}C NMR shieldings and absorption spectra of retinal chromophores are influenced by perturbations from their environments. These calculations successfully revealed the origin of characteristic behavior of spectral data observed for Rh and bR, leading to proposals of a new molecular model for the chromophore-protein interactions in Rh and bR. The findings and conclusions derived from them are summarized as follows.

In Chapter 2, from the results of *ab initio* shielding calculations, the author explored the universal relationships between the conformation around a single bond in linear π-conjugated systems and the NMR shieldings of the unsaturated carbons. The conjugated carbons were classified into two types according to the profiles of conformation dependence of the shieldings. The shieldings of the carbons forming the rotating bond exhibited complicated angular dependence. The author rigorously evidenced that the behavior of such carbon shieldings can be understood by considering the effect of π-orbital modification, a new concept introduced here. On the other hand, the shieldings of the other carbons essentially followed well-known mechanisms including the steric and charge density effects, and so on. One of the most important findings is that the steric effects are reflected predominantly on the out-of-plane element σ_{11}, and the effects originated in electronic perturbation are on the in-plane elements σ_{22} and σ_{33}. This classification is hardly disturbed even when both types of effects simultaneously act during a conformational change. These basic data for the model systems were available to interpret the conformation dependence of ^{13}C shieldings for more complicated compounds like retinal. Combining the data for the direct *ab initio* shielding calculation of 11-*cis*-retinal and for the dienes, the author estimated the preferred

conformation around the C12-C13 bond of the chromophore in Rh. It was concluded that the chromophore takes *s-trans* conformation around the C12-C13 bond.

In Chapter 3, the author formulated a new theory for evaluating the medium effects on the absorption spectra of molecules. This theory is based on a self-consistent reaction field polarizable continuum model (SCRF-PCM), coupled with the configuration interaction (CI) procedure. The author derived the exact expression of contributions of the orientational and electronic polarization of solvent, and the expression of the diagonal element of the CI matrix. In addition, the operator formalism of the reaction field potential, which enabled the derivation of the off-diagonal elements of the CI matrix as well. This theory was implemented into the INDO/S program. It was demonstrated that the calculation for a merocyanine dye well reproduced the solvatochromic shift observed in a variety of solvents with wide ranges of dielectric constant and refractive index.

In Chapter 4, the computational method developed in Chapter 3 was applied to the analysis of the solvatochromic shifts of *all-trans*-retinal, its Schiff base and protonated Schiff base. From regression analysis of the experimental and theoretical data, the author clarified that the solvatochromic shift of these compounds is reproduced as a simple function of the physical parameters (i.e., dielectric constant and refractive index) of solvents. An important finding is that the absorption maxima of these compounds significantly red shift with an increase in refractive index of solvent. On the other hand, the effective refractive index of the chromophore-binding pocket of bR was estimated to be 1.51. This value, combined with literature value of dielectric constant, was used in the estimations of the absorption maxima of bR_{568} and M_{412}. The calculated absorption maxima were in a good agreement with the corresponding experimental values. From decomposition analysis of the calculated data, the author showed that the

polarizable medium effect of the protein matrix makes a sizable contribution (1000 cm^{-1}) to the opsin shift. In addition, the author pointed out that the reference state to measure the opsin shift should be chosen to be the solution of a non-polar and non-basic solvent such as hexane.

In Chapter 5, the author formulated a new method for evaluating the absorption spectra of a chromophore contained in a protein. The "polarizable mosaic model" approximation was shown to correctly predict the electronic rearrangement of molecules, caused by the immediate response of the protein to an external electric field. This approximation, combined with MO calculations, enabled the author to examine the electronic polarization effect on the absorption maxima of bR with explicitly taking into account the individual atoms. Based on the results of electrostatic potential analysis, the author proposed a new molecular model, in which three aromatic residues (Trp86, Trp182 and Tyr185) play a key role in causing the opsin shift of bR. The author compared the results in this chapter with those in Chapter 4, and concluded that these aromatic residues play a role similar to a polarizable medium.

Fortunately, in this dissertation, the author succeeded in proposing a molecular model which can fully explain the opsin shift of bR. The author believes that the opsin shift of Rh can be explained from the same mechanism, although the tertiary structure of this protein has not been published. In the near future, more detailed structural analyses of Rh will prove or disprove this presumption. In this regards, the determination of the C12-C13 conformation is of great significance as a starting point of such analyses.

Two different methods, which have been presented by the author, could be applied to theoretical analyses of various chromophore-containing proteins. The author's interest is also addressed to elucidation of the photo-reaction mechanism of such proteins. For example, the distinct behavior in the photo-isomerization

process of the chromophores in Rh and bR, e.g., the high quantum yield of photo-absorption and the high regio-selectivity of photo-isomerization, might be explained from the same molecular model of the chromophore-protein interaction as proposed in this study.

I believe that this study lays the foundation for quantum chemical analysis of spectroscopic data for photoreceptive proteins.

Acknowledgments

The author gratefully wishes to express his appreciation to Professor Y. Inoue at Tokyo Institute of technology, for his helpful discussion, suggestions and guidance throughout this study. I am deeply indebted to Associate Professor M. Sakurai at Tokyo Institute of technology, for his helpful discussion, particularly valuable suggestions and encouragement throughout this study.

I would like to thank Professors I. Ando and M. Fujihira and Associate Professor H. Ohtani at Tokyo Institute of technology for referring this thesis.

I would gratefully like to thank Dr. Y. Tamura at Nihon Silicon Graphics Cray K. K., for his helpful suggestions.

I would gratefully like to thank Dr. M. Wada at Fujitsu Co. Limited, for his helpful suggestions.

I gratefully thank Nihon Silicon Graphics Cray K. K., for the kind arrangement of the use of the computer systems, Cray YMP8E/8128 and C90.

I gratefully thank the Computer Center, Institute for Molecular Science, Okazaki, Japan, for the kind arrangement of the use of the computer systems, an IBM SP2 cluster system and an NEC SX-3 supercomputer.

I gratefully thank the Computer Center, Tokyo Institute of Technology, Tokyo, Japan, for the use of a Cray C916 system.

Last but not least, I thank all the members of Inoue & Sakurai's laboratory, Tokyo Institute of Technology, for their helpful and joyful collaboration.

北條博彦